Durham E-Theses

Analytic QCD Amplitudes using Finite Field Evaluation Techniques

SARANDREA, FRANCESCO

How to cite:

Use policy

Analytic QCD Amplitudes using Finite Field Evaluation Techniques

Francesco Sarandrea

A Thesis presented for the degree of
Doctor of Philosophy

Institute for Particle Physics Phenomenology
Department of Physics
Durham University
England, UK

February 2023

Analytic QCD Amplitudes using Finite Field Evaluation Techniques

Francesco Sarandrea

Submitted for the degree of Doctor of Philosophy

February 2023

Abstract: In this thesis we present the analytic expressions of different high-multiplicity one-loop scattering amplitudes in Quantum Chromodynamics. The scattering amplitudes are decomposed into combinations of colour-ordered amplitudes. The colour-ordered amplitudes are represented as scalar integrals multiplied by coefficients, which are functions of the kinematics of the external particles. We parametrised the kinematics using momentum-twistor variables, in order to express the coefficients as rational functions. We found the analytic form of the rational coefficients by employing numerical interpolation techniques, which make it possible to reconstruct analytic expressions by sampling their value over finite fields. We computed the expressions of the one-loop corrections to $pp \to \bar{t}tj$ up to second order in the dimensional regulator. We also computed the expressions of the Maximally-Helicity-Violating six-gluon one-loop amplitudes in an arbitrary number of dimensions. We studied different techniques for optimising the reconstruction process, developing original methods for directly reconstructing polynomial expressions of high degree into simpler, partial-fractioned forms.

Contents

List of Tables

List of Figures

Acronyms

BCFW Britto-Cachazo-Feng-Witten.

BSM Beyond the Standard Model.

CDR Conventional Dimensional Reduction.

CDT Catani-Dittmaier-Trocsanyi.

DGLAP Dokshitser-Gribov-Lipatov-Altarelli-Parisi.

DIS Deep Inelastic Scattering.

DR Dimensional Regularisation.

FHD Four Helicity Dimensional.

IBPs Integration By Parts.

IR Infrared.

ISP Irreducible Scalar Product.

KLN Kinoshita-Lee-Nauenberg.

LHC Large Hadron Collider.

LO Leading Order.

MHV Maximally Helicity Violating.

MI Master Integrals.

MPLs Multiple Polylogarithms.

NLO Next to Leading Order.

NNLO Next to Next to Leading Order.

OPP Ossola-Papadopoulos-Pittau.

PDF Parton Distribution Functions.

QCD Quantum Chromodynamics.

QED Quantum Electrodynamics.

QFT Quantum Field Theory.

RSP Reducible Scalar Product.

SM Standard Model.

tHV 't Hooft-Veltmann.

UT Uniform Trascendental.

UV Ultraviolet.

Declaration

The work in this thesis is based on research carried out in the Institute for Particle Physics Phenomenology at Durham University and in the University of Torino. No part of this thesis has been submitted elsewhere for any degree or qualification. Chapter 5 is based on the published work

- S. Badger *et al.*, "One-loop QCD helicity amplitudes for pp $\to \bar{t}tj$ to $O(\epsilon^2)$", *Journal of High Energy Physics*, vol. 2022, no. 6, 2022. DOI: `10.1007/jhep06(2022)066`. [Online]. Available: `https://doi.org/10.1007/jhep06(2022)066` .

Acknowledgements

First and foremost, I would like to thank my supervisor Simon Badger, for the guidance and support he gave me throughout my studies. His help and encouragement have been fundamental to my work, both on an academic and a human level. I am grateful to both the IPPP and University of Torino communities for being such welcoming and stimulating environments to work in. The people I have met in these institutions made me feel at home, regardless of where I was in the world.

Thanks to Bayu Hartanto, Tiziano Peraro, Simone Zoia, Ekta, Matteo Becchetti and Ryan Moodie for the interesting discussions and the help they have given me along the way. I am especially thankful to Ryan Moodie, Jakub Kryś, Simone Zoia, Callum Milloy, Gloria Bertolotti and Henry Truong for taking the time to read parts of the draft of this thesis and give me valuable suggestions. I would also be remiss if I didn't thank my mother, my father and Marco, for putting up with me for the past twenty-nine years.

Chapter 1

Introduction

The ultimate goal of Science, and of theoretical physics in particular, has always been to find a unifying theory which could explain all natural phenomena within one simple model. Tremendous progress has been made in this direction since the introduction of quantum fields to describe the fundamental constituents of Nature. The effectiveness of this paradigm was confirmed in the late sixties, when Abdus Salam and Steven Weinberg used it to unify the Electromagnetic and Weak interactions, two of the four fundamental forces of the Universe [2, 3]. In the following years, further work lead to the formulation of the Standard Model of particle physics (SM), the most complete unified theory known to date [4]. The SM accurately describes the nature of the Strong and Electroweak interactions, as well as the properties of all observable matter in the universe [5]. Its most recent success was the discovery of the Higgs Boson in 2012 [6, 7], which was predicted by the theory as a result of Electroweak symmetry breaking.

Despite being incredibly successful at making predictions at high level of accuracy for many physical observables [8], the Standard Model does not offer the final description of reality at the sub-atomic scale. This is the case since the theory fails to explain a variety of phenomena in cosmology and particle physics [5]. Some of the most interesting problems with the theory are the lack of an explanation for neutrino oscillations, the predicted but never observed charge-parity symmetry breaking via strong interactions in Quantum Chromodynamics (QCD), and the mystery concerning

the true nature of Dark Energy and Dark Matter. Furthermore, the Standard Model appears to be incompatible with General Relativity, and therefore fails to describe gravitational interactions [9].

For this reason the SM is currently regarded as an Effective theory valid up to a finite energy scale. Above such scale, it is expected that new physics will start being detectable and play an important role. The main interest for most of the particle physics community in the past decades has been to look for discrepancies between the predictions of the theory and the experimental results in the laboratory, in order to obtain data which can guide the formulation of more general theories beyond the SM (these are commonly referred to as BSM theories).

The most important type of experiment in particle physics is the study of scatterings and decays of highly energetic particles, most of which are studied in particle accelerators. The biggest particle accelerator in the world is the Large Hadron Collider (LHC), in which it possible to perform experiments at the highest energies permitted by current technology.

The second running period of the LHC (Run 2), which started in 2015 and finished in December 2018, delivered an unprecedented amount of data, with more than $160\,\mathrm{fb}^{-1}$ proton-proton collisions recorded over the whole run [10]. This new set of experiments made it possible to observe collisions at energies as high as 13 TeV, giving the opportunity to test Standard Model predictions at a new energy frontier. In July 2022 the third running period (Run 3) started; it is expected to last for four years, at the energy of 13.6 TeV [11]. Further experimental upgrades will be implemented with the start of the High-Luminosity LHC project [12], scheduled to begin in 2026, which will increase the integrated luminosity of the LHC design value by a factor of 10. In this context, it is crucial to develop and refine theoretical methods to produce phenomenological predictions that can be compared to the experimental results; in this way the LHC data can be exploited to its full potential in the search for new physics [13].

High-precision QCD calculations play a crucial role in the phenomenology of LHC, both because they enable to obtain more accurate estimates of physically relevant quantities such as the strong coupling α_s and the top-quark mass, and also because QCD processes represent the principal source of background at the LHC [13]. Understanding the background processes is of vital importance in

order to isolate interesting rare events.

In the past years it has been observed a decrease in the experimental uncertainty for many observables at the LHC [14]. An example is the mass of the top quark, which has been determined with sub-percentage precision by combining data from the LHC and the Tevatron experiment [15]. On the theory side, the same quantity can be extracted from the calculation of the cross-section of processes with top quarks and a jet as final states. The most recent theoretical predictions have an uncertainty around the percent level [16], which is higher than the experimental ones.

The discrepancy between experimental and theoretical precision is expected to be even greater for Higgs Bosons's cross-sections. Since for many processes involving the Higgs boson the uncertainty is dominated by statistical errors, the increase in LHC luminosity (number of events) is expected to shrink the error bars by approximately a factor of five, making them significantly smaller than the current theoretical ones.

It appears therefore clear that new methods and techniques need to be implemented so that the theoretical work can keep up with the increasing accuracy and precision of the experimental data. An increase in precision in QCD calculations is needed in order to achieve this goal [14].

This thesis aims to present the research of the author, which focused on the study of high-multiplicity scattering amplitudes in QCD. Scattering amplitudes are a fundamental ingredient in the computation of physical observables in quantum field theories (QFTs) and their study is one of the most active areas of research in high-precision phenomenology. In this work we will present the previously unknown analytical expressions of scattering amplitudes for different processes involving five and six particles. In addition to describing the final analytical results, the intention is also to discuss the original methods that have been employed to obtain said expressions. The strengths and limitations of these new computational techniques are discussed, providing information for their general implementation in high-precision phenomenological studies.

This thesis is organised as follows. In Chapter 2, we give a theoretical background, briefly describing the Standard Model and the most relevant features of Quantum Chromodynamics. In Chapter 3 we introduce the modern methods for the computation of scattering amplitudes which were

employed in the projects described in the subsequent chapters. In Chapter 4 we describe the analytic reconstruction of rational functions using sampling over finite fields, giving a detailed description of the algorithms which were used to obtain the expressions of the scattering amplitudes. In Chapter 5 we present the computation of $pp \to \bar{t}tj$ one-loop amplitudes up to second order in the dimensional regulator. Chapter 6 contains a brief review of the history of the computation of one-loop gluon amplitudes. In Chapter 7 we describe the computation of the one-loop six-gluon Maximally-Helicity-Violating (MHV) amplitudes in an arbitrary number of dimensions D. The conclusions are in Chapter 8.

Chapter 2

The Standard Model and High Precision Physics

In this chapter present a brief overview of the fundamental aspects of the theory of the Standard Model (SM), focusing specifically on the theory of Quantum Chromodynamics (QCD). The study of QCD is the most relevant for precision physics, since the strong interactions dominate quantum corrections for most processes observed in particle accelerators. This fact is a consequence of the large value of the strong coupling constant relatively to the other fundamental forces [4, 17].

The discussion will introduce the essential theoretical background to the research presented in this thesis. This chapter is organised as follows. In Section 2.1 we introduce the most relevant features of the SM and explain how QCD and Quantum Electrodynamics (QED) are coherently combined in the same framework. In Section 2.2 we describe the QED Lagrangian, and do the same for the QCD Lagrangian in Section 2.3. Section 2.4 presents the process of renormalisation of QCD, while in Section 2.5 we describe how QCD can be used to model physical events thanks to models in which contributions between soft and hard energy factorise. In Section 2.6 we introduce scattering amplitudes and how they are used to obtain hard cross-sections. In Section 2.7 we delineate the infrared structure of QCD.

2.1 The Standard Model

The SM is a quantum field theory which describes the fundamental constituents of matter and their interactions, with the exception of gravity. Interactions in the SM preserve gauge (local) symmetries expressed by the action of the groups

$$SU(3)_c \times SU(2)_L \times U(1)_Y, \tag{2.1}$$

Group $SU(3)_c$ represents the gauge symmetry of the interactions between coloured quarks and gluons, described by the theory of QCD. The groups $SU(2)_L \times U(1)_Y$ in turn describe the local symmetries of Electroweak interactions between quarks and leptons. The subscripts refer to left-handedness and hyper-charge, respectively.

At temperatures below a certain energy scale (~ 160 GeV) the Electroweak symmetry is spontaneously broken by the Higgs mechanism, following the pattern

$$SU(2)_L \times U(1)_Y \rightarrow U(1)_{EM} \tag{2.2}$$

which gives rise to the gauge group of Electromagnetic interactions, described by the theory of QED. The matter content of the SM consists of fermions, which are the spin-$\frac{1}{2}$ particles listed in Table 2.1 The interactions between fermions are mediated by bosons. In the theory, the bosons are the

	Family 1	Family 2	Family 3	Charge
Quarks	**u** $m_u = 2.2\text{MeV}/c^2$	**c** $m_c = 1.28\text{GeV}/c^2$	**t** $m_t = 173.1\text{GeV}/c^2$	$+\frac{2}{3}$
	d $m_d = 4.7\text{MeV}/c^2$	**s** $m_s = 96\text{MeV}/c^2$	**b** $m_b = 4.18\text{GeV}/c^2$	$-\frac{1}{3}$
Leptons	**e** $m_e = 0.551\text{MeV}/c^2$	**μ** $m_\mu = 105.66\text{MeV}/c^2$	**τ** $m_\tau = 1.7768\text{GeV}/c^2$	-1
	ν_e $m_{\nu_e} < 2.2\text{eV}/c^2$	**ν_μ** $m_{\nu_\mu} < 0.17\text{MeV}/c^2$	**ν_τ** $m_{\nu_\tau} < 18.2\text{MeV}/c^2$	0

Table 2.1: The fermionic content of the Standard Model. All particles have spin-$\frac{1}{2}$. The three leptonic families are listed. We notice how the difference among the three families consists of the different masses of their particles.

$N^2 - 1$ group generators of the three $SU(N)$ groups in Eq. (2.1) in the adjoint representation. We

therefore have 8 bosons associated to $SU(3)_c$ (gluons), the three W_μ^1, W_μ^2 and W_μ^3 bosons associated to $SU(2)_L$ and the one B_μ associated to $U(1)_Y$. After the Electroweak symmetry breaking, the gauge bosons mix and give rise to the physical bosons:

$$W_\mu^\pm = (W_\mu^1 \mp i W_\mu^2)/\sqrt{2} \tag{2.3}$$

$$A_\mu = \sin\theta_W W_\mu^3 + \cos\theta_W B_\mu \tag{2.4}$$

$$Z_\mu = \cos\theta_W W_\mu^3 - \sin\theta_W B_\mu. \tag{2.5}$$

Where θ_W is a dimensionless parameter which depends on the coupling of the bosons.

This thesis will be concerned with the study of physical processes described by QCD theory, which we present in more detail in Section 2.3. For more comprehensive reviews of the SM the reader is referred to the numerous books and reviews present in the literature [4, 5, 9, 18–20].

Before introducing QCD, we briefly higlight the most salient features of QED in Section 2.2. This will help to understand how Lagrangians are constructed in quantum field theories. A comparison of QED and QCD will also allow us to elucidate the higher degree of complexity of the latter theory.

2.2 The QED Lagrangian

QED is an abelian gauge theory with symmetry group $U(1)$. It describes the interaction among spin-$\frac{1}{2}$ fermions and spin-1 vector bosons. The fermions are quarks and leptons in Table 2.1, while the vector bosons are the photons A_μ. The lagrangian of QED is can be split into two parts:

$$\mathcal{L}^{\text{QED}} = \mathcal{L}_{classical} + \mathcal{L}_{gauge}. \tag{2.6}$$

The first term has form

$$\mathcal{L}_{classical} = -\frac{1}{4} F^{\mu\nu} F_{\mu\nu} + \sum_{f=1}^{n_f} \bar{\psi}_f (i\not{D} - m_f)\psi_f, \tag{2.7}$$

where the field strength tensor $F^{\mu\nu}$ and the covariant derivative D are defined as:

$$F^{\mu\nu} = \partial^\mu A^\nu - \partial^\nu A^\mu, \tag{2.8}$$

$$D^\mu = \partial^\mu - ieq_f A^\mu. \tag{2.9}$$

Symbol e represent the electron electromagnetic charge, while q_f is a fraction $-1 < q_f < 1$ specific for the fermion ψ_f. It is convenient to express the coupling in terms of the dimensionless constant

$$\alpha = \frac{e^2}{4\pi}, \tag{2.10}$$

which is the fine structure constant. The coupling has a dependence on the energy scale of the process, we will see this explicitly for the QCD case in Section 2.3.

The form of the covariant derivative gives rise to interactions among fermions and photons in QED. If we derive the equation of motion for the photon field from Eq. (2.7) we obtain:

$$(\Box g^{\mu\nu} - \partial^\mu \partial^\nu)A_\nu = 0. \tag{2.11}$$

The canonical quantisation of the photon field would therefore require the inversion of the 4×4 matrix $k^2 g^{\mu\nu} - k^\mu k^\nu$ in momentum space. This cannot be done directly since the matrix is not invertible. This issue indicates the need of *fixing the gauge* of the theory and motivates the addition of term $\mathcal{L}_{gauge}$ in Eq. (2.6). Fixing the gauge corresponds to imposing local linear constraints which eliminate the redundancy of the gauge symmetries. We can add a *covariant gauge* term

$$\mathcal{L}_{gauge} = -\frac{1}{2\xi}(\partial^\mu A_\mu)(\partial^\nu A_\nu) \tag{2.12}$$

to the classical Lagrangian. As a result of the gauge fixing, it is possible to write the propagator of the photon in momentum space:

$$\tilde{\Delta}_{\nu\mu}(k) = \frac{1}{k^2 - i\epsilon}\left(g_{\mu\nu} - (1 - \xi)\frac{k_\mu k_\nu}{k^2}\right). \tag{2.13}$$

The freedom in the choice of gauge is encoded in the introduction of parameter ξ: different values of ξ represent different gauge choices. The choice $\xi = 0$ is defined as *Landau gauge* and corresponds to te imposition of the constrain:

$$\partial_\mu A^\mu = 0. \tag{2.14}$$

We refer to setting $\xi = 1$ as working in the Feynman gauge. In general we refer to those as R_ξ gauges. Thorough discussions of the quantisation of gauge theories can be found in numerous textbooks [4, 20].

Most of the physical processes discussed in this thesis are described by Quantum Chromodynamics, which we introduce in the next section. We will highlight some of the similarities and differences with QED.

2.3   The QCD Lagrangian

Quantum Chromodynamics is a non-abelian gauge theory with symmetry group $SU(N_c)$, with $N_c = 3$. The subscript c refers to the *colour charge*, which is the name of the charge that fields have under the gauge group. In a similar fashion to Eq. (2.6) we write it as

$$\mathcal{L}^{\text{QCD}} = \mathcal{L}_{\text{classical}} + \mathcal{L}_{\text{gauge}} + \mathcal{L}_{\text{ghost}}, \tag{2.15}$$

where the classical Lagrangian is [18]

$$\mathcal{L}_{\text{classical}} = -\frac{1}{4} G_a^{\mu\nu} G_{\mu\nu}^a + \sum_{f=1}^{n_f} \bar{\psi}_f (i\slashed{D} - m_f)\psi_f. \tag{2.16}$$

The ψ_f are again the fermion fields, but this time they only refer to the quarks and not to the leptons. Their index f runs from 1 to $n_f = 6$ (number of quark flavours). $G_a^{\mu\nu}$ is a tensor field which depends on the gluon field A_a^μ

$$G_a^{\mu\nu} = \partial^\mu A_{\nu a} - \partial^\nu A_{\mu a} + g_s f_{abc} A_b A_c, \tag{2.17}$$

where g_s is the QCD coupling constant. The f^{abc} are the group's structure constant, they form a basis for the group in its adjoint representation. In this convention the latin letters a, b, c index the

gluons, which live in the adjoint representation of the $SU(N_c)$ gauge group, and thus run from 1 to $N_c^2 - 1$. This means that gluon vector fields A_μ can be expressed in the basis $A_\mu = A_\mu^a t^a$, where t^a are the gauge group generators. They are often expressed as

$$t_{ij}^a = \frac{1}{2}\lambda_{ij}^a, \tag{2.18}$$

where λ_{ij}^a are the Gell-Mann matrices [21]. Quarks, in contrast, live in the fundamental representation of $SU(N_c)$ and their indices run from 1 to N_c.

We see that $G_a^{\mu\nu}$ has a similar form to Eq. (2.8), with the addition of a term quadratic in the gluon field. This term needs to be added since QCD is a non-abelian theory. A physical consequence of this is that gluons, differently from photons, are self-interacting particles. This fact plays a crucial role in the difference in complexity between the calculations in QED and QCD: the presence of three and four-gluon interactions greatly increase the number of Feynman diagrams which need to be computed for a specific process in QCD, compared to processes at similar energies in QED. The t^a generators have the property [4]

$$\left[t^a, t^b\right] = if^{abc}t^c, \tag{2.19}$$

and in our presentation we choose the normalisation

$$\mathrm{tr}(t^a t^b) = T_R\delta^{ab}, \qquad T_R = \frac{1}{2}. \tag{2.20}$$

This choice fixes the following relations:

$$t_{ij}^a t_{jk}^a = \delta_{ik}C_F, \qquad C_F = \frac{N_c^2 - 1}{N_c}, \tag{2.21}$$

$$f^{abc}f^{abd} = \delta^{cd}C_A, \qquad C_A = N_c.$$

Constants C_F and C_A are the *Casimirs* of the group.

Like in the case of the photon in QED, it is necessary to add the term $\mathcal{L}_{gauge}$ to the classical Lagrangian in order to have a well defined physical gluon propagator when the theory is quantised.

The gluon propagator in the case of the addition of a covariant term to the Lagrangian is:

$$G_{\nu\mu}^{ab}(k) = \frac{i\delta^{ab}}{k^2 - i\epsilon}\left(\eta_{\mu\nu} - (1-\xi)\frac{k_\mu k_\nu}{k^2}\right). \tag{2.22}$$

Compared to the abelian case, however, the non-abelian theory presents a further complication. The introduction of a covariant gauge term is not sufficient to cancel out unphysical polarisation states of the gluons [19]. A theory with Lagrangian $\mathcal{L}_{classical} + \mathcal{L}_{gauge}$ predict the existence of gluons with polarisation vectors parallel and anti-parallel to their momentum k. Since these are not observed in the real world, it is necessary to introduce a new term to cancel such states. This term has form:

$$\mathcal{L}_{\text{ghost}} = -\bar{c}^a \partial^\mu D_\mu^{ab} c^b. \tag{2.23}$$

The c^a are named *Faddeev-Popov ghosts*, they are anticommuting ghost fields which live in the $SU(N_c)$ adjoint representation and obey the fermionic statistics. They do not correspond to any real physical state. The reader can find in Section 16.2 of [19] a derivation which shows how the introduction of gauge-fixing and ghost terms prevent the redundant integration over the infinite space of physically equivalent gauge configurations.

It is possible to make an alternative choice to the one of a covariant gauge-fixing term: the axial gauge. The benefit of using the axial gauge is that it does not need the introduction of ghost fields. It requires fixing the the gauge field with respect to an arbitrary vector n^μ:

$$\mathcal{L}_{\text{gauge}}^{QCD} = -\frac{1}{2\xi}(n^\mu A_\mu^a)(n^\nu A_\nu^a). \tag{2.24}$$

The gluon propagator is then:

$$G_{\mu\nu}^{ab}(k) = \frac{i\delta^{ab}}{k^2 + i\epsilon}\left(-\eta_{\mu\nu} + \frac{k_\mu n_\nu + k_\nu n_\mu}{k \cdot n} - \frac{(n^2 + \xi k^2)k_\mu k_\nu}{(k \cdot n)^2}\right). \tag{2.25}$$

Such an expression for the propagator is much more complicated than Eq. (2.22), this is the trade-off which is made for avoiding the presence of ghost fields.

In the case in which the reference vector is massless, $n^2 = 0$, we are in the *light-like axial gauge*, and there are only two polarisation states for the spin-1 particles. They then satisfy the following

equation

$$\sum_{s=\pm 1} \epsilon_s^\mu \epsilon_s^{\nu *} = -\eta^{\mu\nu} + \frac{n^\mu k^\nu + n^\nu k^\mu}{n \cdot k}, \qquad (2.26)$$

where $s = \pm 1$ are the two polarisation states,which represent the *helicity* of the particles. These definition will be useful in Chapter 3.

Once the choice of gauge has been made, it is possible to write down the interaction terms of the Lagrangian. These are the non-linear terms which depend on the couplings of the fields:

$$\mathcal{L}_{\mathrm{int}} = g_s A_\mu^a \hat{\psi}_i^f \gamma^\mu t_{ij}^a \psi_j^f - g_s f^{abc}(\partial_\mu A_\nu^a) A^{\mu,b} A^{\nu,c} - \frac{1}{4} g_s^2 (f^{eab} A_\mu^a A_\nu^b)(f^{ecd} A^{\mu,c} A^{\nu,d}) + g_s \hat{c}_i^a \partial^\mu A_\mu^a t_{ij}^c c_j^c.$$

$$(2.27)$$

Each of the terms in Eq. (2.27) is represented by a diagram with its associated Feynman rule. All the QCD Feynman rules are listed in Appendix B. The strong coupling constant in QCD is defined in a similar way to the fine structure constant in Eq. (2.10):

$$\alpha_s = \frac{g_s^2}{4\pi}. \qquad (2.28)$$

2.4   Ultraviolet Divergences and Renormalisation

Since the development of the earliest quantum field theories, it has been known that the direct application of the Feynman rules derived from the interaction terms of Lagrangians cannot be used to compute physical observables at arbitrarily high energies [5]. The computation of quantum corrections, in fact, requires the evaluation of Feynman diagrams with internal loops, as it will be explained in Section 2.6. The momentum of the virtual states k flowing in the internal loops is *unconstrained* and its values must be integrated over the whole energy range $\int_0^\infty dk$, this causes the appearance of divergences. Feynman integrals can evaluate to infinity in the limits $k \to 0$ and $k \to \infty$, these are called respectively *infrared* (IR) *virtual divergences* and *ultraviolet* (UV) *virtual divergences*. In this section we will focus on the latter cases, infrared divergences are discussed in Section 2.7.

We take as an example the simplest one-loop correction to a Feynman propagator displayed in Figure 2.1, following a similar argument to [5]. To compute this correction we must evaluate the Feynman
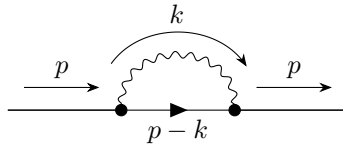
Figure 2.1: The quark self-energy is an example of a divergent Feynman diagram in QCD.

integral

$$I = \int^{\Lambda} \frac{d^4k}{(2\pi)^4} \frac{1}{k^2(p-k)^2},$$
(2.29)

for which we have

$$\lim_{k \to \infty} I = \log(\Lambda).$$
(2.30)

We chose to integrate up to what is called a cutoff scale Λ, in order to explicitly show that the integral diverges at high energies. The physical interpretation of such a behaviour is that our current physical models should be interpreted as effective field theories, only valid up to a specific energy scale. For this reason we cannot model interactions happening at arbitrarily high energy scales (or, equivalently, arbitrarily short distances). A truly complete theory of fundamental interactions is expected to be free of such divergences. Renormalisation should then be understood as a series of techniques which allow to extract physical predictions from a an effective theory, isolating the values of observables at lower energies from unkown high-energy effects.

Introducing a cut-off is an example of the *regularisation* of the divergences. We refer to regularisation to indicate any method which allows to parametrise the dependence of computed quantities on the UV or IR scale. The introduction of a cut-off has the drawback of breaking gauge invariance. In this section we discuss the *dimensional regularisation* (DR) scheme [22], which has been employed in the project discussed in Chapter 5. Other schemes, such as the Pauli-Villars [23], are commonly used. The reader can find discussions and reviews of the methods in many textbooks [4, 5, 19].

The crucial insight behind the DR scheme is that integral of Eq. (2.29) does not diverge for all values of the dimensions D. We therefore compute the integral in an arbitrary number of dimensions. In order to do this, it is possible to express it in a different form introducing a *Feynman parameter x*

so that

$$\frac{1}{k^2(p-k)^2} = \int_0^1 dx \frac{1}{((k-xp)^2 + x(1-x)p^2)^2} = \int_0^1 dx \frac{1}{(l^2+M^2)^2},\qquad(2.31)$$

where we defined $l = k - xp$, $M^2 = x(1-x)p^2$. We can invert the order of integration and substitute $dk \to dl$. We then have the task of computing $\int dl \frac{1}{(l^2+M^2)^2}$, it is convenient to perform a Wick rotation, equivalent to changing the energy component of the four vector l: $l^0 \to il_{\rm E}^0$, defining $l_{\rm E} = \{il^0, l^1, l^2, l^3\}$. Once this is done we obtain integral

$$\int_{-\infty}^{\infty} \frac{d^D l_{\rm E}}{(2\pi)^D} \frac{1}{(l_{\rm E}^2 + M^2)^2} = \frac{(M^2)^{D/2-2}}{(4\pi)^{D/2}} \Gamma[2 - D/2].\qquad(2.32)$$

A common choice is $D = 4 - 2\epsilon$; if we make that substitution and perform the final integral in dx we obtain

$$I(4 - 2\epsilon) = \frac{i}{(4\pi)^2} \left(\frac{1}{\epsilon} - \gamma_{\rm E} - \log(-p^2) - \log(4\pi) \right) + O(\epsilon),\qquad(2.33)$$

where $\gamma_{\rm E}$ is the Euler-Mascheroni constant. We then see that the UV divergence is parametrised as a simple pole with a clear dependence on the dimensionality of the integration measure.

Once the UV divergences have been identified, it is possible to insert counter-terms in the Lagrangian which cancel such divergences and give predictive power to the theory. This is normally done by redefining the fields and parameters in $\mathcal{L}^{\rm QCD}$. One can start by writing the exact two-point function in an interactive quantum field theory. Here we present the fermionic propagator as an example, using the same notation as in Chapter 10 of [19]:

$$D_{\rm F}(x) = \langle\Omega| T(\psi_{\rm bare}(x)\bar\psi_{\rm bare}(0)) |\Omega\rangle = \int \frac{d^4p}{(2\pi)^4} \frac{iZ_2 e^{-ip\cdot x}}{\not{p} - m + i\epsilon}.\qquad(2.34)$$

In Eq. (2.34), $|\Omega\rangle$ represents the vacuum of the interacting theory, while T is a time-ordering operator. We introduce the subscript *bare* to refer to the parameters entering in the Lagrangians such as the ones in Eq. (2.27), these are different from the physical renormalised quantities [19]. We present here the rescaling of the fermions, gauge bosons and ghosts together with the redefinition of

the coupling constant and mass, expressed in the same way as in [24] :

$$\psi_{\text{bare}} = \sqrt{Z_2}\psi, \tag{2.35}$$

$$A^{\mu}_{\text{bare}} = \sqrt{Z_3}A^{\mu}, \tag{2.36}$$

$$c_{\text{bare}} = \sqrt{Z_2^c}c, \tag{2.37}$$

$$g_{s,\text{bare}} = \frac{Z_1}{Z_2\sqrt{Z_3}}g_s = Z_g g_s, \tag{2.38}$$

$$m_{\text{bare}} = Z_m m \tag{2.39}$$

The factors Z_2, Z_3, Z_2^c are *wave-function renormalisation constants*, it is common practice to account for them by rescaling the fields: this procedure is referred to as wave-function renormalisation [20]. One is then free to define the counter-terms δ_i so that $Z_i = 1 + \delta_i$. This allows us to separate the bare Lagrangian from the one containing the counter-terms, obtaining:

$$\mathcal{L}^{\text{QCD}} = \mathcal{L}_{\text{bare}} + \mathcal{L}_{\text{c.t.}}. \tag{2.40}$$

The exact form of the counter-terms δ_i depends on the choice of renormalisation scheme [24]. This freedom is a consequence of the fact that the poles of the renormalisation constants need to be fixed to exactly cancel the poles in epsilon such as the one appearing in Eq.(2.4), but this is not the case for any additional finite term. One possible choice corresponds to the subtraction of only the epsilon poles appearing in the loop integrals; this is referred to as the *minimal subtraction scheme* [20]. A more widely-used scheme is the *modified-minimal-subtraction scheme*, in which in addition to the poles we also subtract a universal constant appearing in all loop integrals [19]. For masses, the *on-shell scheme* is also commonly used: this is defined by the requirement that the quark two-point function vanishes at the position of the on-shell mass [20, 25]. In practice, if we write the renormalised quark propagator in momentum space as

$$\tilde{D}_{\text{F}}(p) = \frac{iZ_2}{\not{p} - m_{\text{bare}} + \Sigma(p,m) + i\epsilon}, \tag{2.41}$$

then we require its inverse $\tilde{D}_{\text{F}}^{-1}(p)$ to vanish at the position of the on-shell mass m. The function

$\Sigma(p, m)$ represents the quark self-energy [25], details on its computation at one loop can be found in many textbooks and reviews [19, 24]. The form of Z_2 is in turn determined by the prescription that the residue at m must be equal to i, therefore having

$$\lim_{p^2 \to m^2} \tilde{D}_{\mathrm{F}}(p) = \frac{i}{\not{p} - m + i\epsilon}.$$ (2.42)

This leads to the following form for the Z_m renormalisation constant: $Z_m = 1 + \Sigma(p, m)|_{p^2 = m^2}$.

We then see that the physical mass is distinct from the bare mass m_{bare} which appears in the Lagrangian, as explained before.

The renormalisability of QCD ensures that the UV divergences for all possible processes can be cancelled by this finite number of counter-terms [19].

In many renormalisation schemes, a distinction is made between the dimensions of the integral measure D and a quantity defined as the *spin dimension d_s* [26]

$$d_s = \eta_\mu^\mu.$$ (2.43)

The spin dimension arises from the contractions of the integrand numerators. Different choices are made in different reduction schemes. In the Conventional Dimensional Reduction (CDR) scheme we have $d_s = D$, in the 't Hooft-Veltman (tHV) scheme $d_s = 4 - 2\epsilon$ [27], while in the Four Helicity Dimensional (FHD) scheme $d_s = 4$ [28].

An important consequence of the change in the dimensions to $D < 4$ in DR is that we need to introduce a dependence of the strong coupling constant on an energy scale μ_{R}, to ensure that $\mathcal{L}^{\mathrm{QCD}}$ retains the correct dimensions. We know that $\mathcal{L}^{\mathrm{QCD}}$ must define a dimensionless action, and changing the number of dimensions to $D < 4$ would yield to a Lagrangian with the wrong mass-dimensions. This fact makes it necessary to introduce the *renormalisation scale μ_{R}*, so that we can redefine the coupling constant as

$$g_S = \mu_{\mathrm{R}}^\epsilon g_S,$$ (2.44)

in this way g_S remains dimensionless. Since μ_{R} was introduced for mathematical convenience, any

real physical observable O_{obs} must be independent of it, having $\frac{\partial O_{\text{obs}}}{\partial \mu_R} = 0$. This must then be true for the bare coupling constant:

$$\frac{\partial g_{S,\text{bare}}}{\partial \mu_R} = 0. \tag{2.45}$$

The condition of Eq. (2.45) imposes a dependence of the renormalised strong coupling on μ_R. This dependence is expressed by the Callan-Symanzik β-function [29, 30]:

$$\beta(\alpha_s) := \frac{d\alpha_s}{d\log(\mu_R^2)} = -\sum_{n=0}^{\infty} \beta_n \left(\frac{\alpha_s}{4\pi}\right)^{n+2}. \tag{2.46}$$

The coefficients of Eq. (2.46) have been computed up until β_4 (five loops) [31, 32]. The behaviour of the strong coupling constant at the variation of the energy scale is defined as the *running of the coupling*. All five β coefficients are positive, indicating that the coupling decreases at higher energies, as shown in Figure 2.2. This property is referred to as the *asymptotic freedom* of the theory, and it shows that perturbative expansions can be used to compute quantities in QCD for processes at sufficiently high energies (hard processes). Processes at lower energies are referred to as soft physics, and need to be modelled using different methods. We will explore these concepts further in the next section. In Section 2.4 we will see how the scale dependence of α_s is related to the cancellation of divergent quantities from the physical theory.

2.5 Physical Observables and Factorisation

The main physical observables computed in particle physics are differential cross-sections [18]. These are quantities which allow us to calculate the probability of a specific scattering or decay process, and their computation consists of several steps.

Firstly, an accurate description of the initial states is required. Such a description is simple if the initial states are fundamental particles, but it presents a significant challenge if they are composite hadrons. In the latter case, Parton Distribution Functions (PDFs) need to be computed [18]. PDFs are not calculated perturbatively, but instead by fitting the theoretical models to the experimental data [34, 35]. This is the case because the quarks and gluons bound in a parton interact at energies much lower than the ones of the observed scattering events in the accelerator. From our discussion
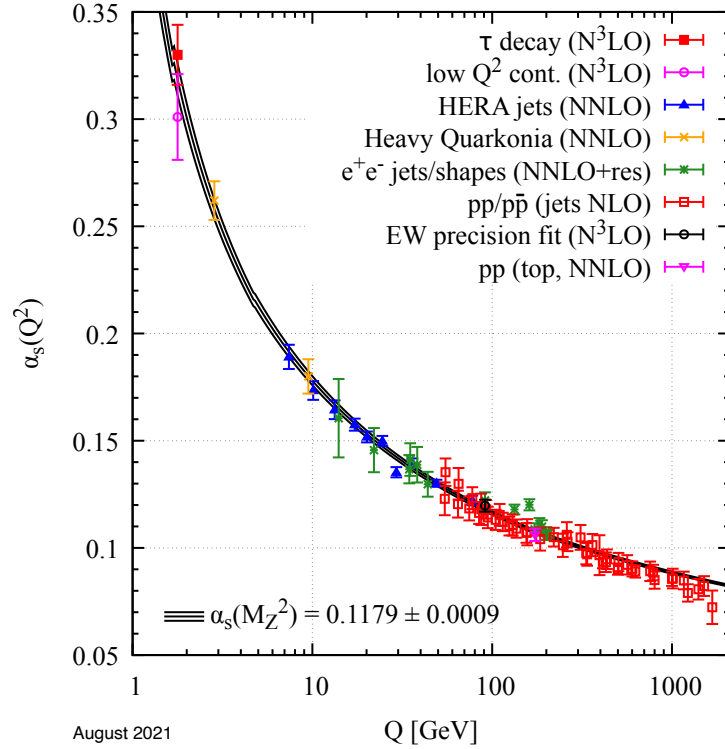
Figure 2.2: Experimental measurements of α_s as a function of the energy Q [33]. The black line shows the theoretical prediction with its confidence interval.

in Section 2.4 we know that this means that the value of α_s in such a regime is not small enough to perform a perturbative expansion. PDFs are universal, which means that once they are computed, their form can be used in all processes having the same partons as initial states [18, 35] .

The scattering of partons is, instead, a hard process happening at higher energies. Such interactions are modelled by fixed-order perturbative calculations, as we will see in Section 2.6 in more detail.

As the last step, in order for the calculations to be comparable with experimental data, it is necessary to model the transition from the high-energy of the scattering event to the low-energy regime, where particles bond into *jets* which can be measured by detectors. This is achieved by simulating the emission of unresolved soft and collinear radiation and of hadronisation processes. Three main classes of hadronisation models are commonly used: independent fragmentation [36], the string models [37] and the cluster models [38].

Hadronisation events are simulated via Monte Carlo event generators such as SHERPA [39], PYTHIA

[40], and HERWIG [41]. Most of the available hadronisation models require the definition of *fragmentation functions* D_{F}, which, like the PDFs, are modelled from empirical data and are assumed to be process-independent.

The values of the PDFs and fragmentation functions depend on a *factorisation scale* μ_F which sets the energy separation between soft and hard processes. The dependence that said functions have on μ_F has the effect of renormalising their divergences, in a similar way to how the strong coupling constant must depend on μ_R to renormalise the bare Lagrangian of QCD, as seen in Section 2.4. In this framework, a parton distribution function $f_i^h(x, \mu_F^2)$ expresses the probability of finding a parton i with a fraction x of the total momentum inside the hardon h. The PDFs have a dependence on the factorisation scale which is expressed by the Dokshitser-Gribov-Lipatov-Altarelli-Parisi (DGLAP) equations [42–44]. Following a similar argument to the one that lead us to Eq. (2.45), we expect the physical cross-section to be independent of the arbitrary factorisation scale μ_F. In a Taylor expansion, the cancellations of α_S-depending terms will be approximate, so at order α_S^k:

$$\mu_F^2 \frac{\partial d\sigma}{\partial \mu_F^2} = 0 + O(\alpha_S^{k+1}). \tag{2.47}$$

Therefore we expect that the dependence of the hadronic cross-section on the factorisation scale will decrease as we reach higher orders in perturbation theory. This fact is verified empirically by employing the method of *scale variation*, in which the cross-section is computed for different values of μ_F [45].

The factorisation theorem allows us to model the whole physical process as a convolution of the quantities contributing to each soft and hard part [4]. We consider the toy example of the process $h_a h_b \rightarrow X$ depicted in Figure 2.3. of two hadrons interacting and producing a final state hadrons X. According to the factorisation theorem, the differential cross-section can be modelled as:

$$d\sigma(h_a h_b \rightarrow X) = \sum_{ij} \int_0^1 dx_1 dx_2 f_{i,h_1}(x_1, \mu_F^2) f_{i,h_2}(x_2, \mu_F^2) \times \tag{2.48}$$

$$d\hat{\sigma}_{ij}(i(x_1 p_a) j(x_2 p_b) \rightarrow \hat{X}, \mu_F^2, \mu_R^2, Q^2) \times D_{\mathrm{F}}(\hat{X} \rightarrow X, \mu_F^2) + O\left(\frac{\Lambda_{QCD}}{Q}\right),$$
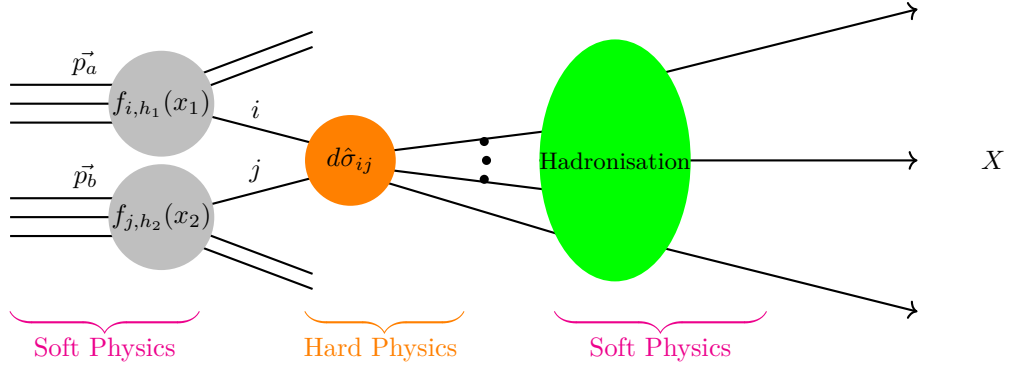
Figure 2.3: Schematic representation of a $h_a h_b \to X$ scattering event. We distinguish the parts of the process described by perturbative (hard) and non-perturbative (soft) quantum field theory. The symbols are the same as the one in Eq. (2.48).

where the initial states have momenta p_a and p_b. The partonic initial states of the hard scattering process are labelled i and j, while the final states of the hard scattering events are represented by $\hat{X}$. The fragmentation function describes the hadronisation process from partons $\hat{X}$ to observables X, as shown in Figure 2.3. We see that Eq. (2.48) is not exact, but has corrections of order $O(\Lambda_{QCD}/Q)$. The critical energy Λ_{QCD} is the energy for which $\alpha_s(\Lambda_{\text{QCD}}) \approx 1$ and the perturbative approach is no longer valid. This shows that the formula is applicable in cases in which the hard scattering energy Q is much higher than Λ_{QCD}. The factorisation theorem has been formally proven only for Deep-Inelastic-Scattering (DIS) processes and Drell-Yan processes [18]. In a Drell-Yan process the final state consists of two oppositely-charged leptons [46].

In the next section we will se how the process-dependent hard scattering cross-section can be computed using scattering amplitudes.

2.6 Scattering Amplitudes

We can now discuss how scattering amplitudes can be used to compute the hard cross-section and how this is related to the QCD Lagrangian of Eq. (2.15). In order to do this we introduce the S-matrix, following [47].

We see from Eq. (2.46) that when working in the hard scattering regime we are justified in treating

the incoming and outgoing states as asymptotically free when far away from the scattering region. If we assume that the scattering happens at time $t = 0$, then we take the states $|\text{in}\rangle$ and $|\text{out}\rangle$ to be at times $t = -\infty$ and $t = +\infty$ respectively. The evolution of the states can be described by the free-state Hamiltonian H_{free} at infinite times and the interaction Hamiltonian H_{int} at the scattering time. So the evolution $|\text{in}\rangle \rightarrow |\text{out}\rangle$ is expressed as

$$|\text{out}\rangle = \exp(iH_{\text{free}}t_{\text{out}})\exp(iH_{\text{int}}(t_{\text{out}} - t_{\text{in}}))\exp(-iH_{\text{free}}t_{\text{in}}) := U(t_{\text{out}}, t_{\text{in}})|\text{in}\rangle. \quad (2.49)$$

We then define the S-matrix as [19]

$$\mathcal{S} := \lim_{\substack{t_{\text{in}} \to -\infty \\ t_{\text{out}} \to +\infty}} U(t_{\text{out}}, t_{\text{in}}) = U(-\infty, \infty). \quad (2.50)$$

We analyse the scattering process $p_a p_b \rightarrow p_1, ..., p_n$, for which we have initial and final momentum eigenstates $|\text{in}\rangle \rightarrow |p_a, p_b\rangle$ and $|\text{out}\rangle \rightarrow |p_1, ..., p_n\rangle$. The S-matrix element related to this process is

$$\langle p_1, ..., p_n | \mathcal{S} | p_a, p_b \rangle, \quad (2.51)$$

and the transition probability from state $|\text{in}\rangle$ to state $|\text{out}\rangle$ is

$$P(\text{in} \rightarrow \text{out}) = |\langle \text{out} | \mathcal{S} | \text{in} \rangle|^2. \quad (2.52)$$

The Lorentz-invariant normalisation of the states is:

$$\langle p' | p \rangle = (2\pi)^3 \delta^{(3)}(p - p'). \quad (2.53)$$

This implies that the first term in the perturbative expansion for the elastic scattering will be $(2\pi)^3 \delta^{(4)}(p_a + p_b - \sum_{i=1}^{n} p_i)$. From this analysis we see that the S-matrix can be decomposed into [47]

$$\mathcal{S} = \mathbf{1} + i\mathcal{T}, \quad (2.54)$$

so that we have:

$$\langle p_1, ..., p_n | \, \mathcal{S} \, | p_a, p_b \rangle = \langle p_1, ..., p_n | p_a, p_b \rangle + i \, \langle p_1, ..., p_n | \, \mathcal{T} \, | p_a, p_b \rangle \,. \tag{2.55}$$

From Eq. (2.55) we see that all the information on the interaction is contained in $\mathcal{T}$. The interactions in the theory are those expressed by Eq. (2.27); H_{int} is derived from $\mathcal{L}_{int}$.

The relation between the S-matrix and the scattering amplitude $\mathcal{A}$ is expressed by [19]

$$\langle p_1, ..., p_n | \, \mathcal{T} \, | p_a, p_b \rangle = i(2\pi)^4 \delta^{(4)}(p_a + p_b - \sum_{i=1}^{n} p_i) \mathcal{A}_{n+2}, \tag{2.56}$$

with the four-dimensional delta function ensuring momentum conservation. The scattering amplitude can be expressed as an expansion in the coupling constant, in the case of QCD it is α_s, so for a scattering event involving $n + 2$ total external states (incoming and outgoing) we have :

$$\mathcal{A}_{n+2} = \alpha_s^m \mathcal{A}_{n+2}^{(0)} + \alpha_s^{m+1} \mathcal{A}_{n+2}^{(1)} + ... + \alpha_s^{m+L} \mathcal{A}_{n+2}^{(L)} + O(\alpha_s^{m+L+1}). \tag{2.57}$$

The order of the coupling m in Eq. (2.57) depends on the process being studied, it can be inferred from the number of vertices in the simplest Feynamn diagrams for the process. The superscript of $\mathcal{A}_{n+2}^{(i)}$ indicates that the term is the i-th in the expansion and it corresponds to the number of loops in the Feynman diagrams which contribute to it. In the literature the term *amplitude* is used to refer to both the left-hand side of Eq. (2.57) and to each of the terms on its right-hand side [48]. In this work we will use the terminology *n-point k-loop amplitude* to refer to $\mathcal{A}_n^{(k)}$. The first term in the expansion is also referred to *tree-level amplitude*, due to the fact that it is obtained by summing Feynman diagrams free of loops [48]. The results in this thesis will concern five and six-point tree-level and one-loop amplitudes. A hard differential cross section $d\sigma(p_a p_b \rightarrow p_1...p_n)$, for which the initial and final states are not composite hadrons, is equal to the amplitude squared divided by the flux of the particles $\mathcal{F}$ and multiplied by a Lorentz-invariant differential phase-space $d\Phi_n$ [49],

$$d\sigma(p_a p_b \rightarrow p_1, .., p_n) = \frac{1}{\mathcal{F}} \left(\overline{\sum} |\mathcal{A}_{n+2}|^2 \right) d\Phi_n. \tag{2.58}$$

The symbol $\overline{\sum}$ is used to indicate that the spins and colour factor of the initial states of the amplitude are averaged, while the spins and colours of the final states are summed. The flux-factor and differential phase-space have form [49]:

$$\mathcal{F} = 4\sqrt{(p_a \cdot p_b)^2 - m_a m_b}, \tag{2.59}$$

$$d\Phi_n = \delta^{(4)}(p_a + p_b - \sum_{i=1}^{n} p_i) \prod_{j=3}^{n} \frac{d^3 p_j}{(2\pi)^2 2E_j} \delta^{(+)}(p_j^2 - m_j^2). \tag{2.60}$$

The $\delta^{(+)}$ functions indicate a restriction to the future light cone, so that $\delta^{(+)}(p^2 - m^2) = \delta(p^2 - m^2)\theta(p^2 - m^2)$. The quantity $d\sigma(p_a p_b \to p_1...p_n)$ is also referred to as *exclusive differential cross-section*, in order to stress the fact that it only describes a scattering event with an exact set of final states. Eq. (2.58) is clearly different from Eq.(2.48), since in the former case there is no need to take into account any PDFs or hadronisation processes.

It possible to perform a perturbative expansion of $d\hat{\sigma}_{ij}$ similar to the one of Eq. (2.57):

$$d\hat{\sigma}_{ij} = \alpha_s^{2m} d\hat{\sigma}_{ij}^{\text{LO}} + \alpha_s^{2m+1} d\hat{\sigma}_{ij}^{\text{NLO}} + \alpha_s^{2m+2} d\hat{\sigma}_{ij}^{\text{NNLO}} + O(\alpha_s^{2m+3}). \tag{2.61}$$

Where LO stands for *Leading Order*, NLO for *Next-to-Leading-Order* and so on; the k-th term in the expansion will be referred to as N^{k}LO. The cross-section $d\sigma_{ij}$ does not have a fixed number of final states, due to the possibility of the emission of *unresolved final states*, i.e. states which have energies below the sensitivity of the detector. For this reason $d\sigma_{ij}$can be referred to as an *inclusive differential cross-section* [4, 19]. This means that each term in the expansion Eq. (2.61) is equal to the sum of different cross-sections of the form of Eq. (2.58), each integrated over the correct final-state space. We show this explicitly for the first terms in the expansion [50]:

$$d\hat{\sigma}_{ij}^{\text{LO}} = \int_{\Phi_n} d\hat{\sigma}^{\text{B}}, \tag{2.62}$$

$$d\hat{\sigma}_{ij}^{\text{NLO}} = \int_{\Phi_n} d\hat{\sigma}^{\text{V}} + \int_{\Phi_{n+1}} d\hat{\sigma}^{\text{R}}. \tag{2.63}$$

Where $d\hat{\sigma}^{\mathrm{B}}$ is referred to as the *Born amplitude*, while $d\hat{\sigma}^{\mathrm{V}}$ and $d\hat{\sigma}^{\mathrm{R}}$ are called *virtual* and *real* corrections respectively [50]. These are expressed in terms of scattering amplitudes as

$$d\hat{\sigma}^{\mathrm{B}} = d\Phi_n |\mathcal{A}_n^{(0)}|^2, \tag{2.64}$$

$$d\hat{\sigma}^{\mathrm{V}} = d\Phi_n (\mathcal{A}_n^{(0)*}\mathcal{A}_n^{(1)} + \mathcal{A}_n^{(1)*}\mathcal{A}_n^{(0)}) = 2\Re(\mathcal{A}^{(0)*}\mathcal{A}^{(1)}), \tag{2.65}$$

$$d\hat{\sigma}^{\mathrm{R}} = d\Phi_{n+1} |\mathcal{A}_{n+1}^{(0)}|^2. \tag{2.66}$$

We can then see that in the NLO case the term *real* or *virtual* distinguishes the case in which the additional particle is virtual in an internal loop from the one in which it is a real final emission. If we go up to NNLO, we will also need to compute *double-real* and *double-virtual* corrections.

In Eqs. (2.67), (2.68) and (2.69) we show the contributions up to order $O(\alpha_s^{2m+3})$ for the three processes of different multiplicity. The colour-coding clarifies which differential cross-sections contribute to which inclusive observable. We stress again that only terms with the same power of α_s are combined, as required to have a sensible Taylor expansion.

$$|\mathcal{A}_{n+2}|^2 = \alpha_s^{2m+2}|\mathcal{A}_{n+2}^{(0)}|^2 + O(\alpha_s^{2m+3}), \tag{2.67}$$

$$|\mathcal{A}_{n+1}|^2 = \alpha_s^{2m+1}|\mathcal{A}_{n+1}^{(0)}|^2 + \alpha_s^{2m+2} 2\Re(\mathcal{A}_{n+1}^{(1)}\mathcal{A}_{n+1}^{(0)*}) + O(\alpha_s^{2m+3}), \tag{2.68}$$

$$|\mathcal{A}_n|^2 = \alpha_s^{2m}|\mathcal{A}_n|^2 + \alpha_s^{2m+1} 2\Re(\mathcal{A}_n^{(1)}\mathcal{A}_n^{(0)*}) + \alpha_s^{2m+2}(2\Re(\mathcal{A}_n^{(2)}\mathcal{A}_n^{(0)*}) + |\mathcal{A}_n^{(1)}|^2) + O(\alpha_s^{2m+3}). \tag{2.69}$$

$$d\hat{\sigma}_{ij}^{\mathrm{LO}} \qquad d\hat{\sigma}_{ij}^{\mathrm{NLO}} \qquad d\hat{\sigma}_{ij}^{\mathrm{NNLO}}$$

The Born cross section is finite in four dimensions and can be directly integrated to obtain the leading order result. The real and virtual corrections, on the other hand, exhibit divergences in certain kinematical limits of the phase-space [50]. This will be topic of the next section.

2.7   Cancellation of Infrared Divergences

In Section 2.4 we have seen that loop integrals exhibit IR virtual divergences. At NLO, these will be present in the expression of the virtual correction $d\hat{\sigma}^V$. Differently from UV divergences, the

IR ones are not cancelled by the addition of the counter-terms after renormalisation. Instead, such divergences are expected to cancel exactly when summed to the real correction $d\hat{\sigma}^R$. From Eq. (2.66) we know that these are the lower order contributions with a higher number of final states, in the limit in which such additional final states are below the energy resolution of the detector. Infrared-safety (the absence of IR singularities from physical observables) is ensured by the Block-Nordsieck [51, 52] and the Kinoshita-Lee-Nauenberg (KLN) theorems [53, 54]. The first theorem states that IR divergences cancel between real and virtual contributions when all indistinguishable final states are added up, while the second proves that in any quantum field theory the transition rate between states of equal energy is free of IR divergences in the limit of massless particles. As a consequence, all quantities $d\hat{\sigma}_{ij}^{\mathrm{LO}}$, $d\hat{\sigma}_{ij}^{\mathrm{NLO}}$, $d\hat{\sigma}_{ij}^{\mathrm{NNLO}}$, ..., are free of IR singularities.

While the previous discussion ensures the absence of IR singularities from inclusive final states at colliders, this is not the case for the initial states in hadronic collisions. In such states collinear singularities do not cancel, and need to be absorbed at the factorisation scale μ_{F} into the so-called *bare* PDFs in order to obtain the physical PDFs described in Section 2.5 [34] . These singularities originate from degenerate collinear states inside protons which cannot be resolved individually [18]; factorization of initial state collinear singularities into parton distributions can be proven to all orders in perturbation theory [55].

In Eq. (2.63) we see that in order to cancel the virtual divergences we need to sum the real correction cross-section integrated over the correct phase-space. Since only tree-level expressions contribute to $d\sigma_{\mathrm{R}}$, clearly its IR divergences are not virtual, i.e. they do not arise from the low-energy limit of the integral over an internal momentum. Instead, they are *real* IR divergences. These can be of two types [56]:

1. collinear singularities, which arise when 2 particles i and j become collinear to each other, meaning $p_i \cdot p_j = 0$,

2. soft singularities, which arise when the energy of one of the massless final particles i goes to zero, $E_i \to 0$.
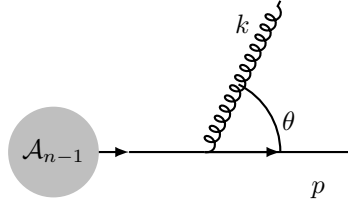
Figure 2.4: An example of the real correction to a $\mathcal{A}_n$ amplitude. The soft limit corresponds to $k \to 0$ and the collinear limit (in the $m \to 0$ case) to $\theta \to 0$.

We illustrate both cases with the simple example of an amplitude $\mathcal{A}_n$ radiating a real gluon from one of its quark final states. This is equivalent to adding a quark virtual line which radiates a real quark of mass m and momentum p and a real gluon of momentum k, as shown in Figure 2.4. The propagator of the virtual quark is

$$\frac{1}{(p+k)^2 - m^2} = \frac{1}{2(p \cdot k)} = \frac{1}{E_p E_k} \frac{1}{1 - \beta_p \cos\theta}, \tag{2.70}$$

where E_k and E_p are the energies of the radiated quark and gluon respectively, and we define $\beta_p = \sqrt{1 - m^2/E_p^2}$. The angle θ is defined in Figure 2.4.

We see that for $E_k \to 0$ we have a divergence since the integration over the space of final state has a dependence on the gluon energy of $\sim E_k dE_k$, while the squared amplitude has a double pole $\frac{1}{E_k^2}$. This is an example of a singluarity originating from a gluon going soft. We also notice that in the massless case ($m \to 0$) the amplitude will diverge for $\cos\theta \to 1$, this corresponds to the massless quark and the gluon going collinear. The IR limits are universal properties of the theory [57].

While the Block-Nordsiek and the KLN theorems formally solve the problem of IR divergences, they do not provide a method for the practical computation of physical cross-sections, since Monte Carlo techniques cannot be employed to perform the integrations of the form of Eq. (2.63). Three main methods have been developed in the field to address this issue: phase-space slicing [58, 59], sector decomposition [60] and subtraction [61–63]. Since the latter method is the one more commonly used in high-precision QCD calculations, we present its general features.

In the subtraction technique, the IR divergences are subtracted at the integrand level, making it possible to perform numerical integration in four dimensions of only regular quantities.

At NLO the method is based on the introduction of a counter-term $d\sigma^A$ [50]:

$$d\hat{\sigma}^{\mathrm{NLO}_{ij}} = \int_{\Phi_{n+1}} (d\hat{\sigma}^{\mathrm{R}} - d\hat{\sigma}^{\mathrm{A}}) + \int_{\Phi_n} \left(d\hat{\sigma}^{\mathrm{V}} + \int_{\Phi_1} d\hat{\sigma}^{\mathrm{A}} \right). \tag{2.71}$$

The counter-term $d\hat{\sigma}^{\mathrm{A}}$ contains the same singularities as $d\hat{\sigma}^{\mathrm{R}}$ but with opposite sign. In this way it is possible to combine the two terms, see that the IR singularities cancel and then safely perform the Monte Carlo integration. The same procedure applies to $d\hat{\sigma}^{\mathrm{V}}$, where its poles are cancelled by the ones of $d\hat{\sigma}^{\mathrm{A}}$ once it has been integrated over the one-parton phase space $\int_{\Phi_1}$. The counter-terms can be systematically computed by exploiting the factorisation properties of the scattering amplitudes in their IR limits (see for example [64] and [65]). The creation of algorithms to obtain counter-terms for general NNLO and N^{3}LO is an active area of research. The reader is refereed to [55], [66] and references therein for a detailed discussion of IR divergences and recent advancements.

The universality of the IR poles and of the factorisation functions ameks it possible to perform strong checks after amplitudes of new processes have been computed. Even if the general form of an amplitude is not known *a priori*, the behaviour in the soft and collinear limits is constrained. We will see an example of such checks on the expressions derived in Chapter 5.

We have seen in this chapter that scattering amplitudes are a fundamental ingredient for the computation of observables in QCD. In Chapter 3 we are going to discuss some modern techniques for their computation at one loop.

Chapter 3

Modern Methods for Scattering Amplitudes

As we have seen in Chapter 2, the standard prescription for the computation of unpolarised QCD cross-sections consists of obtaining the squared scattering amplitude as the first step. This is done by computing all the possible multiplications of the individual Feynman diagrams and then averaging and summing the spins and colours of the initial and final states respectively. This procedure is unfeasible for most processes beyond four-particle scatterings at tree-level due to the high number of Feynman diagrams contributing, which grows higher than factorially with the number of external states [49]. For this reason modern amplitude methods aim at the computation of the whole unpolarised amplitude expression as a complex number, which is then squared to obtain the cross -section. This technique has proven to be extremely effective for high-multiplicity tree and loop computations [49].

The aim of this chapter is to describe these methods, with a particular focus on the ones which were employed to derive the results presented in chapters 5 and 7. The topic of the computation of amplitudes in QCD and Yang-Mills theories is vast, and for a more comprehensive review the reader is referred to [49, 67, 68] and references therein.

A crucial step in most modern amplitude calculations is their decomposition as sums of smaller expressions. Schematically, a one-loop n-gluon QCD amplitude can be decomposed as [68]

$$\mathcal{A}_n^{1-\text{loop}} = \sum_J \sum_c \sum_h A_{n;c}^{[J]}(h), \tag{3.1}$$

where the sums are over the spins J of the internal particles in the loop, the colour factors, indexed by c, and the helicities h of the external states (in our notation indicated as $+$ or $-$). We will refer to the terms $A_{n;c}^{[J]}(h)$ as *sub-amplitudes* in this thesis. It is then convenient to individually compute the independent sub-amplitudes $A_{n;c}^{[J]}(h)$ and later combine them to obtain the full result. This strategy is applied because it allows the calculation to be divided into smaller steps and makes full use of the symmetries of the sub-expressions making up an amplitude, avoiding redundant computations.

This chapter is organised as follows. In sections 3.1 and 3.2 the decomposition of Eq. (3) will be described in greater detail. In the former section we describe the decomposition into colour-ordered sub-amplitudes, in the latter we introduce the spinor-helicity formalism. In Section 3.4 we detail how amplitudes can be expressed using momentum-twistor variables, which will be used to express many results in this thesis. Section 3.5 explains how the unitarity of the S-matrix can be exploited for the computation of amplitudes, while in Section 3.6 we describe an integrand-reduction method which will be essential for the work of Chapter 7. In Section 3.7 we describe an additional decomposition method which proved to be useful in the computation of one-loop gluon amplitudes. The last computational technique presented is the use of complex shifts for one-loop amplitudes, in Section 3.8.

3.1 Colour Decomposition

This section focuses on the colour decomposition part of Eq. (3). We only give explicit results for tree-level amplitudes, while the colour decompositions for the specific one-loop processes studied in this thesis are presented in Section 5.2 and Section 7.2 of chapters 5 and 7 respectively. Most of the theory exposed in this section is an elaboration of [49] and [67]. Observing the Feynman rules in Appendix B we see that each vertex and propagator has a colour factor and a kinematic factor. This fact generalises to amplitudes, making it possible to organise the calculations according to the

colour algebra, in this case $SU(N_c)$

$$\mathcal{A} = \sum_i C_i A_i, \tag{3.2}$$

where C_i is the colour factor [69, 70]. The meaning of Eq. (3.2) is that it is possible to separate the term of the amplitude which depends exclusively on the colour quantum numbers

$a = 1, ..., (N_c^2 - 1)$ (for a $SU(N_c)$ gauge theory) from the part depending exclusively on the momenta p_i and polarisations.

The A_i are referred to as *primitive amplitudes*. At tree-level the primitive amplitudes are specific sub-amplitudes in which external legs have fixed order in colour space, called *colour-ordered amplitudes* or *partial amplitudes* [69]. They can be computed efficiently exploiting the Berends-Giele recursion relations [71]. For the one-loop case, primitive amplitudes correspond to linear combinations of colour-ordered amplitudes, further decomposed according to their internal flavour. Their explicit expression for some five and six-point processes will be seen in chapters 5 and 7.

Working in this framework the squared amplitude becomes

$$\sum_{\text{colours}} |\mathcal{A}|^2 = \sum_{\text{colours}} \sum_i \sum_j A_i^\dagger C_i^\dagger C_j A_j = \sum_{i,j} A_i^\dagger \mathscr{C}_{ij} A_j, \tag{3.3}$$

where we defined the colour matrix $\mathscr{C}_{ij} = \sum_{\text{colours}} C_i^\dagger C_j$.

We then see that A_i can be thought of as a vector in colour space whose entries are independent primitive amplitudes. For n-gluon amplitudes the colour factors are traces obtained by contracting the $SU(N_c)$ generators $\text{Tr}(t^{a_{\sigma(1)}}...t^{a_{\sigma(n)}}) = \text{tr}(\sigma(1)...\sigma(n))$ [67]. Because of the cyclic symmetry of traces, a basis of independent colour structures is obtained by computing all the non-cyclic permutations of the colour indices. Since the overall amplitude is expected to be invariant under the cyclic permutations of the external legs, such a symmetry must also be present for the kinematic parts. This greatly diminishes the complexity of a calculation, since for an n-point amplitude it makes it sufficient to compute $(n-1)!$ independent primitive amplitudes. Further analysis reveals that these partial amplitudes possess a reflection symmetry [72]

$$A(1, ..., n) = (-1)^n A(n, ..., 1), \tag{3.4}$$

which means that there are only $\frac{(n-1)!}{2}$ independent amplitudes. So we have explicitly

$$\mathcal{A}_n^{\text{tree}}(g_1, ..., g_n) = \sum_{\sigma_n \in R_{n-1}} \text{tr}(\sigma(1)...\sigma(n)) \times A(\sigma(1)...\sigma(n)) \tag{3.5}$$

for the group R_{n-1} which is the reflection-independent subset of $S_{n-1} = \frac{S_n}{\mathbb{Z}_n}$ (remembering that $\mathbb{Z}_n$ is the cyclic permutations subset of the group of permutations S_n).

Additional relations can be found among the primitive amplitudes of 3.1, further reducing the set of independent ones. We explicitly state the Kleiss-Kuijf relations [73]

$$A_n(1, \alpha, 2, \beta) = \sum_{\sigma \in \mathrm{OP}\{\alpha\}\{\beta\}} A_n(1, \sigma, 2), \tag{3.6}$$

where $\mathrm{OP}\{\alpha\}\{\beta\}$ indicates all the permutations that keep the relative ordering of sets α and β unchanged.

Taking the Kleiss-Kuijf relations into account, the number of independent primitive amplitudes can be reduced to $(n-2)!$. It is possible to reduce this number further by applying the Bern-Carrasco-Johansson relations, which we do not state explicitly, obtaining a set of only $(n-3)!$ independent expressions. It is worth noticing, however, that in many cases the computations are carried out in a larger over-complete set of primitive amplitudes, instead of the smallest possible one. This is the case because it can happen that the price of a larger set is compensated by the simpler form that the primitive amplitudes assume for a specific choice of colour basis [49].

We quote an expression similar to 3.1 for the tree-level $q\bar{q}gg...g$ amplitude:

$$\mathcal{A}_n^{\text{tree}}(q_1, \bar{q}_2, g_3, ..., g_n) = \sum_{\sigma_{S_{n-2}}} (t^{a_{\sigma(1)}}...t^{a_{\sigma(n)}})_{i_1}^{\bar{i}_2} A_n(1_q, 2_{\bar{q}}, \sigma(3), ..., \sigma(n)), \tag{3.7}$$

where indices i_1 and $\bar{i}_2$ refer to the quark pair. The colour factors can be calculated from the squared diagrams by using the *Fierz Identity* [49, 74]

$$t_{ij}^a t_{kl}^a = \frac{1}{2}(\delta_{il}\delta_{kj} - \frac{1}{N_C}\delta_{ij}\delta_{kl}), \tag{3.8}$$

which is also represented pictorially in Figure 3.1.

3.2 Spinor-Helicity Formalism for On-Shell Kinematics

Once we have discussed the decomposition of amplitudes in colour space, we can address the decomposition according to the helicity of their external particles.
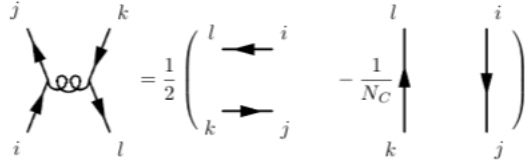
Figure 3.1: Diagrammatic representation of the Fierz identity.

The kinematic part of a QCD amplitude can always be expressed in terms of four-momenta p^μ and their Lorentz-invariant contractions $p^\mu q_\mu = p \cdot q$. It is common in the literature to express squared amplitudes as functions of *Mandelstam invariants* $s_{ij} = (p_i + p_j)^2$ [75]. The introduction of the spinor-helicity formalism, on the other hand, allows us to define the expressions of the gauge-invariant helicity amplitudes $A_{n;c}^{[J]}(h)$ appearing in Eq. (3). The final result can then be obtained by individually squaring each helicity amplitude and then summing them all together [49, 69].

Gauge interactions preserve the chirality of massless fermions, which coincide with their helicities [49]. For massless particles the helicity is defined as the angular momentum component along the momentum direction [67]; this makes it convenient to define a helicity basis. To this end we present the spinor formalism. We will see that one of the main advantages of using spinor variables is that they automatically satisfy the on-shell conditions for massless particles: $p_i^2 = 0$. This property makes many possible helicity amplitudes evaluate to zero, reducing the complexity of the calculations [67].

Massless four-momenta have a $SL(2, \mathbb{C}) \times SL(2, \mathbb{C})$ representation given by the relation

$$p_{\dot{a}a} = p^\mu (\sigma_{\dot{a}a})_\mu \tag{3.9}$$

where p^μ is the $SO(1, 4)$ representation of the momentum and $\sigma_{\dot{a}a}$ are the Pauli matrices as defined in Appendix A.

For a generic p^μ we then have:

$$p_{\dot{a}a} = \begin{pmatrix} -p^0 + p^3 & p^1 - ip^2 \\ p^1 + ip^2 & -p^0 - p^3 \end{pmatrix}, \tag{3.10}$$

$$\tag{3.11}$$

$$\det(p_{\dot{a}a}) = -p^\mu p_\mu = 0. \tag{3.12}$$

Therefore massless momenta are represented by the $SL(2,\mathbb{C}) \times SL(2,\mathbb{C})$ subgroup of 2×2 matrices with zero determinant.

In linear algebra it is a well known fact [67] that 2×2 matrices with vanishing determinant can be written as $p_{\dot{a}a} = -\tilde{\lambda}_{\dot{a}}\lambda_a$, with $\tilde{\lambda}_{\dot{a}}$ and λ_a being two independent 2-component vectors. In the spinor-helicity formalism they are written as:

$$\lambda_a = \langle p|_a \,,$$
$$\tilde{\lambda}_{\dot{a}} = |p]_{\dot{a}}. \tag{3.13}$$

The bra and ket spinors correspond to 2-component Weyl spinors. We recall that for a generic Dirac field $\psi(p) = \int d^4x\, u(p)e^{ip\cdot x} + v(p)e^{-ip\cdot x}$ the four-component spinors satisfy the massless Weyl equations:

$$\not{p}u(p)_\pm = 0,$$
$$v(p)_\pm\not{p} = 0. \tag{3.14}$$

where again the plus and minus label the different helicities of the spinors.

We can then write the spinors using the bra-ket notation:

$$v_+(p) = \begin{pmatrix} |p]_a \\ 0 \end{pmatrix}, \quad v_-(p) = \begin{pmatrix} 0 \\ |p\rangle^{\dot{a}} \end{pmatrix} \tag{3.15}$$

$$\tag{3.16}$$

$$\bar{u}_-(p) = (0, \langle p|_{\dot{a}}), \quad \bar{u}_+(p) = ([p|^a, 0) \tag{3.17}$$

where only outgoing states were considered. The polarisation vectors of spin-1 massless particles

such as photons and gluons can also be expressed in these variables [67]

$$\epsilon_-^{\mu}(p;n) = -\frac{\langle p|\,\gamma^{\mu}\,|n]}{\sqrt{2}[np]}, \qquad \epsilon_+^{\mu}(p;n) = -\frac{\langle n|\,\gamma^{\mu}\,|p]}{\sqrt{2}\,\langle np\rangle}, \qquad (3.18)$$

where the one needs to introduce the arbitrary reference vector $n^{\mu} \neq p^{\mu}$. It is easily verified that the relation $p_{\mu}\epsilon_{\pm}^{\mu}(p;n) = 0$, a consequence of the massless Weyl equation, is satisfied. We can also verify that if the polarisation vectors are represented in this form, they satisfy the polarisation sum expressed by Eq. (2.3).

The metric used to lower and rise indices in this space is the Levi-Civita tensor, defined in Appendix A. It is useful to present some of the most important properties of spinor products [49]

$$\begin{aligned}
p &= -|p]\,\langle p|\,, \\
-\not{p} &= |p\rangle\,[p| + |p]\,\langle p|\,, \\
|p\rangle &= (|p])^{*} & \textbf{Reality Condition}, \\
\langle pq\rangle &= [pq]^{*}, \\
\langle pq\rangle &= -\langle qp\rangle\,, & (3.19) \\
[pq] &= -[qp], & \textbf{Antisymmetry} \\
\langle pq\rangle\,[pq] &= (p+q)^{2} = 2p_{\mu}q^{\mu}, \\
\sum_{k}\langle pk\rangle\,[kq] &= 0, & \textbf{Momentum Conservation}
\end{aligned}$$

$$\langle pq\rangle\,\langle kw\rangle + \langle pk\rangle\,\langle wq\rangle + \langle pw\rangle\,\langle qk\rangle = 0. \qquad \textbf{Schouten Identity}$$

We see that the reality condition on the momenta imposes a relation between angle and square spinors. If, on the other hand, the momenta are allowed to be complex, square and angle spinors are independent from each other [67].

Expressing helicity amplitudes in the spinor formalism can unveil the hidden simplicity of some expressions, which may appear much more complicated if written in terms of momenta. The best

example is given by the Parke-Taylor expression [76] for the so-called *maximally helicity violating* (MHV) amplitudes:

$$A(1^+, 2^+, ..., i^-, ..., j^-, ..., n^+) = \frac{\langle ij \rangle^4}{\langle 12 \rangle \langle 23 \rangle ... \langle n-1, n \rangle}. \tag{3.20}$$

If we perform the operation of *helicity conjugation*, i.e. the change of helicity of all the particles in Eq. (3.20), we obtain the same expression but with all the angle brakets changed to square ones. This is referred to as the *anti-maximally-helicity violating* ($\overline{\text{MHV}}$) amplitude.

3.3 Britto-Cachazo-Feng-Witten Relations

It has been shown [77] that tree-level amplitudes can be computed using recursion relations which exploit their factorisation in specific kinematical limits. The most widely used class of these relations are the Britto-Cachazo-Feng-Witten (BCFW) relations [77, 78]. We briefly review them, since they are of great importance for the computation of amplitudes and they were used to derive results in this thesis.

The basic idea behind the BCFW method consists in applying a shift by a complex number z to two of the massless external momenta of an amplitude. Such a shift is conveniently expressed in spinor form. For example we can shift the legs 1 and 2 of an amplitude in the following way:

$$\langle 1| \rightarrow \langle \hat{1}| = \langle 1| - z \langle 2|,$$
$$|2] \rightarrow |\hat{2}] = |2] + z|1]. \tag{3.21}$$

It is simple to show that such a shift preserves momentum conservation and the square of their norm,

$$\hat{p}_1^2 = \langle \hat{1}\hat{1} \rangle [\hat{1}\hat{1}] = ((\langle 1| - z \langle 2|)(|1\rangle - z|2\rangle)[11] = 0,$$
$$\hat{p}_2^2 = \langle \hat{2}\hat{2} \rangle [\hat{2}\hat{2}] = \langle 22 \rangle ([2| + z[1|)(|2] + z|1]) = 0, \tag{3.22}$$
$$\hat{p}_1 + \hat{p}_2 = \frac{1}{2}(\langle 1| \gamma^\mu |1] - z \langle 2| \gamma^\mu |1] + z \langle 2| \gamma^\mu |2] + \langle 2| \gamma^\mu |1]) = p_1 + p_2,$$

where we used the identity $\langle i| \gamma^\mu |i] = 2p_i$ for massless vectors. The gamma matrices are defined as in the Appendix A.

The shifted amplitude $A(z)$ is a meromorphic function in the complex variable z [49]. The function
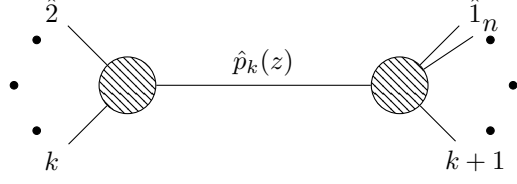
Figure 3.2: The diagram schematically shows the factorisation of the amplitude into two sub-amplitudes of lower multiplicity in the kinematical limit $\hat{p}_k(z) \to 0$.

vanishes as $z \to \infty$ for some specific choices of the shift. In those cases it is possible to exploit Cauchy's theorem to compute the value of the physical unshifted amplitude $A(0)$ by computing the residues of $\frac{A(z)}{z}$

$$\frac{1}{2\pi i} \int_C dz \frac{A(z)}{z} = A(0) + \sum_i \text{Res}\left(\frac{A(z)}{z}\right)\bigg|_{z=z_i} = 0, \tag{3.23}$$

where the z_i are the values at which $A(z)$ is singular and C is the integration contour which encircles all poles, extending to infinity in the complex z-plane.

The values of z_i are those for which the amplitude factorises into two amplitudes of lower multiplicity [49]. For an amplitude with n external legs we can imagine a factorisation into two sub-processes of $k+1$ and $n-k+1$ legs respectively, with the momentum $\hat{p}_k(z)$ being shared between them, as shown in Figure 3.2.

The amplitude will then have a pole for the value z_k which makes momentum $\hat{p}_k(z_k)$ go on-shell. We stress the fact that the two shifted legs (1 and 2 in this case) always need to be in the two different sub-amplitudes. If this was not the case, momentum $\hat{p}_k$ would have no dependence on z and it could not be put on-shell. We then have

$$\begin{aligned}
\hat{p}_k(z_k)^2 &= (\hat{p}_1(z_k) + p_3 + ... + p_k)^2 \\
&= z_k \langle 2| p_{1,...,k} |1] + p_{1,...,k}^2 \\
&= 0,
\end{aligned} \tag{3.24}$$

with $p_{1,...,k} = p_1 + ... + p_k$. The solutions to 3.24 give the position of all the poles in the z plane:

$$z_k = -\frac{p_{1,...,k}^2}{\langle 2| p_{1,...,k} |1]}. \tag{3.25}$$

We then give the form of the amplitude as a sum of the residues of $\frac{A(z)}{z}$ in a similar notation to [49]

$$A(0) = \sum_{h=\pm 1} \sum_{k=3}^{n-1} A(\hat{2}, ..., -\hat{p}^{-h}(z_k)) \frac{i}{p_{1,...,k}^2} A(\hat{p}^{+h}(z_k), ..., n, \hat{1}), \tag{3.26}$$

where we see that we need to sum over the two possible helicity states of the intermediate leg. The helicities have to be opposite for the two sub-amplitudes because the particle is interpreted as incoming in one case and outgoing in the other.

The BCFW relations described above are valid for tree-level amplitudes. We will see in Section 3.8 how some of the results that we have presented can be exploited for the one-loop cases.

3.4 Momentum Twistors

In this section we briefly outline how momentum twistors are constructed and how they are used to represent helicity amplitudes. This discussion is necessary to understand the variables used to express the results of the thesis. We will see how employing momentum-twistor variables gives a rational parametrisation of the kinematics, which means that the scattering amplitude will be a rational function of the variables. This property is extremely convenient for managing the amplitude expressions and for the application of the reconstruction methods which will be presented in Chapter 4.

Twistors were introduced by Penrose [79, 80] in order to obtain a new algebra for Minkowski space-time which describes objects that manifestly exhibit conformal symmetry. The simplest non-trivial twistor Z^α consists of a four-component representation of the conformal group in four dimensions $SO(2, 4)$. In [79], it is noted that $SO(2, 4)$ can be interpreted as the Lorentz group of a six-dimensional space wih signature $(-, -, +, +, +, +)$. Twistor space defines a complex projective three-space $\mathbb{CP}^3$; a point in twistor space corresponds to a null-line in Minkowski space, and lines in twistor space represent a point in Minkowski space [79].

In [81], Hodges extended Penrose's twistor formalism, with the aim to represent a conformal symmetry in *momentum dual space* of colour-ordered amplitudes.

In this section we limit the discussion to the connection between spinor and momentum-twistor variables, referring the reader to [81] for a more detailed exposition. Most of the theoretical parts follow [82] and Chapter 5 of [67].
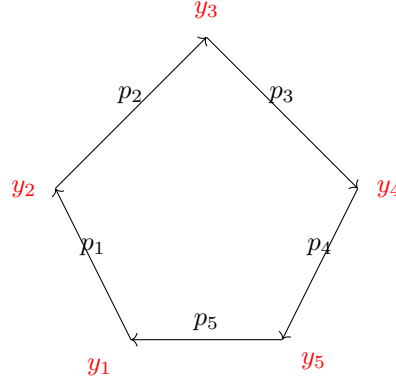
Figure 3.3: The relation between $p_i^{\dot{a}a}$ and $y_i^{\dot{a}a}$ coordinates. The momenta p_i are null-vectors (massless). In this example five incoming momenta were considered.

Momentum dual space, also called *region space* in [81], is defined by coordinates $y_i^{\dot{a}a}$ such that

$$p_i^{\dot{a}a} = y_{i+1}^{\dot{a}a} - y_i^{\dot{a}a}. \tag{3.27}$$

In dual space, y-coordinates can be interpreted as the labels of the vertices of a polygon, while the the canonical p_i represent its sides, as shown in Figure 3.3. The sides of the polygon of Figure 3.3 are null, which means that they describe massless vectors. We see from the construction of Figure 3.3 that the conservation of total momentum for n particles $\sum_i^n p_i = 0$ (in the case in which all the momenta are taken to be incoming or outgoing) is equivalent to having $y_1 = y_{n+1}$ in dual space. We notice that the dual space is well-defined only if the momenta of the amplitude have a fixed ordering, as in the case of colour-ordered expressions.

It is then possible to associate each couple of holomorphic and anti-holomorphic spinor ($\langle i|$, $[i|$) to a momentum-twistor Z_i^α and an dual momentum twistor W_i^α. The momentum twistor depends on spinor variables and a new set of variables $[\mu|_i^a$, which depend on the dual coordinates. We know that spinors satisfy Weyl's massless equation, therefore we combine Eq. (3.27) and (3.14) to find the *incidence relations*, which define the new variable $[\mu|_i$,

$$[\mu|_i^a = \langle i|_{\dot{a}} \, y_i^{\dot{a}a} = \langle i|_{\dot{a}} \, y_{i+1}^{\dot{a}a}. \tag{3.28}$$

This allows us to define a momentum twistor as a four-component vector $Z_i^\alpha = (|i\rangle, [\mu|_i)$ [67]. In our notation the momentum twistors for an n-point amplitude are the columns of a $4 \times n$ matrix of

the form

$$Z = \begin{pmatrix} |1\rangle & |2\rangle & ... & |n\rangle \\ [\mu_1| & [\mu_2| & ... & [\mu_n| \end{pmatrix}. \tag{3.29}$$

The dual momentum twistor is completely determined by the form of Z_i^α via the relation [81, 82]

$$W_{i\alpha} = \frac{\epsilon_{\alpha\beta\gamma\delta} Z_{i-1}^\beta Z_i^\gamma Z_{i+1}^\delta}{\langle i-1, i \rangle \langle i, i+1 \rangle}. \tag{3.30}$$

One important feature of the momenta derived from the momentum twistor is that they are complex, hence the reality condition of Eq. (3.19) no longer holds and holomorphic and anti-holomorphic spinors are independent from each other. Nevertheless, the values of the anti-holomorphic spinors can still be derived from the holomorphic ones and the newly defined coordinates $[\mu|_i$.

From the incidence relations we have [67]

$$|i\rangle^{\dot{b}} [\mu_{i-1}|^a - |i-1\rangle^{\dot{b}} [\mu_i|^a = (|i\rangle^{\dot{b}} \langle i-1|_{\dot{a}} - |i-1\rangle^{\dot{b}} \langle i|_{\dot{a}}) y^{\dot{a}a}, \tag{3.31}$$

but we can also derive

$$\begin{aligned} |i-1\rangle^{\dot{b}} \langle i|_{\dot{a}} &= \epsilon^{\dot{b}\dot{c}} |i-1\rangle_{\dot{c}} \epsilon_{\dot{a}\dot{d}} \langle i|^{\dot{d}} = \\ (\delta_{\dot{a}}^{\dot{b}} \delta_{\dot{d}}^{\dot{c}} - \delta_{\dot{a}}^{\dot{c}} \delta_{\dot{d}}^{\dot{b}}) |i-1\rangle_{\dot{c}} \langle i|^{\dot{d}} &= \delta_{\dot{a}}^{\dot{b}} \langle i, i-1 \rangle - |i-1\rangle_{\dot{a}} \langle i|^{\dot{b}}. \end{aligned} \tag{3.32}$$

Combining Eq. (3.31) and (3.32) we obtain

$$y^{\dot{a}a} = \frac{|i\rangle^{\dot{a}} \langle \mu_{i-1}|^a - |i-1\rangle^{\dot{a}} \langle \mu_i|^a}{\langle i-1, i \rangle}, \tag{3.33}$$

finally giving the relation

$$[i| = \frac{\langle i+1, i \rangle [\mu_{i-1}| + \langle i, i-1 \rangle [\mu_{i+1}| + \langle i-1, i+1 \rangle [\mu_i|}{\langle i-1, i \rangle \langle i, i+1 \rangle}. \tag{3.34}$$

Where we used the properties $p_i^{\dot{a}a} = -|i\rangle^{\dot{a}} [i|^a = y_{i+1}^{\dot{a}a} - y_i^{\dot{a}a}$ from Eq. (3.19).

The kinematic part of a colour-ordered amplitude can the be written in terms of holomorphic spinor products and momentum-twistor 4-brakets [82]

$$\langle ijkl \rangle = \epsilon_{\alpha\beta\gamma\delta} Z_i^\alpha Z_j^\beta Z_k^\gamma Z_l^\delta. \tag{3.35}$$

It is possible to see that a momentum-twistor matrix Z fully specifies an n-momenta phase-space, automatically ensuring masslessness and momentum conservation. We will illustrate this with a simple example.

We consider a $2 \rightarrow 2$ process, and wish to construct a 4×4 momentum-twistor matrix. We know that any choice of the entries of the matrix will give a suitable phase-space point. It is convenient to make a choice such that the momentum-twistor variables x_i have a simple relation with the Mandelstam invariants:

$$Z = \begin{pmatrix} 1 & 0 & 1 & \frac{x_2}{x_1+x_2} \\ 0 & 1 & 1 & 1 \\ 0 & 0 & -x_1 & 0 \\ 0 & 0 & 0 & 1 \end{pmatrix}. \tag{3.36}$$

For a $4 \times n$ matrix, we have $3n - 10$ variables x_i, this is the number of degrees of freedom of an n-point colour-ordered amplitude. We then have the following map from Mandelstam invariants to momentum-twistor variables:

$$s_{12} = \langle 12 \rangle [12] = x_1, \tag{3.37}$$

$$s_{13} = \langle 13 \rangle [13] = x_2, \tag{3.38}$$

$$s_{14} = \langle 14 \rangle [14] = -x_1 - x_2. \tag{3.39}$$

So momentum conservation is expressed as a linear relation: $s_{12} + s_{13} + s_{14} = x_1 + x_2 - x_1 - x_2 = 0$. Any expression which doesn't contain helicity factors can be calculated using the momentum twistor Eq. (3.36) [83]. The information on any helicity factor has to be recovered using a different method, which we outline in the following section.

3.4.1 Reconstruction of the Helicity Information

We can see from Eq. (3.36) that the momentum twistor parametrisation does not preserve the helicity information. Using the mapping described in the previous section on pure-phase expressions yields incorrect results of the kind $\langle 12 \rangle = \langle 13 \rangle = 1$. This fact is a general property of all momentum twistor

parametrisations [83]. It is then clear that in order to obtain a purely rational parametrisation, the phase expression must be discarded at first, and then recovered at the end of the calculation.

For the projects described in this thesis this was done by defining a *helicity factor* $\boldsymbol{\Phi}$ and a *momentum helicity factor* $\boldsymbol{\Phi}_{\mathrm{MT}}$. The helicity factor is a spinor expression transforming correctly under *little group scaling*, ensuring parity invariance.

Upon the transformation acting on spinors as $|i\rangle \to t\,|i\rangle, |i] \to t^{-1}|i]$, with t being any complex number, the amplitude must transform as [67]

$$A(\{|i\rangle, |1], h_1\}, ..., \{t\,|i\rangle, t^{-1}|i], h_i\}) = t^{-2h_i} A(\{|i\rangle, |1], h_1\}, ..., \{|i\rangle, |i], h_i\}). \tag{3.40}$$

Therefore the helicity factor $\boldsymbol{\Phi}$ will need to have a form which ensures the right symmetry. A further constraint on the form of $\boldsymbol{\Phi}$ is given by the dimensions of helicity amplitudes. In four dimensions, an n-particle amplitude must have mass dimension of $4 - n$ [49]. These constraints are sufficient to completely determine 3-particle massless amplitudes [67]. In our case, this information allows us to choose a factor $\boldsymbol{\Phi}$ which restores parity symmetry. One possible standard form of the helicity factor is

$$\boldsymbol{\Phi}(1^{h_1}, ..., n^{h_n}) = \left(\frac{\langle 13\rangle}{[12]\langle 23\rangle}\right)^{h_1} \prod_{i=2}^{n} \left(\frac{\langle 1i\rangle^2 [12]\langle 23\rangle}{\langle 13\rangle}\right)^{h_i}. \tag{3.41}$$

Choosing the example of a four-gluon helicity amplitude $A_{4g}^L(1^-, 2^-, 3^+, 4^+)$, at generic loop order L, we have:

$$\boldsymbol{\Phi}(1^-, 2^-, 3^+, 4^+) = \left(\frac{\langle 14\rangle [12]\langle 23\rangle}{\langle 12\rangle}\right)^2. \tag{3.42}$$

We see that the above term has the correct phase weight; upon little group scaling of $|1\rangle \to t\,|1\rangle, |1] \to t^{-1}|1]$, for example, it scales as $t^{-2\times(-1)} = t^2$.

The momentum helicity factor is then computed by mapping the helicity factor into momentum-twistor variables. Using the parametrisation of Eq. (3.36) we have

$$\boldsymbol{\Phi}_{\mathrm{MT}}(1^-, 2^-, 3^+, 4^+) = x_1^2, \tag{3.43}$$

which does not have a physical meaning.

For this reason, if $A_{4g}^L(1^-, 2^-, 3^+, 4^+)$ is reconstructed with momentum-twistor variables, two operations need to be performed to evaluate it on a phase-space point **p**:

1. divide the expression by $\mathbf{\Phi}_{\mathrm{MT}}(1^-, 2^-, 3^+, 4^+)$,

2. multiply the resulting expression by $\mathbf{\Phi}(1^-, 2^-, 3^+, 4^+)$, evaluated on **p**.

In this way, it is possible to obtain the correct physical value of the expression at any phase-space point.

3.5   On-Shell Methods at One Loop

In this section we expand the discussion of on-shell methods to one loop amplitudes. These techniques have been prolifically applied to one-loop gluon amplitudes in the literature, as we will see in Chapter 6. In a similar fashion to the BCFW discussion, we analyse the structure of amplitudes as complex analytical functions, this time extending it at loop-level.

We will now see what consequences these properties have in relation to unitarity.

3.5.1   Unitarity of the S-matrix

We can define states $|k_m\rangle = |k_1, ..., k_m\rangle$ as the momentum eigenstates of the Hamiltonian of a system. If the set is complete, we have

$$\sum_m \int d\Phi_m \, |k_m\rangle \langle k_m| = \mathbf{1}. \tag{3.44}$$

The Lorenttz invariant phase-space measure $d\Phi_m$ has the same form as in Eq. (2.60). So if we have the contraction between initial state $|i\rangle$ and final state $|f\rangle$ we can write [19]

$$\langle f|i\rangle = \sum_m \int d\Phi_m \, \langle f|k_m\rangle \langle k_m|i\rangle. \tag{3.45}$$

Eq. (3.45) has the consequence that the probability of a transition from state $|i\rangle$ to state $|f\rangle$ can be obtained from the sum over all the multi-particle physical states from the spectrum of the theory,

integrated over their phase-space. We can then write

$$|i\rangle = \sum_m \int d\Phi_m a_m |k_m\rangle, \tag{3.46}$$

where the normalisation of $|m\rangle$ implies $\sum_m |a_m|^2 = 1$. From conservation of probability we know that the sum of the probabilities of the initial state to be scattered into any of the states $|k_m\rangle$ is unity, therefore we derive

$$\mathbf{1} = \sum_m \int d\Phi_m |\langle k_m| \mathcal{S} |i\rangle|^2 = \sum_m \sum_l \int d\Phi_m d\Phi_l a_m a_l \langle m| \mathcal{S}^\dagger \mathcal{S} |k_l\rangle. \tag{3.47}$$

The above relation is satisfied for

$$\mathcal{S}^\dagger \mathcal{S} = \mathbf{1}, \tag{3.48}$$

hence the unitarity of the S-matrix must be imposed in order to ensure the conservation of probability [47]. When combined with Eq. (2.54), the unitarity condition becomes

$$(\mathbf{1} - i\mathcal{T}^\dagger)(\mathbf{1} + i\mathcal{T}) = \mathbf{1} - i\mathcal{T}^\dagger + i\mathcal{T} + \mathcal{T}^\dagger \mathcal{T} = \mathbf{1}, \tag{3.49}$$

from which it follows that

$$i(\mathcal{T} - \mathcal{T}^\dagger) = \mathcal{T}^\dagger \mathcal{T}. \tag{3.50}$$

We will now explore the consequences of unitarity for the specific process of the $2 \to 2$ scattering of particles of equal mass m. Our results can be easily generalised to scatterings of arbitrary multiplicities with unequal masses.

The four particles will have momenta p_1, p_2, p_3 and p_4, all taken to be outgoing. The S-matrix element related to this process is $\langle p_3, p_4| \mathcal{S} |p_1, p_2\rangle$, defining the initial and final momentum eigenstates $|p_1, p_2\rangle$ and $|p_3, p_4\rangle$. Since the scattering is elastic we have $p_1 + p_2 + p_3 + p_4 = 0$. The on-shell conditions $p_i^2 = m^2$ imply $s + u + t = 4m^2$, where we are using a common definition $s = s_{12}, t = s_{13}, u = s_{14}$. Therefore the S-matrix $\mathcal{S}$ can be expressed as a function of only two variables, $\mathcal{S} = \mathcal{S}(s, t)$.

The Lorentz-invariance of the S-matrix implies the equality

$$\langle p_3, p_4 | \, \mathcal{S} \, | p_1, p_2 \rangle = \langle p_1, p_2 | \, \mathcal{S} \, | p_3, p_4 \rangle \tag{3.51}$$

since in the centre of mass frame the exchange of momenta $p_1 \leftrightarrow p_3$ and $p_2 \leftrightarrow p_4$ correspond to a rotation of π around the axis which bisects the angle between p_1 and p_3. Therefore from Eq. (3.50) we obtain

$$\langle p_3, p_4 | \, \mathcal{T} \, | p_1, p_2 \rangle - \langle p_3, p_4 | \, \mathcal{T} \, | p_1, p_2 \rangle^* = -i \, \langle p_3, p_4 | \, \mathcal{T}^\dagger \mathcal{T} \, | p_1, p_2 \rangle \,, \tag{3.52}$$

impliying:

$$2i\mathrm{Im}(\langle p_3, p_4 | \, \mathcal{T} \, | p_1, p_2 \rangle) = \langle p_3, p_4 | \, \mathcal{T} \mathcal{T}^\dagger \, | p_1, p_2 \rangle = \tag{3.53}$$
$$\sum_m \int d\Phi_m \, \langle p_3, p_4 | \, \mathcal{T} \, | k_m \rangle \, \langle p_1, p_2 | \, \mathcal{T} \, | k_m \rangle^* \,.$$

We have seen in Eq. (2.56) that the T-matrix element can be related to the transition scattering amplitude $A(s,t)$. Therefore 3.53 can be used to derive an expression for the imaginary part of $A(s,t)$ [47]:

$$2i\mathrm{Im}(\langle p_3, p_4 | \, A \, | p_1, p_2 \rangle) = \mathrm{Disc}(\langle p_3, p_4 | \, A \, | p_1, p_2 \rangle) = \tag{3.54}$$
$$\sum_m \int d\Phi_m \, \langle p_3, p_4 | \, A \, | k_m \rangle \, \langle p_1, p_2 | \, A \, | k_m \rangle^* \,.$$

We then see that loop amplitues will in general have discontinuities related to their imaginary parts. Above the energy threshold of elastic scattering $s = 4m^2$, new states become available, corresponding to the creation of new particles [75]. This means that for $s > 4m^2$, new terms must be added to the right hand side of Eq. (3.54). New states become available every time the centre-of-mass energy goes above one of the thresholds for the creation of a new particle $s = 4m^2, 9m^2, 16m^2, ...$

We can therefore conclude that the expression $2i\mathrm{Im}[A(s,t)]$ represents a discontinuity starting at the energy of elastic scattering.

It is then possible to expand Eq. (3.54) in the coupling constant and solve the equation order-by-order.

For tree-level and one loop this means having

$$\text{Disc}(A^{(0)}) = 0, \tag{3.55}$$

$$\text{Disc}(A^{(1)}) = \int d\Phi_2 \, \langle p_3, p_4| \, A^{(0)} \, |k_1, k_2\rangle \, \langle p_1, p_2| \, A^{(0)} \, |k_1, k_2\rangle^* . \tag{3.56}$$

Eq. (3.55) and (3.56) are examples of the *Cutkosky rules* [84] directly applied at the amplitude level. If our amplitude is represented as a function $A(s,t)$ then we will see that its discontinuities correspond to the branch cuts of the functions $\log(-\frac{s}{\mu_R^2})$ and $\log(-\frac{t}{\mu_R^2})$ in the complex s-plane and t-plane respectively. These branch cuts are normally referred to as *unitarity cuts*, to stress their relation to the unitarity of the S- matrix [67].

In this framework, the cut in a specific channel is computed as the product of two tree-level amplitudes, summed over all the possible multi-particle states crossing the cut and then integrated over the two-body phase space of the states .

We now quote the relevant dispersion relations which allows us to reconstruct the full analytical form of the amplitude from its discontinuities and simple poles [67],

$$A(s,t) = \frac{\lambda_1}{s-m^2} + \frac{\lambda_2}{t-m^2} + \int_{4m^2}^{\infty} \frac{ds'}{2\pi} \left(\frac{\text{Im}[A(s',t)]}{s'-s} + \frac{\text{Im}[A(s',t)]}{s'-t} \right), \tag{3.57}$$

where λ_1 and λ_2 are the pole residues of $A(s,t)$ at $s = m^2$ and $t = m^2$ respectively. Eq. (3.57) is derived by applying Cauchy's theorem on a contour which moves around the branch cut and then extends to infinity, plus smaller contours which encircle the simple poles. We show the shape of the integration contour in the s-channel in figure 3.4, labelling it Γ. We then see that combining Eqs. (3.54), (3.56) and (3.57) it is possible to fully compute a one-loop amplitude by combining products of tree-level expressions with on-shell legs and integrating them over the appropriate phase-space.

3.5.2 Generalised Unitarity

The unitarity method described above can be expanded to a technique called *generalised unitarity*, first presented in [77]. This method requires the substitution of all the possible combinations of propagators in a Feynmann integral with a delta function

$$\frac{i}{k^2 - p^2} \rightarrow \delta^{(+)}(k^2 - p^2), \tag{3.58}$$
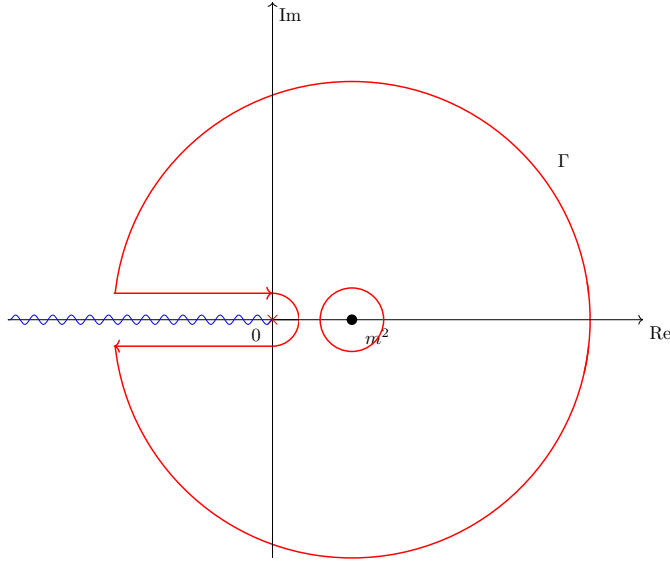
Figure 3.4: The integration contour Γ in the complex s-plane. The one in the t-plane will be identical, with pole in position $t = m^2$.

remembering that in D dimensions at most D propagators can be cut simultaneously. Therefore the method starts by putting on-shell all the sets comprising D propagators, then all the sets of $D-1$ propagators, and so on.

We note that this is similar to performing the standard unitarity cut, but with the difference that in this case a larger set of propagators is put on-shell, not just the ones associated to a specific channel. For this reason this method does not rely specifically on the unitarity of the S-matrix. Cutting all the possible propagators in a given integral is also referred to as computing the *maximal cut* of that integral [67].
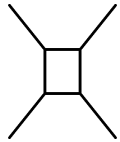
Performing generalised cuts is useful in the case in which the amplitude can be written in a basis of known functions. It is shown in [85] that any one-loop amplitude in D dimensions, when expanded up to order $O(\epsilon^0)$ in the dimensional regulator, can be written as a linear combination of m-gon one-loop scalar integrals, where $m = 1, 2, ..., D$:

$$A^{(1)} = \sum_i c_i^D I_D^i + \sum_j c_j^{D-1} I_{D-1}^j + ... + \sum_k c_k^2 I_2^k. \tag{3.59}$$

In the case in which we want to expand $A^{(1)}$ beyond the $O(\epsilon^0)$ order, we need to include $(D+1)$-gon scalar integrals and their coefficients

$$\sum_l c_l^{D+1} I_{D+1}^l. \tag{3.60}$$

This latter case is the one which applies to the computations in chapters 5 and 7. We name scalar integrals according to their *topology* (pentagon, box, triangle). The topology of an integral is given by the set of the independent denominators of its integrand, corresponding to the internal propagators in specific diagrams. An n-gon integral is then an integral with n denominators. We give here the example of a scalar box integral in D dimensions:

$$I_4 = \int \frac{d^D k}{(2\pi)^D} \frac{1}{k^2(k+p_1)^2(k+p_1+p_2)^2(k-p_4)^2} = \int \frac{d^D k}{(2\pi)^D} \quad \text{} \quad . \tag{3.61}$$

The adjective *scalar* given to the integrals is used in the literature to refer to integrals with numerators equal to one. In general one could have more complicated tensor structures appearing in the numerators, but it is always possible to decompose tensor integrals into scalar ones. One of the most important of these tensor-reduction procedures is the *Passarino-Veltmann* method [86], an example of which is briefly sketched in Appendix D. The integrals that form the basis of an amplitude are called *master integrals* (MIs).

The task of computing a one-loop amplitude can therefore always be reduced to computing the rational coefficients in a given basis. The ability to write amplitudes in the general form of Eq. (3.59) has historically been of fundamental importance for their computations. This is the form in which they will be derived and presented in all the following chapters of this thesis, specifically in chapters 5 and 7.

The crucial insight of [77] is that the contributions to the cut of a specific set of D propagators in the amplitude in Eq. (3.59) will only come from the scalar integral which contains those all those propagators, and it will correspond to the value of the cut of the integral multiplied by its coefficient. Since the Cutkosky rules allow us to obtain the value of unitarity cuts from the knowledge of lower order results, as seen in Section 3.5.1, it is then possible to set up a system of linear equations which

can be solved recursively [67] for all the coefficients in Eq. (3.59). In [77] this procedure was applied to $N = 4$ one-loop amplitudes in $D = 4$ dimensions, which can be expressed in a basis of only scalar boxes I_4^i with no rational terms.

Generalised unitarity makes it possible to directly compute the rational coefficients c_i. In many examples, nevertheless, the high complexity of such calculations makes the method not efficient. In the next section we will see instead how the coefficients can be computed by solving linear systems of equations obtained by numerically sampling the whole amplitude expression.

3.6 Ossola-Papadopoulos-Pittau Integrand Reduction

The Ossola-Papadopoulos-Pittau (OPP) integrand reduction methods were presented in [87], this section summarises the content of the paper, extending the presentation to explain the computation of D-dimensional amplitudes performed in Chapter 7.

The OPP method exploits the one-loop representation of Eq. (3.59) and provides an algorithmical way of finding the rational coefficients given the basis of master integrals. A generic colour-ordered one-loop amplitude with n legs can be written as

$$A_n = \mu_R^{2\epsilon} \int \frac{d^D k}{(2\pi)^D} I_n, \tag{3.62}$$

where the integrand can be expressed as a fraction [88]

$$I_n = \frac{N(k)}{\prod_i D_i}. \tag{3.63}$$

The denominators D_i are of the form $q_i^2 - m_i^2$, with q_i being the momenta flowing in the internal lines with mass m_i; $N(k)$ is a polynomial in the components of the internal loop momentum k. The numerator can be written as the sum of two classes of terms: Reducible Scalar Products (RSPs) and Irreducible Scalar Products (ISPs). The former products can be fully written in terms of the D_i's,

while the rest of the numerator consists of the ISPs. Schematically we write

$$N(k) = \text{RSPs} + \text{ISPs}. \tag{3.64}$$

In order to take into account the the form of the integrand beyond $D = 4$, it is convenient to decompose the internal momentum as $k = \bar{k} + \tilde{k}$, where $\bar{k}$ is taken to be four-dimensional, while $\tilde{k}$ is a $4 - D$ dimensional vector orthogonal to $\bar{k}$: $\bar{k} \cdot \tilde{k} = 0$.

If we then define $\tilde{k} \cdot \tilde{k} = \mu^2$ we find a new form of the denominators,

$$D_i = q_i^2 - m_i^2 + \mu^2, \tag{3.65}$$

which is true in our case since the external momenta p_i are all taken to be four-dimensional, hence we have $\tilde{k} \cdot p_i = 0$. We then see that μ^2 acts as an effective mass, and it must be added to the list of ISPs. The OPP reduction focuses on the reconstruction of the numerator of the integrand, since the denominator factors can be obtained by examining the integral topology.

We will use representation of Eq. (3.59) but including the $D + 1$-dimensional terms of Eq. (3.5.2). This is the case because in this thesis we are interested in the contributions of one-loop amplitudes at NNLO, which require expansions of the amplitudes to higher orders than $O(\epsilon^0)$, remembering that we have $\epsilon = \frac{4-D}{2}$. Having p_i as four-dimensional vectors, the terms in Eq. (3.5.2) will be scalar pentagons with their associated coefficients. We then have

$$A_n = \sum_l e_l I_5^l + \sum_i d_i I_4^i + \sum_j c_j I_3^j + \sum_k b_k I_2^k. \tag{3.66}$$

This was the integral basis of the amplitudes reconstructed in Chapter 7, for which the OPP method

was employed. Pictorially the decomposition can be illustrated as

$$A_n = \sum_l e_l \int d^D k \quad\quad + \sum_i d_i \int d^D k \quad\quad \tag{3.67}$$

$$+ \sum_j c_j \int d^D k \quad\quad + \sum_k b_k \int d^D k \text{—} \bigcirc \text{—} \quad .$$

Using Eq. (3.66), we can conveniently decompose the numerator N as

$$
\begin{aligned}
N(k) = &\sum_{i<j<k<l<m} \dot{e}_{ijklm}(\mu^2) \prod_{\alpha \neq i,j,k,l,m} D_\alpha + \\
&\sum_{i<j<k<l} \left(d_{ijkl} + \tilde{d}_{ijkl}(\bar{k}) + \dot{d}_{ijkl}(\mu^2) \right) \prod_{\alpha \neq i,j,k,l} D_\alpha + \\
&\sum_{i<j<k} \left(c_{ijk} + \tilde{c}_{ijk}(\bar{k}) + \dot{c}_{ijk}(\mu^2) \right) \prod_{\alpha \neq i,j,k} D_\alpha + \\
&\sum_{i<j} \left(b_{ij} + \tilde{b}_{ij}(\bar{k}) + \dot{b}_{ij}(\mu^2) \right) \prod_{\alpha \neq i,j} D_\alpha + \\
&\sum_i \left(a_i + \tilde{a}_i(\bar{k}) + \dot{a}_i(\mu^2) \right) \prod_{\alpha \neq i} D_\alpha + \\
&\tilde{p}(\bar{k}) \prod_\alpha D_\alpha
\end{aligned}
\tag{3.68}
$$

Where we made explicit which terms depend on the four-dimensional momentum, which ones on the effective mass, and which terms are constant (purely dependent on the external momenta). Terms $\tilde{d}, \tilde{c}, \tilde{b}, \tilde{a}$, are spurious, meaning that they evaluate to zero once the integral is performed, but they need to be computed since the decomposition is at the level of the integrand. We remark that it is in theory possible to choose a different parametrisation, for which we also have terms e_{ijklm} coefficients in the topmost line of Eq. (3.68). Nevertheless, we found that the choice of Eq. (3.68) was the most convenient for the work of this thesis.

While knowing Eq. (3.68) in theory makes it possible to reconstruct the analytical form of the numerator by performing multiple numerical evaluations, it would be unfeasible to try and solve the resulting system by brute force. Instead, it is possible to see that many terms in the sum can be set

to zero with a deliberate choice which puts different internal propagators on-shell.

For example we see that a *five-particle cut*, which sets $D_1 = D_2 = D_3 = D_4 = D_5 = 0$ for a specific value of the four-momentum $\bar{k} = \bar{k}^*$ and the effective mass $\mu^2 = \mu^{2*}$, reduces the numerator to the form

$$N(\bar{k}^*, \mu^{2*}) = \dot{e}_{12345}(\mu^{2*}) \prod_{\alpha \neq 1,2,3,4,5} D_\alpha, \tag{3.69}$$

therefore the values of the pentagon coefficients can be computed by solving smaller systems of equations taking all the different five-particle cuts.

Once the pentagon coefficients have been evaluated, the algorithm can be iterated imposing four-particle cuts and so on, allowing a full reconstruction, minimising the computation time and resources.

It is worth stressing that the above analysis slightly differs from the one in [87], which is carried out explicitly in $4 - 2\epsilon$ dimensions. In most cases the OPP method is used to obtain amplitude expressions expanded up to order $O(\epsilon^0)$; this means that the results of the integrals can be expanded and only contributions up to the fixed order are retained in the final result. The five-particle cut is performed in the limit $\mu^2 \to 0$, so that the pentagons are not included into the basis and their contributions are part of a rational remainder.

Explicitly, the class of integrals which are dropped in the $4 - 2\epsilon$ expansion are

$$\int d^{4-2\epsilon} k \mu^2 \quad \vcenter{\hbox{}} \quad = -\epsilon \int d^{6-2\epsilon} k \quad \vcenter{\hbox{}} \tag{3.70}$$

and

$$\int d^{4-2\epsilon} k \mu^2 \quad \vcenter{\hbox{}} \quad = -\epsilon \int d^{6-2\epsilon} k \quad \vcenter{\hbox{}} \quad . \tag{3.71}$$

It is easily seen that the above integrals are of order $O(\epsilon)$ since both the pentagon and the box are finite quantities in six dimensions [89, 90]. In this thesis we will refer to the integrals on

the left-hand-side of Eqs. (3.70) and (3.71) as μ^2-pentagon and μ^2-box. If the decomposition is performed up to higher orders of the dimensional regulator, both the integrals contribute, increasing the complexity of the calculation, as we will see in Chapter 7.

3.7   Supersymmetric Decomposition

In this subsection we introduce an additional type of decomposition for one-loop scattering amplitudes, which is sometimes defined in the literature as *supersymmetric decomposition* [48, 91]. This type of decomposition consists of expressing a sub-amplitude $A_{n;c}^{[J]}$ as the linear combination of the sub-amplitudes originating from different theories, with particles with spin different from J circulating the their internal loops. We will outline the procedure following the exposition of [48].

The method relies on the quantisation of QCD in a different gauge than the one described in Section 2.3. This is called the *background-field gauge* and it splits the gluon field into a classical background field A_μ^B and a quantum one A_μ^Q: $A_\mu = A_\mu^B + A_\mu^Q$. The gauge-fixing condition is then

$$D^{B,\mu} A_\mu^Q = 0, \tag{3.72}$$

where we defined

$$D^{B,\mu} = \partial^\mu - i\frac{g_s}{\sqrt{2}} A^{B,\mu}. \tag{3.73}$$

These choices have the effect of adding terms to the Lagrangian of the theory, creating corresponding Feynamn rules for the vertices mixing the Q and B fields

$$V_{\mu\nu\rho}^{QQB} = \frac{i}{\sqrt{2}}[\eta_{\mu\nu}(k-p)_\rho - 2\eta_{\rho\nu}q_\mu + 2\eta_{\rho\mu}q_\nu], \tag{3.74}$$

$$V_{\mu\nu\rho\lambda}^{QQBB} = -\frac{i}{2}[\eta_{\mu\nu}\eta_{\rho\lambda} + 2\eta_{\mu\lambda}\eta_{\rho\nu} - 2\eta_{\mu\rho}\eta_{\nu\lambda}]. \tag{3.75}$$

For one-loop gluon amplitudes, the field A_μ^Q represents the particle running inside the loop, while the A_μ^B fields are the external legs [92]. We can then compare vertices in Eq. (3.74) and (3.75) to

the Feynamn rules for vertices with scalars s instead of A_μ^Q fields

$$V_\rho^{ssB} = \frac{i}{\sqrt{2}}(k-p)_\rho, \tag{3.76}$$

$$V_{\rho\lambda}^{ssBB} = -\frac{i}{2}\eta_{\rho\lambda}, \tag{3.77}$$

where in the context of one-loop amplitudes, these vertices are the ones contributing to the integrand of the diagrams with external gluon legs and the scalar s running in the loop [48, 92]. We then see that the term of $V_{\mu\nu\rho}^{QQB}$ which depends on the internal momentum k is the same as the one for a complex scalar in all the renormalisation schemes in which the number of physical helicities of the gluon is equal to 2. This is the case for the DR and the FDH scheme.

As a result, it is possible to express part of the numerators of the integrands of the one-loop gluon sub-amplitude in terms of the contributions of a scalar particle. In general, finding the linear relations between the vertices in this gauge allows us to express the particles running in the loop as combinations of particles from different theories.

Further relationships involving fermion loops can be found, following a similar logic to the one presented above. Here we will only present the relevant results, but for a detailed derivation the reader is referred to [48] and [93]. The final result is that the gluon g and the fermion f in the internal loop can be expressed as

$$g = (g + 4f + 3s) - 4(f + s) + s, \tag{3.78}$$

$$f = (f + s) - s, \tag{3.79}$$

that at the level of amplitudes means having

$$A_n^{[1]} = A_n^{\mathcal{N}=4} - 4A_n^{\mathcal{N}=1} + A_n^{\mathcal{N}=0}, \tag{3.80}$$

$$A_n^{[1/2]} = A_n^{\mathcal{N}=1} - A_n^{\mathcal{N}=0}. \tag{3.81}$$

Where $A^{\mathcal{N}=4}$ represents the contribution from a $\mathcal{N}=4$ super Yang-Mills multiplet, comprising one gluon g, four gluinos f and three complex scalars s. $A^{\mathcal{N}=1}$ indicates the contribution of a chiral matter $\mathcal{N}=1$ multiplet, consisting of one fermion and a complex scalar. $A^{\mathcal{N}=0}$ is the contribution from a complex scalar in the loop. Gluon QCD amplitiudes can therefore be obtained by computing the amplitudes in these three theories and combining them. Expressing the amplitude in terms of these supersymmetric components significantly simplifies their calculation in most cases. This is the case since the supersymmetric parts have simpler expressions than the non-supersymmetric ones (see for example [94],[95] and references therein), and in turn the $A^{\mathcal{N}=0}$ sub-amplitudes exhibit a lower complexity than either $A_n^{[1]}$ or $A_n^{[1/2]}$. This fact can be understood if we know that a scalar in the internal loop does not propagate any spin information, giving rise to simpler structures [48].

The supersymmetric decomposition was used in many of the computations of one-loop n-gluon amplitudes, as we will see in Chapter 6. It was also instrumental in obtaining the results of the work detialed in Chapter 7.

3.8   BCFW shifts at One-Loop

In this section we discuss one last technique which can be employed for the computation of parts of one-loop scattering amplitudes. This discussion will be useful to gain a better understanding of the algorithm in Section 4.3.5 and the computations mentioned in the review in Chapter 6. We will use the same notation as in [96].

In order to describe the application of this method we define the distinction between *cut-constructible* and *non cut-constructible* parts of an amplitude. We focus here on amplitudes in $D = 4 - 2\epsilon$ dimensions, expanded to order $O(\epsilon^0)$. Their representation is then

$$A_n = \sum_i d_i I_4^i + \sum_j c_j I_3^j + \sum_k b_k I_2^k + R, \tag{3.82}$$

where we note the presence of the additional rational term R. Coefficients d_i, c_i, b_i can be computed using generalised unitarity in four dimensions as described in Section 3.5.2, so they are referred

to as the cut-constructible part. The R term contains all the contributions from the additional 2ϵ-dimensional parts and it evaluates to zero when the cuts are performed, for this reason it is defined as the non cut-contructible part and needs to be computed by other means. The BCFW-like shifts described in this section are an example of one of such methods.

A complex shift can be performed in the same fashion as for the BCFW-method at tree-level

$$[i| \rightarrow [i| + z[j|, \tag{3.83}$$

$$\langle j| \rightarrow \langle j| - z \langle i|, \tag{3.84}$$

in the MHV case it is convenient to perform the shift on the two negative-helicity legs, since this choice ensures that the amplitude has no pole at $z \rightarrow \infty$ [97]. For the remaining of the section we will work under the assumption $\text{Res}_{z\rightarrow\infty}(\frac{A(z)}{z}) = 0$ for simplicity. The cases in which this condition is not met are discussed in Section 4.3.5, where it is explained how this additional complication is tackled in our computations.

A generic one-loop amplitude can be represented as

$$A_n(z) = C_n(z) + R_n(z), \tag{3.85}$$

splitting it into a cut-constructible and non cut-constructible part. The term $R(z)$ is then constructed by setting all the functions containing branch cuts and π^2 terms to zero in the amplitude.

Despite being a rational function, $R(z)$ cannot be fully obtained from its residues in z via the Cauchy's theorem, since it contains spurious singularities in z which are not physical. Such residues cancel out when $R(z)$ and $C(z)$ are summed in the full expression, but they are present when the two terms are considered in isolation. We will see an example of this in Chapter 6: the function $\frac{\log(r)}{(1-r)^2}$ (part of $C(z)$) has a spurious singularity at $r \rightarrow 1$ which is then cancelled when summed with $\frac{1}{(1-r)}$ (part of $R(z)$) and a regular function $L_1(z)$ is formed.

For this reason it is necessary to perform a *completion* of the expressions

$$\hat{C}_n(z) = C_n(z) + CR_n(z),$$
$$\hat{R}_n(z) = R_n(z) - CR_n(z), \tag{3.86}$$

where $CR_n(z)$ is a non-unique term which makes $\hat{R}_n(z)$ free of spurious singularities.
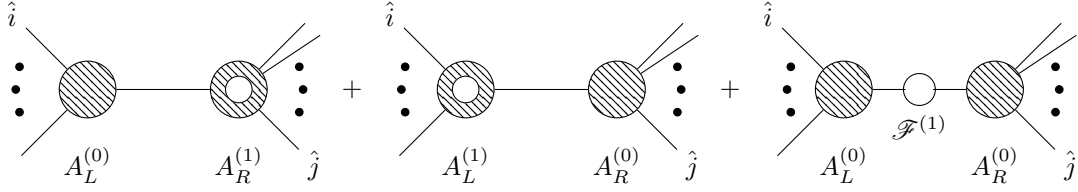
Figure 3.5: Graphical representation of Eq. (3.87). The shaded circles represent the tree-level terms, while the ones with a white circle inside represent one-loop terms. The factorisation function is represented as the loop dressing the right-most propagator. The two shifted legs are labelled i and j.

One aspect to consider is that the newly introduced term is likely to be non-zero for large values of z. In order to correct for this spurious behaviour the value of the term in the limit $z \to \infty$ is computed and subtracted from the amplitudes' expression, This is always possible since $CR_n(z)$ is fully known analytically.

It is then possible to compute $\hat{R}_n(z)$ by summing over the residues at finite z. This corresponds to the sum over the factorisation channels. At MHV the contributions for the $s_{\alpha...\beta}$ channel are

$$A_L^{(0)} \times \frac{i}{s_{\alpha...\beta}} \times A_R^{(1)} + A_L^{(1)} \times \frac{i}{s_{\alpha...\beta}} \times A_R^{(0)} + A_L^{(0)} \times \frac{\mathscr{F}^{(1)}}{s_{\alpha...\beta}} A_R^{(0)}, \tag{3.87}$$

where the factorisation function $\mathscr{F}^{\text{1-loop}}$ represents the insertion of a loop in the propagator as shown in Figure 3.5.

The rational term $\hat{R}_n(z)$ is computed via formula Eq. (3.87) with all the polylogarithms and π^2 in the loop-expressions set to zero. It is important to notice that the factorised rational term $\hat{R}_n(z)$ obtained in such a way will contain all the correct residues for the physical poles. For this reason, it is necessary to compute any potential residue in the physical poles of $\hat{C}R_n(z)$ and subtract it from the overall expression, in order to avoid any double counting. The term which is added to avoid the double counting is represented as O_n in [98],

$$O_n = \sum_{\text{poles } \alpha} \text{Res}_{z=z_\alpha} \left(\frac{\hat{C}R_n(z)}{z} \right). \tag{3.88}$$

In conclusion, the full non cut-constructible part is expressed as $\hat{R}_n(0) + O_n$.

After having described modern methods for the computation of tree and one-loop amplitudes, we will see in the next chapter how they can be implemented in algorithms which were used to derive the results presented in this thesis.

Chapter 4

Analytic Reconstructions using Finite Fields

The methodology employed in this thesis for the analytic computation of QCD amplitudes requires the manipulation of large rational functions in the momentum-twistor variables. Such manipulations give rise to large intermediate expressions in the calculations, which can be orders of magnitudes grater than the final result [99, 100]; this especially becomes a bottleneck for high-multiplicity amplitudes. An effective method for avoiding this problem consist of *black-box interpolation* techniques [14]: the function is evaluated on specific numerical points and the analytic form is reconstructed by performing a numerical interpolation.

As we have seen in Eq. (3.5.2), a one-loop amplitude can be represented as a linear combination of scalar integrals multiplied by coefficients. These coefficients, in specific parametrisations, are represented by rational functions which depends on the kinematic kinematics; for this reason we will now highlight some interpolation algorithms which allow to reconstruct rational functions by evaluating them on a finite number of numerical points. These methods represent the mathematical backbone of the reconstruction algorithms used to obtain the results presented in this thesis. This chapter is organised as follows. In Section 4.1 we describe the general method of numerical interpolation for polynomials and rational functions. In Section 4.2 we define the notion of finite

fields, and how they are used for analytic reconstructions. In Section 7.3 we describe the main techniques which we implemented in order to optimise the reconstruction of polynomials of high complexity. Said techniques were essential to obtain the results presented in chapters 5 and 7.

4.1 Analytic Reconstruction

In this presentation we will follow the same sequence of steps as in [100]. We start with Newton's polynomial representation of a univariate polynomial:

$$f(z) = \sum_{i=0}^{M} c_i \prod_{j=0}^{i-1} (z - y_j) \tag{4.1}$$
$$= c_0 + (z - y_0)(c_1 + (z - y_1)(c_2 + (z - y_2)(... + (z - y_{M-1})c_R))),$$

where M is the polynomial degree and y_i are numbers. This representation makes it straightforward to see how the coefficients c_i can be calculated by recursively evaluating the functions at the various points: $f(y_0), ..., f(y_{M-1})$.

A multivariate polynomial can be reconstructed in the same way by choosing a similar representation to the one of Eq. (4.1) in a specific variable, with the difference that the c_i coefficients will now be polynomials of all the remaining variables:

$$f(z_1, ..., z_n) = \sum_{i=0}^{M_1} c_i(z_2, ..., z_n) \prod_{j=0}^{i-1} (z_1 - y_{i,j}) = \tag{4.2}$$

$$c_0(z_2, ..., z_n) + (z - y_{1,0})(c_1(z_2, ..., z_n) + (z - y_{1,1})(... + (z - y_{1,M-1})c_R(z_2, ..., z_n)))) \quad .$$

We have as the result of the first evaluation $f(y_{1,0}) = c_0(z_2, ..., z_n)$. We can then put $c_0(z_2, ..., z_n)$ in Newton's representation and carry out the procedure iteratively, thereby recustring the whole polynomial. We see that there is an upper bound to the number of needed evaluations: $M_1 \times M_2 \times ... \times M_n$, where M_i are the maximum degrees of the polynomial in each of the z_i variables.

In general the degrees M_i are not known *a priori*, therefore they must be found through the evaluation. This is done easily on a univariate polynomial: every time a new coefficient c_i is

computed, the series is evaluated on one or more random points (different from the y_i's), if the values of the series equal the ones of the full function then we have reached the end of the reconstruction and we know the total degree. The reconstruction is carried out until such condition is met. We then see that the reconstruction is more computationally expensive if the degrees are not known at the beginning and need to be computed on the fly.

We now turn our attention to the reconstruction of rational functions. The equivalent of Newton's formula for univariate rational functions is Thiele's formula, based on the representation:

$$f(z) = c_0 + \cfrac{z - y_0}{c_1 + \cfrac{z - y_1}{c_2 + \cfrac{z - y_2}{... + \cfrac{z - y_{M-1}}{c_N}}}}. \tag{4.3}$$

It can be seen from this representation function that $f(z)$ can be reconstructed with M evaluations in an equivalent way to the polynomial reconstruction. For the multivariate case the reconstruction can be performed again as a series of iterated univariate reconstructions. While this solves the interpolation problem in general, we detail here the specific sequence of steps followed by the algorithm in the FINITEFLOW package [100], since this is the one used to compute most of the results presented in this thesis.

The method exploits the introduction of an auxiliary variable t, as done in [101], costructing the function $h(t, z)$:

$$\begin{aligned} h(t, z_1, ..., z_n) &= f(tz_1, tz_2, ..., tz_n) \\ &= \frac{\sum_i^M p_i(z_1, ..., z_n)t^i}{1 + \sum_i^{M'} q_i(z_1, ..., z_n)t^i}. \end{aligned} \tag{4.4}$$

We note that this representation of a rational function relies on the constant term of its denominator being non-zero, this can be ensured by performing a shift of the z_i variables as proposed in [101]. The function can be reconstructed in the shifted variables and then the inverse shift is performed as the last step, retrieving the correct expression. The constant term can always be set to 1 via an appropriate normalisation.

We can then consider $h(t, z)$ to be a univariate funcion in t and use Thiele's formula to compute the numerator and denominator degrees M and M'. Once this is done, a system of equations can be set up choosing a series numerical values for the variable $t = t'$ and a constant numerical one for $z = z^*$, where we used the shorthand notation $z = z_1, ..., z_n$. The linear system is then composed

by equations such as:

$$f(t'\boldsymbol{z}^*) = \sum_i^M p_i(\boldsymbol{z}^*)(t')^i + \sum_i^{M'} q_i(\boldsymbol{z}^*)f(t'\boldsymbol{z}^*)(t')^i \tag{4.5}$$

for each different value of t'.

If the function is evaluated on a sufficiently high number of t values, we can reconstruct the polynomials p and q on the numerical point z^*. This means that we can obtain the values of those polynomials on numerical points and then use that information to apply Newton's formula recursively and fully reconstruct $p(\boldsymbol{z})$ and $q(\boldsymbol{z})$.

The analytical form of the original function is then simply obtained by evaluating $h(1, \boldsymbol{z})$:

$$f(\boldsymbol{z}) = h(1, \boldsymbol{z}) = \frac{\sum_i^M p_i(z_1, ..., z_n)}{1 + \sum_i^{M'} q_i(z_1, ..., z_n)}. \tag{4.6}$$

4.2 Finite Fields

The above discussion has presented reconstruction techniques which rely on the evaluations of functions over rational numbers. These methods have the issue of the loss of precision in the storing of floating-point numbers in computer memory. The precision needed to perform the reconstruction often requires keeping in memory a high number of digits at each intermediate step, thus recreating the problem of large intermediate expressions and making the method impractical. For this reason it is preferable to perform all the numerical evaluations on integers, which are of finite size and for which the loss of precision is not an issue.

We can consider the set $\mathbb{Z}_n$ of all non-negative integer numbers smaller than n. All rational operations with the exception of division are well defined within the elements of the set modulo number n. If n is prime, $n = p$, then a multiplicative inverse can unambiguously be defined, so that all four arithmetic operations can be performed over it. This allows us to define $\mathbb{Z}_p$ a *prime field* [102]. Crucially, there is a one-to-one map from elements in $\mathbb{Z}_p$ to the ones in $\mathbb{Q}$. Wang's reconstruction algorithm [103, 104] allows to find the image of any number in a prime field to the rationals; given a number of value c in $\mathbb{Z}_p$, the algorithm makes it possible to find integers a and b such that

$$\frac{a}{b} = c \ \mathrm{mod}(p), \tag{4.7}$$

given the condition

$$|a|, \ |b| < \sqrt{\frac{p}{2}}. \tag{4.8}$$

The condition in Eq. (4.8) puts a limit $p \leq 2^{64}$ to the size of the prime, since on most machines integers have maximum size of 64 bit. This limit can be circumvented by exploiting the *Chinese Remainder Theorem*, which states that if the image of a rational number over several prime fields $\mathbb{Z}_{p_1}, \mathbb{Z}_{p_2}, ..., \mathbb{Z}_{p_n}$ is known, it is possible to construct its image over $\mathbb{Z}_{p_1 p_2 ... p_n}$ [105].

The technique of reconstructing over finite fields is widely used by many computer algebra systems [102]. In recent years it has been adopted in the field high-energy physics by many different research groups. Its first application was in [106], where it was used to perform *Itegration by Parts* (IBP) reductions. Subsequent works have applied it to the same end [107, 108]. In [109] it was used to efficiently implement the unitarity method to a multi-loop calculation. Additional examples of such applications can be found in [83, 110, 111].

The theorems that we have introduced in this section make it possible to perform all the computations described in Section 4.1 over prime fields, and only reconvert the expressions to rational numbers as the last step. This avoids the loss of precision issues and significantly speeds up the evaluations.

4.3 Reconstruction Techniques

While the reconstruction over finite fields can in principle be performed on every rational function, it is always convenient to exploit all the knowledge that is available on the function to optimise the computation. In the case of tree-level and one-loop helicity amplitudes, the physical origin of the expressions puts great constraints on the form that they can assume, significantly reducing the number of computations needed to reconstruct them. In this section we will present the methods and algorithms which were employed to perform the reconstructions efficiently. We will illustrate the effect of the various methods on one specific tree-level NMHV six-gluon helicity amplitude: $A_{6g}^{(0)}(-+-+-+)$.

The $A_{6g}^{(0)}(-+-+-+)$ amplitude has the highest complexity out of all the tree-level expressions

and it is referred to as the *alternating helicity amplitude*. It can be represented in spinor variables as in [99]

$$A_{6g}^{(0)}(-+-+-+) = \frac{\langle 5| p_{13}|2]^4}{[12][23]\langle 45\rangle\langle 56\rangle\langle 4| p_{23}|1]\langle 6| p_{12}|3]s_{123}}$$
$$+ \frac{\langle 3| p_{24}|6]^4}{[16]\langle 23\rangle\langle 34\rangle[56]\langle 2| p_{16}|5]\langle 4| p_{23}|1]s_{234}}$$
$$- \frac{\langle 1| p_{35}|4]^4}{\langle 12\rangle[34][45]\langle 16\rangle\langle 2| p_{16}|5]\langle 6| p_{12}|3]s_{345}}.$$

(4.9)

For the following examples the tree amplitude was expressed as a rational function of momentum-twistor variables. As already stated, this is a necessary requirement for the application of the reconstruction techniques illustrated in this chapter. We also use this example to compare two possible parametrisations in the momentum-twistor variables. We call them A and B parametrisations, explicitly they are

$$Z^A =$$

(4.10)

$$\begin{pmatrix} 1 & 0 & \frac{1}{x_1} & \frac{1}{x_1}+\frac{1}{x_1x_2} & \frac{1}{x_1}+\frac{1}{x_1x_2}+\frac{1}{x_1x_2x_3} & \frac{1}{x_1}+\frac{1}{x_1x_2}+\frac{1}{x_1x_2x_3}+\frac{1}{x_1x_2x_3x_4} \\ 0 & 1 & 1 & 1 & 1 & 1 \\ 0 & 0 & 0 & \frac{x_5}{x_2} & x_6 & 1 \\ 0 & 0 & 1 & 1 & x_7 & 1-\frac{x_8}{x_5} \end{pmatrix},$$

$$Z^B = \begin{pmatrix} 1 & 0 & \frac{1}{s_{12}} & \frac{\sigma_1}{s_{12}} & \frac{\sigma_2}{s_{12}} & \frac{\sigma_3}{s_{12}} \\ 0 & 1 & 1 & 1 & 1 & 1 \\ 0 & 0 & 0 & y_1 & y_2 & 1 \\ 0 & 0 & 1 & 1 & \frac{y_2-y_3}{y_1} & \frac{1-y_4}{y_1} \end{pmatrix},$$

(4.11)

where we recall the definition of the momentum twistor Z from Eq. (3.29).

We see that the Z matrices both have 8 independent entries; this is consistent with the 8 degrees of freedom of the 6 gluon momenta $(3 \times 6 - 10 = 8)$. We give the expressions of the variables of both

matrices in terms of spinors and other kinematic invariants. For Z^A

$$x_1 = s_{12},$$
$$x_2 = -\frac{\mathrm{tr}_+(1234)}{s_{12}s_{34}},$$
$$x_3 = -\frac{\mathrm{tr}_+(1345)}{s_{13}s_{45}},$$
$$x_4 = -\frac{\mathrm{tr}_+(1456)}{s_{14}s_{56}},$$
$$x_5 = \frac{s_{23}}{s_{12}},$$
$$x_6 = -\frac{\mathrm{tr}_+(2, p_{34}, 5, 1)}{s_{12}s_{15}},$$
$$x_7 = -\frac{\mathrm{tr}_+(5, 1, p_{23}, p_{234})}{s_{15}s_{23}},$$
$$x_8 = \frac{s_{123}}{s_{12}}.$$

$$(4.12)$$

And for Z^B

$$y_1 = -\frac{s_{23}s_{34}}{\mathrm{tr}_+(1234)},$$
$$y_2 = -\frac{\mathrm{tr}_+(2, p_{34}, 5, 1)}{s_{12}s_{15}},$$
$$y_3 = \frac{\mathrm{tr}_+(5, 1, p_{23}, p_{234})s_{12}s_{34} - \mathrm{tr}_+(1234)\mathrm{tr}_+(2, p_{34}, 5, 1)}{s_{12}s_{15}\mathrm{tr}_+(1234)},$$
$$y_4 = \frac{\langle 13 \rangle \langle 4|p_{23}|1]|}{\langle 23 \rangle \langle 4| 1|2]},$$
$$\sigma_1 = \frac{\langle 13 \rangle \langle 24 \rangle}{\langle 14 \rangle \langle 23 \rangle},$$
$$\sigma_2 = \frac{\langle 13 \rangle \langle 25 \rangle}{\langle 15 \rangle \langle 23 \rangle},$$
$$\sigma_3 = \frac{\langle 13 \rangle \langle 26 \rangle}{\langle 16 \rangle \langle 23 \rangle}.$$

$$(4.13)$$

This amplitude is chosen because it is compact enough but still presents non-trivial features which well exemplify the simplifications made possible by our techniques.

An additional consideration has to be made concerning the phases of the scattering amplitudes. We have already seen in Section 3.4.1 that only phase-free expressions can be expressed in momentum-twistor variables. For this reason before a reconstruction, each amplitude is divided by the momentum helicity factor, as explained in Section 3.4.1. The numerical interpolation that has been discussed in the previous sections is then applied to reconstruct the the phase-free rational part of the amplitude, and the helicity factor is added back at the end of the computation. This will also be the case for the amplitude in all the examples we will discuss in this chapter.

4.3.1 Linear Relations Among the Coefficients

One crucial property which is exploited in the reconstruction of a full QCD amplitude is that the colour-ordered partial amplitudes are not all linearly independent, as stated in 3.1. Instead, knowledge of their associated colour factor can be exploited to find relations among them [73]. Finding such relations is important because it allows to reduce the number of helicity amplitudes that need to be reconstructed to obtain the full-colour expression. Linear relations among functions $c_i(\boldsymbol{x})$ are found by solving the system

$$\sum_i r_i c_i(\boldsymbol{x}) = 0, \tag{4.14}$$

where r_i are rational numbers. Computing the values of the r_i therefore requires many fewer computations than reconstructing the coefficients.

It is often the case that linear combinations of the coefficient are related to known rational functions, in which case the linear system is extended to

$$\sum_i r_i c_i(\boldsymbol{x}) + \sum_i s_i f_i(\boldsymbol{x}) = 0, \tag{4.15}$$

in this case the $f_i(\boldsymbol{x})$ are rational functions which are given as an ansatz and the s_i are rational numbers like the r_i's.

We show the explicit application of the linear relations on the $A_{6g}^{(0)}(-+-+-+)$ amplitude by studying the Kleiss-Kuijf relation

$$
\begin{aligned}
A_{6g}^{(0)}(1^-2^+3^-4^+5^-6^+) = &-A_{6g}^{(0)}(1^-2^+6^+5^-4^+3^-) - A_{6g}^{(0)}(1^-6^+2^+5^-4^+3^-) \\
&- A_{6g}^{(0)}(1^-6^+5^-2^+4^+3^-) - A_{6g}^{(0)}(1^-6^+5^-4^+2^+3^-).
\end{aligned}
\tag{4.16}
$$

it is straightforward to see that Eq. (4.16) is a specific case of Eq. (3.6).

We will use a lighter notation in which the ordering of the external legs is indicated by a label Ω_i, the labels are defined as:

$$
\begin{aligned}
\Omega_1 &= (1^- 2^+ 3^- 4^+ 5^- 6^+) \\
\Omega_2 &= (1^- 2^+ 6^+ 5^- 4^+ 3^-) \\
\Omega_3 &= (1^- 6^+ 2^+ 5^- 4^+ 3^-) \\
\Omega_4 &= (1^- 6^+ 5^- 2^+ 4^+ 3^-) \\
\Omega_5 &= (1^- 6^+ 5^- 4^+ 2^+ 3^-).
\end{aligned}
\tag{4.17}
$$

It is possible to compare the complexity of the amplitudes appearing in Eq. (4.16) by evaluating them over a *univariate slice* modulo a prime number. This means that each variable x_i of the function is substituted in the following way

$$
x_i \rightarrow a_i + b_i t,
\tag{4.18}
$$

where a_i and b_i are integers chosen randomly to avoid spurious cancellations. The result are expressions which only depend on the parameter t. The numerical values are all computed modulo a prime number, in order to reduce the size of the expression. The fact that the substitution makes each variable linear in t makes it possible to compute the total degree of the numerators and denominators from the slice, without the need to reconstruct the full expressions. We recall from Section 4.1 that the degree of the numerator M and denominator M' of a rational function provide the upper bound for the number of numerical points needed for its reconstruction, as expressed by Eq. (4.5). The code takes as an input a list with all the tree amplitudes. We can then gather the information on the degrees for the two different parametrisations.

Parametrisation	$A_{6g}^{(0)}(\Omega_1)$	$A_{6g}^{(0)}(\Omega_2)$	$A_{6g}^{(0)}(\Omega_3)$	$A_{6g}^{(0)}(\Omega_4)$	$A_{6g}^{(0)}(\Omega_5)$
A	28/24	33/29	38/37	32/30	26/21
B	19/18	21/20	25/25	22/22	19/18

Table 4.1: The polynomial degree of the different permutations of the tree amplitudes for both parametrisations. In this notation $\frac{n}{m}$ indicates a numerator of degree n and a numerator of degree m

.

It is shown in Table 4.1 that the expression of $A_{6g}^{(0)}(\Omega_3) = A_{6g}^{(0)}(1^-6^+2^+5^-4^+3^-)$ has the highest polynomial degree in both representations. This means that when performing the reconstruction of the full-colour amplitude it is convenient to avoid the reconstruction of such sub-amplitude and express it in terms of the other ones instead. This procedure has been fully automatised in the code used to derive the amplitudes presented in the following chapters.

In Appendix H one finds an example of the MATHEMATICA code using FINITEFLOW to compute all the possible permutations of $A_{6g}^{(0)}(1^-2^+3^-4^+5^-6^+)$ and finding the linear relations among the resulting expressions.

4.3.2 Factor Matching

One important step that is carried out before starting a reconstruction consists in compiling a list of ansatz factors that we expect parts of the function to factorise into. For tree-level expressions and in the case of one-loop five and six-point helicity amplitudes it was found in many different cases (see for example [1, 109, 112, 113]) that all the factors making up the denominators of the rational coefficients could be guessed in advance, together with some numerator factors. In practice this means that a rational coefficient can be put in the form

$$c(\boldsymbol{x}) = \frac{N(\boldsymbol{x})}{\prod_i D_i(\boldsymbol{x})}, \tag{4.19}$$

and the $D_i(\boldsymbol{x})$, which are irreducible polynomials over $\mathbb{Q}$, can all be included in the ansatz list and therefore don't need to be reconstructed.

The members of the ansatz list for tree-level amplitudes are spinor products and Mandelstam invariants. The first guess for the terms are objects of the form $s_{ij}, s_{ijk}, \langle ij \rangle, [ij]$ and $\langle i| p_{jk} |l]$,

with the indices running over all possible values $i, j, k, l = 1, ..., 6$. Such a list is over-complete, since we expect that not all the terms will be independent of each other. The ansatz is therefore reduced by evaluating all the terms in momentum-twistor variables and only keeping the independent polynomial factors in the resulting expressions. It is convenient to perform this pre-processing step, since having a long list of ansätze will increase the computation time for the evaluation of each individual sample point. The explicit form of the list of ansätze in momentum twistor variables is given in Appendix C.

For the reconstruction of one-loop amplitudes the ansatz list is longer and we included some spinor products and combinations which appear in the denominators of the differential equations for the Master Integrals of a given amplitude [1]. The differential equations become singular as these terms go to zero, so one naturally expects some of them to appear in the denominators of the rational coefficients. This will be exploited for the reconstructions in chapters 5 and 7.

After the ansatz list has been produced, the matching with the rational coefficents is performed over a univariate slice modulo a prime number. This is done by performing substitutions of the type of Eq. (4.18). The result is an expression which only depends on the parameter t and whose factors can be compared with the ones in the ansatz list, evaluated over the same univariate slice. Once again, it is possible to compute the total degree of the numerators and denominators from the slice, as well as the exponents e_i from Eq. (4.19). The total expression is then divided by all the factors that were matched (elevated to the correct exponent), leaving only the unmatched factors. Performing the factor matching allows then to reduce the number of factors that need to be reconstructed, decreasing the number of sample points in the reconstruction.

We show in Table 4.2 the effect of the application of the factor matching to the tree-level amplitude.

Amplitude	Original Degrees	After Matching
$A_{6g}^{(0),\mathrm{A}}(-+-+-+)$	28/24	26/0
$A_{6g}^{(0),\mathrm{B}}(-+-+-+)$	19/18	18/0

Table 4.2: The polynomial degrees of the expressions before and after the factor matching in both parametrisations.

As it was anticipated, we are able to guess all the denominator factors. The notation *number*/0 indicates that no polynomial denominator needs to be reconstructed after the matching. We see that the amplitude has a lower total degree in the second parametrisation. This fact can be used to justify the use of one choice of representation over the other.

Another important set of techniques which can be used to reduce the computational cost of a reconstruction consists in constructing additional polynomial ansätze for the coefficients. In many cases fitting such ansätze requires less computations than directly reconstructing the coefficients. This can be achieved by partial fractioning the expressions, writing them as sums of simpler rational functions. An additional advantage is that the expressions decomposed in such a way are more compact, resulting in files of smaller sizes once they are saved on a computer. In general, a partial fractioning decomposition will generate an ansatz with a higher number of terms. From the point of view of the reconstruction, this has the effect of increasing the evaluation time per single numerical point. This is the case because this method requires to solve a linear system to find the values of the coefficients of the terms in the ansatz. An ansatz with more terms corresponds to an increase in the size of the system. We found, for the coefficients reconstructed in this thesis, that this time increase was balanced in most cases by the fact that a smaller number of points needs to be sampled to fit the total function, since the degrees of the polynomial functions are lower.

Different techniques were developed to perform the partial fractioning on the fly within the FINITEFLOW framework, directly reconstructing expressions in a partial-fractioned form. In the following sections we present three distinct techniques that can be employed to achieve this goal.

4.3.3 Univariate Partial Fractioning

The simplest form of partial fractioning is the one on a univariate function. As discussed in Section 4.1, we can always treat a multivariate function as a univariate one by treating all variables but one as constants. If we have a function depending on variables $\{y, x_1, x_2, ..., x_n\} = \{y, \boldsymbol{x}\}$ we can write it, without loss of generality, as

$$f(y, \boldsymbol{x}) = \frac{N(y, \boldsymbol{x})}{\prod_i^n D_i(y, \boldsymbol{x})^{e_i}}, \tag{4.20}$$

taking only y as a variable.

It is possible that some denominator factors will not have any dependence on y, $\tilde{d}_k = \tilde{d}_k(\boldsymbol{x})$; in this context they will have no effect on the partial fractioning, and we can treat the term $\frac{1}{\tilde{d}_1 \ldots \tilde{d}_n}$ as a factor that multiplies the whole expression and whose reconstruction will be unaffected by the decomposition. For this reason for the rest of the discussion we only treat the d_i that have a y dependence, remembering that the presence of any extra denominator will not change the computations. This is especially true in the cases in which all the denominator factors are guessed via factor matching.

We can write down an ansatz for the partial fractioned expressions with respect to y, the notation will be similar to the one used in [112], where this technique was first used for reconstructions performed with FINITEFLOW:

$$f(y, \boldsymbol{x}) = \sum_i^n \sum_{j=1}^{e_i} \sum_{k=0}^{d_j-1} \frac{n_{ijk}(\boldsymbol{x}) y^k}{D_i(y, \boldsymbol{x})^j} + \Theta(d_N - d_Q) \sum_{i=1}^{d_{NUM}-d_Q} n'(\boldsymbol{x}) y^i + R(\boldsymbol{x}). \qquad (4.21)$$

Where we defined $d_i = \deg(D_i)$, $d_{NUM} = \deg(N)$ and $d_Q = \sum_i^n d_i e_i$, where all the degrees are with respect to the variable y. We see that the rightmost term in Eq. (4.21) is only present if the denominator has a higher total degree than the numerator in the variable y. It is possible to use the above ansatz to set up a linear system for coefficients $n_{ijk}(\boldsymbol{x})$, $n'(\boldsymbol{x})$ and $R(\boldsymbol{x})$, in the case in which all the coefficients $D_i^{e_i}$ are known analytically. This means that the univariate apart can only be used in conjunction with the factor matching algorithm described in the previous section.

We reiterate here a point already mentioned at the end of Section 4.3.2, namely that having a longer ansatz for each coefficient increases the evaluation time per each individual sampled point. This can be understood if we imagine having a generic rational function $f(y, \boldsymbol{x})$, for which we have an ansatz made up of m terms $f_i(y, \boldsymbol{x})$

$$f(y, \boldsymbol{x}) = \sum_i^m c_i(\boldsymbol{x}) f_i(y, \boldsymbol{x}). \qquad (4.22)$$

If we then want to evaluate the function at a specific numerical point, we need to solve a system with m equations to find the values of all the c_i at that point. Therefore, we expect the time to

evaluate the whole function at a single point to scale linearly with the number of terms m [100]. This is indeed what we observed in our work when reconstructing scattering amplitudes.

As stated before, the choice of the variable to partial fraction with respect to is arbitrary; different choices normally lead to very different representations of the expressions. A code in MATHEMATICA was written so to evaluate the impact of the partial fractioning with respect to each different variable, comparing the total degree of the polynomials which needed to be reconstructed after the decomposition. This is done by performing partial fractioning on different univariate slices and allows us to make the choice which most reduces the complexity of the computation.

When the different choices of variable are tested on $A_{6g}^{(0)}(-+-+-+)$, it is found that the one for which there is the biggest drop in complexity is x_8 in parametrisation A and y_4 in parametrisation B. In Table 4.3 we report the polynomial degree of the expression after each stage in the algorithm, to show the simplifications.

Amplitude	Original Degrees	Stage 1	Stage 2	Stage 3
$A_{6g}^{(0),\text{A}}(-+-+-+)$	28/24	26/0	17/11	4/4
$A_{6g}^{(0),\text{B}}(-+-+-+)$	19/18	18/0	11/8	2/0

Table 4.3: The polynomial degree of the expressions to be reconstructed in each stage, when using the univariate partial-fractioning. Again, in this notation n/m indicates a numerator of total degree n and a denominator of total degree m. The total degrees is computed over the remaining variables **x**.

The stages in the table indicate the methods that have been applied in sequence. Stage 1 consists in the matching of factors from the list of ansätze. Once the factors are matched they are multiplied out, reducing the size of the polynomial, as explained in Section 4.3.2. The values for Stage 2 indicate the maximum degrees of the terms in the ansatz of form Eq. (4.21), we notice that the partial fractioning has decreased the complexity of the expression. This is to be expected also because, after the partial fractioning, the expression depends on one fewer variable than the original one. In Stage 3 the terms are again matched with the list of ansätze, dividing out the matched

terms as in Stage 1. We see that again the degrees are lower at each stage for parametrisation B. Having final polynomials of degree 2/0 indicates that all the factors of the denominators have been matched with the ansätze and a polynomial of total degree 2 in the numerator is the only factor left to reconstruct.

We can then see that the power of the partial fractioning in this case consists in recasting the expression in a form from which it is possible to identify most of its factors as ones present in the original ansatz. We will see in the next section what are the differences when a *multivariate* partial fractionning is performed.

4.3.4   Multivariate Apart Reconstruction

After having discussed partial fractioning in one variable, in this section we briefly outline the algorithm we employed to perform the partial fractioning of a function with respect to multiple variables and how it was used within the finite-field reconstruction framework. This decomposition was implemented exploiting the package MULTIVARIATEAPART [114]. We first briefly give some mathematical definitions needed to understand the steps in the algorithm, following the same exposition as [114]. This section will not go into the mathematical details or proofs, for a more comprehensive reading on the topic the reader is redirected to [115].

We start by defining polynomials $p_i(\boldsymbol{x})$ which belong to a *polynomial ring* $\mathbb{Q}[\boldsymbol{x}]$. So that

$$p(\boldsymbol{x}) = \sum_i c_i \boldsymbol{x}^{\alpha_i}, \tag{4.23}$$

where coefficients c_i belong to the field of rational numbers $\mathbb{Q}$, $\boldsymbol{x} = \{x_1..., x_n\}$ are the variables and α_i are vectors of integers. All the polynomials of momentum-twistor variables discussed in this chapter belong to $\mathbb{Q}[\boldsymbol{x}]$.

Since we are considering the dependence of the function on more than just one variable, one essential step consist in defining a *monomial ordering* among the different variables. For a monomial set of twistor variables

$$M \equiv \{x^a \equiv x_1^{a_1} \cdots x_n^{a_n} | a_i \in \mathbb{Z}^{0+}\}, \tag{4.24}$$

a monomial ordering $\prec$ must satisfy the two conditions:

1. $x^a \prec x^b \implies x^{a+c} \prec x^{b+c}$ for all c,

2. $1 \prec x^a$ for all a .

If, for example, the ordering $x \prec y$ is established, then we can order the monomials in polynomial $p(x, y) = x^3 y^2 + y^4 + x^8$ as $\{x^8, x^3 y^2, y^4\}$, and the rightmost term can be interpreted as the *greatest* in this ordering. The *leading term* in the polynomial will then just be the greatest monomial: $\mathrm{LT}(p) = y^4$.

Defining an ordering for the monomials allows us to perform *polynomial reductions*, which will be the key operation to perform the decomposition. If for some term t of polynomial p_1 there exists a polynomial u such that $t = u \times \mathrm{LT}(p_2)$, then we say that p_1 reduces to p_1' modulo polynomial p_2 if $p_1' = p_1 - u \times p_2$ [115].

Polynomial reduction is used to express a polynomial p as a linear combination of other polynomials g_i

$$p(\boldsymbol{x}) = \sum_i f_i(\boldsymbol{x}) g_i(\boldsymbol{x}) + R(\boldsymbol{x}), \tag{4.25}$$

where $f_i(\boldsymbol{x}) \in \mathbb{Q}[\boldsymbol{x}]$ and $R(\boldsymbol{x})$ is a polynomial reminder. We can then define an *ideal I* with *generators* g_i, $I = < g_1(\boldsymbol{x}), ..., g_n(\boldsymbol{x}) >$, as the set of all polynomials for which we can find a decomposition like Eq. (4.25) with $R(\boldsymbol{x}) = 0$ [115]. We will see that the definition of a partial-fractioning method is strictly related, in the implementation of MULTIVARIATEAPART, to the *membership problem* [102, 114]. This problem consists in determining whether a given polynomial belongs to an ideal. The problem is non-trivial in general, since a decomposition of the form of Eq. (4.25) is not unique; it is therefore possible to have $p_i(\boldsymbol{x}) \in I$, but obtaining a general reduction with $R(\boldsymbol{x}) \neq 0$. It is nevertheless possible to compute a *Groebner basis* of the set of the generators, which is a set of polynomials which ensure that a given polynomial $p_i(\boldsymbol{x})$ will be in I if and only if the remainder of its polynomial reduction is zero, thus solving the membership problem [102]. Given a set of generators $g_i(\boldsymbol{x})$, it is always possible to calculate the Groebner basis $\hat{g}_i(\boldsymbol{x}) = \sum_j h_{ij}(\boldsymbol{x}) g_j(\boldsymbol{x})$, where $h_{ij}(\boldsymbol{x})$ are again polynomials.

Calculating a Groebner basis can be computationally expensive, in the most complicated cases

dedicated computer algebra systems such as SINGULAR [116] can be exploited to obtain it. This technology can then be exploited to achieve the decomposition of a function of the form of Eq. (4.19). This is done by taking the set of irreducible denominators D_i and defining the ideal

$$I = < q_1 D_1(\boldsymbol{x}) - 1, q_2 D_2(\boldsymbol{x}) - 1, ..., q_n D_n(\boldsymbol{x}) - 1 >, \tag{4.26}$$

thus introducing the new set of variables q_i. It is important to stress that a new monomial ordering must be defined, including the new variables. The function is then re-written as $c(\boldsymbol{x}, \boldsymbol{q}) = N(\boldsymbol{x})q_1 \ldots q_n$. The next step consists of computing the Groebner basis of I and using it to perform the polynomial reduction of $c(\boldsymbol{x}, \boldsymbol{q})$. We can then express the reduction in terms of the original generators and get

$$N(\boldsymbol{x}) \prod_i q_i(\boldsymbol{x}) = \sum_i f_i(\boldsymbol{x}) \hat{g}_i(\boldsymbol{x}) + R(\boldsymbol{x}) = \sum_i \sum_j f_i(\boldsymbol{x}) h_{ij}(\boldsymbol{x})(q_j(\boldsymbol{x}) D_j(\boldsymbol{x}) - 1) + R(\boldsymbol{x}), \tag{4.27}$$

where again we have the polynomials $f_i(\boldsymbol{x}) \in \mathbb{Q}[\boldsymbol{x}]$.

It is straightforward to see that restoring the condition $q_i(\boldsymbol{x}) = \frac{1}{d_i(\boldsymbol{x})}$ is equivalent to setting the terms $q_i D_i(\boldsymbol{x}) - 1$ to zero. This means that after the reduction, the remainder will be the partial fractioned expression. The use of Groebner basis ensures that the resulting $R(\boldsymbol{x})$ is unique. This procedure does not introduce any new denominator factors.

The above procedure makes it possible to partial fraction a multivariate function of which the analytical expression is known. This is not the case for functions which are being reconstructed with FINITEFLOW, so it is necessary to take a hybrid approach: the rational functions are reconstructed over a n-variate slice, and that expression is then partial fractioned using MULTIVARIATEAPART. Similarly to a univariate slice, an n-variate one is computed by setting all variables to integer numerical values modulo a prime, with the exception of a subset of n of them. Such a slice is fast to evaluate for $n = 2, 3$ (the reconstruction time is of the order of tens of seconds for polynomials known analytically with degrees as high as 90). In most of the applications we employed slices of two variables, so in the rest of the section we will focus on bi-variate slicing, remembering that the

discussion can be straightforwardly extended to an arbitrary number of variables.

We define the rational function as in Section 4.3.3, with the difference that now we have two variables that the function depends on: $\{y_1, y_2\}$. So we write

$$f(y_1, y_2, \boldsymbol{x}) = \frac{N(y_1, y_2, \boldsymbol{x})}{\prod_i^n D_i(y_1, y_2, \boldsymbol{x})^{e_i}}, \tag{4.28}$$

we again only consider the denominators that have a dependence on at least one between y_1 and y_2. The bi-variate slice is then computed by setting the variables $\boldsymbol{x}$ to numerical values, modulo a prime number. The MULTIVARIATEAPART package is then applied to the slice.

We show the steps of the algorithm with the simple example of a function of three variables $\{y_1, y_2, x_3\}$

$$f(y_1, y_2, x_3) = \frac{y_1^3 + y_2^2 x_3^2}{y_1^2(7y_1 + y_2)(y_2 + y_1 x_3)}, \tag{4.29}$$

where we assume to know the three (algebraically independent) denominators $D_1 = x_1$, $D_2 = 7x_1 + x_2$, $D_3 = x_2 + x_1 x_3$ and the powers with which they appear in the function. We take a bi-variate slice by setting $x_3 \to 13$ and evaluating each numerical value modulo a prime number 5 (in the real applications both the random number for the substitution and the prime number need to be much higher, as explained in Section 4.2),

$$f_{sliced} = \frac{y_1^3 + 4y_2^2}{y_1^2(2y_1 + y_2)(3y_1 + y_2)}. \tag{4.30}$$

We can then apply MULTIVARIATEAPART with the ordering $y_1 \prec y_2$ to obtain

$$f_{sliced} = \frac{4}{y_1^2} + \frac{1}{(2y_1 + y_2)} + \frac{1}{y_1(2y_1 + y_2)} - \frac{1}{3y_1 + y_2} - \frac{1}{y_1(3y_1 + y_2)}. \tag{4.31}$$

We recognise $x_1, (2x_1 + x_2), (3x_1 + x_2)$ as D_1, D_2, D_3 respectively, evaluated over the slice. So we are able to fully reconstruct the denominators of the terms in Eq. (4.31). The bi-variate ansatz for the numerator of $f(y_1, y_2, x_3)$ is then obtained by multiplying each term in Eq. (4.31) by the full denominator $x_1^2(2x_1 + x_2)(3x_1 + x_2)$, and substituting any numerical pre-factor with a coefficeint

which will depend on x_3. We then have

$$N(y_1, y_2, x_3) = c_1(7y_1 + y_2)(y_2 + y_1 x3) + c_2 y_1^2(y_2 + y_1 x_3)+$$

$$c_3 y_1(y_2 + y_1 x_3) + c_4 y_1^2(7y_1 + y_2) + c_5 x1(7y_1 + y_2). \tag{4.32}$$

where the coefficeints c_i are all functions of the remaining variable x_3: $c_i \equiv c_i(x_3)$. It is then possible to set-up a linear system to evaluate the coefficients $c_i(x_3)$ over many numerical points. This allows FINITEFLOW to fully reconstruct $N(y_1, y_2, x_3)$.

In many cases which we have studied, the ansatz was longer in the multivariate case than in the univariate one, this means that the multivariate apart reconstruction was convenient only if the decrease in polynomial degrees was great enough to balance this.

Like in the univariate case, the choice of the subsets of variables y_1 and y_2 in Eq. (4.29) is arbitrary. In order to make an optimal choice the same strategy as the one described in the previous section is adopted: a MATHEMATICA script was written in order to compare the degrees of the different ansätze for each different choice of variables. This computation can be done on a *bi-variate* slice, without the need to perform any full reconstruction. It is then possible to choose the variables which minimise the complexity of the complete numerical reconstruction. We apply the bi-variate partial fractioning to the alternating helicity amplitude. The best choice of variables is found to be x_4, x_5 for parametrisation A and y_3, y_4 for parametrisation B. We report the degrees at the different stages as in the previous section.

Amplitude	Original Degrees	Stage 1	Stage 2	Stage 3
$A_{6g}^{(0),\mathrm{A}}(-+-+-+)$	28/24	26/0	17/9	0/0
$A_{6g}^{(0),\mathrm{B}}(-+-+-+)$	19/18	18/0	12/6	0/0

Table 4.4: The polynomial degrees of the expressions to be reconstructed in each stage, when using the multivariate partial fractioning

The degrees after Stage 1 are the same as in Table 4.3 for both parametrisations, since the same factor matching procedure is applied. After Stage 2 we show the degrees of the ansatz for the partial

fractioned expression. In this case the second factor matching performed in Stage 3 matches all the numerator factors of the amplitude in both representations. For such cases one only needs to reconstruct some rational number, and the number of evaluations is much smaller. The evaluation was performed almost instantaneously in these cases for the expressions computed in this thesis.

4.3.5 Partial Fractioning with BCFW-like shifts

In this section we describe a last partial fractioning method which has proven to be useful in the reconstruction of tree-level and one loop helicity amplitudes. The algorithm is based on the application of a complex shift of the same type as the one in Eq. (3.83). Once the shift is performed the rational expressions will have singularities for specific values of the variable z. Since the momentum-twistor parametrisation enables one to express the spinors as two-vectors in twistor variables, Eqs. (3.21) can easily be computed in terms of the x_i, allowing the evaluation of any spinor structure in the shifted phase-space. One additional technical detail comes from the fact that the shift will have a normalisation associated to them, added so that phases are not affected. For a $\{\langle i| , [j|\}$ shift the normalisation has form $\langle i| p_k |j]$ (with $k \neq i, j$), so that the shift assumes the phase-free expression $\frac{z|i\rangle[j|}{\langle i| p_k |j]}$.

We show explicitly the form of the shifted spinors for a $\{\langle 1| , [2|\}$ shift in both parametrisations A and B, since this is the one that we will use on the $A_{6g}^{(0)}(- + - + -+)$ amplitude. Shift with parametrisation A:

$$\langle 1| \to \langle 1| - z \frac{\langle 2|}{\langle 1| 3 |2]} = (1, 0) - \frac{z}{x_1^2 x_5} \times (0, 1) = \left(1, -\frac{z}{x_1^2 x_5}\right), \tag{4.33}$$

$$[2| \to [2| + z \frac{[1|}{\langle 1| 3 |2]} = (-x_1, 0) + z \frac{z}{x_1^2 x_5} \left(\frac{x_8}{x_5} - 1, 1\right) = \left(-x_1 + z \frac{(x_5 - x_8)}{(x_1^2 x_5^2)}, -\frac{z}{x_1^2 x_5}\right). \tag{4.34}$$

Shift with parametrisation B:

$$\langle 1| \rightarrow \langle 1| - z \frac{\langle 2|}{\langle 1| \, 3 | 2]} = (1,0) - z \frac{\sigma_1 - 1}{s_{12}^2 y_1} \times (0,1) = \left(1, -z \frac{\sigma_1 - 1}{s_{12}^2 y_1}\right), \tag{4.35}$$

$$[2| \rightarrow [2| + z \frac{[1|}{\langle 1| \, 3 | 2]} = (-s_{12}, 0) + z \frac{\sigma_3 - 1}{s_{12}^2 y_1} \left(\frac{y_3 - 1}{y_1}, 1\right) = \left(-s_{12} - z \frac{(-1 + \sigma_1)(-1 + y_4)}{s_{12}^2 y_1^2}, -z \frac{\sigma_1 - 1}{s_{12}^2 y_1}\right). \tag{4.36}$$

The algorithm relies on the creation of a list of ansätze for the possible linear poles in z. This can be easily constructed by selecting the terms in the general ansatz list which are phase-free. Since in our case all the denominator factors can be matched, the ansätze for the linear poles are just the terms which are linear in z once they are evaluated in the shifted phase-space. At the tree-level case the position of the poles in z and the factorisation properties of the amplitude have already been discussed in Section 3.3. For one loop expressions, it is possible for the shift to give rise to poles which are not linear in z. Additionally, as briefly discussed in Section 3.8, a shifted one-loop amplitude of arbitrary helicity can have a non-zero residue for $z \rightarrow \infty$. We list the steps followed by the algorithm in order to clarify how these issues are approached.

1. Perform the factor matching to decrease the polynomial degree of the expression.

2. Compute the list of poles ansätze on the shifted phase space (as functions of z and the twistor variables) and then evaluate them on a univariate slice.

3. Evaluate the full function on the same univariate slice and match the denominators with z dependence with the ones in the pole ansatz.

4. For each pole linear in z:

   - solve the equation $pole = \delta$ for z and substitute the solution inside the expression,

   - compute the first term of the Laurent series of the expression around $\delta \rightarrow 0$,

   - perform the factor matching on the residue and then reconstruct it.

5. Subtract all the reconstructed terms from the expression.

6. Perform the factor matching on the remainder and reconstruct it.

So we see that in the algorithm only the residues for linear poles are reconstructed, any additional term which comes from non-linear singularities, together with the singularity at infinity, is treated as a remainder which is computed after all the residues have been subtracted. It is often found that after the residues have been subtracted the reminder has a polynomial degree which is much lower than the one of the original expression, making the reconstruction easier.

We show in Table 4.5 how the algorithm performs when used to reconstruct the alternating helicity amplitude. Since the expression is a tree-level amplitude we do not encounter poles not linear in z or residues at infinity.

Amplitude	Original Degrees	Residue s_{16}	Residue s_{23}	s_{156}	Remainder
$A_{6g}^{(0),A}(-+-+-+)$	28/24	0/0	0/0	0/0	0/0
$A_{6g}^{(0),B}(-+-+-+)$	19/18	0/0	0/0	0/0	0/0

Table 4.5: The polynomial degree of each residue, plus the degree of the remainder after both residues have been subtracted.

After this analysis we see that both the reconstruction which exploits multivariate partial fractioning and the one with BCFW shifts make it possible to decompose the amplitude into factors which were included in the original list of ansätze (the final polynomial degrees were 0/0 in both cases). In order to differentiate between the two methods, we present the expression which are obtained using the two different reconstruction algorithms. We choose to only present the expressions written in the parametrisation B; their form in parametrisation A is less compact but not significantly different for this analysis. In order to have more readable expressions, we write them in terms of the polynomials g_i which were matched from the ansatz list. We give the polynomials explicitly as functions of momentum-twistor variables.

$$A_{6g}^{(0),\text{MVA}}(-+-+-+) = \frac{32g_{15}^4}{y_1 g_1 g_{14} g_{16} g_{17} g_3 g_4} - \frac{32y_1 g_4^3 g_6^3}{g_1 g_{10} g_{13} g_{16} g_3 g_7} + \frac{32y_1 g_3^3 g_8^3}{g_1 g_{11} g_{12} g_{14} g_4 g_7} \tag{4.37}$$
$$+ \frac{32g_6^3}{y_1 y_2 g_1 g_3 g_4 g_9 g_{23}} + \frac{32g_6^4}{y_1 y_2 y_3 g_1 g_{12} g_3 g_4 g_{23}} - \frac{32y_1 g_2^4 g_8^3}{y_2 g_1 g_3 g_4 g_5 g_{24}}$$
$$+ \frac{32y_1 g_2^4 g_8^4}{y_2 g_1 g_{13} g_{18} g_3 g_4 g_{24}}$$

$$A_{6g}^{(0),\text{BCFW}}(-+-+-+) = -\frac{32g_{19}^4 g_{22}}{y_1 g_1 g_{10} g_{11} g_{17} g_{20} g_{21} g_3 g_4} + \frac{32 y_1^3 g_2^4 g_{22} g_8^4}{y_2 g_1 g_{18} g_{21} g_3 g_4 g_5}$$
$$- \frac{32 g_{22} g_6^4}{y_1 y_2 y_3 g_1 g_{20} g_3 g_4 g_9} \tag{4.38}$$

$$\{g_1 = \sigma_1 - 1, g_2 = \sigma_2 - 1, g_3 = \sigma_1 - \sigma_2, g_4 = \sigma_2 - \sigma_3, g_5 = y_3 - y_2 y_4, \tag{4.39}$$

$$g_6 = y_1 \sigma_2 + y_2 - y_1 - \sigma_1 y_2, g_7 = \sigma_1 - \sigma_2 + \sigma_2 y_1 - \sigma_3 y_1 - \sigma_1 y_2 + \sigma_3 y_2, g_8 = y_2 - 1,$$

$$g_9 = \sigma_2 y_1 - \sigma_1 y_2 + y_3,$$

$$g_{10} = \sigma_1 y_1 - \sigma_2 y_1 + \sigma_2 y_1^2 - \sigma_3 y_1^2 - \sigma_1 y_1 y_2 + \sigma_3 y_1 y_2 - y_3 + \sigma_1 y_3 + y_1 y_3 - \sigma_3 y_1 y_3 - y_1 y_4 +$$

$$\sigma_2 y_1 y_4 + y_2 y_4 - \sigma_1 y_2 y_4,$$

$$g_{11} = y_1 y_3 - y_3, g_{12} = y_1 - y_2, g_{13} = -1 + \sigma_2 + y_2 - \sigma_3 y_2,$$

$$g_{14} = y_1 - 1, g_{15} = \sigma_1 + y_1 - \sigma_2 y_1 - 1, g_{16} = y_1 + \sigma_1 - \sigma_3 y_1 - 1, g_{17} = y_4 + y_1 - 1,$$

$$g_{18} = \sigma_2 y_1 - \sigma_3 y_1 y_2 + y_3 - y_2 y_4,$$

$$g_{19} = -\sigma_1 y_1 + \sigma_2 y_1 + \sigma_1 y_1 y_2 - \sigma_2 y_1 y_2 + y_3 - \sigma_1 y_3 - y_1 y_3 + \sigma_2 y_1 y_3 + y_1 y_4 - \sigma_2 y_1 y_4 - y_2 y_4 + \sigma_1 y_2 y_4,$$

$$g_{20} = y_1 - y_2 + y_3, g_{21} = -y_1 + y_1 y_2 - y_3 + y_2 y_4, g_{22} = s_{12}, g_{23} = y_1 \sigma_2 - y_2 \sigma_1\}$$

We notice that the MVA reconstruction gives an expression which is broken down into a larger number of terms, while the output of the BCFW reconstruction is shorter. In this case it appears that the BCFW option is preferable. The difference in $A_{6g}^{(0),\text{MVA}}(-+-+-+)$ and $A_{6g}^{(0),\text{BCFW}}(-+-+-+)$ is quite small, but for more complex one-loop cases a comparison of the size of the output expressions (proportional to the output file size) can indicate which algorithm is preferable for a specific amplitude. We also note that neither Eq. (4.37) nor Eq. (4.38), when written in momentum-twistor variables, is as compact as the amplitude in spinor form of Eq. (4.9). This is not an issue, since all the factors have been matched to an ansatz and can always be labelled in the way done in Eqs. (4.37) and (4.38). For most amplitudes, compact forms such as Eq. (4.9) can only be obtained after they have been computed in some specific representation, and then spinor identities are applied to simplify them. One advantage of the reconstruction methods described in this chapter is that in some cases the expressions can be reconstructed directly in a compact form.

In the next chapter we will see how many of the methods described so far were applied to compute physical amplitudes with massive quarks. We will see that finite field reconstruction methods were essential to obtain the desired analytic form of the amplitudes.

Chapter 5

One-loop QCD Amplitudes for $pp \to t\bar{t}j$ to $O(\epsilon^2)$

5.1 Introduction

This chapter has the main aim of discussing the work presented in [1], in which we compute the helicity amplitudes for the one-loop corrections in QCD to top-quark pair production up to second order in the dimensional regulator ϵ.

NLO corrections to $pp \to ttj$ have been known for a long time [117], putting the precision frontier at NNLO. This process is of particular interest because it is extremely sensitive to the top quark mass [118]. The analytical expressions that we computed are needed to carry out a comprehensive phenomenological study of the process. This is the case since, as we have seen in Section 2.6, the one-loop amplitude enters squared in the computation of the NNLO cross-section; this indicates that its expression must be known up to the $O(\epsilon^2)$ expansion. It must be specified that we know from [119] that a full NNLO result in four dimensions, $O(\epsilon^0)$, can in theory be obtained without the need to compute these one-loop corrections up to second order in ϵ, since various cancellations make them drop out from the final expression. Nevertheless, the procedure described in [119] is only applicable if one has full control on how the double-virtual contribution is computed, as explained

in [120]. Since this is in general not the case, and various contributions are normally computed by different research groups, our results are the most suitable for phenomenological studies.

It is important to stress that obtaining the form of the amplitudes expanded to higher orders in the dimensional regulator ϵ is a highly non-trivial endeavour, and it poses significant computational challenges which are not encountered in the $O(\epsilon^0)$ computation. We have found that the algebraic complexity of the coefficients of the integral basis is comparable with the ones of the same amplitude evaluated at two loops.

In order to perform these computations, we exploited many techniques described in chapters 3 and 4. New methods employed for these specific calculations are also presented. The contents of this chapter will show to the reader how the theoretical methods discussed so far are put into practice for a real phenomenological computation, highlighting how the different techniques are used in a single computational framework which yields high-precision results. The results obtained in the project made it possible to look at the NNLO complexity for the first time, demonstrating that the finite field reconstruction techniques are suited to tackle the complexity of the full NNLO expressions.

This chapter is organised as follows. In Section 5.2 we show how the amplitudes were decomposed according to their colour factors and the quark flavours. The use of spinor-helicity representations for massive fermions is also discussed. In Section 5.3 we describe how we use a specific representation in which each amplitude is expressed as a linear combination of four gauge-invariant phase-free objects. We also outline the steps of the computation, from the creation of the Feynman diagrams to the numerical evaluation of the amplitudes. Sections 5.4 and 5.5 focus on the definition of the MIs basis via the Integration By Parts identities and their numerical evaluation using the differential equation method, while in Section 5.6 we provide details on the renormalisation of the sub-amplitudes. In Section 5.7 we show how partial fractioning the tree-level $\bar{t}tggg$ expressions and collecting the top mass helps in their representation. This discussion helps explaining the choices for the rational reconstruction of the one-loop results in Section 5.8. In Section 5.9 we describe the pole structure of the amplitudes, the results are discussed in Section 5.10.

5.2   Colour Decomposition and Kinematic Setup

We defined the momenta in the two $pp \to t\bar{t}j$ partonic channels as all outgoing. We then must consider the amplitudes for two distinct processes:

- $0 \to t\bar{t}ggg$,

- $0 \to t\bar{t}\bar{q}qg$.

The colour decomposition for the $0 \to t\bar{t}ggg$ amplitude is [121]:

$$
\mathcal{A}^{(L)}(1_{\bar{t}}, 2_t, 3_g, 4_g, 5_g) = g_s^{3+2L} N_\epsilon^L \Bigg\{
$$
$$
\sum_{\sigma \in S_3} (t^{a_{\sigma(3)}} t^{a_{\sigma(4)}} t^{a_{\sigma(5)}})_{i_2}^{\bar{i}_1} A_1^{(L)}(1_{\bar{t}}, 2_t, \sigma(3)_g, \sigma(4)_g, \sigma(5)_g)
$$
$$
+ \sum_{\sigma \in S_3/\mathbb{Z}_2} \delta^{a_{\sigma(3)} a_{\sigma(4)}} (t^{a_{\sigma(5)}})_{i_2}^{\bar{i}_1} A_2^{(L)}(1_{\bar{t}}, 2_t, \sigma(3)_g, \sigma(4)_g, \sigma(5)_g)
$$
$$
+ \sum_{\sigma \in S_3/\mathbb{Z}_3} \mathrm{tr}(t^{a_{\sigma(3)}} t^{a_{\sigma(4)}} t^{a_{\sigma(5)}}) \delta_{i_2}^{\bar{i}_1} A_3^{(L)}(1_{\bar{t}}, 2_t, \sigma(3)_g, \sigma(4)_g, \sigma(5)_g) \Bigg\}.
$$
$$(5.1)$$

S_3 is the group of the six permutations of three elements, while $\frac{S_3}{\mathbb{Z}_2}$ and $\frac{S_3}{\mathbb{Z}_3}$ are smaller symmetry groups of three and two elements each. The normalisation constant is:

$$
N_\epsilon = \frac{e^{\epsilon \gamma_E} \Gamma^2(1-\epsilon) \Gamma(1+\epsilon)}{(4\pi)^{2-\epsilon} \Gamma(1-2\epsilon)} \, .
$$
$$(5.2)$$

The number of loops L is kept generic in these formulas. In this chapter we will apply them for the cases $L = 0, 1$. The strong coupling constant is indicated with g_s. As explained in Chapter 2 , the $(t^a)_i^{\bar{j}}$ matrices represent the fundamental generators of the $SU(N_c)$ gauge group, with $a = 1, ..., N_c^2 - 1$ being the adjoint indices while i and $\bar{j}$ are the fundamental and anti-fundamental ones respectively. We present the decomposition for process $0 \to t\bar{t}\bar{q}qg$ following the same conventions (see for example

[122]):

$$\mathcal{A}^{(L)}(1_{\bar{t}}, 2_t, 3_q, 4_{\bar{q}}, 5_g) = g_s^{3+2L} N_\epsilon^L \Bigg\{$$

$$\delta_{i_1}^{\bar{i}_4} (t^{a_5})_{i_3}^{\bar{i}_2} A_1^{(L)}(1_{\bar{t}}, 2_t, 3_{\bar{q}}, 4_q, 5_g)$$

$$+\delta_{i_2}^{\bar{i}_3} (t^{a_5})_{i_1}^{\bar{i}_4} A_2^{(L)}(1_{\bar{t}}, 2_t, 3_{\bar{q}}, 4_q, 5_g)$$

$$-\frac{1}{N_c} \delta_{i_1}^{\bar{i}_2} (t^{a_5})_{i_3}^{\bar{i}_4} A_3^{(L)}(1_{\bar{t}}, 2_t, 3_{\bar{q}}, 4_q, 5_g)$$

$$-\frac{1}{N_c} \delta_{i_3}^{\bar{i}_4} (t^{a_5})_{i_1}^{\bar{i}_2} A_4^{(L)}(1_{\bar{t}}, 2_t, 3_{\bar{q}}, 4_q, 5_g) \Bigg\}. \tag{5.3}$$

The $A_i^{(L)}$ sub-amplitudes can be further decomposed into rational expressions depending on kinematic invariants, number of colours N_c and number of light flavours n_f (note that the number of heavy flavours is taken to be $n_h = 1$ throughout this chapter, so we omit that extra variable in our expressions). These additional decompositions for the $0 \to \bar{t}tggg$ channel are

$$A_1^{(0)} = A_{1;0}^{(0)} = A^{(0)}, \tag{5.4}$$

$$A_2^{(0)} = 0, \tag{5.5}$$

$$A_3^{(0)} = 0, \tag{5.6}$$

$$A_1^{(1)} = N_c A_{1;1}^{(1)} + \frac{1}{N_c} A_{1;-1}^{(1)} + n_f A_{1;0}^{(1),f} + A_{1;0}^{(1),h} \tag{5.7}$$

$$A_2^{(1)} = A_{2;0}^{(1)}, \tag{5.8}$$

$$A_3^{(1)} = A_{3;0}^{(1)}, \tag{5.9}$$

and for the $0 \to \bar{t}tq\bar{q}g$ channel

$$A_X^{(0)} = A_{X;0}^{(0)}, \tag{5.10}$$

$$A_X^{(1)} = N_c A_{X;1}^{(0)} + \frac{1}{N_c} A_{X;-1}^{(1)} + n_f A_{X;0}^{(1),f} + A_{X;0}^{(1),h}, \tag{5.11}$$

where $X = 1, ..., 4$. The subscripts after the semicolon in the above equations refer to the power of N_c multiplying the expressions.

$0 \to \bar{t}tggg$	$+++++$	$++++-$	$+++-+$
$0 \to \bar{t}t\bar{q}qg$	$+++-+$	$++-++$	$+++--$

Table 5.1: Independent helicity configurations of one-loop amplitudes for both channels. We have three independent ones for each channel. The justification for only considering top quarks with positive helicity comes from the parametrisation of massive quarks given below.

Knowledge of the symmetries of the amplitudes allows us to only compute a subset of all the possible helicity configurations, knowing that the missing expressions can be derived applying specific operations to the computed ones. Parity conjugation allows to exchange the helicities of the massless quarks in the expression

$$A^{(1)}(1_{\bar{t}}^-, 2_t^+, 3_q^-, 4_q^+, 5_g^+) \xrightarrow{h_3 \leftrightarrow h_4} A^{(1)}(1_{\bar{t}}^+, 2_t^-, 3_q^+, 4_q^-, 5_g^+). \tag{5.12}$$

Further symmetries are inherited from the colour structures multiplying the sub-amplitudes, as explained in Section 3.1. The subsets of independent helicities for each channel are listed in Table 5.1.

We now outline how the spinor-helicity formalism was employed to express the helicity states of massive fermions, which made it possible to retain the dependence of the amplitudes on the mass of the top quark. The method employed was presented in [123] and used in other works such as [124], where the reader can find a thorough exposition of the results briefly shown here. The notation used will be the one of [1].

Given a particle of mass m with momentum p such that

$$p^\mu p_\mu = p^2 = m^2, \tag{5.13}$$

we can define an arbitrary massless reference vector n and an additional vector

$$p^{\flat,\mu} = p^\mu - \frac{m^2}{2p \cdot n} n^\mu. \tag{5.14}$$

Vector $p^{\flat,\mu}$ is constructed so to be massless: $(p^\flat)^2 = 0$.

It is then possible to construct spinors

$$u_+(p,m) = \frac{(\not{p}+m)\,|n\rangle}{\langle p^\flat n\rangle}, \qquad u_-(p,m) = \frac{(\not{p}+m)|n]}{[p^\flat n]},$$

$$v_-(p,m) = \frac{(\not{p}-m)\,|n\rangle}{\langle p^\flat n\rangle}, \qquad v_+(p,m) = \frac{(\not{p}-m)|n]}{[p^\flat n]} \tag{5.15}$$

which satisfy the Dirac equation for any generic massless vector n. Explicitly, we see:

$$(\not{p}-m)u_\pm(p,m) \propto (p^2 - m^2) = 0, \tag{5.16}$$

$$(\not{p}+m)v_\pm(p,m) \propto (p^2 - m^2) = 0, \tag{5.17}$$

where we used $\not{p}\not{p} = p^2$, which comes from the properties of the gamma matrices displayed in Appendix A.

The dependence of the spinors on a reference vector has the relevant consequence that positive and negative helicities are no longer independent. This is more clearly seen if $u_\pm(p,m)$ are explicitly expressed in terms of n^μ and $p^{\flat,\mu}$,

$$u_+(p,m) = \frac{(\not{p}^\flat + \frac{m^2}{2p\cdot n}\not{n} + m)\,|n\rangle}{\langle p^\flat n\rangle} = -|p^\flat] + \frac{m}{\langle p^\flat n\rangle}\,|n\rangle\,, \tag{5.18}$$

$$u_-(p,m) = \frac{(\not{p}^\flat + \frac{m^2}{2p\cdot n}\not{n} + m)|n]}{[p^\flat n]} = -|p^\flat\rangle + \frac{m}{[p^\flat n]}|n], \tag{5.19}$$

where the spinor identity $\not{p}^\flat = -|p\rangle^\flat\,[p|^\flat - |p]^\flat\,\langle p|^\flat$ was used. We can then see that by performing a $p^\flat \leftrightarrow n$ inversion on $u_+(p,m)$ we obtain

$$u_+(p,m)|_{p^\flat \leftrightarrow n} = \frac{(\not{p}+m)\,|p^\flat\rangle}{\langle np^\flat\rangle} = \frac{(\not{p}^\flat + \frac{m^2}{2p\cdot n}\not{n} + m)\,|p^\flat\rangle}{\langle np^\flat\rangle} = -\frac{m^2}{2p\cdot n}|n] - \frac{m}{\langle p^\flat n\rangle}\,|p^\flat\rangle\,. \tag{5.20}$$

If we multiply by $\frac{\langle p^\flat n\rangle}{m}$ we have

$$\frac{\langle p^\flat n\rangle}{m}u_+(p,m)|_{p^\flat \leftrightarrow n} = -|p^\flat\rangle + \frac{m}{[p^\flat n]}|n] = u_-(p,m), \tag{5.21}$$

a similar relation holds for $v_\pm$ spinors. As a result of Eq. (5.21), it is only necessary to compute

one helicity configuration for the massive top quarks, and all other possible combinations can be extracted using the symmetries of the spinor constructions. In this work we chose to compute the all positive $++$ configuration, as shown in table 5.1.

From the discussion above we see that there is a need to define two arbitrary massless vectors to parametrise each massive quark. In Section 5.3.1 the choices for different expressions are discussed. In [123] it is shown how a physical interpretation can be given to the spinor parametrisation described above: the decay of the top quark into a massless fermion and a photon, $t \to q\gamma$, with the desired split of its momentum, can give rise to a gauge-invariant amplitude with spinors of the form of Eq. (5.15).

For this project the phase-space of seven massless particles was generated, $q_1, ..., q_7$, related to the momenta p_i of the physical particles as

$$p_1 = q_1 + q_2, \quad p_2 = q_3 + q_4, \quad p_3 = q_5, \quad p_4 = q_6, \quad p_5 = q_7. \tag{5.22}$$

The following constraints are imposed to ensure that momenta p_1 and p_2 are on-shell:

$$q_1 \cdot q_2 = q_3 \cdot q_4, \quad \langle q_2 q_5 \rangle = 0, \quad [q_2 q_5] = 0, \quad \langle q_4 q_5 \rangle = 0, \quad [q_4 q_5] = 0. \tag{5.23}$$

The variables used to express the rational coefficients of the amplitudes are then:

$$s_{34} = (p_3 + p_4)^2, \tag{5.24}$$

$$t_{12} = \frac{s_{12}}{s_{34}}, \tag{5.25}$$

$$t_{23} = \frac{(s_{23} - m_t^2)}{s_{34}}, \tag{5.26}$$

$$t_{45} = \frac{s_{45}}{s_{34}}, \tag{5.27}$$

$$t_{15} = \frac{(s_{15} - m_t^2)}{s_{34}}, \tag{5.28}$$

$$x_{5123} = \frac{\langle 5| \, p_1 p_{45} \, |3\rangle}{\langle 53 \rangle \, s_{12}}. \tag{5.29}$$

In the following section we explain how the amplitudes for the two channels were represented, in line with the choice made for the form of massive spinors.

5.3 Amplitudes Representations

We organise the amplitudes into a basis of spinor structures which parametrise the dependence on the reference spinors $|n_1\rangle$ and $|n_2\rangle$. This choice allows us to express each amplitude as a combination of on-shell, gauge invariant sub-amplitudes $A_x^{(L),[i]}$, $i = 1, ..., 4$. The decomposition has the form displayed in [1]

$$A_x^{(L)}(1_t^+, 2_{\bar{t}}^+, 3^{h_3}, 4^{h_4}, 5^{h_5}; n_1, n_2) = m_t \Phi(3^{h_3}, 4^{h_4}, 5^{h_5}) \sum_{i=1}^{4} \Theta_i(1, 2; n_1, n_2) A_x^{(L),[i]}(1_t^+, 2_{\bar{t}}^+, 3^{h_3}, 4^{h_4}, 5^{h_5}),$$

$$(5.30)$$

where the overall phase assumes the form:

$$\Phi(3^+, 4^+, 5^+) = \frac{[35]}{\langle 34\rangle \langle 45\rangle}, \tag{5.31}$$

$$\Phi(3^+, 4^+, 5^-) = \frac{\langle 5|p_3 p_4|5\rangle}{\langle 34\rangle^2}, \tag{5.32}$$

$$\Phi(3^+, 4^-, 5^+) = \frac{\langle 4|p_5 p_3|4\rangle}{\langle 35\rangle^2}. \tag{5.33}$$

This choice for the Θ are made so that the sub-amplitudes $A_x^{(L),[i]}$ are dimensionless and free of the spinor phase.

We choose different expressions for the Θ's depending on the set of values that we decide the reference spinors can assume. If we decide that the reference spinors n_1 and n_2 can be equal to any

of the two momenta p_3 or p_4, we have:

$$\Theta_1(1,2,n_1,n_2) = \frac{\langle n_1 n_2 \rangle s_{34}}{\langle 1^\flat n_1 \rangle \langle 2^\flat n_2 \rangle},$$

$$\Theta_2(1,2,n_1,n_2) = \frac{\langle n_1 3 \rangle \langle n_2 4 \rangle [34]}{\langle 1^\flat n_1 \rangle \langle 2^\flat n_2 \rangle}, \tag{5.34}$$

$$\Theta_3(1,2,n_1,n_2) = \frac{\langle n_1 3 \rangle \langle n_2 3 \rangle [3|p_4 p_5|3]}{s_{34} \langle 1^\flat n_1 \rangle \langle 2^\flat n_2 \rangle},$$

$$\Theta_4(1,2,n_1,n_2) = \frac{\langle n_1 4 \rangle \langle n_2 4 \rangle [4|p_5 p_3|4]}{s_{34} \langle 1^\flat n_1 \rangle \langle 2^\flat n_2 \rangle}.$$

If instead we decide that n_1 and n_2 can be equal to any of the two momenta p_3 and p_5, we have:

$$\Theta_1(1,2,n_1,n_2) = \frac{\langle n_1 n_2 \rangle s_{35}}{\langle 1^\flat n_1 \rangle \langle 2^\flat n_2 \rangle},$$

$$\Theta_2(1,2,n_1,n_2) = \frac{\langle n_1 3 \rangle \langle n_2 5 \rangle [35]}{\langle 1^\flat n_1 \rangle \langle 2^\flat n_2 \rangle}, \tag{5.35}$$

$$\Theta_3(1,2,n_1,n_2) = \frac{\langle n_1 3 \rangle \langle n_2 3 \rangle [3|p_4 p_5|3]}{s_{34} \langle 1^\flat n_1 \rangle \langle 2^\flat n_2 \rangle},$$

$$\Theta_4(1,2,n_1,n_2) = \frac{\langle n_1 5 \rangle \langle n_2 5 \rangle [5|p_4 p_3|5]}{s_{35} \langle 1^\flat n_1 \rangle \langle 2^\flat n_2 \rangle}.$$

In the rest of the chapter we will refer to the parametrisation of Eq.(5.34) as the $(p_3 - p_4)$ reference choice, while the one of Eq. (5.35) will be the $(p_3 - p_5)$ reference choice. In the following section we discuss the effect that these different choices make on the expression of the amplitude.

5.3.1   On the Choice of Reference Vectors

We can invert Eq. (5.30) to obtain expressions of the sub-amplitudes for the two different choices of reference spinors. For the $(p_3 - p_4)$ reference choice we have

$$A_x^{(L)[1]} = \frac{\langle 1^\flat 3 \rangle \langle 2^\flat 4 \rangle}{\langle 34 \rangle \, m_t s_{34} \Phi(h_3,h_4,h_5)} A_x^{(L)h_3 h_4 h_5}(3,4), \tag{5.36}$$

$$A_x^{(L)[2]} = \frac{1}{m_t \Phi(h_3,h_4,h_5) \langle 34 \rangle s_{34}} (\langle 1^\flat 4 \rangle \langle 2^\flat 3 \rangle A_x^{(L)h_3 h_4 h_5}(4,3) + \langle 2^\flat 4 \rangle \langle 1^\flat 3 \rangle A_x^{(L)h_3 h_4 h_5}(3,4)), \tag{5.37}$$

$$A_x^{(L)[3]} = \frac{\langle 1^\flat 4 \rangle \langle 2^\flat 4 \rangle s_{34}}{m_t \Phi(h_3,h_4,h_5) \langle 34 \rangle^2 [3|p_4 p_5|3]} A_x^{(L)h_3 h_4 h_5}(4,4), \tag{5.38}$$

$$A_x^{(L)[4]} = \frac{\langle 1^\flat 3 \rangle \langle 2^\flat 3 \rangle s_{34}}{m_t \Phi(h_3, h_4, h_5) \langle 34 \rangle^2 [4|p_5 p_3|4]} A_x^{(L)h_4 h_3 h_5}(3, 3).$$ (5.39)

Where we have used a lighter notation: $A_x^{(L)h_3 h_4 h_5}(n_1, n_2) = A^{(L)}(1^+, 2^+, 3^{h_3}, 4^{h_4}, 5^{h_5}; n_1, n_2)$.

The sub-amplitudes for the other choice of reference spinors are calculated by inverting $4 \leftrightarrow 5$.

We then observe that it is more convenient to choose the reference spinors depending on the specific helicity we wish to represent. If we take for example the helicity configuration $(+++-)$, we see that a suitable choice of reference vectors makes some sub-amplitudes evaluate to zero. In our example, the gluon number 5 is the only one with negative helicity, therefore the spinor $\langle 5|$ can only be contracted with the angle brackets of the reference spinors; if we then choose $n_1 = 3$ and $n_2 = 5$, we have

$$A_x^{(L)[2]} \propto (\langle 1^\flat 5 \rangle \langle 2^\flat 3 \rangle A_x^{(L)h_3 h_4 h_5}(5, 3) + \langle 1^\flat 3 \rangle \langle 2^\flat 5 \rangle A_x^{(L)h_3 h_4 h_5}(3, 5)) = 0,$$ (5.40)

$$A_x^{(L)[3]} \propto A_x^{(L)h_3 h_4 h_5}(5, 5) = 0.$$ (5.41)

Sub-amplitde $A_x^{(L)[2]}$ vanishes because of the symmetry properties of the full amplitude, while sub-amplitude $A_x^{(L)[2]}$ is zero because it has to be proportional to $\langle 5, 5 \rangle = 0$ since there is no other possible contraction of leg 5.

Thus we see that for the $(+++-)$ configuration it is convenient to choose $n_1 = 3$ and $n_2 = 5$, while for the $(+ + + - +)$ configuration the $n_1 = 3$ and $n_2 = 4$ choice is more convenient for analogous reasons.

Different choices of reference vectors can also be preferred to preserve symmetries which are observed at the full-amplitude level.

We know that the kinematic part of the amplitudes must present the same symmetries over the permutations of the external legs as their corresponding colour factors; for the leading-colour amplitude, for instance, we have the factor $T(2, 3, 4, 5, 1) = (t^3 t^4 t^5)_2^{\bar{1}}$ which is symmetric under the reordering $(1, 2, 3, 4, 5) \rightarrow (2, 1, 5, 4, 3)$, thus the symmetry must also be present for the kinematic

amplitude. In general, such a symmetry will not be preserved by the sub-amplitudes, but if we make the choice $n_1 = p_3$ and $n_2 = p_5$ we see that each $A_x^{(L)[i]}$ is invariant as well. This is the case since the permutation involves the two inversions $1 \leftrightarrow 2$ and $3 \leftrightarrow 5$: if spinors 3 and 5 are taken as the reference spinors for the massive fermions, inverting their order together with one of the fermion legs will carry the symmetry at the sub-amplitude level. In [1], the following properties were tested

$$
\begin{aligned}
A_x^{(1)[i]}(+ + + + -) &= A_x^{(1)[i]}(+ + - + +), \\
A_x^{(1)[i]}(+ + + - -) &= A_x^{(1)[i]}(+ + - - +),
\end{aligned}
\tag{5.42}
$$

both at tree-level and at one-loop order.

The same test was performed for the sub-leading one-loop colour amplitude $A_{5;4}$ with colour structure $\delta_{\bar{2}}^{\bar{1}}\mathrm{tr}(t^3 t^4 t^5)$, and we fond that the sub-amplitudes are invariant under the same permutations.

5.3.2   Computational Pipeline

We conclude this section with a scheme summarising the steps followed to obtain the full expressions for the amplitudes. Below each block are the names of the software used for that stage of the calculation.
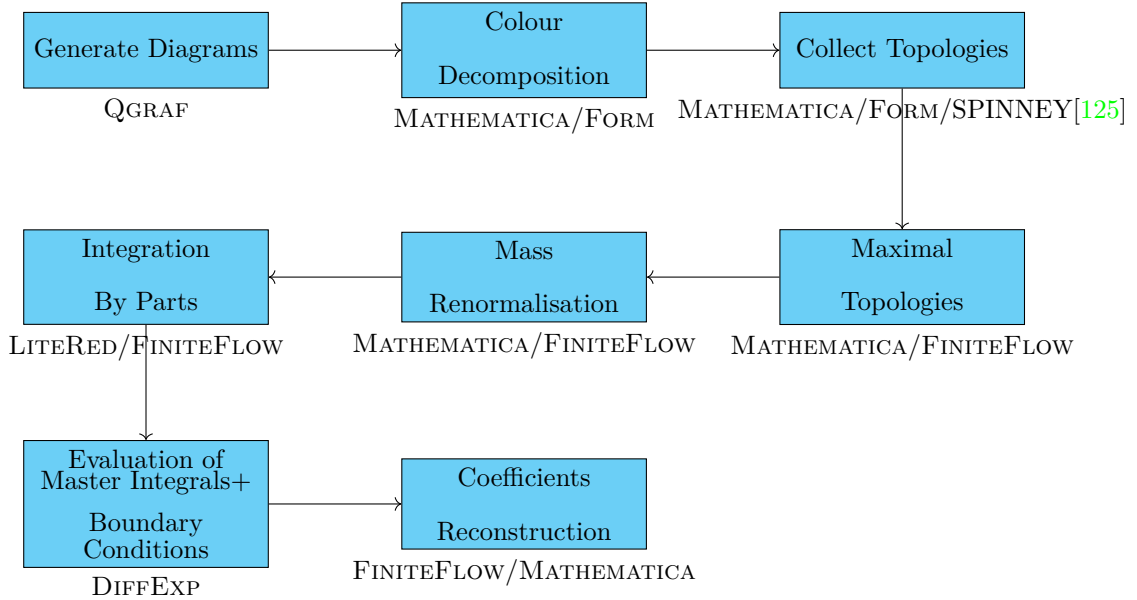
In the following sections we will go into the details of the most salient steps.
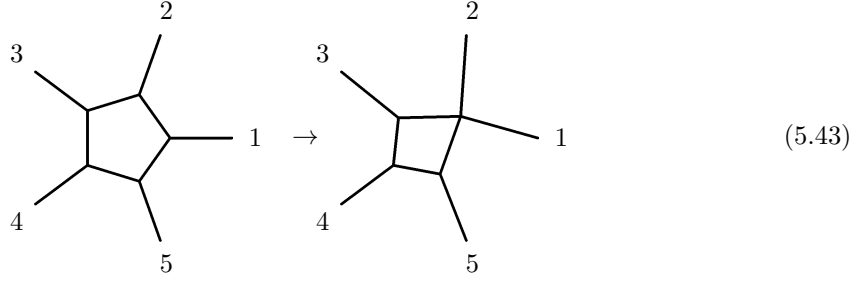
$$(5.43)$$

Figure 5.1: Schematic representation of how pinching the propagator between legs 1 and 2 of the pentagon on the left results in the box on the right.

5.4 Maximal Topologies and Master Integrals

The concept of the topology of an integral in the context of amplitudes has already been introduced in Section 3.5.2, as the set of the independent denominators of their integrands. It is useful to define a smaller set of *maximal topologies*. This is the smallest possible set of topologies which includes all the possible independent propagators. In other words, the topology of any integral appearing in the amplitude can be obtained by taking a sub-set of denominators of one of the maximal topologies. The act of taking a sub-sets of propagators can be referred to as *pinching* the topology. An example is shown in Figure 5.1

For the $pp \to \bar{t}tj$ amplitudes we have four maximal topologies, shown in Figure 5.2.

Each numerator diagram (the numerator associated to a specific topology) is computed using a symbolic value of the the spin dimensions $d_s = g^\mu_\mu$ and the amplitudes are expressed as expansions around $d_s = 2$:

$$A_x^{(L)} = A_x^{(L,0)[i]} + (d_s - 2)A_x^{(L,1)[i]}. \qquad (5.44)$$

The spin dimension d_s is independent of loop integration dimension $D = 4 - 2\epsilon$, so that the amplitudes can be used both in the FDH ($d_s = 4$) or tHV ($d_s = 4 - 2\epsilon$) renormalisation schemes. This additional decomposition doubles the total number of expressions which were reconstructed, but decreases the complexity of each individual one, making it a convenient choice.

The set of master integrals for each topology was computed separately. The master integrals were obtained by solving IBP relations [126, 127].

The IBP reduction is a method which relies on the fact that, as a consequence of translational
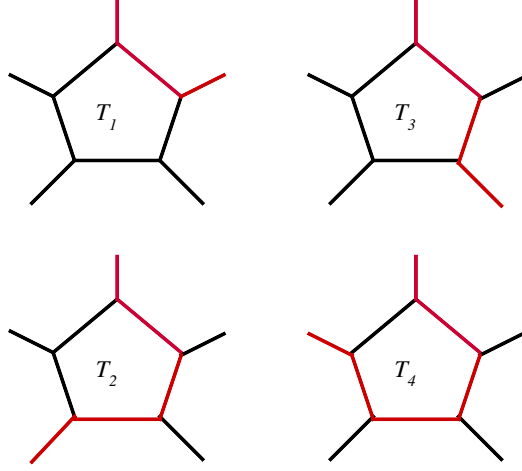
Figure 5.2: The four maximal topologies for the $pp \to \bar{t}tj$ amplitudes. The black lines indicate massless particles, while the red lines indicate massive ones. The image is taken from [1].

invariance, in dimensional regularisation the total derivative of the integrands must evaluate to zero when integrated over the loop-momentum [128]. We can consider an integrand with a generic number of propagators D_i, each raised to an arbitrary power $\nu_i \in \mathbb{Z}$:

$$I(\nu_1, ..., \nu_n) = \frac{N(k)}{D_1^{\nu_1}...D_n^{\nu_n}},\tag{5.45}$$

then we have:

$$\int d^D k \frac{\partial}{\partial k^\mu} k^\mu I(\nu_1, ..., \nu_n) = 0 \tag{5.46}$$
$$\int d^D k \frac{\partial}{\partial k^\mu} p_i^\mu I(\nu_1, ..., \nu_n) = 0,$$

where p_i are the external momenta.

A key insight of this method is that computing the derivatives as in Eq. (5.46) is equivalent to shifting the ν_i by integer numbers. We illustrate this fact with the simple example of a one-loop vacuum massive Feynman integral, taken from [128]

$$F(\nu) = \int \frac{d^D k}{(k^2 - m^2)^\nu},\tag{5.47}$$

which gives:

$$
\begin{aligned}
0 &= \int d^D k \frac{\partial}{\partial k^\mu} \frac{k^\mu}{(k^2 - m^2)^\nu} \\
&= \int d^D k \frac{D}{(k^2 - m^2)^\nu} - 2\nu \frac{k^2}{(k^2 - m^2)^{\nu+1}} \\
&= (D - 2\nu) F(\nu) - 2\nu m^2 F(\nu + 1).
\end{aligned}
\tag{5.48}
$$

The substitution $k = (k^2 - m^2) + m^2$ was used to cast the result in the desired final form. This is an example of how a polynomial numerator k^2 can be re-written in terms of denominators and ISPs $(k^2 - m^2)$ and m^2, as mentioned in Section 3.6.

Eq. (5.48) gives the recurrence relation

$$
F(\nu) = \frac{D - 2\nu + 2}{2(\nu - 1) m^2} F(\nu - 1),
\tag{5.49}
$$

which allows us to express any vacuum integral $F(\nu)$ in terms of the master integral $F(1) = f_1$.

The IBP method can be expanded from this simple example: setting up equations of the form Eq. (5.46) for all the integrals appearing in an amplitude creates a large system of linear equations called an IBP system. More identities are included in the system in addition to Eq. (5.46), stemming from Lorentz invariance and symmetries of the integrals. Solving such system yields the set of independent MIs f_i, none of which can be expressed as a linear combination of the others.

In our project, the reduction to master integrals via IBP reduction was performed automatically using the software LiteRed [129] and FiniteFlow. LiteRed makes use of the Laporta algorithm [130] in order to solve the large system of linear equations.

We find that the the topologies T_1, T_2, T_3, T_4 are described by 15, 21, 17 and 19 MIs respectively. Knowing the symmetry relations between the topologies and their permutations allowed us to obtain a minimal set of 130 MIs f_i. A list of all the MIs can be found in Appendix I.

5.5   Computation of Master Integrals

The computation of the MIs was performed using the differential equation method [131–133]. The differential equations had the form

$$df\vec{f}(\vec{x}, \epsilon) = \epsilon dA(\vec{x})\vec{f}(\vec{x}, \epsilon), \tag{5.50}$$

where d is the total derivative with respect to all the kinematic invariants,

$$\vec{x} = \{d_{12}, d_{23}, d_{34}, d_{45}, d_{15}, m_t^2\}. \tag{5.51}$$

Matrix $A(\vec{x})$ can be written in the form [134]

$$A(\vec{x}) = \sum M_i \log(\alpha_i(\vec{x})), \tag{5.52}$$

where M_i are matrices of rational numbers and $\alpha_i(\vec{x})$ are algebraic functions of the $\vec{x}$ variables. The set of $\alpha_i(\vec{x})$ is sometimes referred to as the *alphabet* of the amplitude [134]. As stated in Section 4.3.2, the knowledge of such functions enables to match all the denominator factors of the rational coefficients of the amplitudes. This point is reiterated in Section 5.8. It is important to stress that for the numerical evaluation of the MIs via a series expansion in ϵ, we did not find it necessary to write $A(\vec{x})$ in form of Eq. (5.52) explicitly.

Matrix $A(\vec{x})$ contains square roots

$$\beta(a, m^2) = \sqrt{1 - \frac{4m^2}{a}}, \tag{5.53}$$
$$\Delta_3(P, Q) = \sqrt{(p \cdot Q)^2 - P^2 Q^2},$$
$$\mathrm{tr}_5 = \sqrt{G(p_3, p_4, p_5, p_1)}.$$

While it is possible to linearise the system and eliminate the square roots, an explicit check for topology T_1 has shown that this causes the polynomial degrees of the coefficients to increase drastically, making solving the system impractical. Indeed, linearising the system would allow us to

obtain an analytic solution in terms of *multiple polylogarithms* (MPLs) [135, 136], but the system of differential equations will involve polynomials of high degree in the linearized variables. This feature impacts significantly the computation since the system of differential equations in the new set of variables is too large to be handled efficiently. In addition, the determination of the phase-space regions, and therefore the analytic continuation, is more complicated [1]. For this reason it was preferable to obtain semi-analytic solutions for the integrals using the software DiffExp [137]. This is a MATHEMATICA package which allows us to integrate Feynman integrals order-by-order in the dimensional regulator ϵ, given a set of differential equations and a boundary condition, i.e. the value of the integral at a specific phase-space point. For completeness we provide the explicit change of variables which linearises the system for topology T_1 in Appendix E. The reader can see that the matrix on the right-hand-side of Eq. (5.50) is in epsilon-factorised (or *canonical*) form [134]. Having the linear differential equations in canonical form greatly simplifies their solution and in principle enables the computation of the MIs as expansions in arbitrarily high powers of ϵ. The computation of the MIs was then performed following these three main steps.

1. Reconstruct the system of differential equations using finite fields with FINITEFLOW for a basis of master integrals $\vec{f'}$ which does not contain square roots. This gives a system which is not in canonical form:

$$d\vec{f'}(\vec{x}, \epsilon) = dA'(\vec{x}, \epsilon)\vec{f'}(\vec{x}, \epsilon). \tag{5.54}$$

2. Put the system in epsilon-factorised form by performing the rotation $\vec{f} = B^{-1}(\vec{x})\vec{f'}$ under which $dA'(\vec{x})$ transforms as

$$dA'(\vec{x}, \epsilon) \rightarrow B^{-1}(\vec{x})A'(\vec{x}, \epsilon)B(\vec{x}) - B^{-1}(\vec{x})dB(\vec{x}) = \epsilon dA(\vec{x}). \tag{5.55}$$

3. Compute the integrals using DIFFEXP. The boundary conditions of a minimal subset of MIs are computed by direct integration of their Feynamn parameter representation at the point

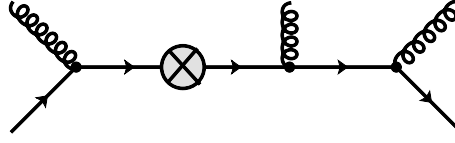$$\vec{x}_0 = (-2, -2, -2, -2, -2, 1). \tag{5.56}$$

Figure 5.3: Example of a counter-diagram added to the $\bar{t}tggg$ amplitude. Image taken from [1].

$B(\vec{x})$ is a diagonal matrix containing the square roots of Eq. (5.53), making the basis transformation trivial. In fact, we find that step 2 is equivalent to setting up the linear system for integrals with uniform trascendental weight (UT integrals). Such integrals at one loop are obtained by dividing each of the MIs by the value of their maximal cut [138]. We observe that the values of the maximal cuts of the master integrals correspond to the arguments of the square roots in the system, confirming the equivalence of the two approaches.

5.6   Wave-Function Renormalisation

The dependence of the amplitudes on the top mass m_t makes it necessary to perform the wave function renormalisation described in Section 2.4, in order to obtain gauge invariant results. This was done by generating diagrams with the appropriate counter-term insertion and adding them to the diagram numerators. An example of such a counter-term diagram is given in Figure 5.3.
The Feynman rule for the counter-term is, as represented in [1],

$$\longrightarrow\!\otimes\!\longrightarrow \;=\; \longrightarrow \left(N_c - \frac{1}{N_c}\right)\left(1 + \frac{(d_{s-2})(1-2\epsilon)}{4(1-\epsilon)}\right) I_2(m_t^2) \tag{5.57}$$

where the black line right after the equal sign represents the rule for a massive fermion propagator and $I_2(m^2)$ is a bubble scalar integral with one massless and one massive propagator, and mass scale m_t^2:

$$I_2(m_t^2) = \longrightarrow\!\bigcirc\!\longrightarrow = \int \frac{d^D k}{(k+p_1)^2(k^2-m_t^2)}. \tag{5.58}$$

The red line represents the massive propagator. Again, the representation is the same used in [1]. This procedure ensured that the amplitude is already gauge invariant at the level of master integrals

and only gauge invariant quantities were reconstructed analytically.

5.7 Tree-Level $t\bar{t}3g$ Amplitudes

We present explicit formulae for the tree-level $t\bar{t}3g$ amplitudes, expressed in terms of spinor variables. This is done because studying the representation of tree-level expressions has been useful to inform the reconstruction methods at one-loop. The expressions are computed starting from the Feynamn diagrams, like for the one-loop case. The final result is an expression in momentum twistor variables, which we then reconverted into spinor variables.

We now describe the method employed to make this conversion, which involves the univariate partial fractioning in terms of the squared top mass m_t^2. We remind the reader that the definitions of the momentum twistor variables are given by Equations (5.25) to (5.29). The univariate partial fractioning method has already been described in Section 4.3.3, but we stress here a difference from the previous exposition: the quantity m_t^2 can itself be represented as a polynomial in the momentum-twistor variables:

$$m_t^2 = \tag{5.59}$$
$$\frac{s_{34}t_{12}(t_{23}t_{51} - t_{23}x_{5123} + t_{45}x_{5123} + t_{12}t_{51}x_{5123} - t_{45}t_{51}x_{5123} - t_{12}x_{5123}^2 + t_{12}^2x_{5123}^2 - t_{12}t_{45}x_{5123}^2)}{t_{45}} \ .$$

We illustrate how the decomposition works starting with a simple two-variables example $N(x,y) = -2x^2 + 2x^3 + 4xy$. In this example $N(x,y)$ will take the role of the numerator of an helicity amplitude. We can interpret this as a function depending only on x, and treat y as a constant. It is then possible to define the factor $\mathbf{X} = x^2 + y$. The polynomial reduction of $N(x,y)$ will then be

$$N(x,y) = (2x-2)\mathbf{X} + \mathbf{R}, \tag{5.60}$$

where the remainder $\mathbf{R}$ is a polynomial which does not have any dependence on $\mathbf{X}$: $\mathbf{R} = 2xy + 2y$. It must be noted again that the choice of x as the dependent variable is arbitrary. If one chooses y instead the reduced form is different

$$N(x,y) = 4x\mathbf{X} + \mathbf{R'}, \tag{5.61}$$

with $\mathbf{R'} = -2x^2 - 2x^3$.

We now repeat this decomposition for the case of a real tree-level numerator. We take the expression for the $A^{(0)[4]}_{t\bar{t}3g}(+++-)$ gauge invariant sub-amplitude. It has the form of a rational function with numerator

$$N = t_{12}t_{23}t_{51} + t_{45}t_{51} + t_{12}t_{51}^2 - t_{12}t_{23}x_{5123} + t_{12}^2t_{23}x_{5123} + t_{12}t_{45}x_{5123} \\ - t_{12}t_{51}x_{5123} + 2t_{12}^2t_{51}x_{5123} - 2t_{12}t_{45}t_{51}x_{5123} - t_{12}^2 + t_{12}^3x_{5123}^2 - t_{12}^2t_{45}x_{5123}^2, \tag{5.62}$$

expressed in the momentum twistor variables described in Section **??**.

We make the choice of taking x_{5123} as the variable of the univariate polynomial. As stated above, the factor that we want to partial fraction with respect to is the top mass m_t^2, which has the form shown in Eq. (5.59). Carrying out the polynomial reduction leads to the result

$$N = \frac{m_t^3 t_{45}}{s_{34}} - m_t t_{51}(-t_{45} - t_{12}t_{51} + t_{45}t_{51} + t_{12}x_{5123} - t_{12}^2x_{5123} + t_{12}t_{45}x_{5123}). \tag{5.63}$$

The decomposed N is then divided by the denominator of the expressions to obtain the partial fractioned result. The crucial step which follows the reduction consists, again, in matching each momentum twistor factor with an equivalent spinor expression, which was included in a list of ansätze. This is the same factor matching technique described in 4.3.2. In this case, the factor matching does not only have the aim of decreasing the degrees of the polynomial, but also of converting an expression in momentum twistor variables to one in spinor ones. For this reason each term in the ansatz is chosen to be free of phase and of homogeneous mass-dimensions, ensuring that the final expression is gauge invariant and of the correct dimensions.

The partial fractioning of the numerators was performed with respect to all the possible twistor variables and it was found that when using x_{5123} the expressions factorised into simpler factors, while this did not happen for the other cases. We will see in Section 5.8 that this special feature of variable x_{5123} was also observed for the one-loop expressions: the partial fractioning with respect to x_{5123} greatly simplified the analytic reconstructions.

The resulting spinor expressions for the $t\bar{t}3g$ tree-level amplitudes are presented below for helicities

$(+++++)$ and $(++++-)$. The $(+++--)$ expressions are in Appendix G. We also display the same expressions as obtained with BCFW-shifts. In this second case the amplitudes are obtained by combining lower-point expressions with the BCFW method described in Section 3.3.

While the amplitudes carry exactly the same physical meaning regardless of the way in which they were computed, it is convenient to compare the different forms in order to study the size of the expressions. We will make considerations on whether a specific choice of representation makes the physical features more transparent. Discussing this for tree amplitudes will allow us to expand on these concepts for one-loop amplitudes in Section 6. For each helicity amplitude we specify the reference vectors chosen in the representation.

Reference Choice $(\mathbf{p_3} - \mathbf{p_4})$

The only non-zero sub-amplitude for the all-plus helicity configuration is $A_{t\bar{t}3g}^{(0)[1]}(++++)$,

$$A_{t\bar{t}3g}^{(0)}(++++) = A_{t\bar{t}3g}^{(0)[1]}(++++) = \frac{m_t^3 [3|p_{12}p_1|5]}{4 s_{34}[35] d_{23} d_{15}}. \tag{5.64}$$

Reference Choice $(\mathbf{p_3} - \mathbf{p_5})$

For the single-minus helicity configuration we have two non-zero sub-amplitudes. The first has the two equivalent expressions

$$A_{t\bar{t}3g}^{(0)[1]}(++++-) = -\frac{m_t \langle 34 \rangle \langle 5| p_2 p_{34} |5\rangle^2}{s_{12} s_{35} \langle 45 \rangle \langle 3| p_2 p_{34} |5\rangle \langle 5| p_3 p_4 |5\rangle} \tag{5.65}$$
$$+ \frac{m_t^3 \langle 34 \rangle^2 \langle 5| 1|4] \langle 5| p_{23}|4][34]}{4 s_{35} \langle 3| p_2 p_{34} |5\rangle \langle 5| p_3 p_4 |5\rangle d_{23} d_{15}[45]},$$

$$A_{t\bar{t}3g}^{(0)[1]\mathrm{BCFW}}(++++-) = -\frac{m_t^3 \langle 35 \rangle \langle 5|1|4]^2}{4 \langle 34 \rangle s_{35}^4 \langle 5| p_{34}p_2 |3\rangle d_{23} d_{15}[45]} + \tag{5.66}$$
$$\frac{m_t \langle 35 \rangle \langle 5| p_2 p_{34} |5\rangle^2}{s_{12} s_{34} s_{35}^4 \langle 34 \rangle \langle 45 \rangle \langle 5| p_{34}p_2 |3\rangle}.$$

We observe that in this case there is no significant difference in the compactness of the expressions. It can be seen that not every factor appearing in the denominators is associated with a physical singularity of the amplitude. We have factors s_{12}, s_{45}, $d_{23} = p_2 \cdot p_3$ and $d_{15} = p_1 \cdot p_5$, which vanish in correspondence of two adjacent legs becoming collinear or a massless leg becoming soft (see Section 2.7), while the terms $\langle 5| p_3 p_4 |5\rangle$ and $\langle 5| p_2 p_{34} |5\rangle$ do not. The second non-zero sub-amplitude has expressions

$$A_{t\bar{t}3g}^{(0)[4]}(+++ +-) = \frac{m_t^3}{4 s_{45} d_{23} d_{15}} + \frac{m_t \langle 4| p_3 p_2 |5\rangle [45]}{2 d_{23} s_{34} s_{45}^2}, \tag{5.67}$$

$$A_{t\bar{t}3g}^{(0)[4]\text{BCFW}}(++++-) = -\frac{m_t \langle 35\rangle}{s_{34} s_{35}^2 \langle 5| p_{34} p_2 |3\rangle} \left[\frac{\langle 5| p_2 p_1 |5\rangle}{\langle 34\rangle \langle 45\rangle} + \frac{m_t^2 \langle 3| 5|4] \langle 5| 1|4][34]}{4 d_{23} d_{15} [45]} \right]. \tag{5.68}$$

We see in this case that the first representation is slighty more compact than the BCFW one. In the first expressions we have a smaller set of denominator factors, we note that all of them correspond to physical poles of the amplitude.

After this brief discussion we conclude that there is no significant difference in the compactness of the tree-level expressions for either choice of representation. What was relevant, however, was to notice that the momentum-twistor variable x_{5123} is the best one if one wants to perform this type of univariate partial fractioning. We will see in the next section that this is consistent with the analysis of the expressions at one-loop.

5.8   Partial Fractioning in Rational Reconstruction

As anticipated in Section 5.7, partial fractioning with respect to x_{5123} proved to be an extremely effective method to improve the reconstruction performance for many of the one-loop amplitudes in the $0 \to ttggg$ channel. In order to verify which expressions would simplify after being partial fractioned, tests were performed on univariate slices. After the univariate slices were partial fractioned, it was possible to estimate in advance the most convenient method to apply. It was found that the partial fractioning was convenient for all the expressions which are of order $(d_s - 2)^1$ in the expansion

shown in Eq. (5.44), while for most of the zeroth order terms it was sufficient to apply the factor matching procedure directly on the full expression.

The list of ansätze was created starting from

$$
\begin{aligned}
&\{\epsilon, 1-\epsilon, 1-2\epsilon, 3-2\epsilon, \\
&\langle 34 \rangle, [34], \langle 3|\,1|4], d_{12}, d_{12} + m_t^2, d_{12} - m_t^2, \\
&d_{13}, s_{12}, s_{13}, s_{34}, s_{12} - s_{34}, s_{13} - s_{24}, \\
&(p_{23} \cdot p_1)^2 - m_t^2 s_{23} = \Delta_3(p_{23}, p_1)^2, \\
&\langle 3|\, p_1 p_{12} |4 \rangle, [3|p_1 p_{12}|4], \langle 3|\, p_1 p_2 |4 \rangle, \\
&[3|p_1 p_2|4], \langle 3|\, p_1 p_2 |3 \rangle, [3|p_1 p_2|3], \langle 3|\, p_2 p_5 p_3 p_1 |4 \rangle + m_t^2 s_{35} \langle 34 \rangle, [3|p_2 p_5 p_3 p_1|4] + m_t^2 s_{35}[34], \\
&\mathrm{tr}_5(3451) = \langle 3|\, p_1 p_5 p_4 |3] - \langle 4|\, p_5 p_5 p_1 |3], \\
&(d_{13} d_{25} - p_3 \cdot p_{24} p_4 \cdot p_{13}) \langle 3|\, p_1 p_{12} |4 \rangle + 2 \langle 34 \rangle d - 13 d_{24} p_5 \cdot p_{34}, \\
&(d_{13} d_{25} - p_3 \cdot p_{24} p_4 \cdot p_{13})[3|p_1 p_{12}|4] + 2[34]d - 13 d_{24} p_5 \cdot p_{34}, \det(Y_5)\},
\end{aligned}
\tag{5.69}
$$

where we defined the *Caley matrix* in the same way as it was done in [85]

$$
(Y_5)_{ij} = -p_{i,j-1}^2 + m_i^2 + m_j^2,
\tag{5.70}
$$

with $p_{i,j-1} = \sum_{k=i}^{j-1} p_k$ and $m_i = \{m_t, 0, m_t, m_t, m_t\}$. Additional terms are then created by performing all the possible permutations of legs 3, 4 and 5 and of legs 1 and 2. Duplicate entries are eliminated when the list is evaluated in momentum-twistor variables. We notice that ansatz 7.14 contains terms which are not all phase-free, and of different mass-dimensions. This is allowed because the ansatz is only needed to match terms and decrease the polynomial complexity in the reconstruction process. The factor matching is not used to try and express the resulting rational coefficients in terms of spinor variables. In Tables 5.2 and 5.3 we show the degrees of the expressions with reference vectors $n^\mu = p_3$ and $p^{\flat\mu} = p_3$, the results are similar for the other spinor projections. As a comparison, we also provide the polynomial degrees of the $O(\epsilon^0)$ expansions of the same

amplitudes in the momentum twistor variables, in Table 5.4 and Table 5.5. These latter expressions were obtained by expanding the terms of the integral bases up to finite order in ϵ. It is possible to observe a significant increase in complexity (i.e. maximum polynomial degrees) when we go beyond $O(\epsilon^0)$. The amplitudes in the $0 \to t\bar{t}\bar{q}qg$ channel on average had lower degrees and it was found that the use of partial fractioning was not needed for their efficient reconstruction.

We reiterate that the efficient numerical evaluation of the finite remainder at one loop, i.e. terms up to $O(\epsilon^0)$, is not the aim of the present study. The evaluation of the basis integrals using generalised series expansions with DIFFEXP will be considerably less efficient than using one-loop integral libraries such as QCDLOOP and ONELOOP, which are used by automated programs such as HELAC-NLO [139, 140] and OPENLOOPS [141, 142]. At NLO these methods have been shown to be quite sufficient for flexible phenomenology (see for example [143] and [144] for their use in studying processes involving $t\bar{t}$ production). For this reason we choose not to include detailed information about the evaluation times of the expressions on specific phase-space points. Past $O(\epsilon^0)$, the main priority is to establish the function basis and analytic complexity up to poly-logarithmic weight four which are necessary for the analytic construction of the two-loop finite remainder, as mentioned in Section 5.1. The pentagon integrals that appear give rise to new basis function that first appears at NNLO. Understanding the differential equations satisfied by these objects is the first (albeit small) step towards a complete understanding of the two-loop function basis for the $pp \to t\bar{t}j$ process.

5.9 Infrared Structure

In [145], Catani, Dittmaier and Trocsanyi (CDT) derived the expressions for the universal pole structure of arbitrary one-loop amplitudes with massless and massive partons in QCD. Such expressions were used in our project to perform checks on the final analytic expressions.

The CDT formulae are written in the colour-space notation introduced in [146]. Colour indices are represented as $c_1 = \{a\} = 1, ..., N_c^2 - 1$ and $c_1 = \{\alpha\} = 1, ..., N_c$ for particles in the adjoint representation (gluons) and fundamental representation (quarks) respectively. Given an orthogonal

Amplitude	Helicity	$d_s - 2$ exp	Original Degrees	Stage 1	Stage 2	Stage 3
$A_{1;1}^{(1)}$	+ + + + +	0	33/24	25/0	17/11	11/5
$A_{1;1}^{(1)}$	+ + + + -	0	48/40	37/0	22/16	15/8
$A_{1;1}^{(1)}$	+ + + - +	0	49/47	43/0	18/18	18/8
$A_{1;1}^{(1)}$	+ + + + +	1	67/58	59/0	22/16	13/10
$A_{1;1}^{(1)}$	+ + + + -	1	99/89	88/0	26/17	15/10
$A_{1;1}^{(1)}$	+ + + - +	1	98/94	95/0	26/25	25/15
$A_{1;-1}^{(1)}$	+ + + + +	1	47/36	36/0	25/18	16/18
$A_{1;-1}^{(1)}$	+ + + + -	1	62/50	47/0	27/27	26/12
$A_{1;-1}^{(1)}$	+ + + - +	1	54/48	47/0	31/25	24/12
$A_{2;0}^{(1)}$	+ + + + +	1	49/47	48/0	25/14	21/0
$A_{2;0}^{(1)}$	+ + + - +	1	79/56	76/0	30/17	24/2
$A_{2;0}^{(1)}$	+ + + + -	1	96/95	90/0	29/29	29/20
$A_{3;0}^{(1)}$	+ + + + +	1	58/53	53/0	29/23	24/17
$A_{3;0}^{(1)}$	+ + + - +	1	96/95	90/0	29/29	29/20
$A_{3;0}^{(1)}$	+ + + + -	1	106/99	99/0	35/29	29/20

Table 5.2: The $\bar{t}tggg$ amplitudes which were all reconstructed with the univariate apart method. They are catalogued according to their helicity and power in the $(d_2 - 2)$ expansion. The stage numbers have the same meaning as in 4.3.3.

basis $\{|c_1, ..., c_n\rangle\}$ the n-particle amplitude $\mathcal{A}_n$ can be written as:

$$\mathcal{A}_n^{c_1,...,c_n}(p_1, m_1, ..., p_n, m_n) = \langle c_1, ..., c_n | \mathcal{A}_n(p_1, m_1, ..., p_n, m_n)\rangle, \tag{5.71}$$

where the dependence on the momenta p_i and the masses m_i is shown explicitly.

The interactions at QCD vertices are then represented by the actions of colour operators $\mathbf{T}_i$. We write the factorisation of one-loop n-leg amplitude $\mathcal{A}_n^{(1)}$ in this notation as:

$$|\mathcal{A}_n^{(1)}\rangle = \mathbf{I}_n |\mathcal{A}_n^{(0)}\rangle + |\mathcal{A}_n^{(1)}\rangle^{\text{fin}} + O(\epsilon) \tag{5.72}$$

where the factor $\mathbf{I}_n$ contains all the $\frac{1}{\epsilon^2}$ and $\frac{1}{\epsilon}$ poles together with their associated colour and kinematic dependence, $|\mathcal{A}_n^{(1)}\rangle^{\text{fin}}$ is the part finite in ϵ.

We see that the divergent part of the amplitude is proportional to the tree-level process [145]. We can therefore infer the pole structure at one-loop order from the one of the real corrections.

Colour	Helicity	$d_s - 2$ exp	Original Degrees	Factors Matched
$A_{1;-1}^{(1)}$	+ + + + +	0	37/27	26/0
$A_{1;-1}^{(1)}$	+ + + + -	0	43/30	28/0
$A_{1;-1}^{(1)}$	+ + + - +	0	35/29	29/0
$A_{1;0}^{(1),f}$	+ + + + +	0	16/10	7/0
$A_{1;0}^{(1),f}$	+ + + + -	0	18/11	7/0
$A_{1;0}^{(1),f}$	+ + + - +	0	15/15	9/0
$A_{1;0}^{(1),h}$	+ + + + +	0	26/14	13/0
$A_{1;0}^{(1),h}$	+ + + + -	0	28/13	13/0
$A_{1;0}^{(1),h}$	+ + + - +	0	21/15	13/0
$A_{2;0}^{(1)}$	+ + + + +	0	32/23	21/0
$A_{2;0}^{(1)}$	+ + + + -	0	43/30	29/0
$A_{2;0}^{(1)}$	+ + + - +	0	34/29	28/0
$A_{3;0}^{(1)}$	+ + + + +	0	31/21	18/0
$A_{3;0}^{(1)}$	+ + + + -	0	43/32	30/0
$A_{3;0}^{(1)}$	+ + + - +	0	35/31	29/0

Table 5.3: The $\bar{t}tggg$ amplitudes which were all reconstructed with the factor matching method. They are catalogued in the same way as in Table 5.2.

In this work we used the following form for factor **I** :

$$\mathbf{I} = N_\epsilon \left(\sum_{j,k=1}^{n} \mathbf{T}_i \cdot \mathbf{T}_j \left(\frac{\mu^2}{|-2d_{jk}|} \right)^\epsilon \mathcal{V}_{ij} - \sum_{j=1}^{n} \Gamma_j \right). \tag{5.73}$$

When a gluon goes soft it always carries away some colour charge [147], this is the reason of the arising of colour correlations $\mathbf{T}_i \cdot \mathbf{T}_j$. The colour-charge operator associated with the emission of a soft gluon of color a by the ith particle is

$$\mathbf{T}_i = \langle a | T_i^a. \tag{5.74}$$

The action of the operator over the space is

$$\langle a, c_1, ..., c_i, ...c_m | T_i^a | b_1, ..., b_i, ..., b_m \rangle = \delta_{c_1 b_1} ... T_{c_i b_i}^a ... \delta_{c_m b_m}. \tag{5.75}$$

The form of the tensor $T_{c_i b_i}^a$ depends on the type of particle i which is radiating the gluon. If the particle is a quark we have $T_{ij}^a = t_{ij}^a$, while if the particle is another gluon $T_{bc}^a = -if_{cab}$, remembering that t_{ij}^a and f_{cab} are the group generators respectively in the fundamental and adjoint representation. The product between colour tensors should then be interpreted as

$$\mathbf{T}_i \cdot \mathbf{T}_j = \mathbf{T}_i^a \mathbf{T}_j^a. \tag{5.76}$$

Amplitude	Helicity	$d_s - 2$ exp	Original Degrees	Factors Matched
$A_{1;1}^{(1)}$	+ + + + +	0	26/15	14/0
$A_{1;1}^{(1)}$	+ + + + -	0	40/29	25/0
$A_{1;1}^{(1)}$	+ + + - +	0	32/29	26/0
$A_{1;1}^{(1)}$	+ + + + +	1	42/34	30/0
$A_{1;1}^{(1)}$	+ + + + -	1	56/48	41/0
$A_{1;1}^{(1)}$	+ + + - +	1	48/48	42/0
$A_{1;-1}^{(1)}$	+ + + + +	1	36/27	20/0
$A_{1;-1}^{(1)}$	+ + + + -	1	52/43	41/0
$A_{1;-1}^{(1)}$	+ + + - +	1	49/45	43/0
$A_{2;0}^{(1)}$	+ + + + +	1	34/25	23/0
$A_{2;0}^{(1)}$	+ + + - +	1	31/27	25/0
$A_{2;0}^{(1)}$	+ + + + -	1	38/29	23/0
$A_{3;0}^{(1)}$	+ + + + +	1	30/22	18/0
$A_{3;0}^{(1)}$	+ + + - +	1	40/36	34/28
$A_{3;0}^{(1)}$	+ + + + -	1	47/37	33/0

Table 5.4: The $\bar{t}tggg$ amplitudes which were all reconstructed with the univariate apart method, up to order $O(\epsilon^0)$. They are catalogued in the same way as in 5.2.

As an example, if a soft gluon is radiated between leg 1 and 2 being respectively a quark and a gluon, we will have

$$\mathbf{T}_1 \cdot \mathbf{T}_2 = t_{i1}^a f^{a2j} = \quad \otimes \quad \tag{5.77}$$

,

therefore we can exploit the known group properties

$$\mathbf{T}_i^2 = \mathbf{T}_i^a \mathbf{T}_i^a = C_i \tag{5.78}$$

for the Casimir operator C_i, which is equal to C_A in the adjoint case and to C_F in the fundamental case.

The functions $\mathcal{V}_{ij}$ contain the kinematic contributions to the soft singularities with colour correlations,

Colour	Helicity	$d_s - 2$ exp	Original Degrees	Factors Matched
$A_{1;-1}^{(1)}$	+ + + + +	0	33/21	22/0
$A_{1;-1}^{(1)}$	+ + + + -	0	40/27	27/0
$A_{1;-1}^{(1)}$	+ + + - +	0	34/27	28/0
$A_{1;0}^{(1),f}$	+ + + + +	0	12/7	3/0
$A_{1;0}^{(1),f}$	+ + + + -	0	17/11	6/0
$A_{1;0}^{(1),f}$	+ + + - +	0	14/14	8/0
$A_{1;0}^{(1),h}$	+ + + + +	0	16/8	13/0
$A_{1;0}^{(1),h}$	+ + + + -	0	24/12	13/0
$A_{1;0}^{(1),h}$	+ + + - +	0	18/15	13/0
$A_{2;0}^{(1)}$	+ + + + +	0	29/19	19/0
$A_{2;0}^{(1)}$	+ + + + -	0	36/26	19/0
$A_{2;0}^{(1)}$	+ + + - +	0	28/24	19/0
$A_{3;0}^{(1)}$	+ + + + +	0	22/12	12/0
$A_{3;0}^{(1)}$	+ + + + -	0	38/30	26/0
$A_{3;0}^{(1)}$	+ + + - +	0	30/28	25/0

Table 5.5: The $\bar{t}tggg$ amplitudes which were all reconstructed with the factor matching method, up to order $O(\epsilon^0)$. They are catalogued in the same way as in Table 5.2.

they are:

$$
\mathcal{V}_{ij} = \begin{cases}
\dfrac{1}{\epsilon^2} & i \text{ and } j \text{ are massless} \\[2ex]
\dfrac{1}{2\epsilon^2} + \dfrac{1}{2\epsilon} \log\left(\dfrac{m_j^2}{-2d_{ij}}\right) - \tfrac{1}{4}\log^2\left(\dfrac{m_j^2}{-2d_{ij}}\right) - \dfrac{\pi^2}{12} & i \text{ massless, } j \text{ massive} \\[2ex]
\dfrac{s_{ij} - (m_i - m_j)^2}{d_{ij}\beta_{ij}\epsilon} \log\left(-\dfrac{1+\beta_{ij}}{1-\beta_{ij}}\right) & \\
-\dfrac{1}{4}\left(\log^2\left(\dfrac{m_j^2}{-2d_{ij}}\right) + \log^2\left(\dfrac{m_j^2}{-2d_{ij}}\right)\right) - \dfrac{\pi^2}{6}, & i \text{ and } j \text{ are massive}
\end{cases}
\tag{5.79}
$$

with $\beta_{ij} = \sqrt{1 - \frac{4m_i m_j}{s_{ij} - (m_i - m_j)^2}}$ expressing the kinematic threshold for the production of a pair of top quarks. Functions Γ_i represent the contributions coming from the hard-collinear regions.

Eq. (5.73) does not include the imaginary parts of $\mathbf{I}_n$, this is the case since they are not needed to compute the poles at the test points used in our paper at order $O(\frac{1}{\epsilon})$. The imaginary contributions can be found in [145].

The poles of each sub-amplitude were computed, and their analytic expression was explicitly given in appendix B of [1]. An ancillary Mathematica file allowed to reproduce the numerical evaluations

of the poles at the test points. They were shown to be all consistent with the CDT formula.

5.10 Results and Conclusion

5.10.1 Master Integral Results

In this section we discuss the results of the numerical evaluations of the MIs performed with DiffExp. As mentioned in Section 5.4, the MIs for each one of the four topologies are evaluated separately, allowing a parallelisation of the computations.

It is important to stress that the four maximal topologies T_1, T_2, T_3 and T_4 are defined with a specific ordering of the external legs: $(1, 2, 3, 4, 5)$ for T_1 and T_2, $(1, 3, 2, 4, 5)$ for T_3 and T_4. This fact makes it necessary to correctly permute the legs to match the ordering of the individual MIs, in order to consider all the possible permutations of the gluon indices $(3, 4, 5)$. DiffExp allows to perform this operation directly in the numerical evaluation. The procedure consists in computing the mapping of the kinematic invariants corresponding to a permutation. We give here an example similar to [1]. If one wants to compute the permutation $(1,2,3,5,4)$ for the topology T_2, it is sufficient to compute how the kinematic invariants transform under the switch $p_4 \to p_5$, $p_5 \to p_4$:

$$\begin{aligned} &\{d_{12} \to d_{12}, d_{23} \to d_{23}, d_{34} \to d_{12} - d_{34} - d_{45} + m_t^2, \\ &\quad d_{45} \to d_{45}, d_{15} \to d_{23} - d_{15}, m_t^2 \to m_t^2\}. \end{aligned} \tag{5.80}$$

Evaluating T_2 with permuted legs $(1, 2, 3, 5, 4)$ at phase-space point

$$\vec{x} = \{d_{12} \to -\frac{11}{7}, d_{23} \to -\frac{7}{5}, d_{34} \to -\frac{5}{27}, d_{45} \to -\frac{17}{5}, d_{15} \to -\frac{11}{17}, m_t^2 \to 1\}, \tag{5.81}$$

will then be equivalent to evaluate T_2 in the standard ordering but at the point

$$\vec{x} = \{d_{12} \to -\frac{11}{7}, d_{23} \to -\frac{7}{5}, d_{34} \to -\frac{2848}{945}, d_{45} \to -\frac{17}{5}, d_{15} \to \frac{45}{17}, m_t^2 \to 1\}. \tag{5.82}$$

This procedure enables to avoid the computation of any new analytic formula.

The numerical value for a specific phase-space point for all the permutations of all the topologies was under one hour on a laptop, 16 digits was the required accuracy.

5.10.2   Amplitude Results

All the expressions for the sub-amplitudes computed in the project were provided in ancillary files to [1]. We have shown in Section 5.8 that the univariate partial fractioning was extremely effective in decreasing the polynomial degrees of many coefficients. This resulted in a decrease of computational time of around a factor of 10 for the overall expression. In [1] we note that the appearance of degrees of order as high as $O(100)$ indicates that it will be challenging to compute corrections to this process at higher loops in this parametrisation, since the complexity is expected to increase significantly.

The comparison of the different expressions for the tree-level $t\bar{t}ggg$ amplitudes did not prove the existence of an optimal choice for their parametrisation, but it showed how studying the partial fractioning at tree-level can inform on the reconstruction strategies at higher loops.

The results of this project and the data collected will be useful for progressing the analytical or semi-analitycal computation of higher order corrections to $pp \to \bar{t}tj$, giving indications of possible future bottlenecks and challenges.

After having discussed the computation of five-points one-loop amplitudes, in the next section we will see how the complexity changes for six-point one-loop expressions.

Chapter 6

Analytic Representations of Gluon Amplitudes

In this chapter we give a brief overview of the history of the computation of n-gluone one-loop scattering amplitudes.

The literature on this topic is extremely vast and the short review in this section does not attempt to cover the work of all the authors which have contributed to it. The main aim will be to present a few of the papers which contained results relevant to the theme of this chapter and to the work carried out in Chapter 7. A graphical representation of the time-line for some of the papaers described in this chapter can be found in Figure 6.1.

Some of the expressions are quoted explicitly, so that the reader can gain a sense of their complexity and the benefits of the chosen parametrisations. This will also be useful for comparisons with the analytical results of Chapter 7, in which a sub-set of the expressions contributing to the six-gluon one-loop amplitudes in D-dimensions is presented.

The first NLO corrections to gluon scattering were computed by Ellis and Sexton in [57]. In their work, the radiative corrections were not computed using amplitudes as the basic blocks of the computations, but rather the cut graphs generated by the interference of the Born amplitudes

with the one-loop ones. This means that the computed quantities are already the squared terms which can be summed to obtain the cross section of the process. For this reason the results can be parametrised using the Mandelstam invariants, without the need for the introduction of spinors. The kinematic invariants are the standard ones for a $2 \to 2$ process introduced in Section 3.5.1. The scattering energy is indicated with Q^2, while $\mu^2 = \mu_{\mathrm{R}}^2$ is the renormalisation scale, as in Section 2.4. These symbols will have the same meaning in all the equations quoted in this chapter. The expression of the squared matrix element is compact enough to be quoted in full

$$\sum |\mathcal{M}^{gg \to gg}|^2 = \frac{1}{4(1-\epsilon)^2 V^2} d(s,t,u), \tag{6.1}$$

with

$$d(s,t,u) = g^4 \mu^{4\epsilon} \Big\{ d^{(4)}(s,t,u) + \frac{\alpha_S}{2\pi} \left(\frac{4\pi\mu^2}{Q^2} \right) \Big[d^{(4)}(s,t,u) \Big(-\frac{4N}{\epsilon^2} + \frac{8T_R - 22N}{3\epsilon} + \frac{20T_R - 67N}{9} \right.$$

$$\left. + N\pi^2 + \left(\frac{11N}{3} - \frac{4T_R}{3} \right) \log \left(\frac{\mu^2}{Q^2} \right) \right) + P(s,t,u) + P(t,u,s) + P(u,t,s) \Big] +$$

$$\frac{\alpha_S}{2\pi} 4V N^2 (f(s,t,u) + f(t,u,s) + f(u,s,t)) \Big\} + O(\epsilon). \tag{6.2}$$

Where we defined the following functions:

$$P(s,t,u) = \frac{16V N^3}{\epsilon} \left(3 - \frac{2tu}{s^2} + \frac{(t^4 + u^4)}{t^2 u^2} \right) \log \left(\frac{s}{Q^2} \right), \tag{6.3}$$

$$f(s,t,u) = N \Big[\left(\frac{2(t^2 + u^2)}{tu} \right) \log^2 \left(-\frac{s}{Q^2} \right) + \left(\frac{4s(t^3 + u^3)}{t^2 u^2} - 6 \right) \log \left(\frac{t}{Q^2} \right) \log \left(\frac{u}{Q^2} \right) + \tag{6.4}$$

$$\left(\frac{4}{3} \frac{tu}{s^2} - \frac{14}{3} \frac{t^2 + u^2}{tu} - 14 - 8 \left(\frac{t^2}{u^2} + \frac{u^2}{t^2} \right) \right) \log \left(-\frac{s}{Q^2} \right) - 1 - \pi^2 \Big] +$$

$$T_R \Big[\left(\frac{10}{3} \frac{t^2 + u^2}{tu} + \frac{16}{3} \frac{tu}{s^2} - 2 \right) \log \left(-\frac{s}{Q^2} \right) - \left(\frac{s^2 + tu}{tu} \right) \log^2 \left(-\frac{s}{Q^2} \right) -$$

$$2 \left(\frac{t^2 + u^2}{tu} \right) \log \left(-\frac{t}{Q^2} \right) \log \left(-\frac{u}{Q^2} \right) + 2 - \pi^2 \Big].$$

The computation in the paper was performed for a generic gauge group $SU(N)$ with generator normalisation T_R. In the paper they also use $V = N^2 - 1$.

The next significant step in one-loop calculations was made by Bern, Dixon and Kosower in 1993 in [148]. In their article, the one-loop matrix elements with five external gluons were computed. Differently from the $2 \rightarrow 2$ case, the building block of the calculation were the analytic expressions of the one-loop amplitudes, whose inteference with the tree-level was then computed to obtain the squared matrix element.

The amplitudes were obtained by employing string-based methods developed in [28] which proved to be efficient for pure-gluonic amplitudes. The obtained expressions were given in a very compact form.

The spinor helicity representation was used to express the amplitudes, which were presented as functions of spinor products $\langle ij \rangle$, $[ij]$ plus the phase-free trace $\text{tr}_5(i, j, k, l) = [ij] \langle jk \rangle [kl] \langle li \rangle - \langle ij \rangle [jk] \langle kl \rangle [li]$. We present here some functions which were used in the formulae:

$$
\begin{aligned}
\text{K}_0(s) &= \frac{1}{\epsilon} - \log(s) + 2 + O(\epsilon), \\
\text{L}_0(r) &= \frac{\log(r)}{1 - r}, \\
\text{L}_1(r) &= \frac{\log(r) + 1 - r}{(1 - r)^2}, \\
\text{L}_2(r) &= \frac{\log(r) - (r - 1/r)/2}{(1 - r)^3}.
\end{aligned}
\tag{6.5}
$$

We see that $\text{K}_0(r)$ is proportional to a scalar bubble integral [89]. Functions $\text{L}_i(r)$ have as arguments the ratios of two Mandelstam invariants. The form of these function is chosen so that they are regular in the limit $r \rightarrow 1$:

$$
\lim_{r \to 1} \text{L}_0 = -1,
\tag{6.6}
$$

$$
\lim_{r \to 1} \text{L}_1 = -\frac{1}{2},
\tag{6.7}
$$

$$
\lim_{r \to 1} \text{L}_2 = \frac{1}{6}.
\tag{6.8}
$$

This choice puts the whole amplitude's expression in a form which is free of spurious singularities of the type $(s_{ij} - s_{kl})^n$, which appear as a result of the reduction of tensor integrals to linear combinations of scalar ones, as seen in the example of Appendix D.

This choice of variables and basis functions has become standard in much of the subsequent literature. Here we quote the expression for one of the colour-leading one-loop helicity amplitudes with a quark in the loop:

$$A_{5;1}^{[1/2]}(1^-, 2^-, 3^+, 4^+, 5^+) = -c_\Gamma \left[\left(\frac{2}{3} V^f + \frac{2}{9} \right) A_5^{\text{tree}} + i(F^f + F^s) \right]. \tag{6.9}$$

With

$$V^f = -\frac{5}{2\epsilon} - \frac{1}{2} \left[\log\left(\frac{\mu^2}{-s_{23}}\right) + \log\left(\frac{\mu^2}{-s_{15}}\right) \right] + 2, \tag{6.10}$$

$$F^f = -\frac{1}{2} \frac{\langle 12 \rangle^2 \left(\langle 23 \rangle [34] \langle 41 \rangle + \langle 24 \rangle [45] \langle 51 \rangle \right)}{\langle 23 \rangle \langle 34 \rangle \langle 45 \rangle \langle 51 \rangle} \frac{\mathrm{L}_0}{s_{15}},$$

$$F^s = -\frac{1}{3} \frac{[34] \langle 41 \rangle \langle 24 \rangle [45] (\langle 23 \rangle [34] \langle 41 \rangle + \langle 24 \rangle [45] \langle 51 \rangle)}{\langle 34 \rangle \langle 45 \rangle} \frac{\mathrm{L}_2(s_{23}/s_{51})}{s_{51}^3} - \frac{1}{3} F^f -$$

$$\frac{1}{3} \frac{\langle 35 \rangle [35]^3}{[12][23] \langle 34 \rangle \langle 45 \rangle [51]} + \frac{1}{3} \frac{\langle 12 \rangle [35]^2}{[23] \langle 34 \rangle \langle 45 \rangle [51]} + \frac{1}{6} \frac{\langle 12 \rangle [34] \langle 41 \rangle \langle 24 \rangle [45]}{s_{23} \langle 34 \rangle \langle 45 \rangle s_{51}}.$$

We draw the attention to the fact that the $\frac{1}{\epsilon}$ pole is contained in the V^f term, which means that its coefficient in the amplitude is proportional to the tree-level expression, as expected [149].

The same authors together with Dunbar continued their work on the topic and in 1994 published a paper [150] in which they constructed ansatze for $\mathcal{N} = 4$ MHV helicity amplitudes with arbitrary number of gluons, exploiting unitarity constraints and knowledge of the collinear limits of the expressions.

These techniques were further developed in [95], where one-loop amplitudes in supersymmetric massless gauge theories were computed from tree-level amplitudes using on-shell methods, as described in Section 3.5. Six-gluon amplitudes at one-loop in $\mathcal{N} = 4$ super-Yang-Mills theory were computed for all helicity configurations, as well as MHV one-loop gluon amplitudes in $\mathcal{N} = 1$ supersymmetric theory with an arbitrary number of external legs. Despite only being concern with amplitudes in supersymmetric theories, the last two papers which we have mentioned must be included in our review because the on-shell methods which they introduce are of pivotal importance for the analytical

computation of scattering amplitudes in QCD. Furthermore, the computed expressions contribute to the full QCD pure-gluon amplitude in the supersymmetric decomposition exposed in Section 3.7. Such a decomposition was used for one of the projects presented in this thesis in Chapter 7, as well as for all papers that we are going to mention in the remainder of this section. The surprising simplicity of amplitudes in $\mathcal{N} = 4$ Super Yang-Mills theory was first remarked in [94], where it was speculated that all such amplitudes would be free of UV singularities. This fact was found to be true in all subsequent calculations. It was shown that supersymmetric amplitudes $A^{\mathcal{N}=4}$ and $A^{\mathcal{N}=1}$ are completely determined by unitarity cuts in four dimensions, since they do not have an additional rational part; they are therefore termed *cut-constructible* amplitudes. These amplitudes were then calculated by applying the generalised unitarity method of Section 3.5.2.

A crucial advantage of this method in this case is that only tree-level $\mathcal{N} = 4$ MHV n-gluon amplitudes are needed to obtain the one-loop result, and they have very compact Parke-Taylor expressions when expressed in spinor variables, as seen in Section 3.20,

$$A_n^{(0)}(1^+, ..., i^-, ..., j^-, ..., n^+) = \frac{\langle ij \rangle^4}{\langle 12 \rangle ... \langle n1 \rangle}. \tag{6.11}$$

For the $\mathcal{N} = 1$ MHV case, one has to consider more diagrams, since the intermediate states can be either fermions or scalars, hence one needs to sum over the two cases to obtain the full cut. Nevertheless, the tree-level amplitudes retain an algebraic simplicity which keeps the computation manageable and the final result compact.

Applying tensor reductions to the integrals in the bases of the amplitudes allows to express them all as combinations of scalar boxes, triangles and bubbles, as expected.

We quote the explicit result for the $\mathcal{N} = 1$ MHV amplitude with the two negative helicity states adjacent, because it is especially compact and it is useful to display the standard notation used in much of the literature

$$A^{\mathcal{N}=1}(1^-, 2^-, 3^+, ..., n^+) = \frac{c_\Gamma(\mu^2) A^{(0)}(1^-, 2^-, 3^+, ..., n^+)}{2} \left(\mathrm{K}_0(t_2^{[2]}) + \mathrm{K}_0(t_n^{[2]}) \right.$$
$$\left. - \frac{1}{t_1^{[2]}} \sum_{m=4}^{n-1} \frac{\mathrm{L}_0(-t_2^{[m-2]}/(t_2^{[m-1]}))}{t^{[m-1]_2}} (\mathrm{tr}_+[\not{p}_1 \not{p}_2 \not{p}_m \not{q}_{m,1}] - \mathrm{tr}_+[\not{p}_1 \not{p}_2 \not{q}_{m,1} \not{p}_m]) \right), \tag{6.12}$$

where the traces over gamma matrices $\text{tr}_+, \text{tr}_-, \text{tr}_5$ are defined in Appendix A. The integral functions are the same as in Eq. (6.5) and the authors of the article use the notation

$$t_i^{[r]} = (p_i + ... + p_{i+r-1})^2, \tag{6.13}$$

$$q_{m,l} = \begin{cases} \sum_{i=m}^{l} k_i, & m \leq l \\ \sum_{i=m}^{n} k_i + \sum_{i=1}^{l} k_i, & m > l. \end{cases} \tag{6.14}$$

A substantial improvement in the paradigm for the computation of cut-constructible amplitudes was made possible by the introduction of generalised unitarity by Britto, Cachazo and Feng in [151], a technique discussed in Section 3.5.2.

Other research groups obtained results for cut-constructible expressions using alternative techniques, such as Bredford, Brandhuber, Spence and Travaglini who in [152] computed the cut-constructible parts of $N = 0$ MHV amplitues using the MHV diagram construction [153].

While the on-shell techniques have made it possible to obtain results for the cut-constructible parts of one-loop gluon amplitudes to very high multiplicities, the computation of the rational parts of the expressions has historically been more challenging. In the remainder of this section we mention three papers in which the authors computed the rational parts needed for the full six-gluon one-loop expressions.

The first full expressions for the simplest six-gluon QCD one-loopn colour-ordered helicity amplitudes were computed by Forde and Kosower in [97]. These are the MHV helicity amplitudes with the two legs of negative helicity being adjacent in colour space, the expressions were computed for an arbitrary number of external states.

In order to obtain the non-cut-constructible parts of the $\mathcal{N} = 0$ amplitudes, the authors employed the method of BCFW shifts at one loop described in Section 3.8. This same method was used in [96] to conclude the computation of the full MHV one-loop amplitudes, by providing the rational expressions for the remaining helicity configurations. The article presents explicit expressions for

six-point MHV helicity amplitudes as functions of spinor variables.

Despite the on-shell recursion method being useful in the MHV calculations, it was not used in [154] to compute the rational parts of the NMHV helicity amplitudes $A_{6g}^{N=0}(1^-, 2^-, 3^+, 4^-, 5^+, 6^+)$ and $A_{6g}^{N=0}(1^-, 2^+, 3^-, 4^+, 5^-, 6^+)$. Instead, the expressions were computed directly from Feynman diagrams, as explained in [155] by the same authors. Their technique consists in expressing the amplitude in the Feynman integral representation, and directly extracting the rational parts.

In principle, it is always possible to obtain the rational coefficients of the amplitude by performing tensor reductions on the integral and reducing them into scalar boxes, triangles and bubbles. Once this is done, one can perform an expansion of the coefficients around $D = 4$ to obtain the rational part of the amplitude. This method is nevertheless not effective for arbitraty high multiplicity due to the complexity of tensor reductions with $n \geq 5$.

The main insight at the basis of the method described in [154] is that it is not necessary to know the complete coefficients from tensor reduction, if one is only interested in the rational part; instead, the reduction only needs to be performed to lower the numerators' degrees by 2. This makes the calculations manageable even for $n = 6$, allowing a diagrammatic approach which gives the rational part as a result of tree-level like calculations. Spinor variables are used once again to express the final answers.

Most of the expressions for the 6-gluon helicity amplitudes can be found in [91], expressed in a consistent notation and fairly compact forms. The amplitudes are split according to their helicities and supersymmetric content, consistently with the majority of the papers in this review. All such expressions are reported explicitly, with the exception of the NMHV contribution with a complex scalar in the loop, since a compact representation for those is not known. Here we directly quote some of the explicit results for the rational coefficients of the amplitude, with the intention of allowing a comparison with the D-dimensional expressions in Section 7.

We quote the $\mathcal{N} = 1$ and $\mathcal{N} = 0$ expressions of the simplest NMHV helicity amplitude :

$$A^{\mathcal{N}=1}(1^-, 2^-, 3^-, 4^+, 5^+, 6^+) = \frac{c_\Gamma}{2}\Bigg[A^{(0)}(1^-, 2^-, 3^-, 4^+, 5^+, 6^+)(\mathrm{K}_0(s_{16}) + \mathrm{K}_0(s_{34})) \tag{6.15}$$

$$- c_1 \frac{\mathrm{L}_0(s_{345}/s_{16})}{s_{16}} - c_2 \frac{\mathrm{L}_0(s_{234}/s_{34})}{s_{34}}$$

$$- c_3 \frac{\mathrm{L}_0(s_{234}/s_{16})}{s_{16}} - c_4 \frac{\mathrm{L}_0(s_{345}/s_{16})}{s_{16}}\Bigg],$$

$$A^{\mathcal{N}=0}(1^-, 2^-, 3^-, 4^+, 5^+, 6^+) = \frac{1}{3}A^{N=1} - \frac{i}{2}\Bigg[c_1 \frac{\mathrm{L}_2(s_{345}/s_{16})}{s_{16}^3} + c_2 \frac{\mathrm{L}_2(s_{234}/s_{34})}{s_{34}^2} + \tag{6.16}$$

$$c_3 \frac{\mathrm{L}_2(s_{234}/s_{16})}{s_{16}^3} + c_4 \frac{\mathrm{L}_2(s_{345}/s_{34})}{s_{34}^2}\Bigg] + c_\Gamma \hat{R}_6,$$

with

$$\hat{R}_6 = X_6 + X_6|_{123456 \to 321654} \tag{6.17}$$

$$X_6 = \frac{i}{6[23]\langle 56\rangle [2|p_{34}|5\rangle}\Bigg[-\frac{[46]^3[25]\langle 56\rangle}{[12][34][61]} - \frac{\langle 13\rangle^3 \langle 25\rangle [23]}{\langle 34\rangle \langle 45\rangle \langle 62\rangle} - \frac{\langle 13\rangle^2 (3[4|2|1\rangle + [4|3|1\rangle))}{\langle 34\rangle \langle 61\rangle} + \tag{6.18}$$

$$\frac{[4|p_{23}|1\rangle^2}{[34]\langle 61\rangle}\left(\frac{[4|2|1\rangle - [4|5|1\rangle}{s_{234}}\right) + \frac{\langle 13\rangle}{\langle 34\rangle} - \frac{[46]}{[61]}\frac{[46]^2(3[4|5|1\rangle + [4|6|1\rangle)}{[34][61]}\Bigg].$$

The coefficients c_i are the same for both expressions, the form of c_1 is

$$c_1 = \frac{[6|p_{345}p_2p_{345}|3\rangle [6|2|3\rangle [6|p_2p_{235}|3\rangle - [6|p_{235}p_2|3\rangle}{[2|p_{235}|5\rangle [61][12]\langle 34\rangle \langle 45\rangle}, \tag{6.19}$$

and all the other coefficients can be obtained permuting the indices of c_1 and performing complex conjugations (in the case of c_3).

Expressions for all six-gluon one-loop helicity amplitudes with one gluon in the loop can also be found in [156]. The authors of this paper employed yet a different computational technique, based on the numerical interpolation of the expressions evaluated over high-precision floating points. These methods differ from the ones described in Chapter 4 and used in Section 5 and Section 7 because the numerical samplings are not preformed over finite fields. The expressions in [156] have the advantage of being all derived using a single framework.
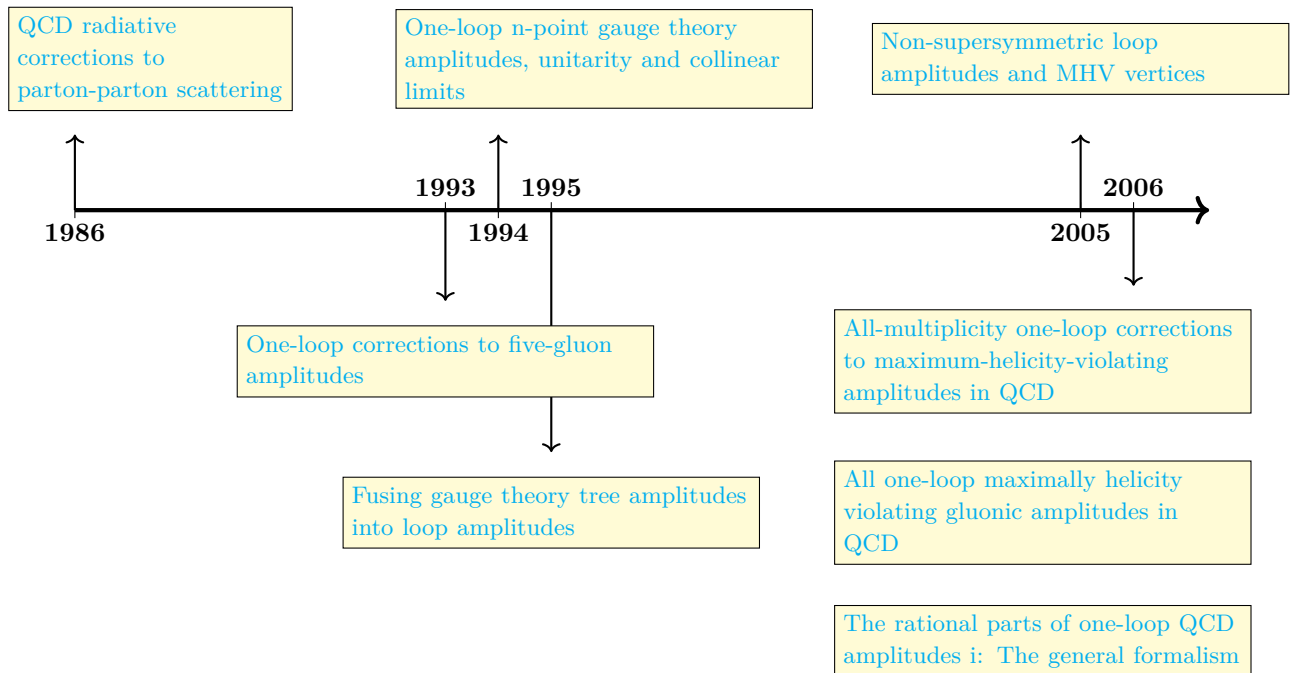
Figure 6.1: Time-ordering of some of the articles reviewed in this chapter. Only the articles which explicitly presented new parts of the gluon amplitudes are shown.

After this brief review, we present the results for D-dimensional six-gluon one-loop amplitudes in the following chapter. Some sub-amplitudes will be quoted explicitly, using the standard notation which was employed in most of the articles discussed so far.

Chapter 7

Six-Gluon Amplitudes in D Dimensions

The development of new techniques has made it possible to obtain cross sections at NNLO for most $2 \to 2$ processes of interest [14], putting the next target at N^{3}LO.

One necessary ingredient for the calculation of N^{3}LO $pp \to 2j$ inclusive cross-sections are analytic expressions for one-loop six-gluon amplitudes. Such expression represent the double-real corrections to the $gg \to gg$ inclusive cross-section, following the description of Section 2.7.

We have already seen in Chapter 6 that full analytic expressions of one-loop six-gluon colour ordered amplitudes in four dimensions have been known for several years [91]. The different parts of these expressions have been computed separately by different groups, using a wide variety of methods such as on-shell recursion relations [96] and direct computation of rational parts from Feynman diagrams [154]. These expressions have been computed as expansions in the dimensional regulator ϵ around $D = 4$ up to order $O(\epsilon^0)$. Nevertheless, these amplitudes need to be computed up to higher order of the dimensional regulator, in order to cancel the IR divergences in the full N^{3}LO four-point cross-section. One of the aims of this project was to compute expressions that can be used to obtain this result. Once again we observe a significant increase in complexity in the expressions, when compared to the four-dimensional ones. This fact makes it impractical to directly apply the

methods which were employed to obtain the $O(\epsilon^0)$ amplitudes to the ones in D dimensions, and motivated the development of novel techniques. The reader can compare the complexity of the D dimensional expressions derived in this chapter (expressed as the polynomial degree of their rational coefficients) with the one of the four-dimensional amplitudes, whose coefficients have polynomial degrees listed in Appendix F.

In this project, the MHV six-gluon one-loop amplitudes were computed in a basis of D-dimensional scalar integrals, without putting any restriction on the number of dimensions D, which is kept as an additional parameter. These amplitudes have an integral basis of the form of Eq. (3.66), and the rational coefficients for such a basis were computed using the OPP reduction method. The external momenta were kept four-dimensional.

It is important to stress that, as stated in Section 3.5.2, and particularly expressed by Eq. (3.59), a true D-dimensional amplitude has an arbitrarily large integral basis (at least up to D-gon topologies). The amplitudes reconstructed in this project do not fall into that category, since the dimensions of their external legs are kept constant, and for this reason they have a well-defined integral basis. We nevertheless refer to them as *D-dimensional amplitudes* for convenience.

A clear consequence of this discussion is the absence of integral topologies with six external legs (hexagons) in the bases of the amplitudes. This is indeed the case, despite these being the scattering amplitudes of six gluons, since it has been proven that the hexagon topologies can be expressed as linear combinations of scalar pentagons [90, 157]. In [90] it is clearly shown that, if the external momenta of an amplitude are kept as four-dimensional, an hexagon integral $I_6[1]$ can be written as:

$$I_6[1] = \frac{1}{2} \sum_i^6 c_i I_5^i[1].$$
(7.1)

In Eq. (7.1), c_i are rational coefficients which depend on the external kinematics: they are computed as the sums of the rows of the inverse Caley matrices. The scalar pentagon integrals $I_5^i[1]$ are obtained by pinching the propagator between legs $i-1$ and i, as in Figure 5.1.

It is also shown in [90] that the pentagon integrals can be written as a linear combinations of scalar boxes, plus the addition of $O(\epsilon)$ terms. This means that the finite part of the scattering amplitudes

can be fully expressed in terms of box, triangle and bubble integrals, as expected. For our case we also need to include the pentagon topologies, since we want to be able to obtain the results up to higher orders in the dimensional regulator ϵ.

Aside from the phenomenological applications, the expressions were also computed in order to study and apply different reconstruction techniques and phase-space parametrisations. A main point of interest is the increase in algebraic complexity of the integral coefficients going from five-point to six-point processes, which created new bottlenecks in the computational pipeline. Different partial fractioning methods were tested on the expressions.

After the full analytic amplitudes were reconstructed, it was possible to evaluate them in various limits of the form $d = 2n - 2\epsilon$ (with integer n). This had the objective to perform checks against expressions in the literature, but also to explore relations among the coefficients and gather data on how to perform future reconstructions. All the expressions for the computed amplitudes can be found at the following link: https://gitlab.com/fsarandrea94/6-gluons_one-loop_d-dimensions.

This chapter is organised as follows. In Section 7.1, we define the variables that the rational expressions were reconstructed in and give expressions for their phases. In Section 7.2, we describe how the amplitudes are decomposed into different sub-amplitudes, specifying the minimal set of expressions which need to be reconstructed to obtain the full information. The reconstruction methods which were used are discussed in Section 7.3, providing details on the complexity on individual sub-amplitudes. The explicit expressions of some of the sub-amplitudes are given in Sections 7.4 and 7.5. In Section 7.6, we explain the method used to derive the amplitudes' formulae in a set number of dimensions ($D = 4, 6, ...$). Conclusions are in Section 7.7.

7.1 Kinematic Set-up

In this section we present the notation for the kinematics, giving explicit definitions of the variables the amplitudes are represented in.

We label the six external gluon momenta as $p_1, ..., p_6$ and we take them to be all outgoing. The

momenta all satisfy the on-shell condition $p_i^2 = 0$ and we use the shorthand notation

$$p_i + ... + p_j = p_{i...j}, \tag{7.2}$$

$$s_{ij} = (p_i + p_j)^2. \tag{7.3}$$

From momentum conservation we have

$$p_1 + p_2 + p_3 + p_4 + p_5 + p_6 = 0. \tag{7.4}$$

Spinor products are again constructed from holomorphic and anti-holomorphic two-component Weyl-spinors, so that $s_{ij} = \langle ij \rangle [ji]$. It is also convenient to use traces over γ matrices, which are defined in Appendix A. Throughout the chapter, we will always assume a cyclic ordering of the six legs $i = 1, ..., 6$ for all the indexed quantities (we will have, for instance, 3+4=1).

The amplitudes have overall phases that depend purely on the helicities: in spinor notation those can be expressed by the Parke-Taylor formulae

$$\Phi(--+++) = A_6^{[0]}(--+++) = \frac{\langle 12 \rangle^4}{\langle 12 \rangle \langle 23 \rangle \langle 34 \rangle \langle 45 \rangle \langle 56 \rangle \langle 61 \rangle}, \tag{7.5}$$

$$\Phi(-+-+++) = A_6^{[0]}(-+-+++) = \frac{\langle 13 \rangle^4}{\langle 12 \rangle \langle 23 \rangle \langle 34 \rangle \langle 45 \rangle \langle 56 \rangle \langle 61 \rangle}, \tag{7.6}$$

$$\Phi(-++-++) = A_6^{[0]}(-++-++) = \frac{\langle 14 \rangle^4}{\langle 12 \rangle \langle 23 \rangle \langle 34 \rangle \langle 45 \rangle \langle 56 \rangle \langle 61 \rangle}. \tag{7.7}$$

The choice of the parametrisation was made trying to minimise the maximum degree of the polynomials which represented the numerators of the coefficients in these variables. While there is no objective definition of a *low* or *high* degree in absolute terms, we set the target of having expressions that could be reconstructed in less than 2×10^4 core hours, which on our 64-cores machines corresponded approximately to 2 weeks as an upper limit. From a thorough study of the coefficients, it was observed that such a time limit corresponded to a polynomial degree lower than 60.

Eqs. (4.10) and (4.11) in Chapter 4 represent two possible parametrisations of the six-point phase-space using momentum-twistor variables. In the reconstruction of the tree-level helicity amplitude $A_{6g}^{(0)}(-+-+-+)$, we found the two choices to be approximately equivalent, meaning that the resulting rational expressions had comparable polynomial degrees. This was not the case for one-loop

expressions, for which parametrisation Z^B has proven to be much more efficient. This is explained in Section 7.3, together with the description of algorithms and manipulations employed to optimise the process.

7.2   Amplitudes' Decomposition

We present the colour decomposition of one-loop n-gluon amplitudes in a $SU(N_c)$ theory as expressed in [158]

$$
\begin{aligned}
\mathcal{A}_n^{1-loop} = N_c \sum_{\sigma \in S_n/\mathbb{Z}} \mathrm{tr}(t^{a_{\sigma_1}}...t^{a_{\sigma_n}}) A_{n;1}^{[1]}(\sigma_1...\sigma_n) + \\
+ \sum_{c=2}^{\lfloor n/2 \rfloor + 1} \sum_{\sigma \in S_n/S_{n;c}} \mathrm{tr}(t^{a_{\sigma_1}}...t^{a_{\sigma_{c-1}}})\mathrm{tr}(t^{a_{\sigma_c}}...t^{a_{\sigma_n}}) A_{n;c}(\sigma_1...\sigma_n) + \\
+ n_f \sum_{\sigma \in S_n/\mathbb{Z}} \mathrm{tr}(t^{a_{\sigma_1}}...t^{a_{\sigma_n}}) A_{n;1}^{[1/2]}(\sigma_1...\sigma_n),
\end{aligned}
\tag{7.8}
$$

where $S_{n;c}$ is the subset of S_n which leaves the trace product invariant. The formula is written for a generic number of colours N_c and quark flavours n_f.

Not all the sub-amplitudes in the above formula are independent: the $A_{n;c>1}$ expressions can be written as linear combinations of the $A_{n;1}^{[1]}$ as shown in [158]

$$
A_{n;c}(1,..,c-1;c,...,n) = (-1)^{c-1} \sum_{\sigma \in \mathrm{COP}_{\{\alpha\}\{\beta\}}} A_{n;1}^{[1]}(\sigma_1,...,\sigma_n),
\tag{7.9}
$$

using notation $\{\alpha\} = \{c-1, c-2, ..., 1\}$, $\{\beta\} = \{c+1, c+2, ..., n\}$ and indicating with $\mathrm{COP}\{\alpha\}\{\beta\}$ the set all the permutations that preserve the cyclic ordering of $\{\alpha\}$ and $\{\beta\}$ independently. It is therefore sufficient to compute the $A_{n;1}^{[1]}$'s to obtain all the necessary information.

We recall that the colour-ordered helicity amplitudes are related to one another through conjugation (inverting all the helicities of an amplitude corresponds to the operation $\langle ij \rangle \leftrightarrow [ij]$ in the spinor representation). As stated in Section 3.1 they also possess symmetries that can be inferred from their corresponding colour factors. In particular for the case of Eq. (7.8), we see that the traces

Supersymmetric Content	Helicity
$\mathcal{N} = 4$	$(--+++)$
$\mathcal{N} = 4$	$(-+-+++)$
$\mathcal{N} = 4$	$(-++-++)$
$\mathcal{N} = 1$	$(--+++)$
$\mathcal{N} = 1$	$(-+-+++)$
$\mathcal{N} = 1$	$(-++-++)$
$\mathcal{N} = 0$	$(--+++)$
$\mathcal{N} = 0$	$(-+-+++)$
$\mathcal{N} = 0$	$(-++-++)$

Table 7.1: The nine independent sub-amplitudes that were computed as fundamental building blocks of the whole one-loop amplitude.

multiplying the $A_{n;1}^{[1]}$ and $A_{n;1}^{[1/2]}$ sub-amplitudes are invariant under a cyclic permutations of the external legs, as was the case for the tree-level n-gluon ones. Since this is known to be a symmetry of the overall amplitude, it must also be present for the kinematic parts, for example we have $A_{n;1}^{[1]}(--++++) = A_{n;1}^{[1]}(-++++-)$ and $A_{n;1}^{[1/2]}(--++++) = A_{n;1}^{[1/2]}(-++++-)$.

We readily see that there are only three independent MHV helicity amplitudes: $(--++++)$, $(-+-+++)$, $(-++-++)$, and all the other ones are obtained by cyclically permuting the helicities within this list.

As an additional step, we perform the supersymmetric decomposition of Section 3.7 on the $A_{n;1}^{[1]}$ and $A_{n;1}^{[1/2]}$ sub-amplitudes. We recall

$$A_n^{[1]} = A_n^{\mathcal{N}=4} - 4A_n^{\mathcal{N}=1} + A_n^{\mathcal{N}=0}, \tag{7.10}$$

$$A_n^{[1/2]} = A_n^{\mathcal{N}=1} - A_n^{\mathcal{N}=0}, \tag{7.11}$$

where again the superscripts indicate either a $\mathcal{N} = 4$ multiplet, a $\mathcal{N} = 1$ chiral multiplet or an $\mathcal{N} = 0$ complex scalar. Expressing the amplitude in terms of these supersymmetric components significantly simplifies the calculations. We then see that there are nine independent sub-amplitudes, which we write in Table 7.1.

Having identified a minimal sub-set of independent sub-amplitudes, we move the discussion to the

methods used to reconstruct their analytical form. Most of the methods were already presented in 4.1; here we show their effect for these specific expressions.

7.3   Reconstruction Techniques

All the sub-amplitudes were computed by performing the OPP reduction described in Section 3.6 and then reconstructing the rational coefficients in the scalar integral basis. Two main facts contribute to making the computation of the amplitude in a generic number of dimensions D more involved than the four-dimensional one.

Firstly, as already mentioned in Section 3.6, the number of master integrals is higher for the case of generic dimensions. This is the case since in four dimensions it is possible to express a pentagon scalar integral as a combination of scalar boxes plus terms of order $O(\epsilon)$, which are normally discarded (see for example [159]). This cannot be done for a generic D, making it necessary to compute the additional coefficients of the pentagons.

Secondly, scalar integrals in four dimensions possess known expansions into special functions, such as the $L_k(\frac{s}{t})$ shown in Eq. (6.5). These expansions allow us to find linear relations and simplifications among the special functions, further reducing the basis onto which the expression is projected and diminishing the complexity of the rational coefficients. In the case in which the number of dimensions is kept as a parameter D such expansions cannot be performed, limiting the number of simplifications which precede the reconstruction step.

Contrary to the five-point case, we observed that there was not a single method which proved to be the most efficient for all the sub-amplitudes. Instead, it was most efficient to use different approaches for different helicity configurations and supersymmetric content.

As a preliminary step, we ran a code which applies the different algorithms to a numerical univariate slice of the amplitude and outputs the degrees of the resulting expressions. In this way it was possible to estimate in advance the most convenient method to apply. In this section we outline the reconstruction methods and how effective they are for the individual amplitudes.

7.3.1 Linear Relations

Linear relations among the integral coefficients can be inferred from properties that we know the amplitude must have once expanded into $2n - 2\epsilon$ dimensions.

One type of relations is derived from the structure of the singularities in the dimensional regulator ϵ. The renormalisation properties of QCD impose that ultraviolet (UV) singularities in one-loop amplitudes must be proportional to the amplitude for the same process at tree level, and the proportionality constant is related to the one-loop beta function β_0 ([149], [72]). This is a consequence of the fact that UV divergences can be cancelled at one loop by the insertion of a finite number of counterterms which correspond to tree diagrams with effective vertices [19].

In four dimensions, only the scalar bubble integrals with numerator equal to one contain UV divergences:

$$I_2^{4-2\epsilon}[1](s_{ij}) = \int \frac{d^{4-2\epsilon}k}{(2\pi)^4} \frac{1}{k^2(p_{ij}+k)^2} = \frac{1}{\epsilon} + \log\left(\frac{s_{ij}}{\mu^2}\right) + 2 + O(\epsilon). \tag{7.12}$$

This analysis brings to the conclusion that the UV divergences of the one-loop amplitude must be proportional to the sum of the coefficients of the logarithm terms coming from the bubble expansions. In order to be true in $4 - 2\epsilon$ dimensions, this must also hold in the generic D-dimensional case. We take as an example the $A_{6g}^{(1)}(--+++)$ amplitude, which only has three such integrals in its basis: $I_2^{4-2\epsilon}[1](s_{23})$, $I_2^{4-2\epsilon}[1](s_{234})$ and $I_2^{4-2\epsilon}[1](s_{16})$. We can then readily verify:

$$\begin{aligned} b_{23;1456} + b_{234;156} + b_{16;2345} &= \frac{1}{3} \frac{\langle 12 \rangle^3}{\langle 23 \rangle \langle 34 \rangle \langle 45 \rangle \langle 56 \rangle \langle 61 \rangle} \\ &= \frac{1}{3} A_{6g}^{(0)}(--+++), \end{aligned} \tag{7.13}$$

where again the coefficient $b_{ij;klmn}$ is the one multiplying $I_2^{4-2\epsilon}[1](s_{ij})$.

These relations were obtained using the same algorithm described in Section 4.3.1, with the tree-level amplitudes given as part of the f_i rational ansätze.

7.3.2   Factor Matching and Partial Fractioning

The factor matching is performed in the same fashion as described in chapters 4 and 5. The factors in the expressions are matched to the ones present in an ansatz, corresponding to the spinor structures evaluated on the same slice. The coefficients are divided out by the matched factors, leaving smaller polynomials to be reconstructed. This operation is completely automatised within the algorithm. The list of ansätze was created starting from

$$\{\langle ij\rangle , [ij], s_{ij}, s_{ijk}, \langle i|\, p_{jk}\,|l], s_{ijk} - s_{ij}, (p_{ij}\cdot p_{kl})^2 - s_{ij}s_{kl}, \mathrm{tr}_5(i,j,k,l)\}, \tag{7.14}$$

with the indices running over all possible values $i, j, k, l = 1, ..., 6$. As already discussed in Section 4.3.2, the resulting list is over-complete. Again, we used the same procedure of evaluating all the terms in momentum-twistor variables and only keeping the independent polynomial factors in the resulting expressions. We see that in comparison with the list of ansätze used for the 6-gluon tree-level amplitudes, we needed to also include spurious denominators arising from integral tensor reductions, such as $(p_{ij}\cdot p_{kl})^2 - s_{ij}s_{kl}$.

Before proceeding with full reconstructions, the factor-matching algorithm was tested on the expressions with both alternative parametrisations Z^A and Z^B. This allowed us to verify which of the two choices would result in a more efficient reconstruction. The results of this comparison are shown in the Table 7.2. In both tables we show how the degree of the most complex coefficient in each amplitude changes after the matching.

It is clear by comparing the two tables 7.2 that the choice Z^B is the most convenient one, since the degrees are lower for every expression. For this reason the parametrisation A was discarded and the amplitudes were not reconstructed in those variables. For the rest of the chapter, all the reconstructed rational expressions should be understood as functions of variables in Eq. (4.12).

For the sake of completeness, we give the transformations from Lorentz invariants to rational

Z^A				
Supersymmetric Content	Helicity	Original Degrees	Reduced	Coeff. of Highest Deg.
$\mathcal{N} = 4$	$(--++++)$	21	0	$I_5[\mu^2](s_{34})$
$\mathcal{N} = 4$	$(-+-+++)$	21	0	$I_5[\mu^2](s_{34})$
$\mathcal{N} = 4$	$(-++-++)$	21	0	$I_5[\mu^2](s_{34})$
$\mathcal{N} = 1$	$(--++++)$	33	13	$I_4^{1m}[\mu^2](s_{234})$
$\mathcal{N} = 1$	$(-+-+++)$	38	27	$I_2(s_{345})$
$\mathcal{N} = 1$	$(-++-++)$	35	23	$I_2(s_{34})$
$\mathcal{N} = 0$	$(--++++)$	78	60	$I_4^{2mH}[\mu^2](s_{23}, s_{61})$
$\mathcal{N} = 0$	$(-+-+++)$	90	66	$I_2[\mu^2](s_{345})$
$\mathcal{N} = 0$	$(-++-++)$	126	118	$I_2[\mu^2](s_{345})$
Z^B				
Supersymmetric Content	Helicity	Original Degrees	Reduced	Coeff. of Highest Deg.
$\mathcal{N} = 4$	$(--++++)$	15	0	$I_5[\mu^2](s_{23})$
$\mathcal{N} = 4$	$(-+-+++)$	15	0	$I_5[\mu^2](s_{23})$
$\mathcal{N} = 4$	$(-++-++)$	15	0	$I_5[\mu^2](s_{23})$
$\mathcal{N} = 1$	$(--++++)$	21	10	$I_4^{1m}[\mu^2](s_{123}, s_{45}, s_{56})$
$\mathcal{N} = 1$	$(-+-+++)$	38	11	$I_4^{2mH}[\mu^2](s_{12}, s_{34})$
$\mathcal{N} = 1$	$(-++-++)$	20	16	$I_2[1](s_{34})$
$\mathcal{N} = 0$	$(--++++)$	44	36	$I_4^{2mH}[\mu^2](s_{23}, s_{16})$
$\mathcal{N} = 0$	$(-+-+++)$	53	46	$I_4^{1m}[\mu^2](s_{123}, s_{45}, s_{56})$
$\mathcal{N} = 0$	$(-++-++)$	78	74	$I_2[\mu^2](s_{345})$

Table 7.2: The degrees of the coefficients before and after the factor matching, in both parametrisations. For each amplitude, only the highest coefficient degree is presented. The last column indicates the scalar integral associated to the most complex coefficient for each case. We notice that the degrees are lower using parametrisation Z^B for every amplitude.

parametrisation in such variables:

$$s_{23} = \frac{s_{12}y_1}{\sigma_1 - 1},$$

$$s_{34} = \frac{s_{12}(y_3 - y_2\sigma_1 + y_1\sigma_2)}{\sigma_1 - \sigma_2},$$

$$s_{45} =$$

$$\frac{s_{12}(-y_2y_4(\sigma_1 - 1) + y_1^2(\sigma_2 - \sigma_3) + y_3(y_1 + \sigma_1 - y_1\sigma_3 - 1) + y_1(\sigma_1 - y_2\sigma_1 + y_4(\sigma_2 - 1) - \sigma_2 + y_2\sigma_3))}{y_1(\sigma_1 - 1)(\sigma_2 - \sigma_3)},$$

$$s_{56} = \frac{s_{12}(y_2y_4 + y_1y_3 - y_1y_4 - y_3)}{y_1(\sigma_2 - \sigma_1)},$$

$$s_{61} = \frac{s_{12}(y_3 - y_2y_4)}{y_1(\sigma_2 - \sigma_3)},$$

$$s_{123} = \frac{s_{12}(y_1 + y_4 - 1)}{\sigma_1 - 1},$$

$$s_{234} = \frac{s_{12}y_3}{\sigma_2 - \sigma_1},$$

$$s_{345} = \frac{s_{12}(y_3 - y_2y_4 + y_1\sigma_2 - y_1y_2\sigma_3)}{y_1(\sigma_2 - \sigma_3)}.$$

(7.15)

We see from the table that the factor matching is very effective in reducing the polynomial degrees of the coefficients of most of the sub-amplitudes, with the notable exception of $N = 0$ and $(-+-+++)$ $(-++-++)$; for these two most complex expressions it is convenient to perform a univariate partial fractioning with respect to the momentum twistor variable y_4.

We display the degrees obtained with the partial fractioning using Table 7.3, which has the same structure as Table 4.3:

Amplitude	Original Degrees	Stage 1	Stage 2	Stage 3
$A_{6g}^{\mathcal{N}=0}(-+-+++)$	53/41	46/0	41/37	32/27
$A_{6g}^{\mathcal{N}=0}(-++-++)$	78/75	74/0	43/38	38/35

Table 7.3: The polynomial degree of the expression to be reconstructed in each stage. The stages are the same as described in Section 4.3.3

.

We see that the degrees are significantly lowered once the univariate apart is performed.

7.3.3   Two Stage Reconstruction

In this section we briefly outline a method employed to reduce the reconstruction time for the most complex expressions.

We recall from Chapter 4 that the reconstruction time for a rational expression corresponds to the time to evaluate the algorithm on a specific numerical point multiplied by the number of points:

$$\textbf{Total Time} = \textbf{Time Per Point} \times \textbf{Number of Points} = \textbf{T} \times \textbf{N}. \tag{7.16}$$

Remembering that we have seen in Section 4.1 that the upper bound on the number of points depends on the number of variables of a polynomial and the maximum degree in each variable. Therefore the number of points to be evaluated increases with higher degrees. The evaluation time per point, on the other hand, is proportional to the length of the ansatz, as we have seen in Section 4.3.3. If the ansatz in the form of Eq. (4.21) or the one for the multivariate case contain many terms, it will take a longer time to evaluate them on a specific point. A trade-off is then observed between the
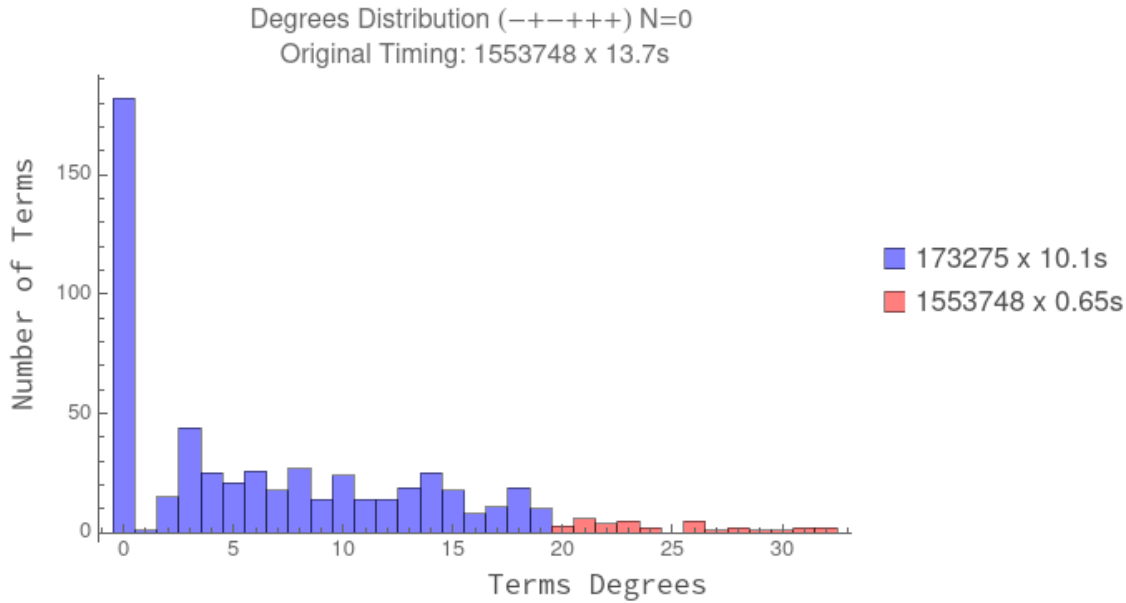
Figure 7.1: The number of ansatz terms grouped according to their polynomial degree. The different colours indicate which terms were reconstructed in Stage 1 (blue) and which in Stage 2 (red), the legend shows how much time each stage took. *Original Timing* refers to the reconstruction time if the split is not performed.

benefit of having a longer ansatz which greatly decreases the maximum degrees, and the time that is taken to evaluate it at every point.

For this reason, it was beneficial to have a preliminary run of the algorithm which evaluated the degrees of every term in the ansatz on univariate slices. This allows us to study how much the degrees varied from term to term. A histogram containing this data for the $A_{6g}^{N=0}(-+-+++)$ is shown in Figure 7.1.

It is apparent from the histogram that the majority of the terms in the ansatz have a polynomial degree which is significantly lower than the ones with the highest complexity. This fact suggests the convenience of performing the reconstruction in two stages:

- **Stage 1:** reconstruct all the terms in the ansatz which have a total degree below a certain threshold, ignoring the most complex ones;

- **Stage 2:** subtract the reconstructed terms from the whole expression and reconstruct the remaining terms in the original ansatz.

We can see the advantage given by the implementation of the two-stage procedure by examining the reconstruction times in both stages.

In Stage 1 the number of terms in the ansatz is not changed (all terms need to be evaluated in order to reconstruct even a portion of the final result) but a lower number of sample points is needed, since we are only interested in reconstructing the polynomials of lowest degree. This means that the reconstruction is performed in a time $\mathbf{N_s} \times \mathbf{T}$, where $\mathbf{N_s}$ is the smaller number of points. We see in Figure 7.1 that the reconstruction time per point is indeed almost equal to the one for the direct reconstruction.

In Stage 2 the total number of points is the same as for the original reconstruction, since the polynomials being reconstructed are those of highest degree, but the time per point is lowered, since many of the terms in the ansatz were already reconstructed in Stage 1. The reconstruction is then performed in $\mathbf{N} \times \mathbf{T_s}$, where $\mathbf{T_s}$ is the smaller reconstruction time.

The total reconstruction time for the two-stage process therefore is $\mathbf{N_s} \times \mathbf{T} + \mathbf{N} \times \mathbf{T_s}$. We have empirically verified that

$$\mathbf{N_s} \times \mathbf{T} + \mathbf{N} \times \mathbf{T_s} < \mathbf{N} \times \mathbf{T}, \tag{7.17}$$

if the majority of the terms have a degree much lower than the highest one.

This case is shown in Figure 7.1, where the highest degree is 32 but more than 90% of the terms are of degree lower than 20. Consiquently, the reconstruction time is reduced by more than a factor of 7:

$$\frac{\mathbf{N_s} \times \mathbf{T} + \mathbf{N} \times \mathbf{T_s}}{\mathbf{N} \times \mathbf{T}} = \frac{173275 \times 10.1s + 1553748 \times 0.7s}{1553748 \times 13.7s} = 7.7. \tag{7.18}$$

Having discussed the reconstruction techniques, in the following sections we present explicit results for some $\mathcal{N} = 4$ and $\mathcal{N} = 1$ helicity amplitudes. The amplitudes are presented in terms of spinor-helicity variables, including their full phase dependence. We will see that the expressions can be written in a compact form.

7.4 $\mathcal{N} = 4$ **Case**

The $\mathcal{N} = 4$ expressions in D dimensions are equal to the $4 - 2\epsilon$ ones, with the addition of order $O(\epsilon)$ pentagons. All three MHV helicity configurations $(- - + + ++, - + - + ++$ and $- + + - ++)$ have the same expression once we divide out by the phase $(A_6^{(0)}(h))$,

$$A_6^{N\,=4}(h) = A_6^{(0)}(h)\left[\sum_i^6 e_i I_5^{[i]}[\mu^2] + d_{12}^{(1)}I_4^{1m}(s_{12}, s_{23}) + d_{61}^{(1)}I_4^{1m}(s_{61}, s_{12}) + d_{14}^{(2)}I_4^{2mE}(s_{23}, s_{56}) + \right.$$
$$d_{56}^{(2)}I_4^{1m}(s_{56}, s_{61}) + d_{36}^{(2)}I_4^{2mE}(s_{45}, s_{12}) + d_{45}^{(1)}I_4^{1m}(s_{45}, s_{56}) + d_{23}^{(1)}I_4^{1m}(s_{23}, s_{34}) +$$
$$\left. d_{25}^{(2)}I_4^{2mE}(s_{34}, s_{16}) + d_{34}^{(1)}I_4^{1m}(s_{34}, s_{45})\right].$$

$$(7.19)$$

We used the following notation for pentagon and box integrals

$$I_5^{[i]}[\mu^2] = \int \frac{d^D k}{(2\pi)^D} \frac{\mu^2}{k^2(k + p_{i,i+1})^2(k + p_{i,i+2})^2(k + p_{i,i+3})^2(k - p_{i+5})^2}, \qquad (7.20)$$

$$I_4^{2mE}(s_{ij}, s_{kl}) = \int \frac{d^D k}{(2\pi)^D} \frac{1}{k^2(k - p_{j+1})^2(k - p_{j+1} - p_{kl})^2(k + p_{ij})^2}, \qquad (7.21)$$

$$I_4^{1m}(s_{ij}, s_{jk}) = \int \frac{d^D k}{(2\pi)^D} \frac{1}{k^2(k - p_i)^2(k - p_{ij})^2(k - p_{ijk})^2}, \qquad (7.22)$$

where the integral coefficients are

$$e_i = \frac{A(i)\mathrm{tr}_5(i + 2, i + 3, i + 4, i + 5)}{\mathrm{tr}_5(1, 2, 3, 4, 5, 6)}, \qquad (7.23)$$

$$d_{ij}^{(1)} = s_{ij}s_{jj+1}, \qquad (7.24)$$

$$d_{ij}^{(2)} = \langle i, p_{i+1i+2}, j, p_{j+1j+2}, i], \qquad (7.25)$$

and we introduced the shorthand notation

$$A(i) = \begin{cases} - |1234561\rangle & i \text{ odd} \\ - |1234561\rangle & i \text{ even.} \end{cases} \qquad (7.26)$$

.

7.5 $\mathcal{N} = 1$ Case

The three independent MHV amplitudes are distinct for the $\mathcal{N} = 1$ case. The integral bases of these amplitudes are the same as for their $4 - 2\epsilon$ versions, with the addition of μ^2 pentagons and boxes. The simplest one of the three is

$$A_6^{\mathcal{N}=1}(--+++) = \tag{7.27}$$

$$A_6^{[0]} \Big[\sum_i^6 e_i I_5^{[i]}[\mu^2] + \sum_i^6 d_i^{1m} I_4^{1m[i]}[\mu^2] + \sum_i^3 d_i^{2mE} I_4^{2mE[i]}[\mu^2] +$$

$$\sum_i^6 d_i^{2mH} I_4^{2mH[i]}[\mu^2] + b_{23;1456} I_2(s_{23}) + b_{234;156} I_2(s_{234}) + b_{16;2345} I_2(s_{16}) \Big]$$

where we used an alternative notation for the three types of box integrals: one-mass ones $(1m)$, two-adjacent masses $(2mH)$ and two non-adjacent masses $(2mE)$.

$$I_4^{2mE[i]} = \int \frac{d^D k}{(2\pi)^D} \frac{\mu^2}{k^2(k + p_{ii+1})^2(k + p_{ii+2})^2(k - p_{i-1})^2},$$

$$I_4^{2mH[i]} = \int \frac{d^D k}{(2\pi)^D} \frac{\mu^2}{k^2(k + p_{ii+1})^2(k + p_{ii+3})^2(k - p_{i-1})^2}, \quad \tag{7.28}$$

$$I_4^{1m[i]} = \int \frac{d^D k}{(2\pi)^D} \frac{\mu^2}{k^2(k + p_{ii+2})^2(k + p_{ii+3})^2(k - p_{i-1})^2}.$$

The function $I_2(s_{ij})$ is the scalar bubble integral

$$I_2(s_{ij}) = \int \frac{d^D k}{(2\pi)^D} \frac{1}{k^2(p_{ij} + k)^2}. \tag{7.29}$$

We find two distinct expressions for the pentagon coefficients, depending if the massive leg takes a contribution from particles with same helicity $(+, +)$ or different helicity $(-, +)$. The coefficients are simpler in the first case

$$e_i = \begin{cases} \dfrac{s_{i+3i+4}s_{i+4i-1}\text{tr}_+(i-1, p_{ii+1}, i+2, p_{i+3i+4})\text{tr}_+(1, 2, 3, 4, 6, 5)}{\text{tr}_5(i+4, i-1, i+3, i+2)\text{tr}_5(1, 2, 3, 4, 5, 6)}, & i \neq 2, 6 \quad \text{(same helicities)} \\[2ex] \dfrac{s_{i+2,i+3}s_{i+3,i+4}s_{i+4,i+5}\text{tr}_+(i-1, p_{ii+1}, i+2, p_{i+3i+4})\text{K}_i}{s_{12}\text{tr5}(i+4, i-1, i+3, i+2)\text{tr}_5(1, 2, 3, 4, 5, 6)}. & i = 2, 6 \quad \text{(different helicities)} \end{cases}$$

$$\tag{7.30}$$

The K_i term is

$$K_i = \frac{\langle i+2|\,i\,|i-1]}{\langle i+2|\,p_{i,i+1}|i-1]}\mathrm{tr}_+(1,6,5,4,2,3) + \frac{\langle i+2|\,p_{i,i+4,i+4}|i-1]}{\langle i+2|\,p_{i,i+1}|i-1]}\mathrm{tr}_+(1,2,3,4,6,5) \qquad (7.31)$$

and the bubble coefficients are

$$\begin{aligned}
b_{ij;klmn} &= \frac{s_{jl}\,\langle il\rangle\,\langle kj\rangle}{(s_{ijl}-s_{ij})\,\langle ik\rangle\,\langle jl\rangle}, \\
b_{ijk;lmn} &= \frac{\mathrm{tr}_+(i,l,m,p_{ijk})-\mathrm{tr}_+(i,l,p_{ijk},m)}{(s_{ijk}-s_{ij})s_{il}} + \frac{\mathrm{tr}_+(i,l,k,p_{ij})-\mathrm{tr}_+(i,l,p_{ij},k)}{(s_{ijk}-s_{mn})s_{il}}.
\end{aligned} \qquad (7.32)$$

We notice how the coefficients of the bubbles with the sum of three momenta on both legs are significantly more complex; this feature is observed in all the helicity amplitudes.

The helicity amplitude in Eq. (7.27) is the simplest of the three; we notice the absence of triangles which are instead present in the other two helicity configurations. While the scalar triangles did not contribute to the amplitudes in their four-dimensional expansion, their coefficients were still computed when we obtained their D-dimensional expressions with the OPP reduction.

7.6 Dimensional Recursion Relations

In this section we present the derivations which are used to relate higher dimensional integrals to the ones in $D = 4 - 2\epsilon$. Such relations are useful since expansions of the box, triangle and bubble integrals in $D = 4 - 2\epsilon$ in terms of special functions are known in the literature up to finite orders in ϵ [160]. Such expansions, as already discussed in Section 7.3.1, instruct us on relations among the rational coefficients.

The reason for this discussion is therefore twofold: on the one hand it instructs on how to obtain the expressions for specific values of space-time dimensions, and on the other it shows how the results for $D > 4$ can be used to infer new relations among the rational coefficients.

As explained in Section 4.3.1, finding that a certain linear combination of coefficients is equal to a known function f_k can be useful to expand the coefficient ansatz and improve the future reconstruction performance of other expressions.

The results presented here are valid for a generic n, but some of these are shown explicitly for the

$n = 4$ and $n = 6$ cases. The $D = 4 - 2\epsilon$ case is particularly important since it allowed us to check that our results were consistent with the literature in the four-dimensional limit.

In our notation, we split the momentum vector in its 4-dimensional and $(D - 4)$-dimensional components respectively: $\bar{k}$ and $\tilde{k}$, and the effective mass is defined as $\tilde{k} \cdot \tilde{k} = \mu^2$. In the integrand reduction method, many integrals in the basis have powers of the effective mass in their numerators: μ^2, μ^4. These integrals can be related to the ones in $D + 2$ and $D + 4$ dimensions via the following steps, as shown in [161]:

$$\int d^D k \mu^{2r} = \int d^4 \bar{k} \int d^{D-4} \tilde{k} \mu^{2r} = \int d^4 \bar{k} \int d\Omega_{D-5} \int_0^\infty \frac{d\mu^2}{2} \mu^{D-6+2r} = \tag{7.33}$$
$$\int d^4 \bar{k} \int d\Omega_{D-5} \frac{\int d^{D-4+2r} \tilde{k}}{\int d\Omega_{D-5+2r}} = \frac{\int d\Omega_{D-5}}{\int d\Omega_{D-5+2r}} \int d^{D+2r} k.$$

The formula for solid angles in general dimensions is

$$\int d\Omega_n = \frac{\pi^{\frac{n+1}{2}}}{\Gamma(\frac{n+1}{2})}, \tag{7.34}$$

this allows us to write the result as an expansion in the dimensional regulator. For example, for $D = 4 - 2\epsilon$ and $r = 1$ we have

$$\int d^{4-2\epsilon} k \mu^2 = -\epsilon \int d^{6-2\epsilon} k, \tag{7.35}$$

which proves the Eqs. (3.70) and (3.71) in Section 3. We also make use of the *lowering dimensional recurrence relation* for one-loop integrals [162, 163],

$$I_n^{d+2} = \frac{(2\mu)[V(p_1, ..., p_n)]^{-1}}{d - n} P(B_1, ..., B_{n+1}) I_n^d, \tag{7.36}$$

where n is the number of external legs and V is the Gram determinant $V(v_1, ..., v_n) = \det G(v_1, ..., v_n)$ as defined in Eq. (A.14). The polynomial P is defined so that

$$P(denominators) = V(k, p_1, ..., p_n), \tag{7.37}$$

with *denominators* indicating the set of denominators appearing in the integrand of I_n^d. The B_i operators act on the integrals as

$$B_i I_n^d(a_1, ..., a_n) = I_n^d(a_1, ..., a_{i-1}, ..., a_n), \tag{7.38}$$

where the a_i are the powers of the denominators appearing in the integral. By combining Eqs. (7.33) and (7.36) we are able to express any of the integrals appearing in the OPP basis in terms of scalar $4 - 2\epsilon$ ones, for which analytic expressions are known.

7.6.1 The $4 - 2\epsilon$ case

The form of the six-gluon one-loop amplitudes in $D = 4 - 2\epsilon$ is well known [91]. As it is clear from the previous section, taking the limit in a specific number of dimensions consists of finding the expansion of the integral basis I_n^d, obtaining a form which has a dependence on the ϵ parameter. This was done for all the integrals appearing in the $\mathcal{N} = 4, \mathcal{N} = 1$ and $\mathcal{N} = 0$ MHV amplitudes up to finite orders in ϵ.

Before presenting the expansions, we give the definitions of the three types of triangle integrals which appear in the bases of $\mathcal{N} = 0$ amplitudes:

$$I_3^{1m}(s_{ij}, s_l) = \int \frac{d^D k}{(2\pi)^D} \frac{1}{k^2 (k + p_l)^2 (k - p_j)^2}, \tag{7.39}$$

$$I_3^{2m}(s_k, s_l) = \int \frac{d^D k}{(2\pi)^D} \frac{1}{k^2 (k + p_k)^2 (k + p_{kl})^2}, \tag{7.40}$$

$$I_3^{3m}(s_j, s_k, s_l) = \int \frac{d^D k}{(2\pi)^D} \frac{1}{k^2 (k + p_j)^2 (k - p_l)^2}. \tag{7.41}$$

As always, integrals $I_3^{1m}[\mu^{2r}]$, $I_3^{2m}[\mu^{2r}]$, $I_3^{3m}[\mu^{2r}]$ have the same expression with μ^{2r} as the numerator of the integrand. The explicit expansions are [89]:

$$I_5^{[i]}[\mu^2] = O(\epsilon),$$

$$I_4[\mu^2](s_{ij}, s_{kl}) = -\frac{1}{6} + O(\epsilon),$$

$$I_4^{1m}(s_{ij}, s_{jk}) = -\frac{2}{s_{ij} s{jk}} \left(\frac{(-s_{ij})^{-\epsilon}}{\epsilon^2} + \frac{(-s_{jk})^{-\epsilon}}{\epsilon^2} - \frac{(-s_{ijk})^{-\epsilon}}{\epsilon^2} + \mathrm{F}^{1m}[s_{ij}, s_{jk}, s_{ijk}] \right) + O(\epsilon),$$

$$I_4^{2mE}(s_{ij}, s_{jk}, p_j, p_l) = -\frac{2}{s_{ij} s_{jk} - p_j^2 p_l^2} \left(\frac{(-s_{ij})^{-\epsilon}}{\epsilon^2} + \frac{(-s_{jk})^{-\epsilon}}{\epsilon^2} - \frac{((-p_j)^2)^{-\epsilon}}{\epsilon^2} - \frac{((-p_l))^{-2\epsilon}}{\epsilon^2} \right.$$
$$\left. + \mathrm{F}^{2mE}[s_{ij}, s_{jk}, p_j, p_l] \right) + O(\epsilon)$$

$$I_4^{2mH}(s_{ij}, s_k, s_l) = -\frac{2}{s_{ij} s_{jk}} \left(\frac{(-s_{ij})^{-\epsilon}}{\epsilon^2} + \frac{(-s_{jk})^{-\epsilon}}{\epsilon^2} - \frac{(-(p_k)^2)^{-\epsilon}}{\epsilon^2} - \frac{(-(p_l)^2)^{-\epsilon}}{\epsilon^2} \right. \tag{7.42}$$

$$\left. + \mathrm{F}^{2mH}[s_{ij}, s_k, s_l] \right) + O(\epsilon),$$

$$I_3[\mu^2](s_{ij}, s_{kl}) = \frac{1}{2} + O(\epsilon)$$

$$I_3^{1m}(s_{ij}, s_k) = -\frac{(-(p_k)^2)^{-\epsilon}}{\epsilon^2 s_k} + O(\epsilon),$$

$$I_3^{2m}(p_k, p_l) = -\frac{(-(p_k)^2)^{-\epsilon} - (-(p_l)^2)^{-\epsilon}}{\epsilon^2 (p_k^2 - p_l^2)} + O(\epsilon),$$

$$I_2[\mu^2](s_{ij}) = -\frac{s_{ij}}{6} + O(\epsilon),$$

$$I_2(s_{ij}) = \frac{1}{\epsilon} - \log(s_{ij}) + 2 + O(\epsilon).$$

Where we used the following notation for the finite part of the boxes $F^{2mE}[s_{ij}, s_{kk}^2]$, $F^{2mH}[s_{ij}, p_k^2, p_l^2]$, $F^{1m}[s_{ij}, s_{kl}, s_{ijk}]$:

$$\begin{aligned}
F^{1m}[s_{ij}, s_{jk}, s_{ijk}] &= -L_2\left(1 - \frac{s_{ikj}}{s_{ij}}\right) - L_2\left(1 - \frac{s_{ikj}}{s_{jk}}\right) - \frac{1}{2}\log\left(\frac{s_{ij}}{s_{jk}}\right) - \frac{\pi^2}{6}, \\
F^{2mE}[s_{ij}, s_{jk}, s_j, s_l] &= -L_2\left(1 - \frac{s_j}{s_{ij}}\right) - L_2\left(1 - \frac{s_j}{s_{jk}}\right) - L_2\left(1 - \frac{s_l}{s_{ij}}\right), \\
&\quad - L_2\left(1 - \frac{s_l}{s_{jl}}\right) + L_2\left(1 - \frac{s_j s_l}{s_{ij} s_{jk}}\right)\log^2\left(\frac{s_{ij}}{s_{jk}}\right), \\
F^{2mH}[s_{ij}, s_{jk}, s_k, s_l] &= -L_2\left(1 - \frac{s_k}{s_{jk}}\right) - L_2\left(1 - \frac{s_k}{s_{jk}}\right) - \frac{1}{2}\log^2\left(\frac{s_{ij}}{s_{jk}}\right).
\end{aligned}$$ (7.43)

The dilogatirhms $\text{Li}_2(x)$ are defined as [89]

$$\text{Li}_2(x) = -\int_0^x \frac{dt}{t}\text{Log}(1-t) = \frac{x}{1^2} + \frac{x^2}{2^2} + \frac{x^3}{3^2} + \dots \quad \text{for}|x| \le 1$$ (7.44)

We verified that, by performing these substitutions for the integrals in the sub-amplitudes in Table 7.1, we obtain the same results as in [91].

7.6.2 The $6 - 2\epsilon$ case

As for the $4 - 2\epsilon$ case, in order to find the $D = 6$ form of the amplitudes it is necessary to expand the integral basis in 6 dimensions. In this case we are mainly interested in the pole structure of the amplitudes, therefore we only show the expansion up to order $O(\frac{1}{\epsilon})$.

The form of some of the integrals was obtained from [164], and for the missing ones the ϵ dependence

was obtained using dimensional recurrence relations derived with LITERED [129],

$$I_5^{[i]}[\mu^2] = O(\epsilon^0),$$

$$I_4^{1m}[\mu^4](s_{ij}, s_{jk}) = \frac{s_{ijk} + s_{ij} + s_{jk}}{60\epsilon} + O(\epsilon^0),$$

$$I_4^{2mE}[\mu^4](s_{ij}, s_{jk}, p_j^2, p_l^2) = \frac{p_j^2 + s_{kl} + p_l^2 + s_{il}}{60\epsilon} + O(\epsilon^0),$$

$$I_4^{2mH}[\mu^4](s_{ij}, p_k^2, p_l^2) = \frac{p_k^2 + p_l^2 + s_{jk} + s_{ij}}{60\epsilon} + O(\epsilon^0),$$

$$I_4^{1m}[\mu^2](s_{ij}, s_{jk}) = \frac{1}{6\epsilon} + O(\epsilon^0),$$

$$I_4^{2mE}[\mu^2](s_{ij}, s_{jk}, p_j^2, p_l^2) = \frac{1}{6\epsilon} + O(\epsilon^0),$$ (7.45)

$$I_4^{2mH}[\mu^2](s_{ij}, p_k^2, p_l^2) = \frac{1}{6\epsilon} + O(\epsilon^0),$$

$$I_3^{1m}[\mu^2](s_{ij}) = -\frac{s_{ij}}{24\epsilon} + O(\epsilon^0),$$

$$I_3^{2m}[\mu^2](p_i^2, p_j^2) = -\frac{p_i^2 + p_j^2}{24\epsilon} + O(\epsilon^0),$$

$$I_3^{3m}[\mu^2](p_i^2, p_j^2, p_k^2) = -\frac{p_i^2 + p_j^2 + p_k^2}{24\epsilon} + O(\epsilon^0),$$

$$I_2(p_i^2)[\mu^2] = \frac{p_i^4}{60\epsilon} + O(\epsilon^0),$$

$$I_2(p_i^2)[1] = \frac{p_i^4}{60\epsilon} + O(\epsilon^0).$$

From the above expansions we see that in six dimensions the amplitudes do not have any pole deeper than $\frac{1}{\epsilon}$. It is interesting to reproduce a similar computation as the one presented in Section 7.3.1, but for $D = 6 - 2\epsilon$. Namely, we compute the ϵ pole of the amplitude, and we verify that it corresponds to a local rational function of the kinematics. In this case the term *local* refers to a function free of spurious poles. We can refer to this function as a *tree-like expression*, since it originates from tree-level diagrams in an effective six-dimensional theory.

For the case of sub-amplitude $A^{\mathcal{N}=0}(- - + + + +)$, we have 63 rational coefficients multiplying the

same number of scalar integrals. After the ϵ expansion we find:

$$
\begin{aligned}
20(c_7 &+ c_9 + c_{11} + c_{13} + c_{15} + c_{17} + c_{19} + c_{21} + c_{23} + c_{25} + c_{27} + c_{29} + c_{31} + c_{33} \\
&+ c_{35} + c_{55}s_{23} + c_{57}s_{234} + c_{59}s_{16}) + 2c_{56}s_{23}^2 + 2c_{60}s_{16}^2 + 2c_{61}s_{34}^2 + 2c_{54}s_{56}^2 \\
&+ 2c_{32}(p_{16} + p_{34})^2 + 2c_{28}(p_{23} + p_{34})^2 + 2c_{63}s_{45}^2 + 2c_{58}s_{234}^2 + 2c_{62}s_{345}^2 \\
&- 5(c_{39}s_{16} + c_{43}s_{23} + c_{49}s_{34} + c_{52}s_{45} + c_{42}s_{56}) + 2c_{22}(p_{12} + p_{45})^2 + 2c_{36}(p_{34} + p_{45})^2 \\
&+ 2c_{14}(p_{23} + p_{56})^2 + 2c_{26}(p_{45} + p_{56})^2 + 2c_{18}(p_{16} + p_{56})^2 = \textbf{local rational function}.
\end{aligned}
\tag{7.46}
$$

As expected, the coefficient of the $O(\frac{1}{\epsilon})$ pole is a rational function free of spurious singularities.

7.7 Conclusion

In this chapter we have presented the details of the computation of the six-gluons MHV helicity amplitudes in a generic number of dimensions D.

The helicity amplitudes were decomposed into combinations of simpler sub-expressions, exploiting the properties known from the formal study of scattering amplitudes presented in chapters 2 and 3. All the sub-amplitudes were represented as a linear combination of one-loop scalar integrals multiplied by rational coefficients which are functions of the external kinematics. Some of the simplest expressions are presented explicitly in a compact form in terms of spinor variables.

Carrying out these computations allowed us to study the effects of the reconstruction over finite fields of rational functions expressed in terms of momentum-twistor variables for amplitudes of high multiplicity. Some valuable tools which were developed in this work were codes which make it possible to automatically estimate the impact of a specific reconstruction method over the polynomial degrees of an expression, without the need to perform the full numerical interpolation. The MATHEMATICA code which was written to achieve this goals directly generates histograms of the form of the one in Figure 7.1, giving a clear indication on which terms contribute the most to the overall complexity of an amplitude and enabling us to perform the reconstruction in multiple stages. The data on the degrees and reconstruction times will be useful when these techniques will be extended to a broader class of amplitudes.

It was possible to write the expressions in terms of spinor variables, by matching factors appearing in the numerators and denominators of the coefficients with spinor structures which were listed in an ansatz. In order to achieve compact expressions, it was necessary to perform some algebra and

apply spinor identities of the type presented in Eq. (3.19). It will probably be beneficial to increase the automatisation level of this procedure in the future, so that it will be possible to directly obtain parts of the amplitude in spinor form.

At the end of the chapter, it was shown how the expressions computed in this project can be used to obtain the explicit analytic form of coefficients of amplitudes in an arbitrary number of dimensions. It was shown with a brief example how these expansions could be exploited to find additional relations among the coefficients of the amplitudes. These ideas have the potential of helping to enlarge the number of useful terms in the ansatz for the reconstruction of the coefficients. The most natural case in which this can be implemented is the NMHV six-gluon one-loop amplitudes. In computing the NMHV expressions, we anticipate to observe a significant increase in complexity due to the higher polynomial degrees of the coefficients in the momentum-twistor parametrisation.

Chapter 8

Conclusions

In this thesis we have studied the computation of high-multiplicity one-loop scattering amplitudes in Quantum Chromodynamics. We presented original results for five-point and six-point amplitudes, both with massive and massless external legs and internal propagators. Together with their analytic expressions, we described the new techniques which were developed in order to optimise their reconstruction.

The new results are useful ingredients for the phenomenological studies of various processes of interest. In particular, the five-point amplitudes will be used to obtain full $pp \to \bar{t}tj$ NNLO results, while the six-point gluon expressions will contribute to studies of $pp \to 2j$ at N^3LO. In both these works, the amplitudes that we obtained were in relatively compact forms. This fact made it possible to find alternative representations in terms of spinor variables of some sub-amplitudes. This is a convenient feature, since having representations which are easily readable can enable us to better understand their physical properties .

The reconstruction via numerical interpolation over finite fields has proven to be an extremely effective method to obtain full analytic expressions, requiring only a relatively modest amount of time and computing resources. Despite the power of these techniques, as implemented in FINITEFLOW, we have seen in this work that it was necessary to integrate them with new tools and strategies to

tackle the computation of the most complex expressions.

It is apparent from the work presented that it is essential to exploit the knowledge about the physical properties of the amplitudes in order to minimise the amount of computations needed to obtain a full result. This starts at the level of the decomposition of the amplitude into sub-amplitudes; we heavily exploited the symmetries relating colour-ordered helicity amplitudes, as well as the ones which arise from their supersymmetric decomposition, in the case of multi-gluon expressions.

At a lower level, we studied the linear relations among the individual rational coefficients of the sub-amplitudes, avoiding the computation of the most complex ones in favour of the ones with lowest polynomial degrees. Some of these relations are known form the general theory, such as the one relating the bubble coefficients, while others could be found by applying the algorithm within FINITEFLOW. The work we have done confirmed that the information about tree-level amplitudes can and must be exploited in the computation of one-loop expressions. In the same way, we expect that the use of analytic one-loop expressions will be useful to construct the ansätze for two-loop amplitudes.

In addition to the study of the physical properties of scattering amplitudes, we found that it was beneficial to investigate the features of some of their parts as purely mathematical objects. This has been possible thanks to the methods that reduce the amplitudes to linear combinations of known Master Integrals. Once such methods were applied, the task of computing them consisted only in the reconstruction of the coefficients which multiply the MIs. These coefficients can in turn be expressed as multivariate polynomials of momentum-twistor variables. It is then possible to exploit some known the properties of polynomials to find efficient ways to reconstruct them. This fact motivated the development of the partial-fractioning techniques presented in the thesis. We have shown how the different algorithms for partial-fractioning enabled us to construct ansätze for the coefficients, in some cases significantly reducing the complexity of a reconstruction.

It should be stressed that the study of the mathematical and physical properties of the expressions are not done separately, but instead one contributes to the other. A clear example of this is the very successful implementation of the factor-matching techinques: the ansätze for parts of the expressions

are created by studying the topologies of the MIs of the amplitude, plus spurious terms originating from integrals reductions, but the efficient matching is made possible by the implementation of a rational parametrisation.

In the projects presented in this thesis, we did not find a single parametrisation or reconstruction technique which was optimal for all amplitudes. Indeed, there was no indication that such a general parametrisation exists at all for the studied processes. Instead, many options had to be tested in advance, in order to find the strategy which best suited each individual expression. While such test could be performed easily and were not excessively time-consuming, it remains an open question whether it could be possible to define *a priori* a rational parametrisation which would be optimal for a specific amplitude. In order to pursue such a line of enquiry, it would be necessary to define an algorithmic way to construct Z-matrices such as the ones in Eqs. (4.10) and (4.10) , starting from physical constraints coming from the scattering amplitude.

The results presented in this work show that the analytic reconstruction of QCD amplitudes using finite field techniques is a valid approach for a variety of processes of phenomenological interest, suggesting that the algebraic complexity of many NNLO and N^3LO may be within reach. This fact makes us look with optimism at future reasearch in this direction.

Appendix A

Mathematical Conventions

We give the explicit expressions of the most used mathematical symbols in this thesis.

Metric Tensor

$$\eta = \begin{pmatrix} -1 & 0 & 0 & 0 \\ 0 & 1 & 0 & 0 \\ 0 & 0 & 1 & 0 \\ 0 & 0 & 0 & 1 \end{pmatrix}. \tag{A.1}$$

Four Vectors

$$x^\mu = (x^0, x^1, x^2, x^3) \tag{A.2}$$

$$x^\mu x_\mu = \eta_{\mu\nu} x^\mu x^\nu = -(x^0)^2 + (x^1)^2 + (x^2)^2 + (x^3)^2 \tag{A.3}$$

. **Levi-Civita Tensor**

$$\epsilon = \begin{pmatrix} 0 & 1 \\ -1 & 0 \end{pmatrix} \tag{A.4}$$

Pauli Matrices

$$\sigma_0 = \begin{pmatrix} 1 & 0 \\ 0 & 1 \end{pmatrix}, \quad \sigma_1 = \begin{pmatrix} 0 & 1 \\ 1 & 0 \end{pmatrix}, \tag{A.5}$$

$$\tag{A.6}$$

$$\sigma_2 = \begin{pmatrix} 0 & -i \\ i & 0 \end{pmatrix}, \quad \sigma_3 = \begin{pmatrix} 1 & 0 \\ 0 & -1 \end{pmatrix}. \tag{A.7}$$

Gamma Matrices

$$\gamma^\mu = \begin{pmatrix} 0 & \sigma^\mu \\ \bar\sigma^\mu & 0 \end{pmatrix}, \quad \gamma^5 = \begin{pmatrix} -\mathbf{1} & 0 \\ 0 & \mathbf{1} \end{pmatrix} \tag{A.8}$$

with

$$\sigma^\mu = \{\sigma_0, \sigma_1, \sigma_2, \sigma_3\}, \tag{A.9}$$

$$\bar\sigma^\mu = \{\sigma_0, -\sigma_1, -\sigma_2, -\sigma_3\}. \tag{A.10}$$

Traces over Gamma Matrices

Traces over gamma matrices can be expressed as multiple products of spinor brackets

$$\mathrm{tr}_+(i...i+n) = \mathrm{tr}((1+\gamma_5)\not p_i \cdots \not p_{i+n}) = \prod_{k=0}^{\frac{n-1}{2}} [i+2k, i+2k+1] \langle i+2k+1, i+2k+2 \rangle, \tag{A.11}$$

$$\mathrm{tr}_-(i...i+n) = \mathrm{tr}((1-\gamma_5)\not p_i \cdots \not p_{i+n}) = \prod_{k=0}^{\frac{n-1}{2}} \langle i+2k, i+2k+1 \rangle [i+2k+1, i+2k+2], \tag{A.12}$$

$$\mathrm{tr}_5(i...i+n) = \mathrm{tr}_+(i...i+n) - \mathrm{tr}_-(i...i+n). \tag{A.13}$$

In Eqs. (A.11), (A.12), (A.13), a cyclical ordering of the n momenta is assumed, meaning that we have $n+1 = 1$.

Gram Matrix

A Gram matrix for a set of vectors in an inner product space is defined as an Hermitian matrix

whose entries are the vector products. So for a set of vectors $\{v_1, .., v_n\}$ we have

$$G(v_1, ..., v_n) = \begin{pmatrix} v_1 \cdot v_1 & v_1 \cdot v_2 & ... & v_1 \cdot p_n \\ \vdots & \ddots & & \\ v_n \cdot v_1 & ... & ... & v_n \cdot v_n \end{pmatrix} . \tag{A.14}$$

Appendix B

QCD Feynman Rules

Here we list the Feynamn rules for internal propagators and vertices in a R_ξ gauge. The colour factors are in red to make their factorisation more explicit. We recall that t_{ij}^a are the colour matrices in the fundamental $SU(N_c)$ representation, while f^{abc} live in the adjoint representation.

$$\alpha\,i \xrightarrow{\ \ p\ \ } \beta\,j \; = \frac{i\delta_{ij}}{p^2+i\epsilon}(\not{p}+m)_{\alpha\beta} \tag{B.1}$$

$$\mu\,a \overset{p}{\,\text{(gluon)}\,} \nu\,b \; = \frac{i\delta^{ab}}{p^2+i\epsilon}(g^{\mu\nu}+(1-\xi)\frac{p^\mu p^\nu}{p^2+i\epsilon}) \tag{B.2}$$

$$a \cdots\blacktriangleright\cdots b \quad = \frac{i\delta^{ab}}{p^2+i\epsilon} \tag{B.3}$$

$$\mu\,a \;=\; -ig_s\gamma^\mu_{\alpha\beta}t^a_{ij} \tag{B.4}$$

$$\mu\,b \;=\; g_s f^{abc} p^\mu \tag{B.5}$$

$$\rho\,c \;=\; -g f^{abc}(g^{\mu\nu}(p1-p2)^\rho + g^{\mu\rho}(p2-p3)^\mu + g^{\rho\mu}(p3-p1)^\nu) \tag{B.6}$$

$$= -ig^2\big(f^{a_1 a_2 b}f^{ba_3 a_4}(g^{\mu_1\mu_3}-g^{\mu_2\mu_4}) + \text{all other permutations}\big) \tag{B.7}$$

Appendix C

Coefficient Ansätze for Tree-Level Six-Gluon Amplitudes

We give here the explicit list of factors in momentum twistor variables which was used to perform the factor matching for the reconstruction of the tree-amplitudes in 4.3.2.

$\{x_1, x_6, x_7, x_8, -1 + x_6, -1 + x_7, -1 + x_8, x_6 - x_7, x_6 - x_8, x_7 - x_8, x_5 - x_6,$

$x_2, -x_4 - x_2 x_5 + x_3 x_5 + x_2 x_6 + x_4 x_6 - x_3 x_5 x_6 - x_2 x_7 + x_2 x_5 x_7, x_4 x_6 -$

$x_3 x_5 x_6 + x_2 x_5 x_7 - x_4 x_8 - x_2 x_5 x_8 + x_3 x_5 x_8$

$x_4 - x_3 x_5, x_2 - x_3 + x_3 x_6 - x_2 x_7, -x_6 + x_3 x_6 + x_7 - x_2 x_7 + x_2 x_8 - x_3 x_8, -1 + x_3, -x_4 + x_3 x_6 - x_2 x_7$

$- x_4 x_6 + x_5 x_6 - x_6^2 + x_3 x_6^2 - x_5 x_7 + x_6 x_7 - x_2 x_6 x_7 + x_4 x_8 + x_2 x_6 x_8 - x_3 x_6 x_8, -x_4 + x_5 - x_6 + x_3 x_6$

$- x_4 + x_2 x_4 - x_2 x_5 + x_3 x_5 + x_2 x_6 - x_2 x_3 x_6 + x_4 x_6 - x_3 x_5 x_6 - x_2 x_7 + x_2^2$

$x_7 + x_2 x_5 x_7 - x_2^2 x_8 + x_2 x_3 x_8 - x_2 x_4 x_8, x_4 - x_2 x_4 + x_2 x_5 - x_3 x_5 - x_2$

$x_6 + x_2 x_3 x_6 - x_4 x_6 + x_3 x_5 x_6 + x_2 x_7 - x_2 x_3 x_7 + x_2 x_4 x_7 - x_2 x_5 x_7$

$- x_4 + x_2 x_4 - x_2 x_5 + x_3 x_5, x_2 - x_3, x_4 x_6 - x_3 x_5 x_6 + x_2 x_5 x_7, x_6 - x_3 x_6 -$

$x_6^2 + x_3 x_6^2 - x_7 + x_2 x_7 + x_6 x_7 - x_2 x_7^2 - x_2 x_8 + x_3 x_8 - x_3 x_6 x_8 + x_2 x_7 x_8$

$$- x_4x_6x_7 - x_2x_5x_6x_7 + x_3x_5x_6x_7 + x_2x_6^2x_7 + x_4x_6^2x_7 - x_3x_5$$

$$x_6^2x_7 - x_2x_6x_7^2 + x_2x_5x_6x_7^2 + x_2x_5x_6x_8 - x_2x_6^2x_8 + x_4x_7x_8 -$$

$$x_3x_5x_7x_8 + x_2x_6x_7x_8 - x_4x_6x_7x_8 - x_2x_5x_6x_7x_8 + x_3x_5x_6x_7x_8, 1 - x_3 - x_6 + x_3x_6 - x_2x_7 + x_2x_8$$

$$- x_2x_5x_7 + x_2x_6x_7 + x_4x_8 + x_2x_5x_8 - x_3x_5x_8 - x_2x_6x_8 - x_4x_6x_8$$

$$+ x_3x_5x_6x_8, x_4 + x_2x_6 - x_3x_6, -x_4 - x_2x_5 + x_3x_5 + x_4x_6 - x_3x_5x_6 + x_2x_5x_7,$$

$$- x_4x_6 + x_5x_6 - x_6^2 + x_3x_6^2 - x_5x_7 + x_6x_7 - x_2x_7^2 + x_4x_8 - x_3x_6x_8 + x_2x_7x_8$$

$$- x_4x_6 + x_3x_5x_6 - x_2x_5x_7 + x_2x_6x_7 + x_4x_6x_7 - x_3x_5x_6x_7 - x_2$$

$$x_7^2 + x_2x_5x_7^2 + x_4x_8 + x_2x_5x_8 - x_3x_5x_8 - x_2x_6x_8 + x_2x_7x_8 - x_4x_7x_8$$

$$- x_2x_5x_7x_8 + x_3x_5x_7x_8, -x_4 + x_5 - x_6 + x_3x_6 - x_2$$

$$x_7 + x_2x_8, x_4 - x_3x_5 + x_2x_7 - x_2x_8 - x_4x_8 + x_3x_5x_8, x_2 - x_3 + x_4,$$

$$x_5 - x_4 + x_2x_4 - x_2x_5 + x_3x_5 + x_2x_6 - x_2x_3x_6 + x_4x_6 - x_3x_5x_6 - x_2x_7 + x_2x_3$$

$$x_7 + x_2x_5x_7 - x_2x_3x_6x_7 + x_2^2x_7^2 - x_2x_4x_8 + x_2x_3x_6x_8 - x_2^2x_7$$

$$x_8, -x_4x_6 + x_3x_5x_6 - x_2x_5x_7 + x_2x_6x_7 + x_4x_8 + x_2x_5x_8 - x_3x_5x_8 - x_2x_6x_8$$

$$x_4 - x_2x_4 + x_2x_5 - x_3x_5 - x_2x_6 + x_2x_3x_6 - x_4x_6 + x_3x_5x_6 + x_2x_7 - x_2^2x_7$$

$$+ x_2x_4x_7 - x_2x_5x_7 - x_2x_3x_6x_7 + x_2^2x_7^2 + x_2^2x_8 - x_2x_3x_8 + x_2x_3x_6x_8$$

$$- x_2^2x_7x_8, x_4x_6 - x_3x_5x_6 + x_2x_6x_7 - x_4x_8 + x_3x_5x_8 - x_2x_6x_8,$$

$$- x_6 + x_3x_6 - x_4x_6 + x_5x_6 + x_7 - x_2x_7 - x_5x_7 + x_2x_8 - x_3x_8 + x_4x_8,$$

$$- x_5 + x_6 - x_7 + x_5x_7 - x_4 + x_2x_4 - x_2x_5 + x_3x_5 + x_4x_6 - x_3x_5x_6 + x_2x_6^2$$

$$- x_2x_3x_6^2 + x_2x_5x_7 - x_2x_6x_7 + x_2^2x_6x_7 - x_2x_4x_8 - x_2^2x_6x_8 + x_2x_3x_6$$

$$x_8, x_4 + x_2x_5 - x_3x_5 - x_2x_6 - x_4x_6 + x_3x_5x_6 - x_2x_5x_7 + x_2x_6x_7,$$

$$- x_4 + x_2x_4 - x_2x_5 + x_3x_5 + x_2x_6 - x_2x_3x_6 - x_2x_7 + x_2^2x_7 - x_2^2x_8 + x_2x_3x_8,$$

$$x_4 - x_3x_5 + x_2x_7, -1 + x_3 - x_4 + x_5, -x_5 + x_6 - x_8 + x_5x_8x_4 - x_2x_4 + x_2x_5 - x_3x_5$$

$$- x_4x_6 + x_3x_5x_6 - x_2x_6^2 + x_2x_3x_6^2 + x_2x_4x_7 - x_2x_5x_7 + x_2x_6x_7 - x_2$$

$$x_3x_6x_7, x_4x_6 + x_2x_5x_6 - x_3x_5x_6 - x_2x_6^2 - x_4x_6^2 + x_3x_5x_6^2$$

$$+ x_2x_6x_7 - x_2x_5x_6x_7 - x_4x_8 - x_2x_5x_8 + x_3x_5x_8$$

$$+ x_4x_6x_8 - x_3x_5x_6x_8 + x_2x_6^2x_8 + x_2x_5x_7x_8 - x_2x_6x_7x_8x_4$$

$$- x_2x_4 + x_2x_5 - x_3x_5 - x_2x_6 + x_2x_3x_6 + x_2x_7 - x_2x_3x_7, x_4x_6 - x_3x_5x_6$$

$$+ x_2x_5x_7 - x_4x_8 - x_2x_5x_8 + x_3x_5x_8 + x_2x_6x_8 - x_2x_7x_8, -x_4x_6 + x_5x_6$$

$$- x_6^2 + x_3x_6^2 - x_5x_7 + x_6x_7 - x_2x_6x_7, x_2 - x_3 - x_6 + x_3x_6 + x_7 - x_2x_7,$$

$$- x_4x_6x_7 + x_3x_6^2x_7 - x_2x_6x_7^2 + x_5x_6x_8 - x_6^2x_8 + x_4x_7x_8 - x_5x_7x_8$$

$$+ x_6x_7x_8 + x_2x_6x_7x_8 - x_3x_6x_7x_8, x_6 - x_3x_6 - x_7 + x_2x_7 + x_3x_6x_7$$

$$- x_2x_7^2 - x_2x_8 + x_3x_8 - x_6x_8 + x_7x_8 + x_2x_7x_8 - x_3x_7x_8, -x_5x_7 + x_6$$

$$x_7 + x_4x_8 - x_3x_6x_8, -1 + x_3 + x_7 - x_3x_8, -x_4 + x_2x_4 - x_2x_5$$

$$+ x_3x_5 + x_2x_6 - x_2x_3x_6 + x_4x_6 - x_3x_5x_6 - x_2x_7 + x_2^2x_7 + x_2x_5x_7, -1 + x_2,$$

$$x_2x_4x_7 - x_2x_3x_6x_7 + x_2^2x_7^2 - x_4x_8 - x_2x_5x_8 + x_3x_5x_8 + x_2x_6x_8 + x_4x_6x_8 - x_3x_5x_6x_8$$

$$- x_2x_7x_8 - x_2^2x_7x_8 + x_2x_3x_7x_8 - x_2x_4x_7x_8 + x_2x_5x_7x_8, x_6 - x_3x_6 + x_2x_7 - x_8$$

$$- x_2x_8 + x_3x_8, -x_4x_7 - x_2x_5x_7 + x_3x_5x_7 + x_2x_6x_7 + x_4x_6x_7 - x_3x_5x_6x_7 - x_2x_7^2$$

$$+ x_2x_5x_7^2 + x_2x_4x_8 - x_2x_3x_6x_8 + x_2x_3x_7x_8 - x_2x_4x_7x_8, -x_6 + x_3x_6 + x_7 - x_3x_8 - x_4x_6$$

$$+ x_2x_4x_6 - x_2x_5x_6 + x_3x_5x_6 + x_2x_6^2 - x_2x_3x_6^2 + x_4x_6^2 - x_3x_5x_6^2 - x_2x_6x_7$$

$$+ x_2^2x_6x_7 + x_2x_5x_6x_7 + x_4x_8 - x_2x_4x_8 + x_2x_5x_8$$

$$- x_3x_5x_8 - x_2^2x_6x_8 + x_2x_3x_6x_8 - x_4x_6x_8 - x_2x_5x_6x_8 + x_3x_5x_6x_8,$$

$$- 1 + x_2 + x_6 - x_2x_7, x_2x_4x_6 - x_2x_5x_6 + x_2x_6^2 - x_2x_3x_6^2 + x_2x_5x_7 - x_2x_6x_7 + x_2^2x_6x_7$$

$$- x_4x_8 - x_2x_5x_8 + x_3x_5x_8 - x_2^2x_6x_8 + x_2x_3x_6x_8 + x_4x_6x_8 - x_2x_4x_6x_8 + x_2x_5x_6x_8 - x_3x_5x_6x_8,$$

$$1 + x_2 - x_3 - x_6 + x_3x_6 - x_2x_7, x_4x_6 - x_3x_5x_6 + x_2x_5x_7 - x_2x_4x_8, x_3,$$

$$x_4 - x_2x_4 + x_2x_5 - x_3x_5 - x_2x_6 + x_2x_3x_6 - x_4x_6 + x_3x_5x_6, -1 + x_2 + x_6 - x_2x_8, -x_2x_4x_6$$

$$+ x_2x_5x_6 - x_2x_6^2 + x_2x_3x_6^2 + x_4x_7 - x_3x_5x_7 + x_2x_6x_7 - x_2x_3x_6x_7 - x_4x_6x_7 + x_2x_4x_6x_7 - x_2x_5x_6x_7$$

$$+ x_3x_5x_6x_7x_6 + x_2x_6 - x_3x_6 - x_6^2 + x_3x_6^2 - x_7 + x_6x_7 - x_2x_6x_7 - x_2x_8 + x_3x_8 - x_3x_6x_8$$

$$+ x_2x_7x_8, -x_4x_6 + x_3x_5x_6 + x_2x_4x_7 - x_2x_5x_7, x_3x_6 - x_2x_7 + x_2x_8 - x_3x_8, -x_2^2 + x_2x_3 - x_4 - x_2x_5$$

$$+ x_3x_5 + x_2x_6 - x_2x_3x_6 + x_4x_6 - x_3x_5x_6 - x_2x_7 + x_2^2x_7 + x_2x_5x_7,$$

$$x_5 - x_6 + x_2x_6x_4 - x_2x_4 + x_2x_5 - x_3x_5 - x_2x_6 + x_2x_3x_6 - x_4x_6 + x_3x_5x_6 + x_2x_7 - x_2^2x_7$$

$$+ x_2x_4x_7 - x_2x_5x_7 - x_2x_3x_6x_7 + x_2^2x_7^2 + x_2^2x_8 - x_2x_3x_8 - x_4x_8 + x_2x_4x_8 - x_2x_5x_8$$

$$+ x_3x_5x_8 + x_2x_6x_8 + x_4x_6x_8 - x_3x_5x_6x_8 - x_2x_7x_8 - x_2^2x_7x_8 + x_2x_3x_7x_8 - x_2x_4x_7x_8$$

$$+ x_2x_5x_7x_8, -x_4x_6 + x_5x_6 - x_6^2 + x_3x_6^2 - x_2x_6x_7 + x_4x_8 - x_5x_8 + x_6x_8 + x_2x_6x_8 - x_3x_6x_8,$$

$x_4 - x_2x_4 + x_2x_5 - x_3x_5 - x_2x_6 + x_2x_3x_6 - x_4x_6 + x_3x_5x_6 + x_2x_7 - x_2x_3x_7 - x_4x_7 + x_2x_4x_7$

$- 2x_2x_5x_7 + x_3x_5x_7 + x_2x_6x_7 + x_4x_6x_7 - x_3x_5x_6x_7 - x_2x_7^2 + x_2x_5x_7^2 + x_2x_4x_8 - x_2x_3x_6x_8$

$+ x_2x_3x_7x_8 - x_2x_4x_7x_8 - x_4x_6 + x_5x_6 - x_6^2 + x_3x_6^2 - x_5x_7 + x_6x_7 + x_4x_8 - x_3x_6x_8,$

$x_2x_6 - x_2x_3x_6 + x_4x_6 - x_3x_5x_6 - x_2x_7 + x_2^2x_7$

$+ x_2x_5x_7 - x_2^2x_8 + x_2x_3x_8 - x_4x_8 - x_2x_5x_8 + x_3x_5x_8,$

$- x_5 + x_6 - x_2x_7, -x_4 + x_2x_4 - x_2x_5 + x_3x_5 + x_2x_6 - x_2x_3x_6 - x_2x_7 + x_2^2x_7$

$- x_2^2x_8 + x_2x_3x_8 + x_4x_8 - x_2x_4x_8 + x_2x_5x_8 - x_3x_5x_8,$

$- x_4 + x_5 - x_6 + x_3x_6 - x_2x_7 - x_4 + x_2x_4 - x_2x_5 + x_3x_5 + x_4x_6 - x_3x_5x_6 + x_2x_5x_7 - x_2x_4x_8,$

$- x_4 + x_3x_6, -x_2 + x_2x_3 - x_4 + x_3x_5, -x_5 + x_6 - x_2x_8,$

$x_4 - x_2x_4 + x_2x_5 - x_3x_5 - x_2x_6 + x_2x_3x_6 + x_2x_7 - x_2x_3x_7 - x_4x_7$

$+ x_2x_4x_7 - x_2x_5x_7 + x_3x_5x_7 - x_4x_6 + x_5x_6 - x_6^2 +$

$x_3x_6^2 - x_5x_7 + x_6x_7 - x_2x_6x_7 + x_4x_8 - x_3x_6x_8$

$+ x_2x_7x_8, x_4 - x_2x_4 + x_2x_5 - x_3x_5 - x_4x_6 + x_3x_5x_6 + x_2x_4x_7 - x_2x_5x_7,$

$- x_4x_6 + x_3x_6^2 - x_2x_6x_7 + x_4x_8 + x_2x_6x_8 - x_3x_6x_8, x_4x_6$

$- x_3x_5x_6 + x_2x_6^2 - x_2x_3x_6^2 + x_2x_5x_7 - x_2x_6x_7 + x_2^2x_6x_7$

$- x_4x_8 - x_2x_5x_8 + x_3x_5x_8 - x_2^2x_6x_8 + x_2x_3x_6x_8$

$- x_4 - x_2x_5 + x_3x_5 + x_2x_6 + x_4x_6 - x_3x_5x_6 - x_2x_7 - x_2^2x_7 + x_2x_3x_7 + x_2x_5x_7 - x_2x_3x_6x_7$

$+ x_2^2x_7^2, -x_4x_6 + x_2x_4x_6 - x_2x_5x_6 + x_3x_5x_6 + x_2x_6^2 - x_2x_3x_6^2$

$$- x_2x_6x_7 + x_2^2x_6x_7 + x_4x_8 - x_2x_4x_8$$

$$+ x_2x_5x_8 - x_3x_5x_8 - x_2^2x_6x_8 + x_2x_3x_6x_8,$$

$$x_4 - x_2x_4 + x_2x_5 - x_3x_5 - x_2x_6 + x_2x_3x_6$$

$$- x_4x_6 + x_3x_5x_6 + x_2x_7 - x_2^2x_7 + x_2x_4x_7 - x_2x_5x_7 - x_2x_3x_6x_7$$

$$+ x_2^2x_7^2, x_4x_6 - x_5x_6 + x_5x_7 - x_4x_8, -x_4 + x_3x_6 - x_3x_7 + x_4x_7,$$

$$- x_4 + x_3x_5 - x_2x_6 + x_2x_3x_6, -x_4 - x_2x_5 + x_3x_5 + x_2x_6$$

$$+ x_4x_6 - x_3x_5x_6 - x_2x_7 + x_2x_5x_7 - x_2^2x_8 +$$

$$x_2x_3x_8 - x_2x_3x_6x_8 + x_2^2x_7x_8, -x_4 + x_2x_4 - x_2x_5 + x_3x_5 + x_2x_6 - x_2x_3x_6,$$

$$x_4 - x_2x_4 + x_2x_5 - x_3x_5 - x_2x_6 + x_2x_3x_6 - x_4x_6 + x_3x_5$$

$$x_6 + x_2x_7 - x_2^2x_7 - x_2x_5x_7 + x_2x_4x_8 - x_2x_3x_6x_8 + x_2^2x_7x_8, x_4 - x_5,$$

$$- x_4 + x_3x_6 - x_2x_7 + x_2x_8 - x_3x_8 + x_4x_8, -x_4 + x_3x_5$$

$$- x_2x_7 + x_2x_3x_7x_4x_6 - x_3x_5x_6 + x_2x_5x_7 - x_4x_8 - x_2x_5$$

$$x_8 + x_3x_5x_8 + x_2x_6x_8 - x_2x_3x_6x_8 - x_2x_7x_8 + x_2^2x_7$$

$$x_8 - x_2^2x_8^2 + x_2x_3x_8^2, -x_4 + x_2x_4 - x_2x_5$$

$$+ x_3x_5 + x_2x_6 - x_2x_3x_6 + x_4x_6 - x_3x_5x_6 - x_2x_4x_7 + x_2x_5x_7$$

$$- x_2x_6x_7 + x_2x_3x_6x_7, x_4x_6 - x_2x_4x_6 + x_2x_5x_6 - x_3x_5x_6 - x_2x_6^2 + x_2x_3x_6^2$$

$$- x_4x_6^2 + x_3x_5x_6^2 + x_2x_6x_7 - x_2^2x_6x_7 - x_2x_5x_6$$

$$x_7 - x_4x_8 + x_2x_4x_8 - x_2x_5x_8 + x_3x_5x_8 + x_2^2x_6x_8 - x_2x_3x_6x_8 + x_4x_6x_8$$

$$+ x_2x_4x_6x_8 - x_3x_5x_6x_8 + x_2x_6^2x_8 - x_2x_3x_6^2x_8 + x_2x_5x_7x_8 - x_2x_6x_7x_8$$

$$+ x_2^2 x_6 x_7 x_8 - x_2 x_4 x_8^2 - x_2^2 x_6 x_8^2 + x_2 x_3 x_6 x_8^2,$$

$$- x_4 + x_5 - x_6 + x_3 x_6 + x_7 - x_3 x_7 + x_4 x_7 - x_5 x_7,$$

$$- x_4 x_6 + x_5 x_6 - x_6^2 + x_3 x_6^2 - x_5 x_7 + x_6 x_7 - x_2 x_6 x_7 + x_4 x_8 + x_6 x_8$$

$$+ x_2 x_6 x_8 - 2 x_3 x_6 x_8 + x_4 x_6 x_8 - x_5 x_6 x_8 - x_7 x_8 + x_2 x_7 x_8 + x_5 x_7 x_8 - x_2 x_8^2$$

$$+ x_3 x_8^2 - x_4 x_8^2, -1 + x_2 + x_5, -x_4 - x_2 x_5 + x_3 x_5 - x_2^2 x_6 + x_2 x_3 x_6$$

$$+ x_4 x_6 - x_3 x_5 x_6 + x_2 x_6^2 - x_2 x_3 x_6^2 + x_2 x_5 x_7 - x_2 x_6 x_7 + x_2^2 x_6 x_7,$$

$$x_4 x_6 - x_3 x_5 x_6 + x_2 x_5 x_7 - x_2 x_3 x_6 x_7 + x_2^2 x_7^2 - x_4 x_8 - x_2 x_5 x_8$$

$$+ x_3 x_5 x_8 + x_2 x_6 x_8 - x_2 x_7 x_8 - x_2^2 x_7 x_8 + x_2 x_3 x_7 x_8, x_4 - x_3 x_5 + x_2 x_7 - x_2 x_3$$

$$x_8, -x_4 + x_2 x_4 - x_2 x_5 + x_3 x_5 + x_2 x_6 - x_2 x_3 x_6 - x_2 x_7 + x_2^2 x_7,$$

$$x_4 x_6 - x_2 x_4 x_6 + x_2 x_5 x_6 - x_3 x_5 x_6 - x_2 x_6^2 + x_2 x_3 x_6^2 - x_4 x_6^2 + x_3 x_5 x_6^2$$

$$+ x_2 x_6 x_7 - x_2^2 x_6 x_7 + x_2 x_4 x_6 x_7 - x_2 x_5 x_6 x_7 - x_2 x_3 x_6^2$$

$$x_7 + x_2^2 x_6 x_7^2 - x_4 x_8 + x_2 x_4 x_8 - x_2 x_5 x_8 + x_3 x_5 x_8 + x_2^2 x_6 x_8 - x_2 x_3 x_6 x_8$$

$$+ x_4 x_6 x_8 - x_3 x_5 x_6 x_8 + x_2 x_6^2 x_8 - x_2 x_4 x_7 x_8 + x_2 x_5 x_7 x_8 - x_2 x_6 x_7 x_8 - x_2^2 x_6 x_7 x_8$$

$$+ x_2 x_3 x_6 x_7 x_8, x_4 - x_2 x_4 + x_2 x_5 - x_3 x_5 - x_2$$

$$x_6 + x_2 x_3 x_6 - x_4 x_6 + x_3 x_5 x_6 - x_2 x_5 x_7 + x_2 x_6 x_7 + x_2 x_4 x_8 - x_2 x_3 x_6 x_8,$$

$$- x_4 + x_5 - x_6 + x_3 x_6 - x_2 x_7 + x_8 + x_2 x_8 - x_3 x_8 + x_4 x_8 - x_5 x_8, -x_4 x_6 + x_5 x_6 - x_6^2$$

$$+ x_3 x_6^2 - x_5 x_7 + 2 x_6 x_7 - x_3 x_6 x_7 + x_4 x_6$$

$$x_7 - x_5 x_6 x_7 - x_7^2 + x_5 x_7^2 + x_4 x_8 - x_3 x_6 x_8 + x_3 x_7 x_8 - x_4 x_7 x_8, x_4\}$$

Appendix D

Passarino Veltmann Reduction

We present a simple example of the application of the Passarino-Veltman reduction [86]. This allow us to see how spurious poles originate when tensor integrals are reduced to linear combinations of scalar ones.

Consider the 2-mass triangle integral

$$I_3^\mu = \int \frac{d^D k}{(2\pi)^D} k^\mu \qquad = \int d^D k \frac{k^\mu}{k^2 (k+p_1)^2 (k-p_3)^2}, \tag{D.1}$$

for which we have $p_1^2 = m_1^2, p_2^2 = m_2^2, p_3^2 = 0$. Looking at the tensor structure of the integral, we see that it can be decomposed into

$$I_3^\mu = C_1 p_1^\mu + C_2 p_3^\mu. \tag{D.2}$$

We can thus reduce the problem to solving the linear system

$$\begin{pmatrix} I \cdot p_{12} \\ I \cdot p_5 \end{pmatrix} = \begin{pmatrix} p_1^2 & p_1 \cdot p_3 \\ p_1 \cdot p_3 & 0 \end{pmatrix} \cdot \begin{pmatrix} C_1 \\ C_2 \end{pmatrix}. \tag{D.3}$$

We can calculate the left hand side of Eq. (D.3) by dotting the external momenta with the integral of Eq. (D). The coefficients are then found by inverting the Gram matrix, defined by Eq. (A.14).

It is then seen that the coefficients will be proportional to $\frac{1}{\Delta}$, where Δ is a Gram determinant

$$\Delta = -\frac{1}{2}(p_1 \cdot p_3) = \frac{1}{4}(p_2^2 - p_1^2). \tag{D.4}$$

Therefore spurious poles will correspond to the values of the Mandelstam's variables which set Δ to zero. In our example, this corresponds to $p_1 = p_2$, so we expect to find spurious poles of the form $\frac{1}{(p_2^2 - p_1^2)^n}$ in the corresponding coefficient.

Appendix E

Change of Variables to Linearise the Differential Equation System

We provide the explicit change of variables which linearises the system for topology T_1, even if these transformations were not ultimately used to obtain the MIs. The transformations map the set of invariants $\{s_{12}, s_{45}, s_{15}, m_t^2, s_{34}\}$ to a new set $\{w, x, y, z, s_{23}\}$ in the following way:

$$s_{45} \rightarrow -\frac{2s_{23}\left(\frac{(z-1)^2}{x^2} + (z+1)^2\right)}{y\left(\frac{\frac{(z-1)^2}{y^2}+(z+1)^2}{x^2} + \left(\frac{1}{y^2} - 1\right)(z+1)^2\right)}, \tag{E.1}$$

$$s_{12} \rightarrow \frac{2s_{23}\left(\frac{1}{y} + 1\right)z\left(\frac{\frac{(z-1)^2}{y}+(z+1)^2}{x^2} + \left(\frac{1}{y} - 1\right)(z+1)^2\right)}{(z^2+1)\left(\frac{\frac{(z-1)^2}{y^2}+(z+1)^2}{x^2} + \left(\frac{1}{y^2} - 1\right)(z+1)^2\right)}, \tag{E.2}$$

$$s_{15} \rightarrow \left(2 \left(\frac{1}{y} - 1 \right) \left(1 + \frac{1}{y} \right)^2 \left(\frac{(z-1)^2}{x^2} + (z+1)^2 \right) \left(\left(\frac{1}{y} - 1 \right) (z+1)^2 + \frac{\frac{(z-1)^2}{y} + (z+1)^2}{x^2} \right) \times \right. \quad \text{(E.3)}$$

$$s_{23}^2 \left(w \left(\left(\frac{1}{y^2} - 1 \right) (z+1)^2 + \frac{\frac{(z-1)^2}{y^2} + (z+1)^2}{x^2} \right)^2 + \left(\left(1 + \frac{1}{x} \right) \left(\frac{1}{y^2} - 1 \right) \left((1-y^2)(z+1)^4 \times \right. \right.$$

$$\left(-y^2(z+1)^2 + (z+1)^2 - 2y(z^2+1) \right) x^5 + (z+1)^2 \left((z^2-1)^2 y^4 - 2(z+1)^2 (z^2+1) y^3 \right.$$

$$+ \left(6z^4 + 20z^2 + 6 \right) y^2 + 2(z+1)^2 (z^2+1) y + (z^2-1)^2 \right) x^4 - 2(z+1)^2 \left(y^4 (z+1)^4 + y^3 (z^2+1) (z+1)^2 \right.$$

$$- (z^2-1)^2 + y(z-1)^2 (z^2+1) + 4y^2 (z-1)^2 (z^2+z+1) \right) x^3 + 2(z+1)^2 \left(-(z^2-1)^2 y^4 \right.$$

$$+ (z+1)^2 (z^2+1) y^3 + 4(z-1)^2 z y^2 + (z-1)^2 (z^2+1) y + (z-1)^4 \right) x^2 + (z+1)^2 \left((z-1)^2 + y^2(z+1)^2 \right)^2 x$$

$$+ (z-1)^2 \left((z-1)^2 + y^2(z+1)^2 \right)^2 \right) s_{23} \right) / (x^5 y^4) \right) \right) / \left(\left(\left(\frac{1}{y^2} - 1 \right) (z+1)^2 + \frac{\frac{(z-1)^2}{y^2} + (z+1)^2}{x^2} \right) \times \right.$$

$$\left(\left(\left(1 + \frac{1}{x} \right)^2 \left(\frac{1}{y^2} - 1 \right)^2 \left((z+1)^4 \left(-y^2(z+1)^2 + (z+1)^2 - 2y(z^2+1) \right)^2 x^6 \right. \right.$$

$$+ 2(z+1)^4 \left((z^2-1)^2 y^4 - 4(z^2+1)^2 y^3 + 2(z^4 + 6z^2 + 1) y^2 + 4(z^2+1)^2 y + (z^2-1)^2 \right) x^5$$

$$- (z+1)^4 \left((z^4 + 12z^3 + 6z^2 + 12z + 1) y^4 - 8(z^4 - 4z^3 + 2z^2 - 4z + 1) y^3 + 2(7z^4 - 8z^3 + 10z^2 - 8z + 7) y^2 + \right.$$

$$16(z-1)^2 (z^2+1) y - (z-1)^2 (3z^2+2z+3) \right) x^4 + 4(z+1)^2 \left((z+1)^2 (z-1)^4 - y^4 (z+1)^4 (z-1)^2 \right.$$

$$+ 4y \left(z^4 + z^3 + 2z^2 + z + 1 \right) (z-1)^2 + 4y^2 \left(z^4 + z^3 + 4z^2 + z + 1 \right) (z-1)^2 + 4y^3 z(z+1)^2 (z^2+1) \right) x^3 -$$

$$(z+1)^2 \left((z+1)^2 (z^4 - 12z^3 + 6z^2 - 12z + 1) y^4 + 12(z^2-1)^2 (z^2+1) y^3 \right.$$

$$+ 2(z-1)^2 (7z^4 - 8z^3 + 18z^2 - 8z + 7) y^2 + 12(z-1)^4 (z^2+1) y - (z-1)^4 (3z^2 - 2z + 3) \right) x^2$$

$$+ 2(z^2-1)^2 \left((z-1)^4 + 4y(z^2+1)(z-1)^2 + y^4 (z+1)^4 + 2y^2 (z^2-1)^2 + 4y^3 (z+1)^2 (z^2+1) \right) x$$

$$+ (z-1)^4 \left((z-1)^2 + y^2(z+1)^2 \right)^2 \right) s_{23}^2 \right) / (x^6 y^4) - w^2 \left(\left(\frac{1}{y^2} - 1 \right) (z+1)^2 + \frac{\frac{(z-1)^2}{y^2} + (z+1)^2}{x^2} \right)^2 \right) \right),$$

$$m_t^2 \rightarrow \frac{s_{23} \left(\frac{1}{y} + 1 \right) \left(\frac{\frac{(z-1)^2}{y} + (z+1)^2}{x^2} + \left(\frac{1}{y} - 1 \right) (z+1)^2 \right)}{\frac{\frac{(z-1)^2}{y^2} + (z+1)^2}{x^2} + \left(\frac{1}{y^2} - 1 \right) (z+1)^2}, \quad \text{(E.4)}$$

$$s_{34} \rightarrow - \left(2s_{23} \left(1 + \frac{1}{y}\right) \left(\left(\frac{1}{y} - 1\right)(z+1)^2 + \frac{\frac{(z-1)^2}{y} + (z+1)^2}{x^2} \right) \times \right.$$

(E.5)

$$\left(\left(s_{23}^2 \left(1 + \frac{1}{x}\right)^2 \left(x^7(z+1)^8 + x^7 y^4 (z+1)^8 - 2x^7 y^2 \left(3z^4 + 4z^3 + 10z^2 + 4z + 3\right)(z+1)^4 \right.\right.\right.$$

$$- 4x^6 y \left(z^2 + 1\right)\left(-y^2(z-1)^2 + (z-1)^2 - 2y\left(z^2+1\right)\right)(z+1)^4$$

$$+ x^5 \left(- \left(\left(z^4 + 4z^3 + 22z^2 + 4z + 1\right) y^4\right) - 8(z-1)^2\left(z^2+1\right) y^3 + \left(-6z^4 + 28z^2 - 6\right) y^2 + 8(z-1)^2\left(z^2+1\right) y \right.$$

$$+ (z-1)^2\left(3z^2 + 10z + 3\right)\big)(z+1)^4 + x^3 \left(-(z+1)^2\left(z^4 + 4z^3 - 26z^2 + 4z + 1\right) y^4 + 8\left(z^2-1\right)^2\left(z^2+1\right) y^3 \right.$$

$$+ 2(z-1)^2\left(z^4 + 8z^3 + 30z^2 + 8z + 1\right) y^2 + 8(z-1)^4\left(z^2+1\right) y + (z-1)^4\left(3z^2 + 14z + 3\right)\big)(z+1)^2$$

$$+ 2(z-1)^4\left((z-1)^2 + y^2(z+1)^2\right)^2 + x(z-1)^2\left(z^2 + 6z + 1\right)\left((z-1)^2 + y^2(z+1)^2\right)^2$$

$$+ 4\left(x - xz^2\right)^2 \left(-\left(z^2-1\right)^2 y^4 - (z+1)^2\left(z^2+1\right) y^3 + 4(z-1)^2 z y^2 - (z-1)^2\left(z^2+1\right) y + (z-1)^4 \right)$$

$$+ 2x^4\left(z^2-1\right)^2\left(\left(z^2-1\right)^2 y^4 - 2\left(z^2-1\right)^2 y^2 - 4\left(z^2+1\right)^2 y + \left(z^2-1\right)^2\right)\bigg) \left(\frac{1}{y^2} - 1\right)^2 \bigg)/\left(x^7 y^4\right)$$

$$+ 2s_{23} w \left(1 + \frac{1}{x}\right) \left(\frac{(z-1)^2}{x^2} + (z+1)^2\right) \left(\left(\frac{1}{y^2} - 1\right)(z+1)^2 + \frac{\frac{(z-1)^2}{y^2} + (z+1)^2}{x^2} \right)^2 \left(\frac{1}{y^2} - 1\right)$$

$$+ w^2 \left(\left(\frac{1}{y^2} - 1\right)(z+1)^2 + \frac{\frac{(z-1)^2}{y^2} + (z+1)^2}{x^2} \right)^2 \bigg) \bigg) / \left(\left(\frac{1}{x^2} - 1\right) \left(\left(\frac{1}{y^2} - 1\right)(z+1)^2 \right.\right.$$

$$+ \frac{\frac{(z-1)^2}{y^2} + (z+1)^2}{x^2} \bigg) \left(\left(s_{23}^2 \left(1 + \frac{1}{x}\right)^2 \left(\frac{1}{y^2} - 1\right)^2 \left((z+1)^4\left(-y^2(z+1)^2 + (z+1)^2\right.\right.\right.$$

$$- 2y\left(z^2+1\right)\big)^2 x^6 + 2(z+1)^4\left(\left(z^2-1\right)^2 y^4 - 4\left(z^2+1\right)^2 y^3 + 2\left(z^4 + 6z^2 + 1\right) y^2 + 4\left(z^2+1\right)^2 y + \left(z^2-1\right)^2\right) x^5$$

$$- (z+1)^4\left(\left(z^4 + 12z^3 + 6z^2 + 12z + 1\right) y^4 - 8\left(z^4 - 4z^3 + 2z^2 - 4z + 1\right) y^3\right.$$

$$+ 2\left(7z^4 - 8z^3 + 10z^2 - 8z + 7\right) y^2 + 16(z-1)^2\left(z^2+1\right) y - (z-1)^2\left(3z^2 + 2z + 3\right)\big) x^4$$

$$+ 4(z+1)^2\left((z+1)^2(z-1)^4 - y^4(z+1)^4(z-1)^2 + 4y\left(z^4 + z^3 + 2z^2 + z + 1\right)(z-1)^2\right.$$

$$+ 4y^2\left(z^4 + z^3 + 4z^2 + z + 1\right)(z-1)^2 + 4y^3 z(z+1)^2\left(z^2+1\right)\big) x^3$$

$$- (z+1)^2\left((z+1)^2\left(z^4 - 12z^3 + 6z^2 - 12z + 1\right) y^4 + 12\left(z^2-1\right)^2\left(z^2+1\right) y^3 + 2(z-1)^2 \times \right.$$

$$\left(7z^4 - 8z^3 + 18z^2 - 8z + 7\right) y^2 + 12(z-1)^4\left(z^2+1\right) y - (z-1)^4\left(3z^2 - 2z + 3\right)\big) x^2$$

$$+ 2\left(z^2-1\right)^2\left((z-1)^4 + 4y\left(z^2+1\right)(z-1)^2 + y^4(z+1)^4 + 2y^2\left(z^2-1\right)^2 + 4y^3(z+1)^2\left(z^2+1\right)\right) x$$

$$+ (z-1)^4\left((z-1)^2 + y^2(z+1)^2\right)^2\bigg)\bigg) / \left(x^6 y^4\right) - w^2 \left(\left(\frac{1}{y^2} - 1\right)(z+1)^2 + \frac{\frac{(z-1)^2}{y^2} + (z+1)^2}{x^2} \right)^2 \bigg)\bigg).$$

Appendix F

Degrees of Six-Gluon One-Loop Amplitudes in Four Dimensions

We present here the polynomial degrees of the six-gluon one-loop sub-amplitudes in four dimensions. We remind the reader that by this nomenclature we mean amplitudes expressed in a basis of scalar integrals, which were expanded around $D = 4 - 2\epsilon$ dimensions up to order $O(\epsilon^0)$. The resulting expressions are linear combinations of the special functions shown in Eq. (7.42).

We notice that the degrees of most of the sub-amplitudes are lower than the ones in D dimensions, shown in Table 7.2.

Supersymmetric Content	Helicity	Original Degrees	Reduced
$\mathcal{N} = 4$	$(--++++)$	5	0
$\mathcal{N} = 4$	$(-+-+++)$	5	0
$\mathcal{N} = 4$	$(-++-++)$	5	0
$\mathcal{N} = 1$	$(--++++)$	8	5
$\mathcal{N} = 1$	$(-+-+++)$	13	10
$\mathcal{N} = 1$	$(-++-++)$	19	16
$\mathcal{N} = 0$	$(--++++)$	27	27
$\mathcal{N} = 0$	$(-+-+++)$	56	55
$\mathcal{N} = 0$	$(-++-++)$	68	62

Table F.1: The degrees of the coefficients of six-gluon one-loop sub-amplitudes in four dimensions, before and after the factor matching. The amplitudes are expressed in the parametrisation B. For each sub-amplitude, only the highest coefficient degree is presented.

Appendix G

$0 \to \bar{t}tggg$ MHV Tree-Level Amplitudes

Reference Choice $(\mathbf{p_3} - \mathbf{p_4})$ We present here the explicit expressions for the MHV tree-level amplitudes, computed suing the two methods described in Section 5.7.

$$A_{t\bar{t}3g}^{(0)[1]}(+++--) = \frac{m_t\langle 4|p_{23}p_1|3\rangle\langle 4|2|3][45]^2}{d_{23}d_{15}s_{34}\langle 4|3|5][5|p_{12}p_2|3]} + \frac{m_t[3|p_1p_2|3]}{s_{12}s_{34}[5|p_{12}p_2|3]}\left(\frac{\langle 3|p_{12}|3]\langle 4|2|3][45]^2}{s_{45}[34][53]} - \frac{s_{45}d_{13}}{\langle 5|4|3]}\right)$$

(G.1)

$$A_{t\bar{t}3g}^{(0)[1]\text{BCFW}}(+++--) = -\frac{m_t^2 s_{45}\langle 3|1|4]\langle 5|1|4][34]}{s_{34}\langle 34\rangle\langle 3|p_2p_{34}|5\rangle\langle 3|2|3]\langle 5|1|5][3|p_4p_5|3]} -$$

(G.2)

$$\frac{m_t^2\langle 35\rangle\langle 4|p_{23}|4]\langle 5|1|4][34][45]}{s_{34}\langle 34\rangle\langle 3|p_2p_{34}|5\rangle\langle 3|2|3]\langle 5|1|5][3|p_4p_5|3]} -$$

$$\frac{\langle 3|p_1p_{34}|5\rangle\langle 5|p_2p_{34}|5\rangle[45]^2}{s_{12}s_{34}\langle 34\rangle^2\langle 3|p_2p_{34}|5\rangle[3|p_4p_5|3]} - \frac{\langle 35\rangle\langle 4|p_2p_{34}|5\rangle\langle 5|p_2p_{34}|5\rangle[45]^2}{s_{12}s_{34}\langle 34\rangle^2\langle 3|p_2p_{34}|5\rangle[3|p_4p_5|3]}$$

$$A_{t\bar{t}3g}^{(0)[2]}(+++--) = \frac{m_t^3 \langle 4|1|3] s_{45}^2 \langle 45 \rangle \langle 4|2|3]}{s_{34} s_{35}^2 \langle 34 \rangle d_{23} d_{15} [5|p_{12}p_2|3]} - \frac{m_t s_{45} \langle 45 \rangle}{s_{34} s_{35}^2 [5|p_{12}p_2|3]} \left[\frac{2 \langle 45 \rangle [53] \langle 3p_{12}3] [3|p_1p_2|3]}{s_{12} s_{34}} + \right.$$

$$\left. \frac{s_{45} \langle 4|2|3] (\langle |4p_{23}p_1|4 \rangle \langle 3|2|3] + \langle 4|p_{23}p_1|3 \rangle \langle 4|2|3])}{\langle 34 \rangle d_{23} d_{15}} \right] \tag{G.3}$$

$$A_{t\bar{t}3g}^{(0)[3]}(+++--) = -\frac{m_t s_{45} [45] \langle 4|1|5] \langle 4|2|3]^2}{s_{34} d_{23} d_{15} \langle 34 \rangle^2 [3|p_1p_2|3][5|p_{12}p_2|3]} - \frac{m_t s_{45} [53]}{s_{12} s_{34}^2 [5|p_{12}p_2|3]} \tag{G.4}$$

$$A_{t\bar{t}3g}^{(0)[3]\text{BCFW}}(+++--) = \frac{m_t s_{45} [45]}{[34][5|p_{12}p_2|3]} \left[\frac{\langle 45 \rangle \langle 4|1|5] \langle 4|2|3]^2}{4 d_{15} d_{23}} + \right. \tag{G.5}$$

$$\left. \frac{\langle 34 \rangle [3|p_1p_2|3] \langle 4|5|3]^2}{s_{12} s_{45} [34]} \right]$$

$$A_{t\bar{t}3g}^{(0)[4]}(+++--) = \frac{m_t^3 \langle 35 \rangle^2 d_{13} [45]^2 \langle 4|2|3]}{[4|p_2p_1|4] s_{34} d_{23} d_{15} [3|p_2p_{12}|5] \langle 45 \rangle} + \tag{G.6}$$

$$\frac{m_t \langle 3|5|4] \langle 4|p_{23}p_1|3 \rangle \langle 4|2|3][34]}{s_{34}^2 d_{15} [5|p_{12}p_2|3] \langle 45 \rangle [4|p_2p_1|4]]} - \frac{m_t \langle 35 \rangle^2 \langle 3|p_{12}|3][45][3|p_1p_2|3]}{s_{12} s_{34} [34] \langle 45 \rangle^2 [4|p_2p_1|4][5|p_{12}p_2|3]}$$

$$A_{t\bar{t}3g}^{(0)[4]\text{BCFW}}(+++--) = \frac{\langle 35 \rangle [45]^3}{\langle 34 \rangle^2 \langle 45 \rangle [35]} \left[-\frac{m_t^2 \langle 45 \rangle d_{13} \langle 4|2|3]}{d_{23} d_{15} [3|p_2p_{34}|5]} + \right. \tag{G.7}$$

$$\left. \frac{\langle 3|p_{12}|3]^2 [3|p_1p_2|3]}{s_{12} [45][34][3|p_2p_{12}|5]} - \frac{\langle 45 \rangle \langle 4|p_{23}p_1||3 \rangle \langle 4|2|3]}{\langle 34 \rangle d_{15} [3|p_2p_{34}|5]} \right]$$

Once again we can distinguish between the denominator factors which are responsible for soft and collinear singularities in some kinematic limits and the ones which give rise to spurious singularities when they approach zero. The terms which belong to the former category are $\{s_{12}, d_{15}, d_{23}, s_{34}, \langle 34 \rangle, [34], \langle 45 \rangle\}$, while those beloging to the latter are $\{[5|p_{12}p_2|3], [4|p_2p_1|4], s_{35}, [3|p_1p_2|3]\}$.

Appendix H

Linear Relations with FiniteFlow

We show here an example of how the FINITEFLOW package can be used to find linear relations among sub-amplitudes. This also gives us the chance of showing how the package was used to perform different computations which were useful for the research discussed in the thesis.

We start by defining a function **MapToMT**[expression] which maps an expressions in spinor variables to the equivalent one in momentum-twistor variables, for a given parametrisation.

```
In[1]=MapToMT[ang[1,3]*sq[3,1],PSanalytic]
Out[1]= s[1,2](se[1]-y[4])/(se[1]-1)
```

In the code we have $\langle ij \rangle = \text{ang}[i,j]$, $[ij] = \text{sq}[i,j]$. We want to compute all the $6! = 720$ permutations of the external legs of $A_{6g}^{(0)}(-+-+-+)$. If we look at the effect of one of the permutations, such as

$$A_{6g}^{(0)}(1^-,2^+,3^-,4^+,5^-,6^+) \xrightarrow{\text{permutation}} A_{6g}^{(0)}(2^+,1^-,6^+,3^-,4^+,5^-), \tag{H.1}$$

we see that this can be computed by evaluating the sub-amplitude $A_{6g}^{(0)}(-+-+-+)$ with the standard ordering, and then permuting the external legs in the correct way. Instead of re-deriving the amplitudes with the permuted external momenta every time, we define function **perm**[ord] to perform a permutation of the external legs directly on the momentum-twistor expressions. For each permutation we find the corresponding change of variables that give the correct final result.

```
perm[ord_List]:=MTsubstitutions /.Rule[a_,b_]:>Rule[a,MapToMT[b
                    /.Thread[Rule[Range[6],ord]]];
```

The list **MTsubstitutions** the list of rules of Eq. (4.13).

This method works on phase-free expressions, hence all the helicity amplitudes will need to be divided by their phase before the rules are applied. The permutation of the phases must therefore be done directly on the spinor variables. For this reason we define a function **phase**[hel,ord] that permutes the spinors and only afterwards we convert the expression into momentum twistors with **phaseMT**[hel,ord]. This can be done since the phases are known analytically for each helicity configuration.

```
phase["-++++-"]=ang[1,6]^4/(ang[1,2]*ang[2,3]*ang[3,4]*ang[4,5]*ang[5,6]*ang[6,1]);

phase["-+-+-+"] = ang[1,3]*ang[3,5]*ang[5,1]/ang[2,4]/ang[4,6]/ang[6,2];

phase["-++-+-"] = ang[1,4]*ang[4,6]*ang[6,1]/ang[2,3]/ang[3,5]/ang[5,2];

phase["-+-++-"] = ang[1,3]*ang[3,6]*ang[6,1]/ang[2,4]/ang[4,5]/ang[5,2];

phase["--++-+"]=  ang[1,2]*ang[2,5]*ang[5,1]/ang[3,4]/ang[4,6]/ang[6,3];


phase[hel_,ord_List]:=phase[hel] /.ang[i__]:>(ang[i] /.Thread[Rule[Range[6],ord]]);
phaseMT[hel_,ord_List]:= MapToMT[phase[hel,ord]];
```

In order to reduce the number of computations, we exploit the cyclic and reflection symmetries presented in Section 3.1. We conclude that we only have four independent helicity configurations: $\{(---+++), (--+-++), (--++-+), (-+-+-+)\}$. We write the function **findHelAndPerm**[perm] which indicates how each permutation can be expressed as one of those four sub-amplitudes with the right ordering of its legs:

```
indepHelList={"---+++","--+-++","--++-+","-+-+-+"};


findHelAndPerm[perm_]:=Module[{helList,n,hel,permTrial},
                    helList=perm/.{1->"-",2->"+",3->"-",4->"+",5->"-",6->"+"};
                    n=0;
                    While[n<6,
                            hel=StringJoin[RotateLeft[helList,n]];
                            permTrial=RotateLeft[perm,n];
                            If[MemberQ[indepHelList,hel],
                                Return[{hel,permTrial}];
                                ,
                                hel=StringJoin[Reverse@RotateLeft[helList,n]];
                                permTrial=Reverse@permTrial;
                                If[MemberQ[indepHelList,hel],
                                    Return[{hel,permTrial}];
                                    ];
                                ];
                            n=n+1;
                        ];
                        Print["No match found!"];
                        Abort[];
                    ];
```

Two examples are

```
In[2]=findHelAndPerm[{5,6,2,1,4,3}]

Out[2]:={"--+-++", {5, 3, 4, 1, 2, 6}}


In[2]=findHelAndPerm[{3,4,6,5,2,1}]

Out[2]:={"--+-++", {3, 1, 2, 5, 6, 4}}
```

Figure H.1: The node firstEval evaluates the helicity amplitude in momentum-twistor variables. The node phaseEval evaluates the phase in the same variables. The output node phaseFreeNode divides the expression by the phase, giving a physically meaningful expression.

Once we have all the needed analytic expressions, we can set up the FiniteFlow graph to find the linear relations. The first step consits in creating a graph which evaluats a sub-amplitude and divides it by its phase.

```
FFNewGraph[graph,in,vrs];

FFAlgRatExprEval[graph,firstEval,{in},vrs,{expr}];

FFAlgRatExprEval[graph,phaseEval,{in},vrs,

{1/MaptoMT[phase["---+++"]]}];

FFAlgMatMul[graph,phaseFreeNode,{firstEval,phaseEval},1,1,1];

FFGraphOutput[graph,phaseFreeNode];
```

In the graph we evaluate the sub-amplitude and the phase in two separate nodes, and then multiplies them together. We represent it graphically in Figure H.1. We create a graph of this kind for each one of the 720 sub-amplitudes. These graphs are then embedded into another graph, **graphNew**, so that each of them becomes a node in the larger structure. The permutations are performed by evaluating the phase-free functions using a new set of variables, obtained with **perm**[ord]. We stress that within FiniteFlow all the operations are performed only on numerical quantities modulo finite fields, and the analytic result is only reconstructed after the graph is evaluated. This means that we are able to perform a change of variables without ever needing to explicitly write the form of the

expressions. We present the code used to create **graphNew**,whose output is a list of the expressions of all the 720 sub-amplitudes. We show its structure in Figure H.2 with a simplified example with only two sub-amplitudes for readability.

```
listOfAmps=findHelAndPerm/@Permutations[{1,2,3,4,5,6}];
FFNewGraph[graphNew,in,vrs];
Do[
    Print["LS=",ls];
    FFNewGraph[graph,in,vrs];
    expr=DiagramNumerator[ls[[1]],topo[]] /.INT[i__,{},topo[]]:>i;
    FFAlgRatExprEval[graph,firstEval,{in},vrs,{expr}];
    FFAlgRatExprEval[graph,phaseEval,{in},vrs
    {1/(MapToMT[phase[ls[[1]]]])}];
    FFAlgMatMul[graph,phaseFreeNode,{firstEval,phaseEval},1,1,1];
    FFGraphOutput[graph,phaseFreeNode];
    vrsNew=vrs /.perm[ls[[2]]] //Simplify;


    FFAlgRatExprEval[graphNew, evalNode[ls],{in},vrs,vrsNew];
    FFAlgSimpleSubgraph[graphNew,subNode[ls],{evalNode[ls]},graph];
    FFAlgRatExprEval[graphNew,phaseNode[ls],{in},vrs
    {phaseMT[ls[[1]],ls[[2]]]}];
    FFAlgMatMul[graphNew,phaseFullNode[ls
    {phaseNode[ls],subNode[ls]},1,1,1];


    ,{ls,listOfAmps}];
    FFDeleteGraph[graph];
    FFAlgChain[graphNew,chainNode,Table[phaseFullNode[ls
    {ls,listOfAmps}]];
    FFGraphOutput[graphNew, chainNode];
```

The linear relations among the sub-amplitudes are found by evaluating **graphNew** over many
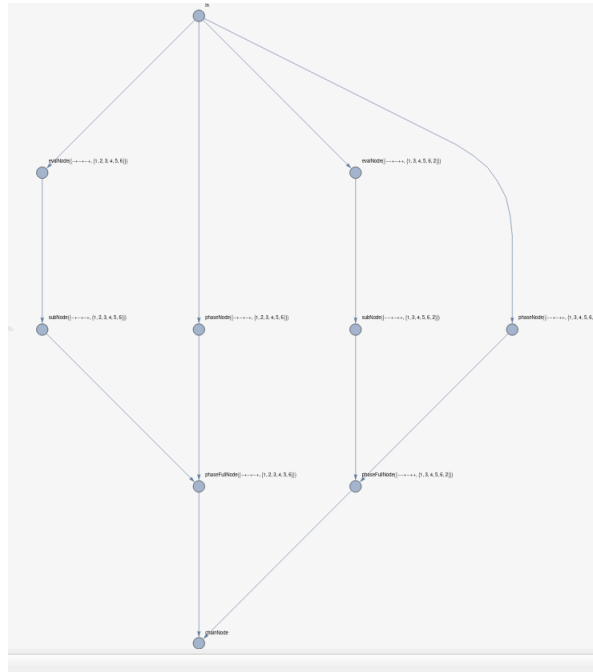
Figure H.2: A n example of the graph which has two permutations of the helicity amplitude as outputs. The one used to find all the KK-relations evaluates 720 permutations, each in a different node.

random numerical points and then solving a linear system.

This is done by our function **GetLinearRelationsFromEvaluationsSimple**. We also use functions **GetSlice**, which evaluates the graph on a univariate slice, as introduced in 4.3.1, and **GetDegree**, which evaluates the maximum polynomial degree of the slice.

```
nSamplePoints=800;

{slicerules,slicedgraph}=GetSlice[graphNew,vrs];

numdegs=(GetDegree/@slicedgraph)/.deg[a_,b_]:>a;

rndpts = Table[RandomInteger[{10^4,10^10},Length[vrs]],nSamplePoints];

batcheval=FFGraphEvaluateMany[graphNew,rndpts];

linrels=GetLinearRelationsFromEvaluationsSimple[batcheval,rndpts,0,numdegs,

{"ExtraCoefficients"->{},"ExtraCoefficientsVariables"->{}}]
```

The output of the code is

```
found 800 evaluations for 720 coefficients
system has closed
found 696 linear relations
number of indep. coeffs in evaluations 24
maximal degree before linear relations: 27
maximal degree after linear relations: 23
```

$$\{\{f[6] \to -f[4] - f[5] + f[11] + f[53] + f[67], \ f[7] \to -f[1] - f[3] + f[12] + f[26] + f[79], \ f[8] \to -f[2] - f[11] - f[12] - f[26],$$
$$f[9] \to f[3] - f[5] + f[11] - f[25] - f[26] - f[29] - f[43] - f[79], \ f[10] \to f[5] - f[11] - f[12] + f[29] + f[43],$$
$$f[13] \to -f[1] - f[2] - f[3] - f[73], \ \boxed{\cdots 685 \cdots}, \ f[716] \to -f[28] - f[29] - f[38] - f[67], \ f[717] \to f[5] - f[11] - f[12] + f[29] + f[43],$$
$$f[718] \to f[25], \ f[719] \to -f[1] - f[3] - f[22] + f[26] + f[32] + f[79] + f[81], \ f[720] \to f[1]\}, \ \{\}\}$$

large output   **show less**   **show more**   **show all**   set size limit...

We see that 696 linear relations were found, leaving a total of $(6-2)! = 24$ independent sub-amplitudes, as expected.

Appendix I

Master Integrals for $pp \to \bar{t}tj$ at $O(\epsilon^2)$

We list here the basis of Master Integrals used to reconstruct the amplitudes in Chapter 5. We distinguish the integrals coming from each of the four master topologies shown in Eq. (???).

We use the notation

$$\mathcal{I}^{T_i,[D]}_{a_1 a_2 a_3 a_4 a_5} = \int \frac{d^D k}{(2\pi)^D} \frac{1}{D_1^{a_1} D_2^{a_2} D_3^{a_3} D_4^{a_4} D_5^{a_5}}. \tag{I.1}$$

We now give the expressions of the five denominators D_i for each topology, together with the MIs.

For T_1

$$D_1 = k^2, \quad D_2 = (k - p_1)^2 - m_t^2, \quad D_3 = (k - p_1 - p_2)^2, \tag{I.2}$$

$$D_4 = (k + p_1 + p_5)^2, \quad D_5 = (k + p_5)^2$$

$$f_1^{T_1} = \epsilon^3 \mathrm{tr}_5(1,2,3,4,5,6) \mathcal{I}_{1,1,1,1,1}^{T_1[6-2\epsilon]}, \tag{I.3}$$

$$f_2^{T_1} = \epsilon^2 2 d_{23} s_{34} \mathcal{I}_{0,1,1,1,1}^{T_1[4-2\epsilon]}, \tag{I.4}$$

$$f_3^{T_1} = \epsilon^2 2 s_{34} s_{45} \mathcal{I}_{1,0,1,1,1}^{T_1[4-2\epsilon]}, \tag{I.5}$$

$$f_4^{T_1} = \epsilon^2 2 d_{15} s_{45} \mathcal{I}_{1,1,0,1,1}^{T_1[4-2\epsilon]}, \tag{I.6}$$

$$f_5^{T_1} = \epsilon^2 2 d_{23} s_{12} \mathcal{I}_{1,1,1,0,1}^{T_1[4-2\epsilon]}, \tag{I.7}$$

$$f_5^{T_1} = \epsilon^2 2 d_{23} s_{12} \mathcal{I}_{1,1,1,0,1}^{T_1[4-2\epsilon]}, \tag{I.8}$$

$$f_6^{T_1} = \epsilon^2 2 d_{23} s_{12} \mathcal{I}_{1,1,1,1,0}^{T_1[4-2\epsilon]}, \tag{I.9}$$

$$f_7^{T_1} = \epsilon^2 \Delta(p_{23}, p_1) \mathcal{I}_{1,1,0,1,0}^{T_1[4-2\epsilon]}, \tag{I.10}$$

$$f_8^{T_1} = \epsilon^2 \Delta(p_{15}, p_2) \mathcal{I}_{0,1,1,0,1}^{T_1[4-2\epsilon]}, \tag{I.11}$$

$$f_9^{T_1} = \epsilon^2 \beta(s_{12}, m_t^2) \mathcal{I}_{1,1,1,0,0}^{T_1[4-2\epsilon]}, \tag{I.12}$$

$$f_{10}^{T_1} = \epsilon s_{12} \mathcal{I}_{2,0,1,0,0}^{T_1[4-2\epsilon]}, \tag{I.13}$$

$$f_{11}^{T_1} = \epsilon s_{23} \mathcal{I}_{0,2,0,1,0}^{T_1[4-2\epsilon]}, \tag{I.14}$$

$$f_{12}^{T_1} = \epsilon s_{34} \mathcal{I}_{0,0,2,0,1}^{T_1[4-2\epsilon]}, \tag{I.15}$$

$$f_{13}^{T_1} = \epsilon s_{45} \mathcal{I}_{2,0,0,1,0}^{T_1[4-2\epsilon]}, \tag{I.16}$$

$$f_{14}^{T_1} = \epsilon s_{15} \mathcal{I}_{0,2,0,0,1}^{T_1[4-2\epsilon]}, \tag{I.17}$$

$$f_{15}^{T_2} = \epsilon m_t^2 \mathcal{I}_{0,2,0,1,0}^{T_1[4-2\epsilon]}. \tag{I.18}$$

For T_2 we have

$$D_1 = k^2 - m_t^2, \quad D_2 = (k - p_1)^2, \quad D_3 = (k - p_1 - p_2)^2 - m_t^2, \tag{I.19}$$

$$D_4 = (k + p_4 + p_5)^2 - m_t^2, \quad D_5 = (k + p_5)^2 - m_t^2$$

$$f_1^{T_2} = \epsilon^3 \mathrm{tr}_5(1,2,3,4,5,6) \mathcal{I}_{1,1,1,1,1}^{T_2[6-2\epsilon]}, \tag{I.20}$$

$$f_2^{T_2} = \epsilon^2 4 d_{34} d_{23} \beta\left(\frac{2d_{23}d_{34}}{d_{23} - d_{15}}, m_t^2\right) \mathcal{I}_{1,0,1,1,1}^{T_2[4-2\epsilon]}, \tag{I.21}$$

$$f_3^{T_2} = \epsilon^2 4 d_{34} d_{45} \beta\left(-\frac{2d_{45}d_{34}}{d_{35}}, m_t^2\right) \mathcal{I}_{1,0,1,1,1}^{T_2[4-2\epsilon]}, \tag{I.22}$$

$$f_4^{T_2} = \epsilon^2 4 d_{15} d_{45} \beta\left(\frac{2d_{15}d_{45}}{d_{15} - d_{23}}, m_t^2\right) \mathcal{I}_{1,1,0,1,1}^{T_2[4-2\epsilon]}, \tag{I.23}$$

$$f_5^{T_2} = \epsilon^2 2 d_{15} s_{12} \beta(s_{12}, m_t^2) \mathcal{I}_{1,1,1,0,1}^{T_2[4-2\epsilon]}, \tag{I.24}$$

$$f_6^{T_2} = \epsilon^2 2 d_{23} s_{12} \beta(s_{12}, m_t^2) \mathcal{I}_{1,1,1,1,0}^{T_2[4-2\epsilon]}, \tag{I.25}$$

$$f_7^{T_2} = \epsilon^2 2 d_{34} \mathcal{I}_{0,0,1,1,1}^{T_2[4-2\epsilon]}, \tag{I.26}$$

$$f_8^{T_2} = \epsilon^2 2 d_{45} \mathcal{I}_{1,0,0,1,1}^{T_2[4-2\epsilon]}, \tag{I.27}$$

$$f_9^{T_2} = \epsilon^2 2 d_{23} \mathcal{I}_{0,1,1,1,0}^{T_2[4-2\epsilon]}, \tag{I.28}$$

$$f_{10}^{T_2} = \epsilon^2 2 d_{15} \mathcal{I}_{1,1,0,0,1}^{T_2[4-2\epsilon]}, \tag{I.29}$$

$$f_{11}^{T_2} = \epsilon^2 \Delta(p_{23}, p_1) \mathcal{I}_{1,1,0,1,0}^{T_2[4-2\epsilon]}, \tag{I.30}$$

$$f_{12}^{T_2} = \epsilon^2 \Delta(p_{15}, p_2) \mathcal{I}_{0,1,1,0,1}^{T_2[4-2\epsilon]}, \tag{I.31}$$

$$f_{13}^{T_2} = \epsilon^2 2 (d_{12} - d_{45} + m_t^2) \mathcal{I}_{1,0,1,1,0}^{T_2[4-2\epsilon]}, \tag{I.32}$$

$$f_{14}^{T_2} = \epsilon^2 2 (d_{12} - d_{34} + m_t^2) \mathcal{I}_{1,0,1,0,1}^{T_2[4-2\epsilon]}, \tag{I.33}$$

$$f_{15}^{T_2} = \epsilon^2 2 (d_{15} - d_{23}) \mathcal{I}_{0,1,0,1,1}^{T_2[4-2\epsilon]}, \tag{I.34}$$

$$f_{16}^{T_2} = \epsilon s_{12} \beta(s_{12}, m_t^2) \mathcal{I}_{1,0,2,0,0}^{T_2[4-2\epsilon]}, \tag{I.35}$$

$$f_{17}^{T_2} = \epsilon s_{45} \beta(s_{45}, m_t^2) \mathcal{I}_{2,0,0,1,0}^{T_2[4-2\epsilon]}, \tag{I.36}$$

$$f_{16}^{T_2} = \epsilon s_{34} \beta(s_{34}, m_t^2) \mathcal{I}_{0,0,1,0,2}^{T_2[4-2\epsilon]}, \tag{I.37}$$

$$f_{19}^{T_2} = \epsilon s_{23} \mathcal{I}_{0,1,0,2,0}^{T_2[4-2\epsilon]}, \tag{I.38}$$

$$f_{20}^{T_2} = \epsilon s_{15} \mathcal{I}_{0,1,0,0,2}^{T_2[4-2\epsilon]}, \tag{I.39}$$

$$f_{21}^{T_2} = \epsilon m_t^2 \mathcal{I}_{2,1,0,0,0}^{T_2[4-2\epsilon]}. \tag{I.40}$$

For T_3

$$D_1 = k^2, \quad D_2 = (k - p_1)^2 - m_t^2, \quad D_3 = (k - p_1 - p_2)^2 - m_t^2, \tag{I.41}$$

$$D_4 = (k + p_4 + p_5)^2, \quad D_5 = (k + p_5)^2$$

$$f_1^{T_3} = \epsilon^3 \text{tr}_5(1,2,3,4,5,6)\mathcal{I}_{1,1,1,1,1}^{T_3[6-2\epsilon]}, \tag{I.42}$$

$$f_2^{T_3} = \epsilon^2 4 d_{24} d_{45}\mathcal{I}_{0,1,1,1,1}^{T_3[4-2\epsilon]}, \tag{I.43}$$

$$f_3^{T_3} = \epsilon^2 4 d_{15} d_{45}\mathcal{I}_{1,0,1,1,1}^{T_3[4-2\epsilon]}, \tag{I.44}$$

$$f_4^{T_3} = \epsilon^2 4 d_{24} d_{45}\mathcal{I}_{1,1,0,1,1}^{T_3[4-2\epsilon]}, \tag{I.45}$$

$$f_5^{T_3} = \epsilon^2 4 d_{15} d_{13}\mathcal{I}_{1,1,1,0,1}^{T_3[4-2\epsilon]}, \tag{I.46}$$

$$f_6^{T_3} = \epsilon^2 4 d_{23} d_{13}\beta(-\frac{2d_{13}d_{23}}{d_{45}}, m_t^2)\mathcal{I}_{1,1,1,1,0}^{T_3[4-2\epsilon]}, \tag{I.47}$$

$$f_7^{T_3} = \epsilon^2 \Delta(p_{13}, p_2)\mathcal{I}_{1,0,1,1,0}^{T_3[4-2\epsilon]}, \tag{I.48}$$

$$f_8^{T_3} = \epsilon^2 \Delta(p_{15}, p_2)\mathcal{I}_{1,1,0,1,0}^{T_3[4-2\epsilon]}, \tag{I.49}$$

$$f_9^{T_3} = \epsilon^2 2 d_{23}\mathcal{I}_{0,1,1,1,0}^{T_3[4-2\epsilon]}, \tag{I.50}$$

$$f_{10}^{T_3} = \epsilon^2 2 d_{13}\mathcal{I}_{1,1,1,0,0}^{T_3[4-2\epsilon]}, \tag{I.51}$$

$$f_{11}^{T_3} = \epsilon^2 2(d_{15} - d_{24})\mathcal{I}_{0,1,1,0,1}^{T_3[4-2\epsilon]}, \tag{I.52}$$

$$f_{12}^{T_3} = \epsilon^2 s_{13}\mathcal{I}_{1,0,2,0,0}^{T_3[4-2\epsilon]}, \tag{I.53}$$

$$f_{13}^{T_3} = \epsilon^2 s_{23}\mathcal{I}_{0,2,0,1,0}^{T_3[4-2\epsilon]}, \tag{I.54}$$

$$f_{14}^{T_3} = \epsilon^2 s_{24}\mathcal{I}_{0,0,2,0,1}^{T_3[4-2\epsilon]}, \tag{I.55}$$

$$f_{15}^{T_3} = \epsilon^2 s_{45}\mathcal{I}_{2,0,0,1,0}^{T_3[4-2\epsilon]}, \tag{I.56}$$

$$f_{16}^{T_3} = \epsilon^2 s_{15}\mathcal{I}_{0,2,0,0,1}^{T_3[4-2\epsilon]}, \tag{I.57}$$

$$f_{17}^{T_3} = \epsilon^2 m_t^2\mathcal{I}_{1,0,2,0,0}^{T_3[4-2\epsilon]} \tag{I.58}$$

For T_4 we have

$$D_1 = k^2 - m_t^2, \quad D_2 = (k - p_1)^2, \quad D_3 = (k - p_1 - p_2)^2, \tag{I.59}$$

$$D_4 = (k + p_4 + p_5)^2 - m_t^2, \quad D_5 = (k + p_5)^2 - m_t^2$$

$$f_1^{T_4} = \epsilon^3 \mathrm{tr}_5(1,2,3,4,5,6) \mathcal{I}_{1,1,1,1,1}^{T_4[6-2\epsilon]}, \tag{I.60}$$

$$f_2^{T_4} = \epsilon^2 4 d_{24} d_{45} \beta(\frac{2 d_{24} d_{45}}{d_{24} - d_{13}}, m_t^2) \mathcal{I}_{1,0,1,1,1}^{T_4[4-2\epsilon]}, \tag{I.61}$$

$$f_3^{T_4} = \epsilon^2 4 d_{15} d_{45} \beta(\frac{2 d_{23} d_{45}}{d_{23} - d_{15}}, m_t^2) \mathcal{I}_{1,1,0,1,1}^{T_4[4-2\epsilon]}, \tag{I.62}$$

$$f_4^{T_4} = \epsilon^2 4 d_{15} d_{13} \mathcal{I}_{1,1,1,0,1}^{T_4[4-2\epsilon]}, \tag{I.63}$$

$$f_5^{T_4} = \epsilon^2 4 d_{23} d_{13} \mathcal{I}_{1,1,1,1,0}^{T_4[4-2\epsilon]}, \tag{I.64}$$

$$f_6^{T_4} = \epsilon^2 4 d_{24} d_{23} \mathcal{I}_{0,1,1,1,1}^{T_4[4-2\epsilon]}, \tag{I.65}$$

$$f_7^{T_4} = \epsilon^2 \Delta(p_{13}, p_2) \mathcal{I}_{1,0,1,1,0}^{T_4[4-2\epsilon]}, \tag{I.66}$$

$$f_8^{T_4} = \epsilon^2 \Delta(p_{23}, p_1) \mathcal{I}_{1,1,0,1,0}^{T_4[4-2\epsilon]}, \tag{I.67}$$

$$f_9^{T_4} = \epsilon^2 2 (d_{23} - d_{15}) \mathcal{I}_{0,1,0,1,1}^{T_4[4-2\epsilon]}, \tag{I.68}$$

$$f_{10}^{T_4} = \epsilon^2 2 d_{15} \mathcal{I}_{0,1,0,1,1}^{T_4[4-2\epsilon]}, \tag{I.69}$$

$$f_{11}^{T_4} = \epsilon^2 2 d_{45} \mathcal{I}_{1,0,0,1,1}^{T_4[4-2\epsilon]}, \tag{I.70}$$

$$f_{12}^{T_4} = \epsilon^2 2 d_{24} \mathcal{I}_{0,0,1,1,1}^{T_4[4-2\epsilon]}, \tag{I.71}$$

$$f_{13}^{T_4} = \epsilon^2 2 (d_{13} - d_{24}) \mathcal{I}_{0,1,0,1,1}^{T_4[4-2\epsilon]}, \tag{I.72}$$

$$f_{14}^{T_4} = \epsilon \beta(s_{45}, m_t^2) \mathcal{I}_{1,0,0,2,0}^{T_4[4-2\epsilon]}, \tag{I.73}$$

$$f_{15}^{T_4} = \epsilon s_{13} \mathcal{I}_{1,0,0,2,0}^{T_4[4-2\epsilon]}, \tag{I.74}$$

$$f_{16}^{T_4} = \epsilon s_{24} \mathcal{I}_{0,0,1,0,2}^{T_4[4-2\epsilon]}, \tag{I.75}$$

$$f_{17}^{T_4} = \epsilon s_{15} \mathcal{I}_{0,1,0,2,0}^{T_4[4-2\epsilon]}, \tag{I.76}$$

$$f_{18}^{T_4} = \epsilon s_{23} \mathcal{I}_{0,1,0,2,0}^{T_4[4-2\epsilon]}, \tag{I.77}$$

$$f_{19}^{T_4} = \epsilon m_t^2 \mathcal{I}_{0,1,0,2,0}^{T_4[4-2\epsilon]}. \tag{I.78}$$

Bibliography

[1] S. Badger, M. Becchetti, E. Chaubey, R. Marzucca, and F. Sarandrea, "One-loop QCD helicity amplitudes for pp $\rightarrow \bar{t}tj$ to $O(\epsilon^2)$", *Journal of High Energy Physics*, vol. 2022, no. 6, 2022. DOI: 10.1007/jhep06(2022)066. [Online]. Available: https://doi.org/10.1007/jhep06(2022)066.

[2] A. Salam and J. Ward, "Electromagnetic and weak interactions", *Physics Letters*, vol. 13, no. 2, pp. 168–171, 1964. DOI: 10.1016/0031-9163(64)90711-5. [Online]. Available: https://doi.org/10.1016/0031-9163(64)90711-5.

[3] S. Weinberg, "A model of leptons", *Physical Review Letters*, vol. 19, no. 21, pp. 1264–1266, 1967. DOI: 10.1103/physrevlett.19.1264. [Online]. Available: https://doi.org/10.1103/physrevlett.19.1264.

[4] M. D. Schwartz, *Quantum field theory and the standard model*. Cambridge University Press, 2014.

[5] A. Zee, *Quantum field theory in a nutshell*. Princeton university press, 2010, vol. 7.

[6] B. Laforge and A. Collaboration, "Search for a low mass standard model higgs boson with the ATLAS detector at the LHC", in *AIP Conference Proceedings*, AIP, 2013. DOI: 10.1063/1.4826710. [Online]. Available: https://doi.org/10.1063/1.4826710.

[7] C. M. and, "OBSERVATION OF a NEW BOSON AT a MASS OF 125 GEV WITH THE CMS EXPERIMENT AT THE LHC", in *The Thirteenth Marcel Grossmann Meeting*, WORLD SCIENTIFIC, 2015. DOI: 10.1142/9789814623995_0019. [Online]. Available: https://doi.org/10.1142/9789814623995_0019.

[8] G. Gabrielse, S. Fayer, T. Myers, and X. Fan, "Towards an improved test of the standard model's most precise prediction", *Atoms*, vol. 7, no. 2, p. 45, 2019. DOI: 10.3390/atoms7020045. [Online]. Available: https://doi.org/10.3390/atoms7020045.

[9] W. N. Cottingham and D. A. Greenwood, *An Introduction to the Standard Model of Particle Physics*. Cambridge University Press, 2007. DOI: 10.1017/cbo9780511791406. [Online]. Available: https://doi.org/10.1017/cbo9780511791406.

[10] "Measurement of top quark pair production in association with a Z boson in proton-proton collisions at $\sqrt{s} = 13$ TeV", CERN, Geneva, Tech. Rep., 2019. [Online]. Available: https://cds.cern.ch/record/2666205.

[11] S. Fartoukh *et al.*, "LHC Configuration and Operational Scenario for Run 3", CERN, Geneva, Tech. Rep., 2021. [Online]. Available: https://cds.cern.ch/record/2790409.

[12] C. O. B. and, "Precision luminosity measurement with the CMS detector at HL-LHC", in *Proceedings of The Ninth Annual Conference on Large Hadron Collider Physics — PoS(LHCP2021)*, Sissa Medialab, 2021. DOI: 10.22323/1.397.0261. [Online]. Available: https://doi.org/10.22323/1.397.0261.

[13] G. Luisoni and S. Marzani, "QCD resummation for hadronic final states", *Journal of Physics G: Nuclear and Particle Physics*, vol. 42, no. 10, p. 103 101, 2015. DOI: 10.1088/0954-3899/42/10/103101. [Online]. Available: https://doi.org/10.1088/0954-3899/42/10/103101.

[14] A. Huss, J. Huston, S. Jones, and M. Pellen, *Les houches 2021: Physics at tev colliders: Report on the standard model precision wishlist*, 2022. DOI: 10.48550/ARXIV.2207.02122. [Online]. Available: https://arxiv.org/abs/2207.02122.

[15] "First combination of Tevatron and LHC measurements of the top-quark mass", CERN, Geneva, Tech. Rep., 2014, All figures including auxiliary figures are available at https://atlas.web.cern.ch/Atla arXiv: 1403.4427. [Online]. Available: https://cds.cern.ch/record/1669819.

[16] S. Alioli *et al.*, "Phenomenology of $t\bar{t}j + X$ production at the lhc", *Journal of High Energy Physics*, vol. 2022, no. 5, 2022. DOI: 10.1007/jhep05(2022)146. [Online]. Available: https://link.springer.com/article/10.1007/JHEP01(2012)137.

[17] J. W. Rohlf and P. J. Collings, "Modern physics from α to Z^0", *Physics Today*, vol. 47, no. 12, pp. 62–63, 1994. DOI: 10.1063/1.2808751. [Online]. Available: https://doi.org/10.1063/1.2808751.

[18] R. K. Ellis, W. J. Stirling, and B. R. Webber, *QCD and collider physics*. Cambridge university press, 2003.

[19] M. E. Peskin, *An introduction to quantum field theory*. CRC press, 2018.

[20] M. Srednicki, *Quantum field theory*. Cambridge University Press, 2007.

[21] M. Gell-Mann, "Symmetries of baryons and mesons∗", in *The Eightfold Way*, CRC Press, 2018, pp. 216–233. DOI: 10.1201/9780429496615-30. [Online]. Available: https://doi.org/10.1201/9780429496615-30.

[22] G. 't Hooft and M. J. G. Veltman, "Regularization and Renormalization of Gauge Fields", *Nucl. Phys. B*, vol. 44, pp. 189–213, 1972. DOI: 10.1016/0550-3213(72)90279-9.

[23] W. Pauli and F. Villars, "On the invariant regularization in relativistic quantum theory", *Rev. Mod. Phys.*, vol. 21, pp. 434–444, 3 1949. DOI: 10.1103/RevModPhys.21.434. [Online]. Available: https://link.aps.org/doi/10.1103/RevModPhys.21.434.

[24] M. L. Mangano, *Introduction to qcd*, 1999.

[25] P. Marquard, A. V. Smirnov, V. A. Smirnov, M. Steinhauser, and D. Wellmann, "$\bar{M}S$-on-shell quark mass relation up to four loops in qcd and a general su(n) gauge group", *Physical Review D*, vol. 94, no. 7, 2016. DOI: 10.1103/physrevd.94.074025. [Online]. Available: https://doi.org/10.1103%2Fphysrevd.94.074025.

[26] W. B. Kilgore, "Regularization schemes and higher order corrections", *Physical Review D*, vol. 83, no. 11, 2011. DOI: 10.1103/physrevd.83.114005. [Online]. Available: https://doi.org/10.1103/physrevd.83.114005.

[27] G. 't Hooft and M. Veltman, "Regularization and renormalization of gauge fields", *Nuclear Physics B*, vol. 44, no. 1, pp. 189–213, 1972. DOI: 10.1016/0550-3213(72)90279-9. [Online]. Available: https://doi.org/10.1016/0550-3213(72)90279-9.

[28] Z. Bern and D. A. Kosower, "The computation of loop amplitudes in gauge theories", *Nuclear Physics B*, vol. 379, no. 3, pp. 451–561, 1992. DOI: 10.1016/0550-3213(92)90134-w. [Online]. Available: https://doi.org/10.1016/0550-3213(92)90134-w.

[29] C. G. Callan, "Broken scale invariance in scalar field theory", *Phys. Rev. D*, vol. 2, pp. 1541–1547, 8 1970. DOI: 10.1103/PhysRevD.2.1541. [Online]. Available: https://link.aps.org/doi/10.1103/PhysRevD.2.1541.

[30] K. Symanzik, "Small distance behaviour in field theory and power counting", *Communications in Mathematical Physics*, vol. 18, no. 3, pp. 227–246, 1970. DOI: 10.1007/bf01649434. [Online]. Available: https://doi.org/10.1007/bf01649434.

[31] P. A. Baikov, K. G. Chetyrkin, and J. H. Kühn, "Five-Loop Running of the QCD coupling constant", *Phys. Rev. Lett.*, vol. 118, no. 8, p. 082 002, 2017. DOI: 10.1103/PhysRevLett.118.082002. arXiv: 1606.08659 [hep-ph].

[32] T. Luthe, A. Maier, P. Marquard, and Y. Schroder, "The five-loop Beta function for a general gauge group and anomalous dimensions beyond Feynman gauge", *JHEP*, vol. 10, p. 166, 2017. DOI: 10.1007/JHEP10(2017)166. arXiv: 1709.07718 [hep-ph].

[33] P. D. Group *et al.*, "Review of Particle Physics", *Progress of Theoretical and Experimental Physics*, vol. 2022, no. 8, Aug. 2022, 083C01, ISSN: 2050-3911. DOI: 10.1093/ptep/ptac097. eprint: https://academic.oup.com/ptep/article-pdf/2022/8/083C01/45434185/ptac097_19_miscellaneous_searches_and_searches_in_other_sections.pdf. [Online]. Available: https://doi.org/10.1093/ptep/ptac097.

[34] J. J. Ethier and E. R. Nocera, "Parton Distributions in Nucleons and Nuclei", *Ann. Rev. Nucl. Part. Sci.*, vol. 70, pp. 43–76, 2020. DOI: 10.1146/annurev-nucl-011720-042725. arXiv: 2001.07722 [hep-ph].

[35] J. Gao, L. Harland-Lang, and J. Rojo, "The structure of the proton in the LHC precision era", *Physics Reports*, vol. 742, pp. 1–121, 2018. DOI: 10.1016/j.physrep.2018.03.002. [Online]. Available: https://doi.org/10.1016/j.physrep.2018.03.002.

[36] R. D. Field and R. P. Feynman, "Quark elastic scattering as a source of high-transverse-momentum mesons", *Physical Review D*, vol. 15, no. 9, pp. 2590–2616, 1977. DOI: `10.1103/physrevd.15.2590`. [Online]. Available: `https://doi.org/10.1103/physrevd.15.2590`.

[37] X. Artru and G. Mennessier, "String model and multiproduction", *Nuclear Physics B*, vol. 70, no. 1, pp. 93–115, 1974. DOI: `10.1016/0550-3213(74)90360-5`. [Online]. Available: `https://doi.org/10.1016/0550-3213(74)90360-5`.

[38] R. D. Field and S. Wolfram, "A QCD model for e^+e^-- annihilation", *Nuclear Physics B*, vol. 213, no. 1, pp. 65–84, 1983. DOI: `10.1016/0550-3213(83)90175-x`. [Online]. Available: `https://doi.org/10.1016/0550-3213(83)90175-x`.

[39] E. Bothmann *et al.*, "Event generation with sherpa 2.2", *SciPost Physics*, vol. 7, no. 3, 2019. DOI: `10.21468/scipostphys.7.3.034`. [Online]. Available: `https://doi.org/10.21468/scipostphys.7.3.034`.

[40] T. Sjöstrand *et al.*, "An introduction to PYTHIA 8.2", *Computer Physics Communications*, vol. 191, pp. 159–177, 2015. DOI: `10.1016/j.cpc.2015.01.024`. [Online]. Available: `https://doi.org/10.1016/j.cpc.2015.01.024`.

[41] J. Bellm *et al.*, "Herwig 7.0/herwig ++ 3.0 release note", *The European Physical Journal C*, vol. 76, no. 4, 2016. DOI: `10.1140/epjc/s10052-016-4018-8`. [Online]. Available: `https://doi.org/10.1140/epjc/s10052-016-4018-8`.

[42] G. Altarelli and G. Parisi, "Asymptotic freedom in parton language", *Nuclear Physics B*, vol. 126, no. 2, pp. 298–318, 1977, ISSN: 0550-3213. DOI: `https://doi.org/10.1016/0550-3213(77)90384-4`. [Online]. Available: `https://www.sciencedirect.com/science/article/pii/0550321377903844`.

[43] V. Gribov and L. Lipatov, "Deep inelastic electron scattering in perturbation theory", *Physics Letters B*, vol. 37, no. 1, pp. 78–80, 1971. DOI: `10.1016/0370-2693(71)90576-4`. [Online]. Available: `https://doi.org/10.1016/0370-2693(71)90576-4`.

[44] Y. L. Dokshitzer, "Calculation of the Structure Functions for Deep Inelastic Scattering and e+ e- Annihilation by Perturbation Theory in Quantum Chromodynamics.", *Sov. Phys. JETP*,

vol. 46, pp. 641–653, 1977. [Online]. Available: https://inis.iaea.org/search/search.aspx?orig_q=RN:9409980.

[45] L. A. Harland-Lang and R. S. Thorne, "On the consistent use of scale variations in PDF fits and predictions", *The European Physical Journal C*, vol. 79, no. 3, 2019. DOI: 10.1140/epjc/s10052-019-6731-6. [Online]. Available: https://doi.org/10.1140\%2Fepjc\%2Fs10052-019-6731-6.

[46] S. D. Drell and T.-M. Yan, "Partons and their applications at high energies", *Annals of Physics*, vol. 66, no. 2, pp. 578–623, 1971. DOI: 10.1016/0003-4916(71)90071-6. [Online]. Available: https://doi.org/10.1016/0003-4916(71)90071-6.

[47] R. J. Eden, P. V. Landshoff, D. I. Olive, J. C. Polkinghorne, and P. Roman, "The analytic s-matrix", *American Journal of Physics*, vol. 35, no. 11, pp. 1101–1102, 1967. DOI: 10.1119/1.1973770. [Online]. Available: https://doi.org/10.1119/1.1973770.

[48] L. Dixon, *Calculating scattering amplitudes efficiently*, 1996. DOI: 10.48550/ARXIV.HEP-PH/9601359. [Online]. Available: https://arxiv.org/abs/hep-ph/9601359.

[49] L. J. Dixon, "A brief introduction to modern amplitude methods", in *Journeys Through the Precision Frontier: Amplitudes for Colliders*, WORLD SCIENTIFIC, 2015. DOI: 10.1142/9789814678766_0002. [Online]. Available: https://doi.org/10.1142/9789814678766_0002.

[50] S Catani and M. Seymour, "Nlo calculations in qcd: A general algorithm", *Nuclear Physics B - Proceedings Supplements*, vol. 51, no. 3, pp. 233–242, 1996, Proceedings of the 1996 Zeuthen Workshop on Elementary Particle Theory: QCD and QED in Higher Orders, ISSN: 0920-5632. DOI: https://doi.org/10.1016/S0920-5632(96)90030-4. [Online]. Available: https://www.sciencedirect.com/science/article/pii/S0920563296900304.

[51] F. Bloch and A. Nordsieck, "Note on the radiation field of the electron", *Phys. Rev.*, vol. 52, pp. 54–59, 2 1937. DOI: 10.1103/PhysRev.52.54. [Online]. Available: https://link.aps.org/doi/10.1103/PhysRev.52.54.

[52] D. Yennie, S. Frautschi, and H Suura, "The infrared divergence phenomena and high-energy processes", *Annals of Physics*, vol. 13, no. 3, pp. 379–452, 1961, ISSN: 0003-4916. DOI: `https://doi.org/10.1016/0003-4916(61)90151-8`. [Online]. Available: `https://www.sciencedirect.com/science/article/pii/0003491661901518`.

[53] T. D. Lee and M. Nauenberg, "Degenerate systems and mass singularities", *Phys. Rev.*, vol. 133, B1549–B1562, 6B 1964. DOI: `10.1103/PhysRev.133.B1549`. [Online]. Available: `https://link.aps.org/doi/10.1103/PhysRev.133.B1549`.

[54] T. Kinoshita, "Mass singularities of feynman amplitudes", *Journal of Mathematical Physics*, vol. 3, no. 4, pp. 650–677, 1962. DOI: `10.1063/1.1724268`. eprint: `https://doi.org/10.1063/1.1724268`. [Online]. Available: `https://doi.org/10.1063/1.1724268`.

[55] N. Agarwal, L. Magnea, C. Signorile-Signorile, and A. Tripathi, *The infrared structure of perturbative gauge theories*, 2021. DOI: `10.48550/ARXIV.2112.07099`. [Online]. Available: `https://arxiv.org/abs/2112.07099`.

[56] S. Catani and M. Grazzini, "Infrared factorization of tree-level qcd amplitudes at the next-to-next-to-leading order and beyond", *Nuclear Physics B*, vol. 570, no. 1-2, pp. 287–325, 2000.

[57] R. Ellis and J. Sexton, "QCD radiative corrections to parton-parton scattering", *Nuclear Physics B*, vol. 269, no. 2, pp. 445–484, 1986. DOI: `10.1016/0550-3213(86)90232-4`. [Online]. Available: `https://doi.org/10.1016/0550-3213(86)90232-4`.

[58] L. J. Bergmann, "Next-to-leading-log qcd calculation of symmetric di-hadron production", Jan. 1989. [Online]. Available: `https://www.osti.gov/biblio/7188277`.

[59] B. W. Harris and J. F. Owens, "Two cutoff phase space slicing method", *Phys. Rev. D*, vol. 65, p. 094 032, 9 2002. DOI: `10.1103/PhysRevD.65.094032`. [Online]. Available: `https://link.aps.org/doi/10.1103/PhysRevD.65.094032`.

[60] T. Binoth and G. Heinrich, "An automatized algorithm to compute infrared divergent multi-loop integrals", *Nuclear Physics B*, vol. 585, no. 3, pp. 741–759, 2000, ISSN: 0550-3213. DOI: `https://doi.org/10.1016/S0550-3213(00)00429-6`. [Online]. Available: `https://www.sciencedirect.com/science/article/pii/S0550321300004296`.

[61] S Catani, "A general algorithm for calculating jet cross sections in NLO QCD", *Nuclear Physics B*, vol. 510, no. 1-2, pp. 503–504, 1998. DOI: 10.1016/s0550-3213(97)00753-0. [Online]. Available: https://doi.org/10.1016/s0550-3213(97)00753-0.

[62] R. K. Ellis, D. A. Ross, and A. E. Terrano, "Calculation of event-shape parameters in e^+e^- annihilation", *Phys. Rev. Lett.*, vol. 45, pp. 1226–1229, 15 1980. DOI: 10.1103/PhysRevLett.45.1226. [Online]. Available: https://link.aps.org/doi/10.1103/PhysRevLett.45.1226.

[63] S. Catani, S. Dittmaier, M. H. Seymour, and Z. Trócsányi, "The dipole formalism for next-to-leading order QCD calculations with massive partons", *Nuclear Physics B*, vol. 627, no. 1-2, pp. 189–265, 2002. DOI: 10.1016/s0550-3213(02)00098-6. [Online]. Available: https://doi.org/10.1016/s0550-3213(02)00098-6.

[64] S Catani and M. Seymour, "NLO calculations in QCD: A general algorithm", *Nuclear Physics B - Proceedings Supplements*, vol. 51, no. 3, pp. 233–242, 1996. DOI: 10.1016/s0920-5632(96)90030-4. [Online]. Available: https://doi.org/10.1016/s0920-5632(96)90030-4.

[65] A. G.-D. Ridder, T. Gehrmann, and E. N. Glover, "Antenna subtraction at nnlo", *Journal of High Energy Physics*, vol. 2005, no. 09, p. 056, 2005. DOI: 10.1088/1126-6708/2005/09/056. [Online]. Available: https://dx.doi.org/10.1088/1126-6708/2005/09/056.

[66] W. J. T. Bobadilla *et al.*, "May the four be with you: Novel IR-subtraction methods to tackle NNLO calculations", *The European Physical Journal C*, vol. 81, no. 3, 2021. DOI: 10.1140/epjc/s10052-021-08996-y. [Online]. Available: https://doi.org/10.1140/epjc/s10052-021-08996-y.

[67] H. Elvang and Y. tin Huang, *Scattering Amplitudes in Gauge Theory and Gravity*. Cambridge University Press, 2015. DOI: 10.1017/cbo9781107706620. [Online]. Available: https://doi.org/10.1017/cbo9781107706620.

[68] R. K. Ellis, Z. Kunszt, K. Melnikov, and G. Zanderighi, "One-loop calculations in quantum field theory: from Feynman diagrams to unitarity cuts", *Phys. Rept.*, vol. 518, pp. 141–250, 2012. DOI: 10.1016/j.physrep.2012.01.008. arXiv: 1105.4319 [hep-ph].

[69] M. L. Mangano and S. J. Parke, "Multi-parton amplitudes in gauge theories", *Physics Reports*, vol. 200, no. 6, pp. 301–367, 1991. DOI: 10.1016/0370-1573(91)90091-y. [Online]. Available: https://doi.org/10.1016/0370-1573(91)90091-y.

[70] F. Berends and W. Giele, "The six-gluon process as an example of weyl-van der waerden spinor calculus", *Nuclear Physics B*, vol. 294, pp. 700–732, 1987. DOI: 10.1016/0550-3213(87)90604-3. [Online]. Available: https://doi.org/10.1016/0550-3213(87)90604-3.

[71] F. Berends and W. Giele, "Recursive calculations for processes with n gluons", *Nuclear Physics B*, vol. 306, no. 4, pp. 759–808, 1988. DOI: 10.1016/0550-3213(88)90442-7. [Online]. Available: https://doi.org/10.1016/0550-3213(88)90442-7.

[72] H. Elvang and Y.-t. Huang, *Scattering amplitudes*, 2013. DOI: 10.48550/ARXIV.1308.1697. [Online]. Available: https://arxiv.org/abs/1308.1697.

[73] R. Kleiss and H. Kuijf, "Multigluon cross sections and 5-jet production at hadron colliders", *Nuclear Physics B*, vol. 312, no. 3, pp. 616–644, 1989. DOI: 10.1016/0550-3213(89)90574-9. [Online]. Available: https://doi.org/10.1016/0550-3213(89)90574-9.

[74] P. B. Pal, *Representation-independent manipulations with dirac matrices and spinors*, 2007. DOI: 10.48550/ARXIV.PHYSICS/0703214. [Online]. Available: https://arxiv.org/abs/physics/0703214.

[75] S. MANDELSTAM, "Determination of the pion-nucleon scattering amplitude from dispersion relations and unitarity. general theory", in *Memorial Volume for Stanley Mandelstam*, WORLD SCIENTIFIC, 2017, pp. 151–167. DOI: 10.1142/9789813207851_0020. [Online]. Available: https://doi.org/10.1142/9789813207851_0020.

[76] S. J. Parke and T. R. Taylor, "Amplitude for *n*-gluon scattering", *Physical Review Letters*, vol. 56, no. 23, pp. 2459–2460, 1986. DOI: 10.1103/physrevlett.56.2459. [Online]. Available: https://doi.org/10.1103/physrevlett.56.2459.

[77] R. Britto, F. Cachazo, and B. Feng, "New recursion relations for tree amplitudes of gluons", *Nuclear Physics B*, vol. 715, no. 1-2, pp. 499–522, 2005. DOI: 10.1016/j.nuclphysb.2005.02.030. [Online]. Available: https://doi.org/10.1016/j.nuclphysb.2005.02.030.

[78] R. Britto, F. Cachazo, B. Feng, and E. Witten, "Direct proof of the tree-level scattering amplitude recursion relation in yang-mills theory", *Physical Review Letters*, vol. 94, no. 18, 2005. DOI: `10.1103/physrevlett.94.181602`. [Online]. Available: `https://doi.org/10.1103/physrevlett.94.181602`.

[79] R. Penrose, "Twistor algebra", *Journal of Mathematical Physics*, vol. 8, no. 2, pp. 345–366, 1967. DOI: `10.1063/1.1705200`. [Online]. Available: `https://doi.org/10.1063/1.1705200`.

[80] R. Penrose and M. MacCallum, "Twistor theory: An approach to the quantisation of fields and space-time", *Physics Reports*, vol. 6, no. 4, pp. 241–315, 1973. DOI: `10.1016/0370-1573(73)90008-2`. [Online]. Available: `https://doi.org/10.1016/0370-1573(73)90008-2`.

[81] A. Hodges, "Eliminating spurious poles from gauge-theoretic amplitudes", *Journal of High Energy Physics*, vol. 2013, no. 5, 2013. DOI: `10.1007/jhep05(2013)135`. [Online]. Available: `https://doi.org/10.1007/jhep05(2013)135`.

[82] S. Badger, "Automating QCD amplitudes with on-shell methods", *Journal of Physics: Conference Series*, vol. 762, p. 012 057, 2016. DOI: `10.1088/1742-6596/762/1/012057`. [Online]. Available: `https://doi.org/10.1088/1742-6596/762/1/012057`.

[83] S. Badger, H. Frellesvig, and Y. Zhang, "A two-loop five-gluon helicity amplitude in QCD", *Journal of High Energy Physics*, vol. 2013, no. 12, 2013. DOI: `10.1007/jhep12(2013)045`. [Online]. Available: `https://doi.org/10.1007/jhep12(2013)045`.

[84] R. E. Cutkosky, "Singularities and discontinuities of feynman amplitudes", *Journal of Mathematical Physics*, vol. 1, no. 5, pp. 429–433, 1960. DOI: `10.1063/1.1703676`. [Online]. Available: `https://doi.org/10.1063/1.1703676`.

[85] D. B. Melrose, "Reduction of feynman diagrams", *Il Nuovo Cimento A*, vol. 40, no. 1, pp. 181–213, 1965. DOI: `10.1007/bf02832919`. [Online]. Available: `https://doi.org/10.1007/bf02832919`.

[86] G. Passarino and M. J. G. Veltman, "One Loop Corrections for e+ e- Annihilation Into mu+ mu- in the Weinberg Model", *Nucl. Phys. B*, vol. 160, pp. 151–207, 1979. DOI: `10.1016/0550-3213(79)90234-7`.

[87] G. Ossola, C. G. Papadopoulos, and R. Pittau, "Reducing full one-loop amplitudes to scalar integrals at the integrand level", *Nuclear Physics B*, vol. 763, no. 1-2, pp. 147–169, 2007. DOI: 10.1016/j.nuclphysb.2006.11.012. [Online]. Available: https://doi.org/10.1016/j.nuclphysb.2006.11.012.

[88] F. del Aguila and R Pittau, "Recursive numerical calculus of one-loop tensor integrals", *Journal of High Energy Physics*, vol. 2004, no. 07, pp. 017–017, 2004. DOI: 10.1088/1126-6708/2004/07/017. [Online]. Available: https://doi.org/10.1088/1126-6708/2004/07/017.

[89] R. K. Ellis and G. Zanderighi, "Scalar one-loop integrals for QCD", *Journal of High Energy Physics*, vol. 2008, no. 02, pp. 002–002, 2008. DOI: 10.1088/1126-6708/2008/02/002. [Online]. Available: https://doi.org/10.1088/1126-6708/2008/02/002.

[90] Z. Bern, L. Dixon, and D. A. Kosower, "Dimensionally regulated one-loop integrals", *Physics Letters B*, vol. 302, no. 2-3, pp. 299–308, 1993. DOI: 10.1016/0370-2693(93)90400-c. [Online]. Available: https://doi.org/10.1016/0370-2693(93)90400-c.

[91] D. C. Dunbar, "The six gluon one-loop amplitude", *Nuclear Physics B - Proceedings Supplements*, vol. 183, pp. 122–136, 2008. DOI: 10.1016/j.nuclphysbps.2008.09.093. [Online]. Available: https://doi.org/10.1016/j.nuclphysbps.2008.09.093.

[92] G. C. NAYAK, "GAUGE FIXING IDENTITY IN THE BACKGROUND FIELD METHOD OF QCD IN PURE GAUGE", *International Journal of Modern Physics A*, vol. 25, no. 20, pp. 3885–3898, 2010. DOI: 10.1142/s0217751x10050172. [Online]. Available: https://doi.org/10.1142/s0217751x10050172.

[93] Z. Bern, L. Dixon, and D. A. Kosower, "PROGRESS IN ONE-LOOP QCD COMPUTATIONS", *Annual Review of Nuclear and Particle Science*, vol. 46, no. 1, pp. 109–148, 1996. DOI: 10.1146/annurev.nucl.46.1.109. [Online]. Available: https://doi.org/10.1146/annurev.nucl.46.1.109.

[94] M. B. Green, J. H. Schwarz, and L. Brink, "N = 4 yang-mills and n = 8 supergravity as limits of string theories", *Nuclear Physics B*, vol. 198, no. 3, pp. 474–492, 1982. DOI: 10.1016/0550-3213(82)90336-4. [Online]. Available: https://doi.org/10.1016/0550-3213(82)90336-4.

[95] Z. Bern, L. Dixon, D. C. Dunbar, and D. A. Kosower, "Fusing gauge theory tree amplitudes into loop amplitudes", *Nuclear Physics B*, vol. 435, no. 1-2, pp. 59–101, 1995. DOI: `10.1016/0550-3213(94)00488-z`. [Online]. Available: `https://doi.org/10.1016/0550-3213(94)00488-z`.

[96] C. F. Berger, Z. Bern, L. J. Dixon, D. Forde, and D. A. Kosower, "All one-loop maximally helicity violating gluonic amplitudes in QCD", Tech. Rep., 2006. DOI: `10.2172/885511`. [Online]. Available: `https://doi.org/10.2172/885511`.

[97] D. Forde and D. A. Kosower, "All-multiplicity one-loop corrections to maximum-helicity-violating amplitudes in QCD", *Physical Review D*, vol. 73, no. 6, 2006. DOI: `10.1103/physrevd.73.061701`. [Online]. Available: `https://doi.org/10.1103/physrevd.73.061701`.

[98] Z. Bern, L. Dixon, D. C. Dunbar, and D. A. Kosower, "Fusing gauge theory tree amplitudes into loop amplitudes", *Nuclear Physics B*, vol. 435, no. 1-2, pp. 59–101, 1995. DOI: `10.1016/0550-3213(94)00488-z`. [Online]. Available: `https://doi.org/10.1016/0550-3213(94)00488-z`.

[99] G. D. Laurentis and D. Maître, "Extracting analytical one-loop amplitudes from numerical evaluations", *Journal of High Energy Physics*, vol. 2019, no. 7, 2019. DOI: `10.1007/jhep07(2019)123`. [Online]. Available: `https://doi.org/10.1007/jhep07(2019)123`.

[100] T. Peraro, "FiniteFlow: Multivariate functional reconstruction using finite fields and dataflow graphs", *Journal of High Energy Physics*, vol. 2019, no. 7, 2019. DOI: `10.1007/jhep07(2019)031`. [Online]. Available: `https://doi.org/10.1007/jhep07(2019)031`.

[101] A. Cuyt and W. shin Lee, "Sparse interpolation of multivariate rational functions", *Theoretical Computer Science*, vol. 412, no. 16, pp. 1445–1456, 2011. DOI: `10.1016/j.tcs.2010.11.050`. [Online]. Available: `https://doi.org/10.1016/j.tcs.2010.11.050`.

[102] J. von zur Gathen and J. Gerhard, *Modern Computer Algebra*. Cambridge University Press, 2013. DOI: `10.1017/cbo9781139856065`. [Online]. Available: `https://doi.org/10.1017/cbo9781139856065`.

[103] P. S. Wang, "A p-adic algorithm for univariate partial fractions", in *Proceedings of the fourth ACM symposium on Symbolic and algebraic computation - SYMSAC '81*, ACM Press, 1981. DOI: 10.1145/800206.806398. [Online]. Available: https://doi.org/10.1145/800206.806398.

[104] P. S. Wang, M. J. T. Guy, and J. H. Davenport, "P-adic reconstruction of rational numbers", *ACM SIGSAM Bulletin*, vol. 16, no. 2, pp. 2–3, 1982. DOI: 10.1145/1089292.1089293. [Online]. Available: https://doi.org/10.1145/1089292.1089293.

[105] D. Pei, A. Salomaa, and C. Ding, *Chinese remainder theorem: applications in computing, coding, cryptography.* World Scientific, 1996.

[106] A. von Manteuffel and R. M. Schabinger, "A novel approach to integration by parts reduction", *Physics Letters B*, vol. 744, pp. 101–104, 2015. DOI: 10.1016/j.physletb.2015.03.029. [Online]. Available: https://doi.org/10.1016/j.physletb.2015.03.029.

[107] A. von Manteuffel and R. M. Schabinger, "Planar master integrals for four-loop form factors", *Journal of High Energy Physics*, vol. 2019, no. 5, 2019. DOI: 10.1007/jhep05(2019)073. [Online]. Available: https://doi.org/10.1007/jhep05(2019)073.

[108] J. Henn, T. Peraro, M. Stahlhofen, and P. Wasser, "Matter dependence of the four-loop cusp anomalous dimension", *Physical Review Letters*, vol. 122, no. 20, 2019. DOI: 10.1103/physrevlett.122.201602. [Online]. Available: https://doi.org/10.1103/physrevlett.122.201602.

[109] S. Abreu, J. Dormans, F. F. Cordero, H. Ita, and B. Page, "Analytic form of planar two-loop five-gluon scattering amplitudes in QCD", *Physical Review Letters*, vol. 122, no. 8, 2019. DOI: 10.1103/physrevlett.122.082002. [Online]. Available: https://doi.org/10.1103/physrevlett.122.082002.

[110] S. Badger, B. Biedermann, P. Uwer, and V. Yundin, "Numerical evaluation of virtual corrections to multi-jet production in massless QCD", *Computer Physics Communications*, vol. 184, no. 8, pp. 1981–1998, 2013. DOI: 10.1016/j.cpc.2013.03.018. [Online]. Available: https://doi.org/10.1016/j.cpc.2013.03.018.

[111] S. Badger, H. B. Hartanto, J. Kryś, and S. Zoia, "Two-loop leading colour helicity amplitudes for $W^{\pm}\gamma + j$ production at the LHC", *Journal of High Energy Physics*, vol. 2022, no. 5, 2022. DOI: `10.1007/jhep05(2022)035`. [Online]. Available: `https://doi.org/10.1007/jhep05(2022)035`.

[112] S. Badger *et al.*, "Virtual QCD corrections to gluon-initiated diphoton plus jet production at hadron colliders", *Journal of High Energy Physics*, vol. 2021, no. 11, 2021. DOI: `10.1007/jhep11(2021)083`. [Online]. Available: `https://doi.org/10.1007/jhep11(2021)083`.

[113] S. Badger, E. Chaubey, H. B. Hartanto, and R. Marzucca, "Two-loop leading colour QCD helicity amplitudes for top quark pair production in the gluon fusion channel", *Journal of High Energy Physics*, vol. 2021, no. 6, 2021. DOI: `10.1007/jhep06(2021)163`. [Online]. Available: `https://doi.org/10.1007/jhep06(2021)163`.

[114] M. Heller and A. von Manteuffel, "MultivariateApart: Generalized partial fractions", *Computer Physics Communications*, vol. 271, p. 108 174, 2022. DOI: `10.1016/j.cpc.2021.108174`. [Online]. Available: `https://doi.org/10.1016/j.cpc.2021.108174`.

[115] D. Cox, J. Little, and D. OShea, *Ideals, varieties, and algorithms: an introduction to computational algebraic geometry and commutative algebra*. Springer Science & Business Media, 2013.

[116] W. Decker, G.-M. Greuel, G. Pfister, and H. Schönemann, Singular *4-3-0 — A computer algebra system for polynomial computations*, `http://www.singular.uni-kl.de`, 2022.

[117] S. Dittmaier, P. Uwer, and S. Weinzierl, "Hadronic top-quark pair production in association with a hard jet at next-to-leading order QCD: Phenomenological studies for the tevatron and the LHC", *The European Physical Journal C*, vol. 59, no. 3, pp. 625–646, 2008. DOI: `10.1140/epjc/s10052-008-0816-y`. [Online]. Available: `https://doi.org/10.1140/epjc/s10052-008-0816-y`.

[118] S. ALIOLI, J. FUSTER, A. IRLES, S. MOCH, P. UWER, and M. VOS, "A new observable to measure the top quark mass at hadron colliders", *Pramana*, vol. 79, no. 4, pp. 809–812, 2012. DOI: `10.1007/s12043-012-0374-6`. [Online]. Available: `https://doi.org/10.1007/s12043-012-0374-6`.

[119] S. Weinzierl, "Does one need the $O(\epsilon)$- and $O(\epsilon^2)$-terms of one-loop amplitudes in a next-to-next-to-leading order calculation ?", *Physical Review D*, vol. 84, no. 7, 2011. DOI: `10.1103/physrevd.84.074007`. [Online]. Available: `https://doi.org/10.1103/physrevd.84.074007`.

[120] G. Bertolotti, P. Torrielli, S. Uccirati, and M. Zaro, "Local analytic sector subtraction for initial- and final-state radiation at NLO in massless QCD", *Journal of High Energy Physics*, vol. 2022, no. 12, 2022. DOI: `10.1007/jhep12(2022)042`. [Online]. Available: `https://doi.org/10.1007/jhep12(2022)042`.

[121] Z. Bern, L. Dixon, and D. A. Kosower, "One-loop corrections to two-quark three-gluon amplitudes", *Nuclear Physics B*, vol. 437, no. 2, pp. 259–304, 1995. DOI: `10.1016/0550-3213(94)00542-m`. [Online]. Available: `https://doi.org/10.1016/0550-3213(94)00542-m`.

[122] Z. Kunszt, A. Signer, and Z. Trócsányi, "One-loop radiative corrections to the helicity amplitudes of QCD processes involving four quarks and one gluon", *Physics Letters B*, vol. 336, no. 3-4, pp. 529–536, 1994. DOI: `10.1016/0370-2693(94)90568-1`. [Online]. Available: `https://doi.org/10.1016/0370-2693(94)90568-1`.

[123] R. H. Kleiss and W. J. Stirling, "Spinor techniques for calculating $p\bar{p} \to W^{\pm}Z^0 + \text{jets}$", *Nucl. Phys. B*, vol. 262, pp. 235–262, 1985. DOI: `10.1016/0550-3213(85)90285-8`. [Online]. Available: `https://cds.cern.ch/record/160513`.

[124] C. Schwinn and S. Weinzierl, "On-shell recursion relations for all born QCD amplitudes", *Journal of High Energy Physics*, vol. 2007, no. 04, pp. 072–072, 2007. DOI: `10.1088/1126-6708/2007/04/072`. [Online]. Available: `https://doi.org/10.1088/1126-6708/2007/04/072`.

[125] G. Cullen, M. Koch-Janusz, and T. Reiter, "Spinney: A form library for helicity spinors", *Computer Physics Communications*, vol. 182, no. 11, pp. 2368–2387, 2011. DOI: `10.1016/j.cpc.2011.06.007`. [Online]. Available: `https://doi.org/10.1016/j.cpc.2011.06.007`.

[126] F. V. Tkachov, "A Theorem on Analytical Calculability of Four Loop Renormalization Group Functions", *Phys. Lett. B*, vol. 100, pp. 65–68, 1981. DOI: `10.1016/0370-2693(81)90288-4`.

[127] K. G. Chetyrkin and F. V. Tkachov, "Integration by Parts: The Algorithm to Calculate beta Functions in 4 Loops", *Nucl. Phys. B*, vol. 192, pp. 159–204, 1981. DOI: `10.1016/0550-3213(81)90199-1`.

[128] V. A. Smirnov, *Feynman integral calculus.* Berlin, Heidelberg: Springer, 2006.

[129] R. Lee, "Presenting litered: A tool for the loop integrals reduction", *arXiv preprint arXiv:1212.2685*, 2012. DOI: `10.48550/ARXIV.1212.2685`. [Online]. Available: `https://arxiv.org/abs/1212.2685`.

[130] S. Laporta, "High precision calculation of multiloop Feynman integrals by difference equations", *Int. J. Mod. Phys. A*, vol. 15, pp. 5087–5159, 2000. DOI: `10.1142/S0217751X00002159`. arXiv: `hep-ph/0102033`.

[131] A. V. Kotikov, "Differential equations method: New technique for massive Feynman diagrams calculation", *Phys. Lett. B*, vol. 254, pp. 158–164, 1991. DOI: `10.1016/0370-2693(91)90413-K`.

[132] E. Remiddi, "Differential equations for feynman graph amplitudes", *Il Nuovo Cimento A*, vol. 110, no. 12, pp. 1435–1452, 1997. DOI: `10.1007/bf03185566`. [Online]. Available: `https://link.springer.com/article/10.1007/BF03185566`.

[133] T. Gehrmann and E. Remiddi, "Differential equations for two-loop four-point functions", *Nuclear Physics B*, vol. 580, no. 1-2, pp. 485–518, 2000. DOI: `10.1016/s0550-3213(00)00223-6`. [Online]. Available: `https://doi.org/10.1016/s0550-3213(00)00223-6`.

[134] J. M. Henn, "Multiloop integrals in dimensional regularization made simple", *Physical Review Letters*, vol. 110, no. 25, 2013. DOI: `10.1103/physrevlett.110.251601`. [Online]. Available: `https://doi.org/10.1103/physrevlett.110.251601`.

[135] A. B. Goncharov, "Multiple polylogarithms, cyclotomy and modular complexes", *Mathematical Research Letters*, vol. 5, no. 4, pp. 497–516, 1998. DOI: `10.4310/mrl.1998.v5.n4.a7`. [Online]. Available: `https://doi.org/10.43102Fmrl.1998.v5.n4.a7`.

[136] A. B. Goncharov, *Multiple polylogarithms and mixed tate motives*, 2001. arXiv: `math/0103059 [math.AG]`. [Online]. Available: `https://arxiv.org/abs/math/0103059`.

[137] M. Hidding, "DiffExp, a mathematica package for computing feynman integrals in terms of one-dimensional series expansions", *Computer Physics Communications*, vol. 269, p. 108 125, 2021. DOI: 10.1016/j.cpc.2021.108125. [Online]. Available: https://doi.org/10.1016/j.cpc.2021.108125.

[138] A. Primo and L. Tancredi, "On the maximal cut of feynman integrals and the solution of their differential equations", *Nuclear Physics B*, vol. 916, pp. 94–116, 2017. DOI: 10.1016/j.nuclphysb.2016.12.021. [Online]. Available: https://doi.org/10.1016/j.nuclphysb.2016.12.021.

[139] A. van Hameren, C. Papadopoulos, and R Pittau, "Automated one-loop calculations: A proof of concept", *Journal of High Energy Physics*, vol. 2009, no. 09, pp. 106–106, 2009. DOI: 10.1088/1126-6708/2009/09/106. [Online]. Available: https://iopscience.iop.org/article/10.1088/1126-6708/2009/09/106.

[140] G. Bevilacqua *et al.*, "HELAC-NLO", *Computer Physics Communications*, vol. 184, no. 3, pp. 986–997, 2013. DOI: 10.1016/j.cpc.2012.10.033. [Online]. Available: https://www.sciencedirect.com/science/article/pii/S0010465512003761?via/3Dihub.

[141] F. Cascioli, P. Maierhöfer, and S. Pozzorini, "Scattering amplitudes with open loops", *Physical Review Letters*, vol. 108, no. 11, 2012. DOI: 10.1103/physrevlett.108.111601. [Online]. Available: https://journals.aps.org/prl/abstract/10.1103/PhysRevLett.108.111601.

[142] F. Buccioni *et al.*, "OpenLoops 2", *The European Physical Journal C*, vol. 79, no. 10, 2019. DOI: 10.1140/epjc/s10052-019-7306-2. [Online]. Available: https://link.springer.com/article/10.1140/epjc/s10052-019-7306-2.

[143] G. Bevilacqua, H. Hartanto, M. Kraus, and M. Worek, "Top quark pair production in association with a jet with next-to-leading-order QCD off-shell effects at the large hadron collider", *Physical Review Letters*, vol. 116, no. 5, 2016. DOI: 10.1103/physrevlett.116.052003. [Online]. Available: https://doi.org/10.11032Fphysrevlett.116.052003.

[144] T. Ježo, *Nlo matching for $t\bar{t}b\bar{b}$ production with massive b quarks*, 2018. arXiv: 1808.09311 [hep-ph]. [Online]. Available: https://pos.sissa.it/316/089.

[145] S. Catani, S. Dittmaier, and Z. Trócsányi, "One-loop singular behaviour of QCD and SUSY QCD amplitudes with massive partons", *Physics Letters B*, vol. 500, no. 1-2, pp. 149–160, 2001. DOI: `10.1016/s0370-2693(01)00065-x`. [Online]. Available: `https://doi.org/10.1016/s0370-2693(01)00065-x`.

[146] S Catani and M. Seymour, "NLO calculations in QCD: A general algorithm", *Nuclear Physics B - Proceedings Supplements*, vol. 51, no. 3, pp. 233–242, 1996. DOI: `10.1016/s0920-5632(96)90030-4`. [Online]. Available: `https://doi.org/10.1016/s0920-5632(96)90030-4`.

[147] S. Catani and M. Grazzini, "The soft-gluon current at one-loop order", *Nuclear Physics B*, vol. 591, no. 1-2, pp. 435–454, 2000. DOI: `10.1016/s0550-3213(00)00572-1`. [Online]. Available: `https://doi.org/10.1016/s0550-3213(00)00572-1`.

[148] Z. Bern, L. Dixon, and D. A. Kosower, "One-loop corrections to five-gluon amplitudes", *Physical Review Letters*, vol. 70, no. 18, pp. 2677–2680, 1993. DOI: `10.1103/physrevlett.70.2677`. [Online]. Available: `https://doi.org/10.1103/physrevlett.70.2677`.

[149] Y. tin Huang, D. A. McGady, and C. Peng, "One-loop renormalization and the s-matrix", *Physical Review D*, vol. 87, no. 8, 2013. DOI: `10.1103/physrevd.87.085028`. [Online]. Available: `https://doi.org/10.1103/physrevd.87.085028`.

[150] Z. Bern, L. Dixon, D. C. Dunbar, and D. A. Kosower, "One-loop n-point gauge theory amplitudes, unitarity and collinear limits", *Nuclear Physics B*, vol. 425, no. 1-2, pp. 217–260, 1994. DOI: `10.1016/0550-3213(94)90179-1`. [Online]. Available: `https://doi.org/10.1016/0550-3213(94)90179-1`.

[151] R. Britto, F. Cachazo, and B. Feng, "Generalized unitarity and one-loop amplitudes in super-yang-mills", *Nuclear Physics B*, vol. 725, no. 1-2, pp. 275–305, 2005. DOI: `10.1016/j.nuclphysb.2005.07.014`. [Online]. Available: `https://doi.org/10.1016/j.nuclphysb.2005.07.014`.

[152] J. Bedford, A. Brandhuber, B. Spence, and G. Travaglini, "Non-supersymmetric loop amplitudes and MHV vertices", *Nuclear Physics B*, vol. 712, no. 1-2, pp. 59–85, 2005. DOI: `10.1016/j.nuclphysb.2005.01.032`. [Online]. Available: `https://doi.org/10.1016/j.nuclphysb.2005.01.032`.

[153] F. Cachazo, P. Svrcek, and E. Witten, "MHV vertices and tree amplitudes in gauge theory", *Journal of High Energy Physics*, vol. 2004, no. 09, pp. 006–006, 2004. DOI: 10.1088/1126-6708/2004/09/006. [Online]. Available: https://doi.org/10.1088/1126-6708/2004/09/006.

[154] Z.-G. Xiao, G. Yang, and C.-J. Zhu, "The rational parts of one-loop QCD amplitudes III: The six-gluon case", *Nuclear Physics B*, vol. 758, no. 1-2, pp. 53–89, 2006. DOI: 10.1016/j.nuclphysb.2006.09.006. [Online]. Available: https://doi.org/10.1016/j.nuclphysb.2006.09.006.

[155] Z.-G. Xiao, G. Yang, and C.-J. Zhu, "The rational parts of one-loop QCD amplitudes i: The general formalism", *Nuclear Physics B*, vol. 758, no. 1-2, pp. 1–34, 2006. DOI: 10.1016/j.nuclphysb.2006.09.008. [Online]. Available: https://doi.org/10.1016/j.nuclphysb.2006.09.008.

[156] G. Laurentis and D. Maître, "Extracting analytical one-loop amplitudes from numerical evaluations", *JHEP*, vol. 07, p. 123, 2019. DOI: 10.1007/JHEP07(2019)123. arXiv: 1904.04067 [hep-ph].

[157] D. Melrose, "Reduction of feynman diagrams", *Il Nuovo Cimento A (1965-1970)*, vol. 40, no. 1, pp. 181–213, 1965.

[158] L. Dixon, "New color decompositions for gauge amplitudes at tree and loop level", Tech. Rep., 1999. DOI: 10.2172/15092. [Online]. Available: https://doi.org/10.2172/15092.

[159] Z. Bern, L. J. Dixon, and D. A. Kosower, "Dimensionally regulated one loop integrals", *Phys. Lett. B*, vol. 302, pp. 299–308, 1993, [Erratum: Phys.Lett.B 318, 649 (1993)]. DOI: 10.1016/0370-2693(93)90400-C. arXiv: hep-ph/9212308.

[160] A. Denner and S. Dittmaier, "Scalar one-loop 4-point integrals", *Nucl. Phys. B*, vol. 844, pp. 199–242, 2011. DOI: 10.1016/j.nuclphysb.2010.11.002. arXiv: 1005.2076 [hep-ph].

[161] Z. Bern and A. Morgan, "Massive loop amplitudes from unitarity", *Nuclear Physics B*, vol. 467, no. 3, pp. 479–509, 1996. DOI: 10.1016/0550-3213(96)00078-8. [Online]. Available: https://doi.org/10.1016/0550-3213(96)00078-8.

[162] O. V. Tarasov, "Connection between feynman integrals having different values of the space-time dimension", *Physical Review D*, vol. 54, no. 10, pp. 6479–6490, 1996. DOI: 10.1103/physrevd.54.6479. [Online]. Available: https://doi.org/10.1103/physrevd.54.6479.

[163] R. Lee, "Space–time dimensionality as complex variable: Calculating loop integrals using dimensional recurrence relation and analytical properties with respect to", *Nuclear Physics B*, vol. 830, no. 3, pp. 474–492, 2010. DOI: 10.1016/j.nuclphysb.2009.12.025. [Online]. Available: https://doi.org/10.1016/j.nuclphysb.2009.12.025.

[164] S. Badger, C. Brønnum-Hansen, F. Buciuni, and D. O'Connell, "A unitarity compatible approach to one-loop amplitudes with massive fermions", *Journal of High Energy Physics*, vol. 2017, no. 6, 2017. DOI: 10.1007/jhep06(2017)141. [Online]. Available: https://doi.org/10.1007/jhep06(2017)141.